Physiological role of sensory axon bifurcation in DRG neurons mediated by Npr2-dependent cGMP signaling

Inaugural-Dissertation
to obtain the academic degree
Doctor rerum naturalium (Dr. rer. nat.)

Submitted to the Department of Biology, Chemistry and Pharmacy
of Freie Universität Berlin

by

Philip Tröster
from Heidelberg, Germany

Berlin, 2015

This thesis was prepared between September 2009 and February 2015 at the Max-Delbrück Center for Molecular Medicine, Department of Developmental Neurobiology, under the supervision of Prof. Dr. Fritz G. Rathjen.

1st Reviewer: Prof. Dr. Fritz G. Rathjen

2nd Reviewer: Prof. Dr. Carmen Birchmeier-Kohler

Disputation date: 29.06.2015

Acknowledgements

First and foremost, I would like to express my sincere gratitude to my supervisor, Prof. Dr. Fritz G. Rathjen, for giving me the great opportunity to pursue a PhD in his group and for his continuous support and guidance through the course of this work.

I would like to extend my appreciation to my committee member, Prof. Dr. Carmen Birchmeier-Kohler, for agreeing to be the second reviewer of my thesis and for the possibility to use her laboratory to perform the ES cell cultivation and Southern blot analysis.

Moreover, I am particularly grateful for the supervision by Dr. habil. Hannes Schmidt. Thanks for taking so much time for explanations and answering my questions. Your support, advice, encouragement, and patience were deeply appreciated.

I emphatically thank SFB665 for funding my research and conference travels.

I would also like to thank all associates of the MDC Transgene Core Facility. Special thanks to Andrea Leschke for teaching me how to handle mouse embryonic stem cells and the friendly and excellent support.

Furthermore, I would like to thank Dr. Gunnar Dittmar and Dr. Oliver Popp from the MS Core Facility for the MS analysis.

I would also like to acknowledge the assistance of the FACS Core Facility at the MDC in the receptor activity experiment.

I would like to give very special thanks to Karola Bach for her friendly and excellent help in the organization of mice breedings.

Very big thanks to all past and present members of the Rathjen lab for support, discussions, advice and company. In particular, I would like to express my heartfelt thanks to my student, Jenni, for being my busy bee in the lab. Furthermore, I would like to extend my sincere gratitude to Mechthild, Hanna, and Anne for their assistance in laboratory experiments as well as the pleasant atmosphere in our laboratory. I would also like to thank my cGMP signaling colleagues, Gohar and Alexandre, for our constructive discussions. Last, but not least, I would like to address a huge "thank you" to my coffee-break companions namely Claudia, Florian, and Vincent.

I would also like to sincerely thank my entire family for their love and encouragement during the past years. A special thanks to my uncle Thomas, my great aunt Gudrun, and my sister Marie.

I would like to dedicate this dissertation to my wonderful parents, Irene and Klaus, for their unconditional love and the amazing chances they have given me over the years. You have always encouraged me to question things and look at life from all angles preparing me for my path through life. Thanks for everything.

Lastly, I would like to thank my fiancée Joana. Your unwavering love is undeniably the bedrock upon which the past ten years of my life have been built.

INDEX

LIST OF ABBREVIATIONS

aa	amino acid
ANP	arterial natriuretic peptide
BNP	B-type natriuretic peptide
bp	base pairs
BioID	proximity-dependent biotin identification
cGKI	cGMP-dependent kinase I
cGMP	cyclic guanosine monophosphate
cKO	conditional knockout
cn	autosomal recessive gene for achondroplasia
CNP	C-type natriuretic peptide
Cre	cyclization recombination
ddH_2O	distilled deionized water
DMEM	Dulbecco`s Modified Eagle Medium
DREZ	dorsal root entry zone
DRG	dorsal root ganglion/ganglia
E	embryonic day
E. coli	*Escherichia coli*
EDTA	ethylenediaminetetraacetic acid
ES	embryonic stem
FCS	fetal calf serum
Flp	flippase
FRT	flippase recognition target
GC	guanylyl cyclase
gSC	genomic subclone
GTP	guanosine triphosphate
G418	geneticin
IRES	internal ribosome entry site
kb	kilobase pairs
kDa	kilodalton
KHD	kinase homology domain

KO	knockout
LB	lysogeny broth
lbab	long bone abnormality
LBD	ligand binding domain
LIF	leukemia inhibitory factor
loxP	Locus of Crossover in P1
Neo	neomycin
Npr1	natriuretic peptide receptor 1 (A)/ guanylyl cyclase A (GC-A)
Npr2	natriuretic peptide receptor 2 (B)/ guanylyl cyclase B (GC-B)
Npr3	natriuretic peptide receptor 3 (C)
MS	mass spectrometry
OD	optical density
P	postnatal day
PAGE	polyacrylamide gel electrophoresis
PBS	phosphate buffered saline
PCR	polymerase chain reaction
pDTA	plasmid diphtheria toxin A
PFA	paraformaldehyde
rec	recombinant
RT	room temperature
RT-PCR	reverse transcription polymerase chain reaction
SC	spinal cord
SDS	sodium dodecyl sulfate
SOB	super optimal broth
SOC	super optimal broth with catabolic repressor
SSC	saline-sodium citrate
TAE	Tris-acetate-EDTA
TBS	Tris-buffered saline
TEMED	Tetramethylethylenediamine
TFB	transformation buffer
TMD	transmembrane domain
Tris	Tris(hydroxymethyl)aminomethane

UV	ultraviolet
V	volt
v/v	volume/volume
wt	wildtype
w/v	weight/volume
YFP	yellow fluorescent protein
^{32}P	phosphorus-32

ABSTRACT

The complexity of the nervous system is in part based on spacious axonal branches that are created during embryonic development and expanded after birth. However, the signaling mechanisms which regulate the formation of these complex axon ramifications are still not sufficiently understood. Studies on afferent axon projections from sensory dorsal root ganglia (DRG) neurons into the spinal cord have demonstrated that growth cone splitting (bifurcation) of these axons at the dorsal root entry zone into two daughter branches which elongate either in caudal or rostral direction is controlled by a cGMP-signaling cascade. This signaling path is activated by extracellular binding of C-type natriuretic peptide (CNP) to the transmembrane natriuretic peptide receptor 2 (Npr2) causing the intracellular guanylyl cyclase domain of the receptor to convert guanosine triphosphate (GTP) into cyclic guanosine monophosphate (cGMP). The second messenger cGMP subsequently activates cGMP-dependent protein kinase I alpha (cGKIα) which in turn phosphorylates so far unknown target proteins most likely involved in the regulation of the cytoskeletal structure of the growth cone.

The aim of the thesis was twofold with respect to the bifurcation-inducing cGMP signaling cascade: (1) the generation of a floxed Npr2 mouse model for behavioral studies in order to gain first *in vivo* insights into the physiological function of axon bifurcation at the dorsal root entry zone, and (2) the investigation of mechanisms that regulate Npr2 activity as well as the search for potential protein interactions of components of the cGMP signaling cascade.

(1) The generation of a conditional Npr2 knockout mouse was necessary for the analysis of behavioral consequences caused by impaired axon bifurcation due to the fact that Npr2-mediated cGMP signaling also contributes to the development and function of other tissues such as bone by endochondral ossification and the meiotic arrest of oocytes. Therefore, the loss of Npr2 function had to be confined to DRG neurons in order to allow interpretable behavioral studies and to clarify whether the transmission of sensory stimuli by afferent axons is hampered by impaired axonal branching in the spinal cord. For this purpose, the Cre-*loxP* recombination system was used as a genetic tool and a transgenic mouse model was generated containing two *loxP* target sites that flank exon 17 and exon 18 of the *Npr2* gene. Whereas a first attempt to generate a

floxed Npr2 mouse unfortunately resulted in a hypomorphic phenotype due to a splice site mutation, the second attempt succeeded with the creation of the intended conditional Npr2 mouse mutant.

Using the Wnt1-Cre mouse as a driver for Cre expression, experimental animals were generated which displayed undisturbed bone development in combination with impaired axon bifurcation. First behavioral studies (Hargreaves test) have revealed that the acute pain perception is significantly reduced in these animals due to the lack of axon bifurcation. Further behavioral studies with regard to nociceptive, mechanoreceptive and proprioceptive perception are planned to confirm the hypoalgesic phenotype and to characterize the role of axonal branching at the dorsal root entry zone in more detail. In general, the floxed Npr2 mouse provides a valuable tool for the investigation of Npr2-related phenotypes and therefore should be instrumental in studies of bone development, oogenesis or other Npr2-mediated physiological processes.

(2) In order to analyze the regulation of Npr2 activity, site-directed mutagenesis of Npr2 followed by subsequent determination of the receptor activity revealed that cGMP production by the guanylyl cyclase domain of the receptor depends on the phosphorylation of five phosphorylation sites (Ser-513, Thr-516, Ser-518, Ser-523 and Ser-526) within the kinase homology domain of Npr2. Furthermore, to ascertain whether the cGMP signaling pathway is engaged in cross-talk with other proteins or signaling pathways, the proximity-dependent biotin identification (BioID) labeling assay based on the promiscuous biotin ligase BirA* was applied to screen for potential interaction partners of Npr2 and cGKIα in cell lines. Thus, a number of Npr2-specifically and cGKIα-specifically purified proteins were identified by mass spectrometry. The *in vitro* data of the biotin labeling assay provided first information about new potential interactors of the cGMP signaling cascade. However, it remains for future studies to experimentally confirm the actual link to cGMP signaling and the participation in axon bifurcation.

ZUSAMMENFASSUNG

Die Komplexität des Nervensystems basiert zum Teil auf weitläufigen axonalen Verzweigungen einzelner Nervenzellen, die während der Embryonalentwicklung angelegt und nach der Geburt weiter ausgebaut werden. Die axonalen Verzweigungen werden dabei von Signalmechanismen reguliert, deren genaue Funktionsweisen meist noch unverstanden sind. Untersuchungen an den Axonen von sensorischen Spinalganglienneuronen im Rückenmark haben gezeigt, dass die Gabelung (Bifurkation) der sensorischen Axone, die beim Einwachsen in das Rückenmark entsteht, von einer cGMP-Signalkaskade kontrolliert wird. Dieser Signalweg wird durch die Bindung von C-Typ-natriuretische Peptid (CNP) an die extrazelluläre Domäne des membranständigen natriuretischen Peptidrezeptors 2 (Npr2) aktiviert. Daraufhin führt die intrinsische Guanylatzyklase-Aktivität des Rezeptors zur Bildung von cyclischem Guanosinmonophosphat (cGMP) im Zellinneren der sensorischen Axone. Dieses cGMP aktiviert die cGMP-abhängige Proteinkinase I alpha (cGKIα), die bislang unbekannte Zielproteine an- und abschalten kann, die sehr wahrscheinlich regulativ auf die Zytoskelettstruktur des Wachstumskegels wirken. Dabei entstehen zwei Tochteraxone, die konträr zueinander in rostraler und kaudaler Richtung entlang der Rückenmarksegmente weiterwachsen. Fehlt ein Mitglied der cGMP-Signalkaskade, wächst das Hauptaxon ohne zu bifukieren in nur einer Richtung im Rückenmark weiter.

Die Zielsetzung der Doktorarbeit umfasste zwei Schwerpunkte hinsichtlich dieser axonalen Verzweigung im Rückenmark: (1) die Herstellung einer gefloxten Npr2 Mausmutante für verhaltensbiologische Untersuchungen, um erste *In-vivo*-Erkenntnisse über die physiologische Funktion der axonalen Verzweigung zu gewinnen und (2) die Untersuchung von Regulationsmechanismen, die die Aktivität von Npr2 kontrollieren sowie die Suche nach weiteren Proteinen, die mit der cGMP-Signalkaskade interagieren und dabei eine Rolle für die axonale Verzweigung spielen können.

(1) Die Erzeugung einer konditionellen Npr2-Mausmutante, bei der das *Npr2* Gen nur in den sensorischen Neuronen deaktiviert wird, war notwendig, da auch das Längenwachstum von Knochen (enchondrale Ossifikation) und der meiotische Arrest von Oozyten durch Npr2-vermittelte cGMP-Signaltransduktion reguliert wird. Vor allem die Umgehung der Kleinwüchsigkeit durch eine konditionelle Npr2-defiziente Mausmutante

war entscheidend, um interpretierbare Verhaltensstudien durchführen zu können. Eine gefloxte Npr2 Mausmutante, bei der zwei *loxP*-Sequenzen das Exon 17 und Exon 18 des *Npr2* Gens flankieren, wurde hergestellt, um mit Hilfe des Cre/*loxP*-Rekombinationssystem eine konditionelle Npr2-defiziente Mausmutante zu erzeugen. Allerdings wies die erste erzeugte gefloxte Npr2-Mausmutante auf Grund von Punktmutationen im Bereich der Exon-Intron-Grenzen bereits einen hypomorphen Phänotyp auf. Erst mit einer mutationsfreien, gefloxten Npr2-Maus und mittels der Wnt1-Cre-Maus konnte eine konditionelle Npr2-defiziente Mausmutante mit normaler Knochenentwicklung, aber ohne Bifurkation der sensorischen Axone im Rückenmark, erzeugt werden. Erste verhaltensbiologische Untersuchungen (Hargreaves Test) haben gezeigt, dass die akute Schmerzwahrnehmung von Tieren mit axonaler Bifurkationsstörung im Rückenmark reduziert ist. Weitere bereits konzipierte Untersuchungen werden die funktionelle Rolle der axonalen Verzweigung bezüglich der nozizeptiven, mechanorezeptiven und propriozeptiven Reizwahrnehmung im Detail charakterisieren. Die erzeugte gefloxte Npr2-Mausmutante ist darüber hinaus ein wertvolles Mausmodell, mit dessen Hilfe die Funktion der Npr2-vermittelten cGMP-Signaltransduktion auch in anderen Npr2-abhängigen physiologischen Prozessen, wie der Knochenentwicklung oder der Oogenese, untersucht werden kann.

(2) Die Analyse der In-vitro-Aktivität von Npr2-Mutanten, die durch ortsgerichtete Mutagenese verändert worden sind, hat gezeigt, dass die Phosphorylierung des Rezeptormoleküls für die enzymatische Aktivität von großer Bedeutung ist. Nur wenn fünf Phosphorylierungsstellen (Ser-513, Thr-516, Ser-518, Ser-523 und Ser-526) innerhalb der Kinase-Homologie-Domäne von Npr2 phosphoryliert sind, kann der Ligand CNP die Guanylatzyklase-Aktivität des Rezeptors und somit die cGMP-Produktion induzieren. Um mögliche Interaktionspartner der cGMP-Signalkaskade nachzuweisen, die an der Rezeptorregulation oder der Strukturveränderung des Zytoskeletts beteiligt sind, wurde eine Biotin-Markierungs-Analyse (BioID) basierend auf der promisken Biotin-Protein-Ligase BirA* etabliert. BirA*-Hybridproteine von Npr2 und cGKIα wurden in Zellen exprimiert, um Nachbarschaftsverhältnisse von Npr2 und cGKIα durch Biotinylierung aufzuspüren. Durch massenspektrometrische Analyse wurden Proteine bestimmt, die jeweils spezifisch für Npr2 oder cGKIα nachgewiesen werden konnten und somit potentielle Interaktionspartner der cGMP-Signalkaskade sind.

1. INTRODUCTION

1.1 Neuronal network

Accurate neuronal wiring during development is crucial for regular adult brain function. All functions of the brain in sensory perception, motor behaviour, learning, memory and cognition require complex and highly specific neuronal circuitry (Man et al., 2013). Thereby, the neuronal network is composed of series of interconnected neurons whose axon terminals transmit signals to higher order neurons. The directional flow of information within the nervous system relies on the distinctive morphological property of single nerve cells to polarize (Dotti and Banker, 1987) and to connect with multiple synaptic targets by axon pathfinding along with extensive axonal branching to form elaborate terminal arbours (Gibson and Ma, 2011; Schmidt and Rathjen, 2010). Since my research is focused on sensory axon bifurcation at the dorsal root entry zone, a brief introduction about axon development in general and sensory neuron development in the dorsal root ganglia will be given in the following chapters. Furthermore, the known members of the bifurcation-inducing cGMP signaling cascade and their reported mutations in mice and humans will be described in more detail.

1.2 Axonal Guidance

The axon development is based neuronal polarization, axonal growth and guidance, axon branching, and presynaptic differentiation (Barnes and Polleux, 2009). During embryonic and early postnatal development axons follow precise pathways and establish predictable connections. For that, growth cones which are the expanded motile tips of growing axons are steered to their target regions by chemorepulsive and chemoattractive guidance factors present in their microenvironment (Tessier-Lavigne and Goodman, 1996). The communication between the neuronal growth cone and guidance cues affects appropriate remodeling of the cytoskeleton to promote locomotion and shape change. Intracellularly, the coordinated assembly of dynamic cytoskeletal polymers, microtubules and filamentous actin, is controlled by signaling cascades which are initiated by guidance cue receptors and propagated by second messenger pathways (i.e., GTPases, protein kinases, and protein phosphatases) (Dent et al., 2011). Several cues that guide axons take an attractive or repellent effect at both

short and long range. Beyond that, they can be linked to intermediate or final targets providing the information required for selective guidance of distinct neuronal populations. Four prominent families of instructive guidance cues have been extensively studied in the past decades: netrins, slits, semaphorins, and ephrins. In combination with their receptors (netrins – DCC, neurogenin, and UNC-5 receptors; slits – ROBO receptors; semaphorins – neuropilin and plexin receptors; ephrins – EPH receptors), they define axon trajectories *in vivo* by affecting assembly and disassembly of growth cone cytoskeletal components (Kolodkin and Tessier-Lavigne, 2011). However, several additional factors can contribute to guidance of axon outgrowth. Growth factors such as brain-derived neurotrophic factor, neurotrophin-3, hepatocyte growth factor, glial-derived neurotrophic factor, neuregulin, and fibroblast growth factors have been linked to an attractive guidance effect that can be specific for neuronal subtypes (Ebens et al., 1996; Kramer et al., 2006a; López-Bendito et al., 2006; O'Connor and Tessier-Lavigne, 1999; Shirasaki et al., 2006). Furthermore, extracellular matrix proteins such as cell-adhesion molecules of the immunoglobulin or cadherin superfamilies as well as morphogens like Wnt and sonic hedgehog are intimately involved in axon guidance (Charron et al., 2003; Hattori et al., 2009; Salinas and Zou, 2008).

1.3 Axonal branching

Over decades, scientists investigating the neural development have mainly focused on mechanisms of axon guidance, while axon branching has received less attention despite its importance in establishing neural circuits (Kalil and Dent, 2013; Schmidt and Rathjen, 2010). Branching contributes to the tremendous complexity of neuronal circuits and allows neurons to develop unique patterns of connectivity. Axon branches shape topographic maps and they enable neurons to communicate with a number of neurons in different parts of the brain, simultaneously. In order to connect with synaptic targets in widely separated regions of the nervous system, single axons need to generate branches that extend interstitially from the axon shaft, elongate and finally arborize at specific target regions. Thereby, axonal branches determine the tremendous individual morphology, connectivity and structural plasticity of each neuronal cell type (Figure 1). Beside morphological differences in extension length and arborisation rate, axonal branches emerge at highly diverse time points during development.

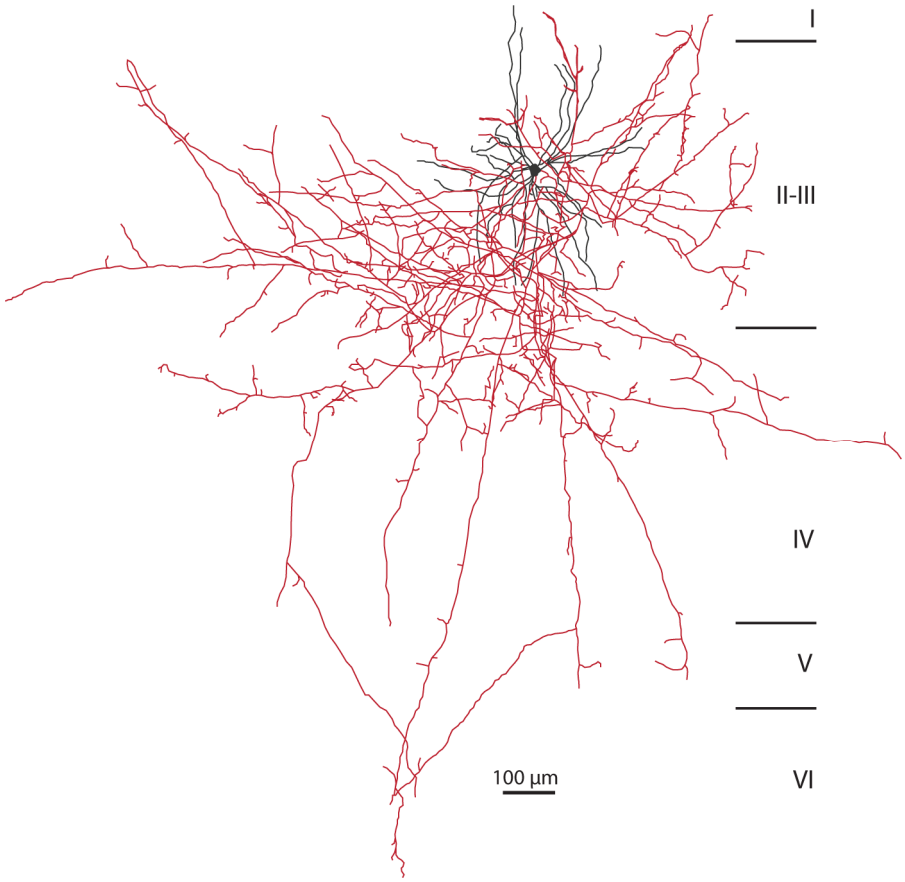

Figure 1: Axonal branching defines the distinct morphology and connectivity of each neuronal cell type. The reconstruction of a GABAergic neuron in the visual cortex illustrates the complexity of axonal branching in the brain. Cell soma and dendrites are in black whereas the highly arborized axon is in red (adapted from (Tamás et al., 1997)). Roman numbers indicate the cortical layers.

A wide range of branches create major neuronal pathways during early stages that persist throughout lifetime, whereas subsequent branches that arise at later and adult stages of neuronal development can often be remodelled by neural activity (Gibson and Ma, 2011). Despite the multiplicity of branches, the literature commonly differentiates between three primary modes of axonal branch formation (Figure 2). The most advanced kind of axonal branching by far is the arborisation of axon terminals leading to the formation of tree-like arbours with higher-order branches that re-branch at the target region. On the contrary, the plainest conformation of axonal branches is shaped by bifurcation. For that, the extending growth cone divides in the form of a T-junction and generates two daughter branches that grow away from each other. The third general axon branching process is collateral branching also termed as interstitial branching. Collateral branches are initially extended either orthogonally or slantingly

along the axon shaft far from the nerve terminal and innervate tissue that is not typically entered by the main axon (Schmidt and Rathjen, 2010). This interstitial branching can be decelerated and appears even days after the main axon has bypassed the target region (O'Leary et al., 1990).

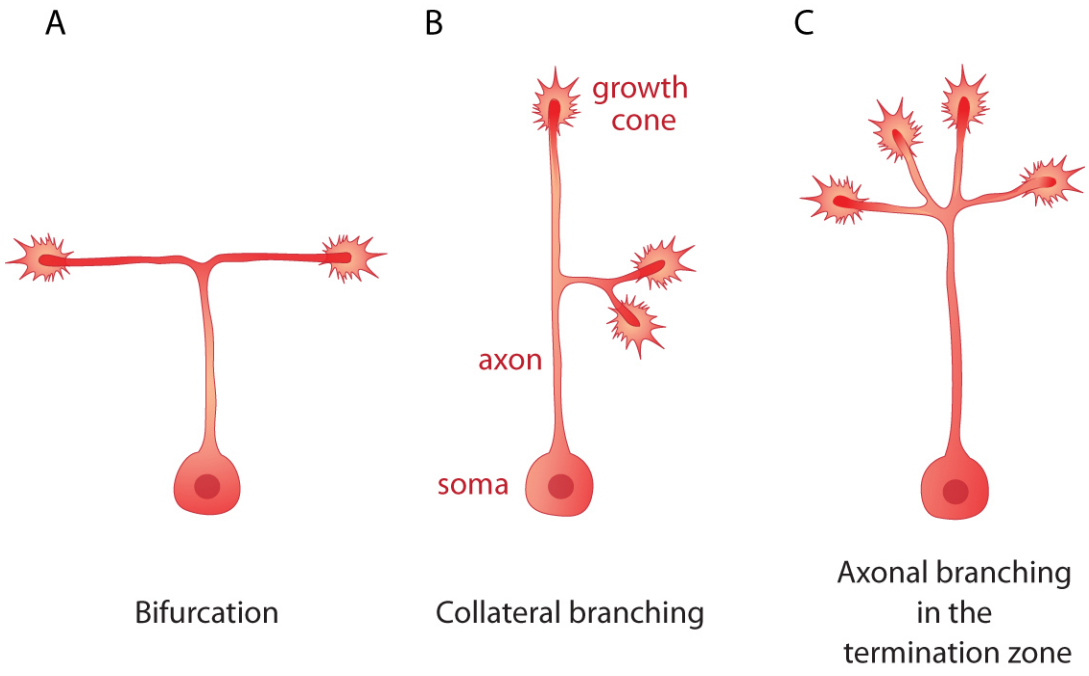

Figure 2: Three different modes of axonal branch formation. (A) Growth cone splitting results in bifurcation of the stem axon into two daughter branches. (B) Collateral branching also termed interstitial branching means the formation of daughter branches along the primary axon shaft. (C) Axonal branching in the termination zone leads to the complex formation of tree-like arbours.

The regulation of these various axonal branching modes is based on distinct signal transduction pathways that are similar to signaling mechanism found during axonal guidance (Dent et al., 2003). Several extracellular cues activate signaling cascades and transcriptional programs which trigger the polymerisation or depolymerisation of the actin and tubulin cytoskeleton to regulate branching. Thereby, the initiation of novel branches has to be tightly restricted spatio-temporally in order to suppress continuous branching after the first branch formation and to have no effect on parental axon guidance (Schmidt and Rathjen, 2010). It should be noted, that no single pathway from receptor to the cytoskeleton has been completely defined to this day. Many extracellular and intracellular factors, that influence axonal branching, have been demonstrated to take effect only in cell culture systems *in vitro*, whereas the proof of

principle *in vivo* is often fragmentary or still missing. The broad range of potential branch-inducing factors momentarily contains axon guidance cues like ephrins, slit2, netrin-1 and semaphorin 3A (Dent et al., 2004; Galimberti et al., 2010; Wang et al., 1999), growth factors such as fibroblast growth factor 2 (Szebenyi et al., 2001), morphogens like Wnt and sonic hedgehog (Bodmer et al., 2009; Gong et al., 2009), calcium transients (Hutchins and Kalil, 2008), electrical activity (Ruthazer et al., 2003), neuritin (Cantallops et al., 2000), transcription factors such as serum response factor (Wickramasinghe et al., 2008), cell adhesion molecules like cadherin-6B or anosmin (Barnes et al., 2010; Gianola et al., 2009), and neurotrophin-3, nerve growth factor, and brain-derived neurotrophic factor (Lentz et al., 1999; Marler et al., 2008; Patel et al., 2003).

1.4 Primary sensory neurons

As part of the peripheral nervous system primary afferent neurons provide sensory innervation to the skin, muscles, joints, fascia, bones, and viscera to convey nociceptive, mechanoreceptive, and proprioceptive stimuli to the central nervous system. The stimulus information which is mediated by those sensory neurons includes touch, pressure, itching, temperature, pain, and body balance and movement. Their cell bodies are located either in the cranial sensory ganglia or in the dorsal root ganglia (DRG), the latter of which are in lateral position to the spinal cord in the vertebral column. DRG neurons are pseudounipolar neurons possessing a stem axon that has split into two branches. The distal process sends a branch to target tissues of the periphery such as skin and muscles, whereas the branch of the proximal process innervates the spinal cord or the medulla. Thereby, DRG neurons start out to be bipolar at early embryonic stages and go through pseudo-unipolarisation by fusion of the peripheral and central axon to become unipolar neurons (Matsuda et al., 1996). Sensory DRG neurons provide an excellent and plain system to study axonal growth and branching because all three subtypes of axonal branching are represented (axon bifurcation at the dorsal root entry zone, interstitial branching of collaterals growing into the spinal cord, and terminal branching in the grey matter). Additionally, sensory DRG neurons have given fundamental insights into the genetic regulation of nerve cell diversification.

1.5 Development and subtype differentiation of primary sensory neurons

The developmental origin of primary afferent neurons is the multipotent trunk neural crest which is the source of many cell types, including sensory, sympathetic and enteric neurons of the PNS. Neural crest cells (NCCs) delaminate from the neural tube which is regulated by precise spatiotemporal signals and migrate ventrally between the dermamyotome and the neural tube to generate the dorsal root ganglia (Le Douarin and Kalcheim, 1999). Initiation of the neural crest migration is guided by the growth factor bone morphogenetic protein (BMP) and Wnt signaling pathways. The expression of Wnt factors which is maintained by BMP leads to an epithelial-to-mesenchymal transition of dorsal neural tube cells into NCCs (García-Castro et al., 2002). Two accurately described Wnt factors which are determinative in directing NCCs towards the sensory lineage are *Wnt1* and *Wnt3a* (Ikeya et al., 1997). The process of delamination and migration goes on along with cytoskeletal reorganization, downregulation of N-cadherin and cadherin 6, and changing of the cell adhesion properties in order to increase the cell motility (Nakagawa and Takeichi, 1998). The murine NCCs start to exit the neural tube in a chain-like structure (Kasemeier-Kulesa et al., 2005) between embryonic day 8.5 and 10 (Serbedzija et al., 1990). During NCC migration, the sensory neuron lineage is formed by three waves of neurogenesis (Ma et al., 1999; Maro et al., 2004). Thereby, successive expression of distinct transcription factors such as neurogenin-1 or neurogenin-2, forkhead transcription factor Foxs1 or Foxs2, and brain-specific homeobox/POU domain protein 3A (Brn3a) is decisive for sensory neuron lineage and sensory subtype differentiation (Bertrand et al., 2002; Montelius et al., 2007). Moreover, the subsequent expression of runt-related transcription factors (Runx1, Runx2, and Runx3) causing the expression of distinct tropomyosin-receptor-kinases (TrkA, TrkB, and TrkB), respectively, is fundamental for the final differentiation of sensory DRG neurons into nociceptors, mechanoreceptors, and proprioceptors (Chen et al., 2006; Kramer et al., 2006b). Migrating NCCs of the first wave of neurogenesis differentiate into Runx3 and TrkC-positive proprioceptive neurons as well as TrkB/TrkC, TrkB, tyrosine receptor kinase RET, or TrkB/RET-positive mechanoreceptive neurons (Chen et al., 2006; Kramer et al., 2006b). NCCs of the second wave proliferate into Runx3 and TrkC-positive

proprioceptive and mechanoreceptive neurons as well as Runx1 and TrkA-positive nociceptive sensory neurons (Chen et al., 2006; Frank and Sanes, 1991; Marmigère et al., 2006). Derived from boundary cap cells, the third wave of neurogenesis generates Runx1 and TrkA-positive nociceptive neurons and glia cells (Hjerling-Leffler et al., 2005; Maro et al., 2004). The large myelinated proprioceptive neurons innervate deep structures in the periphery like muscle spindles or Golgi tendon organs in order to sense limb movement and position. The proximal process of proprioceptive neurons projects either into the ventral spinal cord to synapse directly with motoneurons (Mears and Frank, 1997) or into the intermediate zone of the spinal cord where they are connected to interneurons (Riddell and Hadian, 2000). Mechanoreceptive neurons primarily innervate the skin in order to convey the sensation of touch, pressure and vibration. Their proximal process terminates in distinct or partially overlapping laminae of the dorsal horn which in detail are laminae II, III, IV, and V (Li et al., 2011). Nociceptive neurons innervate either cutaneous or visceral receptive fields and are involved in pain perception, thermoception and pruriception. Thereby, the proximal process of thinly myelinated, more rapidly conducting Aδ fibers projects into laminae I and V of the dorsal horn, whereas unmyelinated, slowly conducting C fibers terminate in laminae I or II (Basbaum et al., 2009). Considering the speed of transmission, Aδ fibers are thought to transduce well-localized fast or “first” pain, whereas C fibers mediate inaccurately localized slow or “second” pain. Furthermore, the nociceptive C fibers can be subdivided into IB4+ (nonpeptidergic) and IB4- (peptiderigic) nociceptors based on the presence or absence of the plant isolectin receptor (Stucky and Lewin, 1999). While the peptidergic afferents expressing capsaicin and heat receptor TRPV1 can perceive inflammation and noxious heat stimuli as pain, the nonpeptidergic neurons primarily contribute to mechanical pain perception (Cavanaugh et al., 2009).

1.6 A cGMP signaling cascade controls axon bifurcation of primary sensory neurons

The migration of neural crest cells and their differentiation into sensory subtypes is early on accompanied by a rapid axonal outgrowth to the dorsolateral margin of the spinal cord. In the mouse, the sensory axon enters the spinal cord at the dorsal root entry zone around embryonic day 10. There, the growth cone of sensory axons splits into two

daughter axons that extend longitudinally either in rostral or caudal direction over several segments. After a waiting period of two days, the two stem axons start to sprout collaterals that project into the grey matter of the spinal cord where they finally arborize (Ozaki and Snider, 1997). Previous studies have demonstrated that a distinct cGMP signaling pathway is essential for the first-order bifurcation of sensory axons at the dorsal root entry zone (Schmidt et al., 2002, 2007, 2009; Zhao and Ma, 2009).

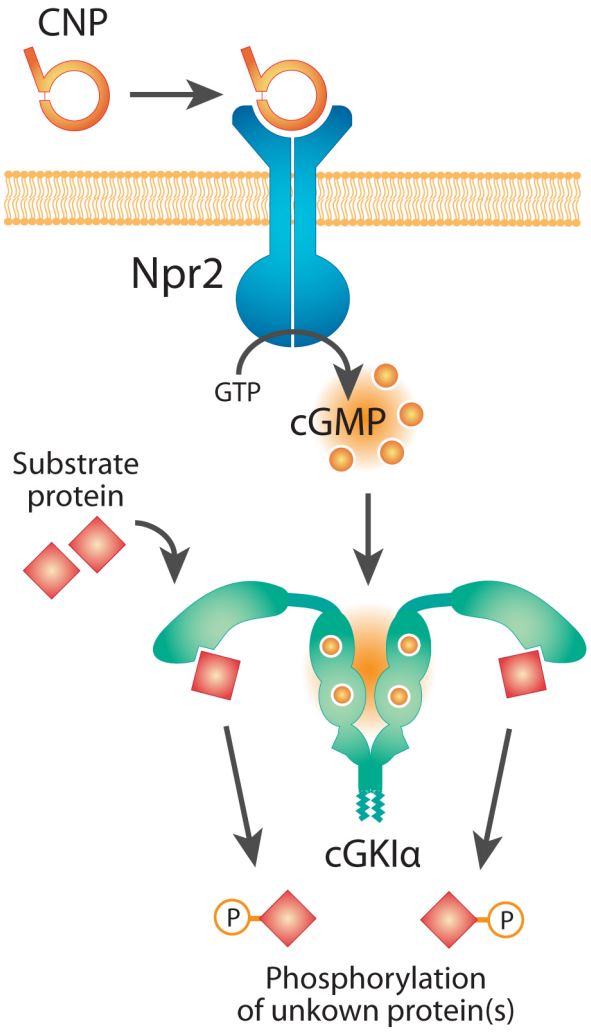

Figure 3: A cyclic guanosine monophosphate signaling cascade is essential for axon bifurcation at the dorsal root entry zone of the spinal cord. Upon binding of the ligand CNP, the receptor guanylyl cyclase Npr2 generates cGMP from GTP. Second messenger cGMP then activates cGKIα which in turn phosphorylates so far unknown targets within the growth cone of sensory DRG neurons. The absence of any component of the cGMP signaling cascade results in impaired axon bifurcation at the dorsal root entry zone. CNP: C-type natriuretic peptide; Npr2: natriuretic peptide receptor 2; cGKIα: cGMP-dependent kinase I alpha; GTP: guanosine triphosphate; cGMP: cyclic guanosine monophosphate; the scheme of cGKIα is adapted from (Vaandrager et al., 2005).

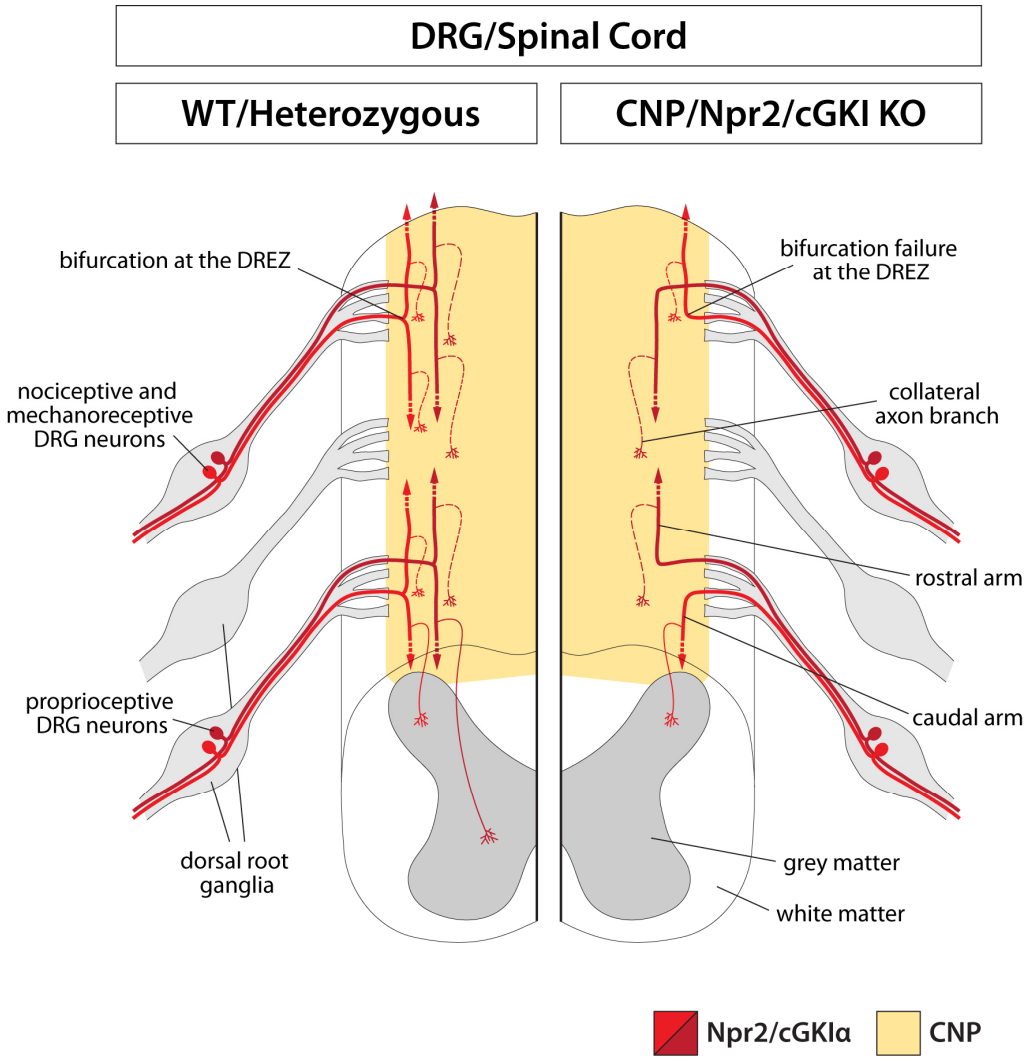

Figure 4: Axon bifurcation of sensory DRG neurons at the dorsal root entry zone of the spinal cord relies on the CNP/Npr2/cGKIα signaling cascade. Axons of sensory DRG neurons enter the spinal cord at the dorsal root entry zone (DREZ) where they bifurcate into two daughter axons that extend longitudinally in rostral or caudal directions. After a waiting period, collaterals are generated from these stem axons that terminate in dorsal or ventral sublaminae of the spinal cord to form terminal arbors. Nociceptive and mechanoreceptive axons terminate in dorsal layers whereas proprioceptive axons synapse with motor neurons in the ventral part of the spinal cord. Axonal branching errors that are caused by absence of the cGMP signaling cascade are represented schematically on the right. In the absence of CNP, Npr2 or cGKIα in mouse mutants, sensory axons still enter the spinal cord but do not bifurcate and instead turn only either in rostral or caudal direction. The formation of collaterals is not affected by the absence of this cGMP signaling cascade. Sensory axons that either enter the spinal cord or grow to the body periphery are drawn in red and express Npr2 and cGKIα; Nociceptive and mechanoreceptive axons are illustrated in light red and proprioceptive axons in dark red; CNP which is secreted by dorsal horn neurons is illustrated in yellow.

This cGMP signaling pathway is composed of the C-type natriuretic peptide (CNP), the natriuretic peptide receptor 2 (Npr2), and the cyclic guanosine monophosphate-dependent kinase I alpha (cGKIα) (Figure 3). The ligand CNP which is secreted by dorsal horn neurons initiates the event of axon bifurcation by binding to the transmembrane receptor Npr2 expressed in sensory DRG neurons. As a result, the intracellular guanylyl

cyclase domain of the activated receptor synthesizes cGMP from GTP. The second messenger cGMP subsequently activates cGKIα which in turn phosphorylates downstream phosphorylation targets in the growth cone of sensory axons which most likely contribute to the process of growth cone splitting. The absence of one component of this cGMP signaling pathway causes impaired axon bifurcation *in vivo* (Schmidt et al., 2002, 2007, 2009; Zhao and Ma, 2009). Instead of splitting up into two daughter branches, sensory axons turn only in one direction (Figure 4). However, the continuative axon development is not disturbed by losing the Npr2-mediated cGMP signaling. The number of collateral branches which sprout from the sensory stem axon to penetrate the dorsal or ventral mantle layer seem to be normal in case of impaired axon bifurcation (Stonkute, 2010). Visualization by DiI tracing of single growth cones at the dorsal root entry zone have evidenced that the two daughter branches are formed by growth cone splitting (Schmidt et al., 2007). On the contrary, it has also been postulated that the sensory axon initially turns in one direction at the dorsal root entry zone and that the second branch is subsequently formed by interstitial branching which is hypothetically induced by interplay between CNP and repulsive guidance cues (Gibson and Ma, 2011). However, Slit/Robo interaction in sensory DRG neurons has been demonstrated to keep the daughter branches outside of the central canal of the spinal cord while they elongate in caudal or rostral direction (Ma and Tessier-Lavigne, 2007). At a functional level, patch clamp recordings at the dorsal horn after capsaicin application have revealed reduced synaptic input on secondary neurons caused by impaired axon bifurcation (Schmidt et al., 2007, 2009). Interestingly, Npr2-mediated cGMP signaling is also involved in first-order axon branching of other primary afferent neurons apart from sensory DRG neurons. The bifurcation of all cranial sensory ganglia neurons is controlled by the same cGMP signaling pathway found in sensory DRG neurons (Ter-Avetisyan et al., 2014). Cranial sensory ganglia neurons bifurcate into descending and ascending branches that elongate along the lateral margin of the hindbrain (Erzurumlu and Killackey, 1983; Erzurumlu et al., 2010). Also spiral ganglion neurons bifurcate in dependency of Npr2-mediated cGMP signaling in order to establish precise connections between hair cells in the cochlea and neurons in the auditory brainstem (Appler and Goodrich, 2011).

1.7 Ligand: C-type natriuretic peptide

The natriuretic peptide family consists of three signaling molecules that are structurally related but genetically and functionally diverse: atrial natriuretic peptide (ANP), B-type or brain natriuretic peptide (BNP), and C-type natriuretic peptide (CNP). These peptides have wide influence on the regulation of homeostatic, cardiovascular, skeletal, nervous and reproductive processes by activating particulate guanylyl cyclases and increasing intracellular cGMP concentrations. There are three known receptors for natriuretic peptides termed natriuretic peptide receptor 1 (Npr1), natriuretic peptide receptor 2 (Npr2), and natriuretic peptide receptor 3 (Npr3). Npr2 is highly specific for CNP with a binding affinity three times greater than for ANP or BNP (Koller et al., 1991). CNP is encoded by the *NPPC* gene which expresses a polypeptide of 126 amino acid residues that needs to be cleaved into a biologically active form (Figure 5). After the signal peptide is detached from the intracellularly generated Prepro-CNP, Pro-CNP gets secreted and further processed by an extracellular protease which is currently unknown (Potter et al., 2009). The proteolytic conversion results either in CNP-53 containing 53 C-terminal amino acids of Pro-CNP or in CNP-22 with 22 C-terminal amino acids. Both share the same 17 amino acid ring structure and are capable to induce cGMP production by binding to natriuretic peptide receptors 2 (Yeung et al., 1996). The half-life of CNP is only 2.6 minutes in humans, what is the shortest of all of the natriuretic peptides, which means that natriuretic peptides are rapidly cleared from the body in general (Hunt et al., 1994). Thereby, the CNP clearance is accomplished by receptor-mediated clearance, proteolytic degradation, or rather by a combination of both (Potter, 2011a). Npr3 lacking the intracellular guanylyl cyclase domain can bind all natriuretic peptides and mediates the natriuretic peptide clearance by internalisation and subsequent degradation (Cohen et al., 1996). Although the internalisation is speculated to occur through a clathrin-dependent mechanism, the molecular transport system required for this process is not known (Potter, 2011a). On the contrary, extracellular proteases such as neprilysin and insulin-degrading enzyme can abolish CNP by proteolytic degradation at initial cleavage sites (Ralat et al., 2011; Watanabe et al., 1997). CNP is expressed by precursor cells and neurons of the dorsal horn and the rhombencephalon where it participates in the Npr2-mediated axon bifurcation (Schmidt et al., 2009; Ter-Avetisyan et al., 2014). In the

peripheral nervous system, CNP is released by Schwann cells (Kishimoto et al., 2008). Furthermore, CNP is slightly expressed in other tissues such as heart and brain and it is found at higher concentrations in bones stimulating longitudinal growth and glycosaminoglycan synthesis (Chusho et al., 2001; Mericq et al., 2000).

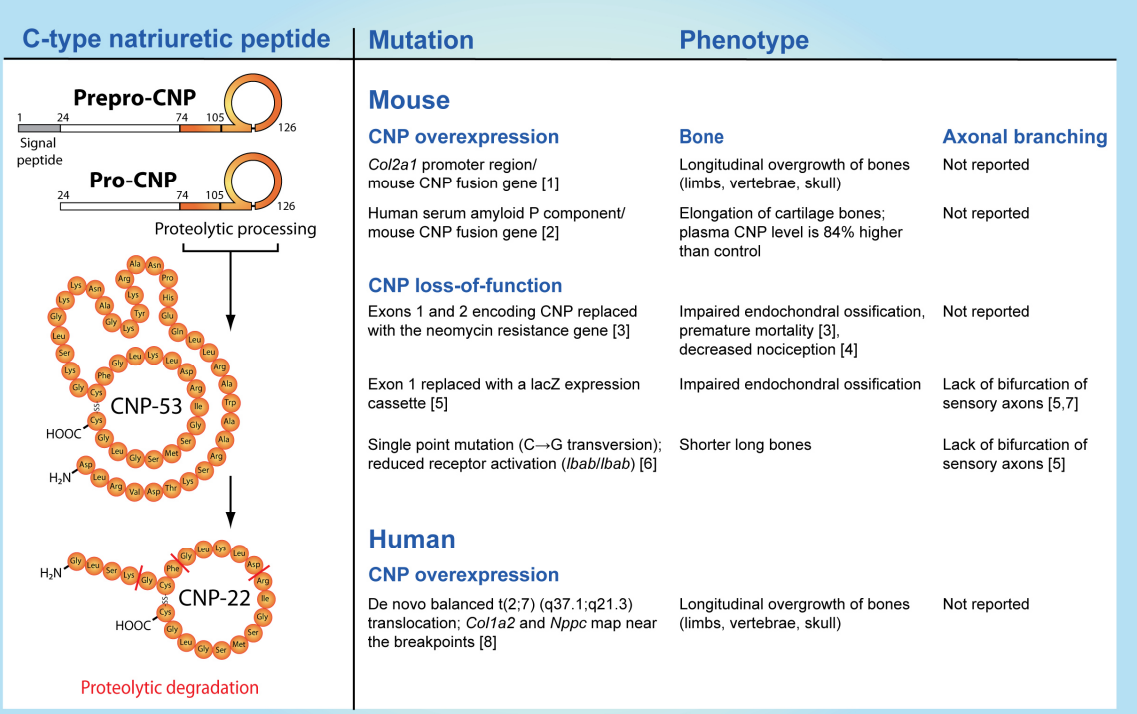

Figure 5: C-type natriuretic peptide (CNP). CNP is a polypeptide of 126 amino acid residues. The cleavage of Prepro-CNP is essential for the biological activity of CNP-53 or CNP-22. After cleavage of the signal peptide, CNP-53 is secreted and further processed to CNP-22 by an extracellular protease which is currently not known. CNP exerts its biological responses by binding and activating Npr2 which generates cGMP from GTP at the intracellular side. Reported spontaneous and directed CNP mutations in mouse and in humans together with their phenotypic expression are listed in tabular form. References: [1] (Yasoda et al., 2004), [2] (Kake et al., 2009), [3] (Chusho et al., 2001), [4] (Kishimoto et al., 2008), [5] (Schmidt et al., 2009), [6] (Jiao et al., 2007), [7] (Zhao and Ma, 2009), [8] (Bocciardi et al., 2007).

1.8 Receptor: Natriuretic peptide receptor 2

The natriuretic peptide receptor 2 (Npr2) also termed guanylyl cyclase B (GC-B) or B-type natriuretic peptide receptor (NPR-B) belongs to a receptor family of seven particulate guanylyl cyclases which all have a cGMP synthesizing activity in common (Potter, 2011b). Furthermore, Npr2 is a member of the natriuretic peptide receptor family which is characterized by binding natriuretic peptides to their extracellular ligand-binding domain (Potter et al., 2006). Three single membrane-spanning natriuretic

peptide receptors have been identified. Npr1 and Npr2 are particulate guanylyl cyclases that catalyze the synthesis of cGMP. Npr3 in turn lacks the guanylyl cyclase domain and therefore the intrinsic enzymatic activity. Npr1 is specific for ANP and BNP, Npr3 can bind all three natriuretic peptides, and Npr2 is activated in a paracrine manner only by CNP (Schulz et al., 1989). In vertebrates, Npr2 is encoded by the *Npr2* gene. Npr2 is integrated into the membrane as a single membrane spanning, noncovalent homodimer and CNP binding leads to no further oligomerization (Chinkers and Wilson, 1992). Npr2 consists of five primary functional domains: a large extracellular ligand-binding domain, a single membrane-spanning region, a juxtamembrane protein kinase homology domain (KHD), a α-helical hinge region involved in dimerization, and a C-terminal guanylyl cyclase catalytic domain (Potter and Hunter, 2001) (Figure 6). Crystal structure analysis of the extracellular ligand-binding domain of Npr1 has demonstrated that the natriuretic peptide binds to the receptor at a stoichiometry of 1:2 (van den Akker et al., 2000). Structural modeling studies have indicated that CNP binds to Npr2, similarly (Yoder et al., 2008). Further crystal structure comparison of natriuretic peptide-bound and non-bound Npr1 has revealed that ligand binding causes the two receptor monomers to undergo an intermolecular twist along with slight intramolecular conformational change (Ogawa et al., 2004). ANP binding is supposed to provoke a twist motion of the two extracellular domains which in turn produces a wheel-like counterclockwise rotation by 24° of the two juxtamembrane domains without essential change in the interdomain distance. Reorientation of the intracellular domains couples the active sites of the guanylyl cyclase domains in optimal proximity and orientation to give rise to guanylyl cyclase activity (Ogawa et al., 2004). Given the fact that Npr1 and Npr2 have the same overall molecular topology, it is most likely that the catalytic activity of NPR2 is based on the same ligand-induced rotation mechanism. Multiple phosphorylation sites have been identified within the intracellular juxtamembrane protein kinase homology domain of Npr2 (Yoder et al., 2010), whose phosphorylation and dephosphorylation acts like an on-off switch for the catalytic receptor activity (Yoder et al., 2012). In the process, phosphorylation is required for initial ligand binding, receptor activation and subsequent catalytic activity, whereas dephosphorylation leads to an inactivation or desensitization of Npr2 (Potter, 1998; Potter and Hunter, 1998). It has been shown that in absence of ligand CNP, Npr2 is highly phosphorylated at five residues (Ser-513, Thr-516, Ser-518,

Ser-23, and Ser-526). Elimination of all of the phosphorylation sites results in a completely dephosphorylated receptor whose CNP-induced cyclase activity was decreased by at least 90 percent (Potter, 1998). The kinase or kinases that are involved in the phosphorylation of Npr2 have not been identified yet. Beside the appropriate phosphorylation status, the glycosylation of extracellular asparagine residues additionally affects ligand binding of Npr2 and displays size heterogeneity of the receptor protein when fractionated by SDS-PAGE. Five of seven extracellular asparagine residues that are suggested to be glycosylated have been mutated by amino acid exchange and analyzed. Thereby, the mutation of asparagine-24 to asparagine acid resulted in a 90 percent loss in CNP binding, which is speculated to be caused by improper folding or cellular targeting of the receptor (Fenrick et al., 1997). Another receptor regulatory element is adenosine triphosphate (ATP) that increases the activity of Npr2 by binding to an unknown intracellular site (Potter, 2011c). A recently postulated Npr2 activation model proposed that the binding of CNP to the extracellular domain enables ATP to bind to the kinase homology domain which derepresses the catalytic domain and elevates the maximum rate of cGMP formation (Duda et al., 1993, 2011). In another model, ATP is constitutively bound to an allosteric site in the guanylyl cyclase domain that in turn is essential for the activation of Npr2 under physiologic conditions. Here, the binding of CNP enables ATP to reduce the Hill coefficient and decreases the Michaelis constant at the same time by displacing GTP at the allosteric site in the catalytic domain (Robinson and Potter, 2012). Mechanisms for the receptor inhibition are debated to be the consequence of a cross-talk between Npr2 and other signaling pathways as well as calcium-dependent. Factors that have been shown to desensitise Npr1 and/or Npr2 *in vitro* are among others arginine-vasopressin (Abbey and Potter, 2002), angiotensin II (Haneda et al., 1991), endothelin (Tokudome et al., 2004), and sphingosine-1-phosphate (Abbey-Hosch et al., 2004). All of these agents interact with either serpentine or tyrosine kinase receptors that can activate phospholipase C (PLC) which in turn produces diacylglycerol and inositol triphosphate. The blocking of protein kinase C (PKC), which is directly activated by diacylglycerol, can disable the angiotensin-II-dependent (Haneda et al., 1991) and endothelin-1-dependent (Tokudome et al., 2004) desensitization of Npr1 and Npr2, respectively, leading to the assumption that PKC could participate in the process.

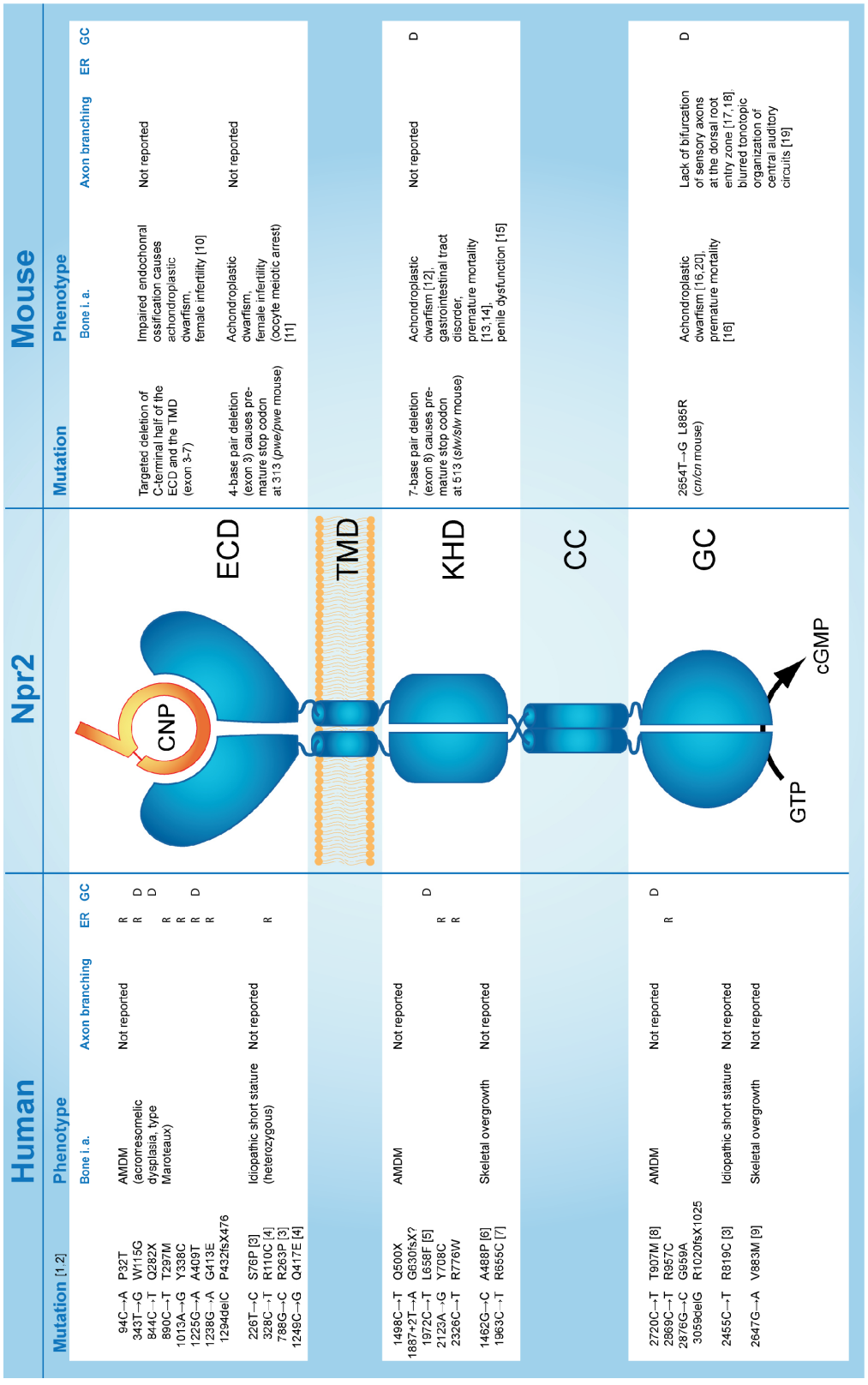

Figure 6: Natriuretic peptide receptor (Npr2). Scheme of the homodimeric receptor guanylyl cyclase Npr2 illustrates the basic topology of the receptor which consists of an extracellular ligand-binding domain (ECD), a hydrophobic membrane spanning region (TMD), a kinase homology domain (KHD), a dimerization segment termed coiled-coil domain (CC) and a guanylyl cyclase domain (GC) at the C-terminus. Reported spontaneous and directed Npr2 mutations in mouse and in humans together with their phenotypic expression are listed in tabular form. Additionally, the location of the mutation is shown with respect to the particular receptor domain. References: [1] (Bartels et al., 2004), [2] (Hume et al., 2009), [3] (Vasques

et al., 2013), [4] (Amano et al., 2014), [5] (Hachiya et al., 2007), [6] (Miura et al., 2014), [7] (Hannema et al., 2013), [8] (Khan et al., 2012), [9] (Robinson et al., 2013), [10] (Tamura et al., 2004), [11] (Geister et al., 2013), [12] (Sogawa et al., 2007), [13] (Sogawa et al., 2010), [14] (Sogawa et al., 2013), [15] (Sogawa et al., 2014), [16] (Tsuji and Kunieda, 2005), [17] (Ma and Tessier-Lavigne, 2007), [18] (Schmidt et al., 2007), [19] (Lu et al., 2014), [20] (Shapiro et al., 2014).

But although PKC-dependent dephosphorylation of serine-523 is a proven inhibitory mechanism for Npr2 *in vitro* (Potter and Hunter, 2000), further studies using PKC inhibitor GF-109203X or chronic downregulation of PKC showed little to none contribution to the desensitization process under physiological conditions (Potter, 2005). Moreover, the inositol triphosphate-calcium part of the phospholipase C pathway seems to play a decisive role in the desensitization of Npr2 by indirectly reducing the amount of phosphate associated with the receptor (Potthast et al., 2004). Arginine-vasopressin and sphingosine-1-phosphate that inhibit the activity of Npr2 also elevate intracellular calcium concentration, whereas the addition of a cell-permeable calcium-chelator blocks most of the inhibitory response (Potthast et al., 2004). A calcium-dependent cellular signaling mechanism is thought to decreases the maximal velocity of the guanylyl cyclase activity (Abbey-Hosch et al., 2005). Recently, the calcium-dependent inhibition of Npr2 guanylyl cyclase activity has been confirmed in cumulus cells where the activity of Npr2 prevents the resumption of meiosis during oocyte maturation (Wang et al., 2013).

Npr2 is highly expressed in cranial sensory ganglia neurons (Ter-Avetisyan et al., 2014) and dorsal root ganglia neurons (Schmidt et al., 2007), but it is also found in chondrocytes, lung, brain, heart, vascular smooth muscle, fibroblasts, uterus and ovary (Chrisman and Garbers, 1999; Doyle et al., 2002; Drewett et al., 1995; Nagase et al., 1997).

1.9 Protein kinase: cGMP-dependent kinase I alpha

The cGMP-dependent protein kinases I (cGKI) and cGMP-dependent protein kinases II (cGKII) are homodimeric serine/threonine kinases that are activated by second messenger cGMP. In mammals, the cGKI gene *prkg1* encodes for two isozymes namely cGKIα and cGKIβ. The two isoforms differ from each other in the first 90 to 100 N-terminal amino acids due to transcription of two alternative exons. Both cGMP-

dependent protein kinases are mainly composed of a regulatory domain and a catalytic domain (Figure 7).

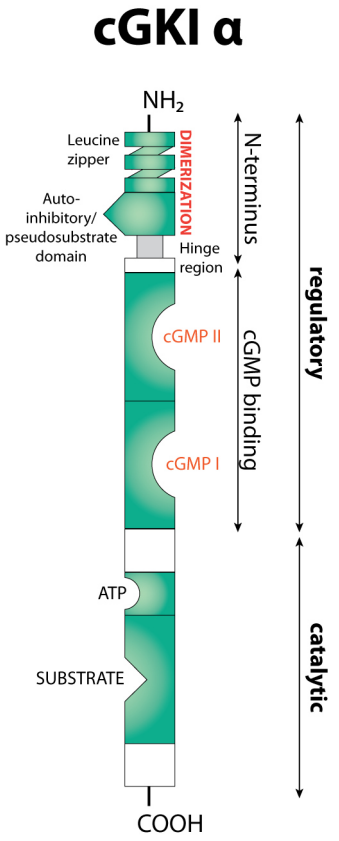

Figure 7: cGMP-dependent kinase I alpha (cGKIα). The serine/threonine kinase cGKI is composed of a regulatory segment and a catalytic domain. In mammals, cGKI is expressed in two isoforms, designated α and β, that are distinct in their N-terminal segments which regulate homodimerization, cGMP affinity and the substrate binding of the isoenzymes. Only the α-isoform of cGKI is expressed in the DRG neurons. The cGKI-deficient mice show impaired axon bifurcation of sensory DRG neurons at the dorsal root entry zone but no severe abnormalities in bone growth (Schmidt et al., 2002, 2007; Zhao et al., 2009). However, diminished perception of pain was reported for cGKI knockout mice (Tegeder et al., 2004). In humans, there is no reported disorder arising directly from the mutated cGKI. Scheme of cGKIα is adopted from (Hofmann et al., 2009).

The regulatory domain can be further classified in an N-terminal domain and a cGMP binding domain containing a high affinity and a low affinity binding pocket for cGMP. By the time all four cGMP binding sites of the homodimer are occupied, the allosteric interaction induces a substantial alteration in the secondary structure of the kinase causing a more elongated molecule (Wall et al., 2003). Binding of cGMP additionally unblocks the inhibition of the catalytic domain by the N-terminal autoinhibitory/pseudosubstrate domain. The catalytic center containing ATP and substrate binding pockets is thereby exposed and can phosphorylate serine/threonine residues in target proteins. The substrate specificity of the kinase is controlled by the N-

terminal hinge region, the autoinhibitory/pseudosubstrate domain, and the leucine zipper domain which is pivotal for the dimerization (Hofmann et al., 2009).

Only the alpha form of cGKI is expressed in sensory neurons and the first evidence of impaired axon bifurcation at the dorsal root entry zone was obtained from cGKIα knockout mice (Schmidt et al., 2002). However, the phosphorylation targets of cGKIα which could be involved in axon bifurcation are unidentified by now. Beside the activation of cGKIα in sensory neurons, Npr2-mediated cGMP signaling can also induce the activation of cGKII. During endochondral ossification, the Npr2-mediated cGMP signaling affects cGKII instead of cGKI in order to guarantee proper longitudinal bone growth (Miyazawa et al., 2002).

1.10 Mutations in CNP, Npr2, and cGKI of the mouse

Directed or spontaneous gene deletions in mice are elementary for the investigation of regular gene functions. Thus, the components of the bifurcation-inducing cGMP signaling pathway were discovered by the analysis of distinct knockout mice. However, beside the impaired axon bifurcation at the dorsal root entry zone, the absence of CNP, Npr2, or cGKIα leads to a broad field of non-neuronal phenotypes in mice indicating that the Npr2-mediated cGMP signaling is involved in several physiological processes. Since the aim of my thesis was the generation of a conditional Npr2 knockout mouse for behavioral studies, the general knowledge about Npr2-related mouse phenotypes is essential to ensure that the tissue-specific disruption of the Npr2 gene activity is in fact restricted to the nervous system without affecting other Npr2-dependent physiological processes.

For instance, the spontaneously mutated *cn*/*cn* mouse which was used as Npr2 loss-of-function model for the analysis of impaired axon bifurcation (Schmidt et al., 2007) was primarily recorded in the context of disproportionate dwarfism caused by disturbed chondrogenesis during endochondral ossification (Silberberg and Lesker, 1975; Tsuji and Kunieda, 2005). In this mouse, a point mutation (T2654G) within exon 18 of *Npr2* leads to a single amino acid exchange (L885R) which completely disrupts the guanylyl cyclase activity of Npr2 (Tsuji and Kunieda, 2005). Starting at day 7 after birth, homozygous mice develop a phenotype of short limbs, short tail, and domed skull which gradually becomes more prominent. Histological analyses have revealed thinner tibial epiphyseal

growth plates and substantially reduced hypertrophic chondrocyte zones for *cn*/*cn* mice suggesting that the dwarf phenotype is evoked by impeded longitudinal bone growth (del Marco, 1981; Wikström et al., 1986). Achondroplasia caused by impaired endochondral ossification was also reported for *slw*/*slw* mice containing a seven base pair deletion in the kinase homology domain of Npr2 leading to a premature stop codon (Sogawa et al., 2007) and for Npr2 knockout mice lacking half of the extracellular ligand binding domain (Tamura et al., 2004). For both Npr2 knockout animals, data about axonal branching are not available. However, recent investigation of Npr2 knockout mice containing a LacZ expression cassette instead of exon 1 of *Npr2* showed impaired bifurcation what makes it highly plausible that all Npr2 knockout mutants manifest the sensory axon bifurcation phenotype (Ter-Avetisyan et al., 2014).

The fact that CNP affects the bifurcation of sensory axons at the dorsal root entry zone was demonstrated by using a CNP knockout mouse containing a LacZ expression cassette instead of exon 1 of *NPPC* (Schmidt et al., 2009). This mutant showed impaired axon bifurcation and an achondroplastic bone phenotype. Also other CNP-deficient mouse mutants suffer from severe dwarfism, but only the *lbab*/*lbab* mouse which contains a cytosine to guanine transversion in the amino acid sequence of CNP was screened for the lack of axon bifurcation so far (Chusho et al., 2001; Jiao et al., 2007; Kishimoto et al., 2008). An interesting point is the inducible overgrowth of cartilage bones by CNP overexpression. Two independently designed mouse mutants showed longitudinal overgrowth of limbs, vertebrae, and skull due to an 84 % higher CNP expression level compared to control animals (Kake et al., 2009; Yasoda et al., 2004).

The influence of cGKIα on sensory axon bifurcation was revealed by analyzing cGKIα-deficient mice (Schmidt et al., 2002, 2007). Even so this mouse mutant shows impaired axon bifurcation, the bone development is unaffected due to the fact that Npr2-mediated cGMP signaling in chondrocytes addresses cGKII instead of cGKIα (Chikuda et al., 2004). However, cGKIα knockout mice decease at the age of 3 to 6 weeks, presumably due to malnutrition or inflammation of the peritoneum (Pfeifer et al., 1999). Furthermore, cGKIα-deficient mice exhibit an intense expansion of stomach and intestine combined with an indication for pyloric stenosis. Experiments with muscle strips from stomach and pylorus have shown that the NO/cGMP-dependent relaxation of intestinal smooth muscles is disturbed in cGKIα-deficient mice (Pfeifer et al., 1998).

Moreover, the vascular tone regulated by vascular smooth muscle cells and the contractile force of the heart is adversely affected, which could also lead to the premature mortality (Bäumner and Nawrath, 1995; Feil et al., 2002).

Premature mortality has also been described for CNP and Npr2 knockout mice, albeit to differing degrees. While more than half of CNP-deficient mice decease before weaning and only 30 % reach an age over 100 days (Chusho et al., 2001), the mortality of Npr2-deficient mice (*cn/cn* mouse) is less than 10 % until postnatal day 100 (Tsuji and Kunieda, 2005). In both cases, the cause of death is still unknown. On the contrary, a study of Npr2-deficient mice (*slw/slw* mouse) revealed a gastrointestinal tract disorder causing early death due to defective intestinal muscles activity (Sogawa et al., 2010). Milk retention in the stomach and distention of the intestinal tract with gas was detected in affected animals which primarily die before weaning.

Another physiological process which is irritated by malfunctioning Npr2-mediated cGMP signaling is the ovarian follicle development. The meiotic arrest of oocytes is maintained in CNP-deficient mice (*lbab/lbab* mouse) as well as Npr2-deficient mice (*cn/cn* mouse and *pwe/pwe* mouse) (Geister et al., 2013; Kiyosu et al., 2012). In all cases, the oocyte maturation is prevented and homozygous female mice are infertile showing no sign of pregnancy at any time. An overview about the CNP- and Npr2-related phenotypes in mice is illustrated in Figure 5 and Figure 6.

1.11 Spontaneous mutations in CNP, Npr2, and cGKI of humans

Abnormal bone growth in humans is the only phenotype so far that was linked to Npr2-mediated cGMP signaling. Several distinct mutations in *Npr2* have been reported to cause a particular form of human skeletal dysplasia termed acromesomelic dysplasia type Maroteaux (AMDM). AMDM is a rare autosomal-recessive genetic disorder with a prevalence of approximately one out of one million. This skeletal dysplasia is characterized by an extreme short stature, malformed bones in the limbs and spine and a body disproportion. Radiographic examination of newborns reveals no misshapen bones or abnormal growth plates and the birth length and weights are normal (Bartels et al., 2004). The skeletal growth declines sharply after birth in such a way that adult patients with AMDM reach only heights of more than 5 standard deviations below the mean (Bartels et al., 2004). Even parental heterozygous carriers exhibit a body shape

that is already below the average but properly proportioned (Bartels et al., 2004). However, neither neurological deficits nor female infertility nor reduced life expectancy have been reported in patients with AMDM. Several heterozygous mutations in *Npr2* were linked to a growth impairment observed in children with idiopathic short stature (ISS) (Vasques et al., 2013). The dominant negative effect caused by heterozygous Npr2 mutations was also found in 2 % of Japanese patients with short stature (Amano et al., 2014). This is in contrast to the bone phenotype observed in mice, where only the endochondral ossification of homozygous animal is affected. In humans, base-pair substitutions are found within the ligand binding domain, the kinase homology domain, and the guanylyl cyclase domain of Npr2 (Bartels et al., 2004). Several of these Npr2 mutations result in poor protein targeting to the plasma membrane or in endoplasmic reticulum protein retention (Hume et al., 2009). Other Npr2 missense mutations inhibit the guanylyl cyclase activity without affecting ligand binding (Hachiya et al., 2007).

Loss-of-function mutations are not found in the human CNP gene until now. But overexpression of CNP based on balanced translocation of *NPPC* has been demonstrated to cause skeletal overgrowth (Bocciardi et al., 2007; Moncla et al., 2007). The plasma level of CNP was almost twofold higher in patients carrying the *NPPC* mutation. In general, genome-wide association studies revealed that elevated CNP plasma levels correlate with larger height (Estrada et al., 2009).

Recently, two studies of distinct Npr2 mutations have linked skeletal overgrowth in humans with a gain-of-function of Npr2. The missense mutation (A488P) of Npr2 was identified in a four-generation family with overgrowth syndrome but normal serum level of proCNP (Miura et al., 2014). In vitro transfection of the receptor protein mutant revealed overactivated cGMP synthesis independent from CNP stimulation. Furthermore, a Npr2 mutation (R655C) localized in the kinase homology domain of the receptor causes extremely tall stature highlighting the regulatory importance of the KHD (Hannema et al., 2013). Whether the CNP/Npr2/cGKIα signaling pathway is implicated in sensory axon bifurcation in humans has not been investigated so far. Therefore, the study of neurological deficits in patients with AMDM could give first indication.

To my knowledge, homozygous mutations in the *prkg1* gene that encodes for cGKIα are not identified in humans up to date. An overview about the CNP- and Npr2-related phenotypes in humans is illustrated in Figure 5 and Figure 6.

2. PREFACE AND OBJECTIVE

The first aim of this thesis was the generation of a floxed Npr2 mouse model for behavioral studies in order to gain first *in vivo* insights into the physiological function of sensory axon bifurcation at the dorsal root entry zone. Since previous patch clamp recordings have demonstrated that the bifurcation failure leads to reduced synaptic input of second-order neurons in the spinal cord, the question arises whether the mutated axonal branching has an impact on sensory perception in animals or not. The results of behavioral testing will help to understand why nature has chosen to project the proximal branch of sensory neurons to the spinal cord in a T-branch manner.

The second aim of this thesis was to provide insights into mechanisms that regulate the Npr2 activity as well as the search for potential protein-protein interactions of components of the cGMP signaling cascade. More specifically, is the catalytic Npr2 activity controlled by the phosphorylation status of the kinase homology domain and what are downstream targets of the cGMP signaling pathway that are involved in the formation of sensory axon bifurcation.

2.1 Role of Npr2-mediated axon bifurcation in sensory perception: Generation of a floxed Npr2 mouse for behavioral studies

In order to perform interpretable behavioral tests that can reveal modifications of sensory perception in animals with impaired axon bifurcation, it is essential that mutant and wild-type mice show no difference concerning size, mobility and bone structure. However, axon bifurcation-deficient CNP and Npr2 knockout mice develop for example prominent achondroplastic dwarfism and the axon bifurcation-deficient cGKI knockout mouse, that would prevent the bone phenotype, suffers from premature mortality to a large extent. Therefore, conventional knockout animals of CNP, Npr2, and cGKI were disqualified for our purposes and the generation of a conditional knockout mouse model was inevitable in order to study the regular function of sensory axon bifurcation at the dorsal root entry zone. Npr2 was chosen as target gene for the genetic modification due to its central role within the cGMP signaling cascade. The strategy for the conditional Npr2 knockout mouse was designed on the basis of the Cre-*loxP* recombination system.

Therefore, a floxed Npr2 mouse mutant containing two *loxP* sites flanking exon 17 and exon 18 of *Npr2* was generated. The Cre-recombinase-inducible excision of exon 17 and exon 18 was selected in order to specifically disrupt the guanylyl cyclase domain activity of Npr2 referring to the exon 18 point mutation in Npr2-deficient cn/cn mice (Tsuji and Kunieda, 2005). Since Wnt1-Cre and Isl1-Cre mice have been demonstrated to induce DRG-specific Cre-recombinase expression at early embryonic stages, both were intended to be used for the generation of DRG-specific conditional Npr2 knockouts (Hu et al., 2011; Scott et al., 2011). After confirming the impaired axon bifurcation of sensory neurons and the correct bone development in the mice, it was planned to characterize the sensory perception by behavioural studies with respect to nociception, mechanoreception, and proprioception.

2.2 Regulation of Npr2 activity and potential cGMP signaling cascade interactions

Since sensory axons bifurcate only once at the dorsal root entry zone, the production of cGMP by the guanylyl cyclase domain of Npr2 is most likely tightly regulated. So far, the exact regulation of Npr2 activity at the growth cone of DRG neurons is unknown. The termination of cGMP signaling by degradation of cGMP via phosphodiesterase 2A or by degradation of ligand CNP via the scavenger receptor Npr3 has been shown to be non-essential for appropriate axon bifurcation (Dr. Hannes Schmidt, personal communication). Therefore, it was suggested that Npr2 itself might be an important determinant for the regulation of the intracellular cGMP level. Since multiple *in vitro* studies by Lincoln R. Potter have revealed that the phosphorylation status of the kinase homology domain of Npr2 plays a crucial role for the receptor activation and desensitization, five different receptor mutants were cloned to analyze how phosphorylation and dephosphorylation of the kinase homology domain can influence the guanylyl cyclase activity of Npr2. Especially, two Npr2 mutants either with glutamate or alanine substitutions at five phosphorylation sites (Ser-513, Thr-516, Ser-518, Ser-523 and Ser-526) were cloned in order to mimic constitutive phosphorylation or constitutive dephosphorylation of the kinase homology domain of Npr2.

Because previous *in vitro* studies by Lincoln R. Potter and others have also suggested that a cross-talk between the cGMP signaling cascade and other signaling pathways

might be involved in desensitization of Npr2 activity and because the phosphorylation targets of cGKIα which contribute to axon bifurcation are unknown, it was intended to search for potential protein-protein interaction of components of the cGMP signaling cascade. Therefore, a recently published proximity-dependent biotin labeling assay (BioID) based on the promiscuous biotin ligase BirA* was applied using BirA* fusion proteins of Npr2 and cGKIα (Roux et al., 2012).

3. MATERIALS

3.1 Buffers, solution and media

Name	Composition and preparation
Agarose gel	0.8-3.5% (w/v) agarose was dissolved in 1xTAE by boiling in microwave oven. 0.01% (v/v) ethidium bromide was added, mixed gently and poured slowly into a gel tray.
BCIP staining solution	20mg/ml 5-Bromo-4-chloro-3-indolyl phosphate dissolved in 100% di-methyl formamide.
CHAPS +protease inhibitors	1% (w/v) CHAPS was dissolved in 1xTBS and protease inhibitors were added; leupeptin hemisulfate salt, pepstatin A, aprotinin to final concentration of 10µM and PMSF (phenylmethylsulfonyl fluoride) to final concentration of 0.1µM. 2ml aliquots were stored at -20°C.
Church buffer (500ml)	0.5M NaH_2PO_4 and 1mM EDTA from 0.5M stock solution was mixed in 450ml ddH_2O; pH value was adjusted to 7.2 with 0.1M NaOH. 1% (w/v) BSA was dissolved at 68°C. After cooling, 7% (w/v) SDS was added and filled up to 500ml. Buffer solution was filtered; aliquots (50 ml) were stored at -20°C.
Denaturation buffer	0.5M NaOH and 1M HCl; freshly prepared of 2M NaOH and 4M HCl stock solution.
Depurination buffer	250mM HCl; freshly prepared of the 2.5M HCl stock solution.
DNA loading buffer (10x)	25% (v/v) Ficoll, 100mM Tris-HCl pH 7.4, 100mM EDTA was dissolved at 65°C. Afterwards 0.25% (w/v) Xylene cyanol was added.
DMEM cell culture medium	500ml DMEM (high glucose/+GlutaMAX) was supplemented with 10% FBS and 1x Penicillin/Streptomycin (final conc. 100 U/ml).
ES cell medium	DMEM (500ml), 90ml FCS, 6ml non-essential amino acids, 6ml Penicillin/Streptomycin (final conc. 100 U/ml), 1.2ml β-mercaptoethanol, 180µl LIF (Leukemia Inhibitory Factor) and 400µg/ml G418 (Geneticin); stored at 4°C.
ES freezing medium	ES cell medium was freshly mixed with 25% (v/v) FCS and 10% (v/v) DMSO before use.
ES lysis buffer	10mM Tris-HCl pH 7.5, 10mM EDTA, 10mM NaCl, 0.5% (w/v) N-lauroylsarcosine; stored at RT.
Feeder (EF) medium	ES cell medium with only 60ml FCS and without LIF and G418; stored at 4°C.
F11 lysis buffer	150mM NaCl, 50mM Tris-HCl pH 7.5, 5mM EDTA pH 8.0; pH was adjusted to 7.4 with 0.1M HCl. Add protease inhibitors before use; leupeptin hemisulfate salt, pepstatin A, aprotinin with final concentration of 10µM and PMSF with 0.1µM
F12 cell culture medium	500ml F-12 Nutrient Mixture medium was supplemented with 15% FBS, 1x Penicillin/Streptomycin (final conc. 100 U/ml), and 1x HAT (final conc. 100µM hypoxanthine, 0.4µM aminopterin, 16µM thymidine).
Laemmli Sample Buffer (5x)	Laemmli Sample buffer consisted of 300 mM Tris-HCl pH 6.8, 50% (v/v) glycerol, 25% (v/v) β-mercaptoethanol, 10% (w/v) sodium dodecyl sulfate, and 0.05% (v/v) bromophenol blue. Aliquots were stored at -20°C.
LB medium	1% (w/v) Bacto-Tryptone, 0.5% (w/v) Bacto-Yeast-Extract, 1% (w/v) NaCl dissolved in ddH2O. The LB medium was autoclaved and stored at 4°C.
LB agar	1.5% (w/v) agar was added to LB-medium, autoclaved and stored at 4°C.
Mowiol mounting medium	2.4g Mowiol 4-88 and 6g glycerol mixed in 6ml ddH_2O for 6h; add 12 mL of 0.2M Tris-HCl (pH 8.5); heat to 50°C for 10 min with mixing; centrifugation at 5000g for 15min; add DABCO to 2.5% and store at -20°C.
NBT staining solution	50mg/ml nitro blue tetrazolium dissolved in 70% di-methyl formamide.

Name	Composition and preparation
NZY$^+$ Broth	2g NZ amine (casein hydrolysate), 1g yeast extract, 1g NaCl was dissolved in 200ml ddH_2O, pH adjusted to 7.5 using NaOH and then autoclaved. Before use, 2.5ml 1M $MgCl_2$, 2.5ml 1M $MgSO_4$ and 4ml 20% (w/v) glucose was added and filter-sterilized.
PBS/EDTA solution	5mM EDTA dissolved in 1xPBS; autoclaved and stored at 4°C.
PFA solution 4% (500ml)	350ml ddH_2O was heated to 60°C and 20g PFA was added. A few drops of 4M NaOH were pipetted until the solution became clear. After cooling, 50ml 10xPBS was added to the solution. After filling up to 500ml and adjusting the pH to 7.2, the solution was filtered, aliquoted (50ml) and stored at -20°C.
Ponceau S staining solution	0.1% (w/v) Ponceau S in 5% (v/v) acetic acid.
Running buffer (WB)	25mM Tris, 190 mM glycine, 0.1% SDS; adjusted to pH 8.3 using 32% HCl.
SOB medium	2% (w/v) Bacto-Tryptone, 0.5% (w/v) Bacto-Yeast-Extract, 10mM NaCl, 2.5mM KCl was autoclaved in ddH_2O. 10mM $MgCl_2$ and 10mM $MgSO_4$ was added, filter-sterilized and stored at 4°C.
SOC medium	20mM added to SOB medium, filter-sterilized and stored at 4°C.
SSC buffer (20x)	3M NaCl and 0.3M sodium citrate dissolved in ddH_2O; pH was adjusted to 7.0 with 0.1M HCl. Buffer was sterile filtered.
Southern washing buffer I	1xSSC, 1% (v/v) SDS.
Southern washing buffer II	1xSSC, 0.1% (v/v) SDS.
Southern washing buffer III	0.5xSSC, 0.1% (v/v) SDS.
Southern washing buffer IV	0.2xSSC, 0.1% (v/v) SDS.
Southern washing buffer V	0.1xSSC, 0.1% (v/v) SDS.
Staining solution for AP	Substrate buffer containing 80µl BCIP solution and 60µl NBT solution per 10ml; mixed freshly for each staining.
Substrate buffer for AP	100mM Tris-HCl pH 9.5, 100mM NaCl, 5mM $MgCl_2$.
TAE (50x)	242g Tris Base, 57.1 ml glacial acetic acid and 100ml 0.5M EDTA (pH 8.0); filled up to 1 liter with ddH_2O.
TBS (10x)	0.5M Tris-HCl pH 7.6 and 1.5M NaCl; adjusted to pH 7.4 using 32% HCl.
TFB1 buffer	100mM $RbCl_2$, 50mM $MnCl_2$, 30mM potassium acetate, 10mM $CaCl_2$; pH of 5.8 adjusted with 0.2N acetic acid. 15% (v/v) glycerol was added, sterile filtered and stored at 4°C.
TFB2 buffer	10mM MOPS, 10mM $RbCl_2$, 75mM $CaCl_2$; pH of 7.0 adjusted with NaOH, then 15% (v/v) glycerol was added, sterile filtered and stored at 4°C.
Transfer buffer	25mM Tris, 190mM glycine and 20% methanol; adjusted to pH 7.4 using 32% HCl; stored at 4°C.
Blocking buffer (WB)	5% (w/v) BSA and 0.5% (v/v) Tween-20 diluted in 1xTBS; aliquots were stored at -20°C.
Washing buffer (WB)	0.5% (v/v) Tween-20 diluted in 1xTBS.

3.2 Restriction enzymes

Name	Company	Name	Company
*Afl*III	New England Biolabs	*Nhe*I-HF	New England Biolabs
*Afl*II	New England Biolabs	*Not*I	Fermentas
*Bam*HI	Fermentas	*Not*I-HF	New England Biolabs
*Bam*HI-HF	New England Biolabs	*Pac*I	Fermentas
*Bln*I	Thermo Scientific	*Pst*I	Fermentas
*Bst*XI	Fermentas	*Sac*I	Fermentas
*Dpn*I	Stratagene	*Sac*II	Fermentas
*Eco*RI	Fermentas	*Sal*I	Fermentas
*Eco*RI-HF	New England Biolabs	*Sal*I-HF	New England Biolabs
*Eco*RV	Fermentas	*Sma*I	New England Biolabs
*Eco*RV-HF	New England Biolabs	*Spe*I	New England Biolabs
*Hin*dIII	Fermentas	*Xba*I	New England Biolabs
*Hin*dIII-HF	New England Biolabs	*Xho*I	New England Biolabs

3.3 Polymerases

Name	Company
FastGene *Taq* DNA Polymerase	Nippon Genetics
Klenow Fragment, exo$^-$	Fermentas
Pfu DNA Polymerase (recombinant)	Fermentas
Q5 High-Fidelity DNA Polymerase	New England Biolabs
TaKaRa LA Taq Polymerase	Takara Shuzo Corporation
Taq DNA Polymerase (recombinant)	Invitrogen
T4 DNA Ligase	Fermentas
T4 Polynucleotide kinase	Fermentas

3.4 Embryonic stem (ES) cells

ES cell line	Provided by
AB2.1	the group of Prof. Dr. Thomas Willnow
E14.1	the group of Prof. Dr. Carmen Birchmeier-Kohler
R1	the group of Prof. Dr. Carmen Birchmeier-Kohler
SV129$_{(TCF)}$	Transgene Core Facility of the Max Delbrück Center for Molecular Medicine

3.5 Laboratory kit

Name	Company
Amersham cGMP Enzyme Immunoassay Biotrak (EIA) System (dual range)	GE Healthcare
Genomic DNA buffer Set	Qiagen
Genomic-tip 500/G	Qiagen
High Pure PCR Template Preparation Kit	Roche
Invisorb DNA Fragment CleanUP	Invitek
QuikChange II XL Site-Directed Mutagenesis Kit	Stratagene
Plasmid Mini/Midi/Maxi Kit	Qiagen

Name	Company
Prime-IT RmT Random Primer Labeling Kit	Stratagene
SuperSignal West Dura Chemiluminescent Substrate	Thermo Scientific

3.6 Antibiotics

Name	Stock solution and storage	Company
Ampicillin	100mg/ml in ddH_2O, at -20°C	Sigma-Aldrich
Chloramphenicol	34mg/ml in 100% ethanol, at -20°C	Sigma-Aldrich
Geneticin (G418)	100mg/ml in ddH_2O, at -20°C	Invitrogen
Kanamycin	100mg/ml in ddH_2O, at -20°C	Sigma-Aldrich
Penicillin/streptomycin	100x concentrated liquid	Invitrogen
Tetracycline hydrochloride	5mg/ml in 50% ethanol, at -20°C	Boehringer

3.7 Bacterial strains

Name	Company or provided by
Escherichia coli DH5α	Invitrogen
Escherichia coli DH10B	Invitrogen
Escherichia coli DY380	the group of Prof. Dr. Carmen Birchmeier-Kohler
Escherichia coli EL350	the group of Prof. Dr. Carmen Birchmeier-Kohler
Escherichia coli EL250	the group of Prof. Dr. Carmen Birchmeier-Kohler
Escherichia coli XL10-Gold	Stratagene

3.8 Antibodies

Name	Used dilution/concentration		From
	WB	IHC	
Goat-α-Rabbit-Alexa488	-	1:300	Jackson ImmunoResearch
Guinea pig-α-cGKIα	1:10000	1:4000	AG Rathjen
Guinea pig-α-Npr2	1:10000	1:4000	AG Rathjen
PGCB-201AP (1.2 mg/ml)	1:500	1:200	FabGennix Inc.
Rb-α-Npr2	1:500	1:200	AG Rathjen

3.9 Chemicals and materials

Name	Company
Acetic acid	Merck
Acryl amide	Bio-Rad
Agarose NEEO Ultra-Quality	Carl Roth
Alkaline Phosphatase (AP)	Roche
Aprotinin	Carl Roth
Amersham Hybond-N+ nylon membrane	GE Healthcare
Amersham Hyperfilm MP	GE Healthcare
BA85 Nitrocellulose membrane	Schleicher & Schuell

Name	Company
Bacto-Tryptone	Becton, Dickinson Company
Bacto-Yeast-Extract	Becton, Dickinson Company
(+)-Biotin, cryst. research grade	Serva
Bromophenol Blue	Sigma-Aldrich
CHAPS	Merck
CNP-22	Biomol
Copper(II) chloride dihydrate	Sigma-Aldrich
DAPI	Dianova
DirectPCR Lysis Reagent	Peqlab
dNTPs	Invitrogen and Takara Co.
DMEM, high glucose (31966-047)	Gibco/Invitrogen
EDTA	Merck
Ethanol	Merck
Ethidium bromide	AppliChem
Fetal Bovine Serum (FBS)	Gibco
F11 cell line	CLS cell lines service
F-12 Nutrient Mixture	Gibco
Gelatin solution (2%)	Sigma-Aldrich
Glycerol	Merck
HAT Supplement (50x)	Gibco
HEK293 cell line	CLS cell lines service
Hydrochloride acid 32% solution	Merck
illustra MicroSpin G50 Columns	GE Healthcare
Isofluran	Baxter
Isopropanol	Merck
Leupeptin hemisulfate salt	Sigma-Aldrich
LIF (Leukemia Inhibitory Factor)	Invitrogen
Magnesium chloride	Merck
Manganese chloride	Merck
Methanol	Merck
Mitomycin C	Sigma-Aldrich
Molecular mass standards for SDS-PAGE	Bio-Rad
Monosodium phosphate	Merck
Non-essential amino acids solution	Invitrogen
Opti-MEM	Invitrogen
PBS (L182-50)	Biochrom
Penicillin-Streptomycin (10000 U/ml)	Invitrogen
Pepstatin A	Sigma-Aldrich
PFA (Paraformaldehyde)	Merck
Phenol-Chloroform-Isoamyl (25:24:1)	Sigma-Aldrich
Pierce High Sensitivity Streptavidin HRP Conjugate	Thermo Scientific
Poly-D-Lysine	Sigma-Aldrich
Ponceau S	Sigma-Aldrich
Potassium acetate	Sigma-Aldrich
Potassium carbonate	Sigma-Aldrich

Name	Company
Potassium permanganate	Sigma-Aldrich
Proteinase K	Roche
SDS solution	Bio-Rad
Silver nitrate	Sigma-Aldrich
Sodium acetate	Merck
Sodium chloride	Merck
Sodium citrate	Merck
Streptavidin Agarose Resin	Thermo Scientific
TCA (2,4,6-Trichloroanisole)	Sigma-Aldrich
TEMED (Tetramethylethylenediamine)	GE Healthcare
Tris	Merck
Triton X-100	Merck
Trypsin	Invitrogen
Tween-20	Sigma-Aldrich
Ultrafree-MC Durapore PVDF (0.45 µm)	Amicon
β-mercaptoethanol	Sigma-Aldrich
^{32}P-dCTP (312H)	Perkin-Elmer

3.10 Laboratory equipment

Name	Company
Axiovert135	Zeiss
BD FACSAria II Cell Sorter	BD Biosciences
BioPhotometer	Eppendorf
BioMax MP1015	Kodak
Chemi Doc	Bio-Rad
Centrifuge 5804	Eppendorf
Contamat FH111M contamination monitor	Thermo Scientific
Gene Pulser Xcell System	Bio-Rad
Hybridization oven	Peqlab
LSM710 confocal microscope	Zeiss
Mastercycler Gradient	Eppendorf
Maxigel M system PerfectBlue	Peqlab
Microplate Reader 3550	Bio-Rad
MicroPulser Electroporator	Bio-Rad
Mini Trans-Blot Cell	Bio-Rad
PeqSTAR 96 universal gradient	Peqlab
Powerpac 300	Bio-Rad
Sonorex TK 52 H	Bandelin
Sorvall M150 centrifuge	Thermo Scientific
Sorvall RC6+ centrifuge	Thermo Scientific
Spring Scissors 15006-09	F.S.T.
Stemi DRC stereomicroscope	Zeiss
Stemi SV11 stereomicroscope	Zeiss
TC10 Automated Cell Counter	Bio-Rad
UV crosslinker	Fisher Scientific

4. METHODS

4.1 Molecular biology

Molecular biological and microbiological methods were performed in accordance with standard protocols from *Molecular Cloning: A Laboratory Manual* (Sambrook and W Russell, 2001) and *Current Protocols in Molecular Biology* (Wiley Online Library). Applied laboratory kits were used pursuant to the instruction manual provided by the manufacturer. Further supplementary techniques and slight modifications from standard protocols are listed in the following sections.

4.1.1 Bacterial culture

Several bacterial strains were used for the amplification of plasmid DNA, the initiation of homologous DNA recombination or the flippase-mediated and Cre-recombinase mediated DNA excision. Individual growth conditions, intended use and applied antibiotics are listed in Table 1-3.

Bacterial strain	Usage	Growth condition
DH5α	Chemical transformation (heat shock at 42°C for 2 min)	
	Amplification of pBluescript II KS+ plasmids, bicistronic Npr2 constructs and BioID constructs	LB medium at 37°C (100µg/ml ampicillin for antibiotic selection)
DH10B	Electroporation (0.1 cm cuvette, 1.8 kV voltage, one pulse)	
	Clean amplification of subclone, mini-targeting vector, and targeting vector DNA after successful homologous recombination steps	LB medium at 37°C (100µg/ml ampicillin for antibiotic selection)
	Amplification of BAC DNA	LB medium at 37°C (20µg/ml chloramphenicol)
	Combination of induced mini-λ DNA with BAC DNA	LB medium at 32°C (12.5µg/ml chloramphenicol, 12.5µg/ml tetracycline)
	Recombination of mini-λ-BAC DNA into pDTA plasmid flanked with homology arms	LB medium at 32°C (100µg/ml ampicillin)
DY380	Electroporation	
	Amplification of mini-λ DNA	LB medium at 32°C (12.5µg/ml tetracycline)
	Amplification of pDTA plasmid carrying Npr2 locus DNA	LB medium at 32°C (100µg/ml ampicillin)
	Recombination of loxP1-mini-targeting and loxP2-mini-targeting into pDTA-Subclones	LB medium at 32°C (30µg/ml kanamycin)

Table 1

Bacterial strain	Usage	Growth condition
EL250	Electroporation	LB medium at 32°C (100µg/ml ampicillin)
	Confirmation of functional Flp target sites	
EL350	Electroporation	LB medium at 32°C (100µg/ml ampicillin)
	Confirmation of functional Cre target sites	
XL10-Gold	Chemical transformation	LB medium at 37°C (100µg/ml ampicillin)
	Plasmid amplification after site-directed mutagenesis	

Table 2

Antibiotics	Usage	Bacterial strains
Ampicillin	100µg/ml final concentration	DH5α, DH10B, DY380, EL250, EL350
Chloramphenicol	20µg/ml final concentration	DH10B
Kanamycin	30µg/ml final concentration	DH5α, DY380
Tetracycline hydrochloride	12.5µg/ml final concentration	DY380
Tetracycline/ chloramphenicol	12.5µg/ml final concentration (each)	DH10B

Table 3

4.1.2 Heat-shock transformation of *E.coli*

Chemically competent DH5α bacteria were prepared by inoculation of 100 ml LB medium with 1 ml of an overnight bacterial culture followed by incubation at 37°C with shaking until the OD_{600} reached about 0.5. The culture was cooled on ice for 10 min and then centrifuged at 1500 g and 4°C for 10 min. The pellet was resuspended in 30 ml pre-chilled TFB1 buffer and placed on ice for 10 min followed by another centrifugation step at 1500 g and 4°C for 10 min. The pellet was resuspended in 4 ml pre-chilled TFB2 buffer and cooled on ice for 10 min. The competent bacteria were subdivided into 100 µl aliquots on ice and stored at -80°C, immediately. The transformation of chemo-competent bacteria was executed using the following procedure.

1. *Chemically competent DH5α bacteria were thawed on ice for 20 min.*
2. *10 µl ligation product or plasmid DNA (≤100 ng) was added.*
3. *Incubated on ice for 20 min.*
4. *Heat shock at 42°C for 2 min.*
5. *Incubated on ice for 1.5 min.*
6. *390 µl pre-warmed LB medium was added.*
7. *DH5α bacteria were incubated for 60 min at 37°C with shaking.*
8. *DH5α bacteria were centrifuged at 5500 g for 1 min; the supernatant was removed.*

9. *The pellet was resuspended in 150 µl LB medium and plated on LB agar plate with antibiotic.*

4.1.3 Bacterial transformation of *E.coli* by electroporation

Electro-competent bacteria were prepared by pre-cultivating a single colony in 2 ml LB medium with appropriate antibiotic and shaking overnight at 32°C. 50 ml LB medium with appropriate antibiotic were inoculated by 100 µl of the overnight culture and incubated with shaking at 32°C until OD_{600} reached about 0.5. After cooling on ice with occasional shaking for 10 min, bacterial culture was centrifuged for 10 min at 1500 g and 4°C and the pellet was resuspended in 50 ml of 10% (v/v) ice-cold glycerol. This step was repeated once. After a final centrifugation step, the pellet was resuspended in 200 µl of 10% (v/v) ice-cold glycerol, divided into 50 µl aliquots and stored at -80°C. The electroporation was executed using the following procedure.

1. *Electroporation cuvette (0.1 cm gap width), 1.5 ml tube, electro-competent bacteria and DNA (~100 ng) were chilled on ice.*
2. *50 µl electro-competent bacteria and DNA was mixed in the 1.5 ml tube and transferred into the cuvette.*
3. *Cuvette was placed into MicroPulser Electroporator and electroporated with one pulse at 1800 Volt.*
4. *1 ml SOC medium was added to the cuvette and then transferred into a new 1.5 ml tube.*
5. *Incubation for 1 h at 32°C (non-recombinogenic bacteria at 37°C) with shaking.*
6. *100-300 µl were plated onto a LB agarose plate containing appropriate antibiotic.*

4.1.4 Isolation of plasmid DNA

The Plasmid Mini Kit, Plasmid Midi Kit and Plasmid Maxi Kit from Qiagen were used to isolate plasmid DNA from bacterial cultures according to the manufacturer´s protocols.

4.1.5 DNA restriction digest

Restriction digests were generally carried out using the operating instructions of the enzyme producing companies. Samples for molecular cloning and DNA ligation were incubated at 37°C for 6 hours or overnight. Samples for restriction analysis to prove successful molecular cloning were incubated at 37°C for 3 hours. The applied standard preparation is displayed in the following table.

Standard restriction enzyme digestion

Plasmid DNA or PCR product (0.5-5 µg)	x µl
Sterile ddH_2O	x µl
10x Enzyme Buffer	2 µl
Endonuclease (10-20 U/µl)	0.5-1 µl
Total volume	20 µl

4.1.6 DNA ligation

Linearized and purified vector DNA was treated with calf-intestinal alkaline phosphatase (CIP) to prevent recircularization and to improve the yield of vector containing the appropriate insert. After incubation of 1 hour at 37°C, the vector DNA fragment was again purified using Invisorb DNA Fragment CleanUP from Invitek. Insert DNA was treated with T4 Polynucleotide Kinase to label the free hydroxyl end of the 5´ DNA and improve the ligation reaction. After incubation of 1 hour at 37°C, the enzymatic activity was heat-inactivated for 20 min at 85°C. Quantitative agarose gel electrophoresis was carried out to quantify the vector and insert DNA in reference to Lambda DNA/*Hin*dIII Marker. The precise molar ratio of 3:1 between insert and vector was calculated and used subsequently for the ligation preparation.

$$x\ \mu l\ insert\ per\ 1\ \mu l\ vector = \frac{3\ x\ vector\ quantity\ (ng)\ x\ insert\ length(bp)}{vector\ length\ (bp)\ x\ insert\ conc.\ (ng/\mu l)}$$

Standard ligation preparation

Linearized plasmid vector (100 ng)	x µl
Insert (3:1 molar ratio)	x µl
Nuclease-free H_2O	x µl
10x T4 DNA ligation buffer	1 µl
T4 DNA ligase (1 U/µl)	1 µl
Total volume	10 µl

The ligation reaction was incubated either overnight at 16°C or at room temperature for 2 hours. The complete 10 µl ligation preparation was mixed with 100 µl competent DH5α bacteria, chemical transformed, and plated on LB-agar plates which contained antibiotics for positive selection. Vector plasmids of single bacteria colonies were

purified by DNA mini-preparation, analyzed by restriction digest and DNA sequence analysis.

4.1.7 Agarose gel electrophoresis

Agarose gels with variant pore sizes (0.8-3.5% (w/v) agarose) were used depending on the length of DNA fragments of interest. DNA samples were mixed with 10x DNA loading buffer and separated by gel electrophoresis in 1x TAE buffer at 110 Volt for a minimum of 60 min. 7 µl of 1kb DNA ladder was loaded as reference for the DNA size. After the run, the gel was visualized under UV light by the Gel Documentation system and pictured using the ChemiDoc software from Bio-Rad.

4.1.8 Oligonucleotides preparation and DNA sequence analysis

Oligonucleotides used for molecular cloning or mouse genotyping were produced by the Eurofins Genomics Company (Ebersberg, Germany). All DNA sequence analyses were performed by the same company. Samples to be sequenced were prepared in accordance with the operating instructions of the company.

4.1.9 PCR amplification for Npr2 targeting vector and DNA probe cloning

Polymerase-chain-reaction (PCR) was used for the amplification of distinct DNA fragments which were required for the downstream ligation reactions of Npr2 targeting vector cloning and the generation of DNA probes. The *Pfu* DNA Polymerase, which exhibits 3´→5´ exonuclease (proofreading) activity, was used for each reaction to guarantee an accurate amplification. As a first step, the amplified DNA fragments were cloned into a pBluescript II KS (+) vector by blunt end ligation, sequenced, and subsequently excised by restriction digest for further ligation reactions. The single steps of Npr2 targeting vector cloning are explicitly illustrated in the result section. The following schemes represent the standard pipetting preparation and PCR cycling program which were used. Table 4 and Table 5 catalogue the primer pairs giving information about their assignments, the amplified band size, and their localization within the genomic DNA of the Npr2 locus. Letters in red indicate the sites for the restriction endonucleases that were introduced.

Pipetting scheme

Components	50 µl reaction	Final conc.
nuclease-free H_2O	38 µl	N/A
10x PCR Buffer with $MgSO_4$	5 µl	1x
dNTP Mix (2.5 mM each)	2 µl	400 µM
Primer for (50 µM)	1 µl	1 µM
Primer rev (50 µM)	1 µl	1 µM
Pfu Polymerase (2.5 U/µl)	1 µl	2.5 Unit
Template DNA	2 µl	≤ 250 ng

PCR cycling protocol

Step	Temperature	Duration	Cycles
Initial denaturation	95°C	3 min	1
Denature	95°C	30 sec	35
Anneal	57-61°C	30 sec	
Extent	72°C	2 min/kb	
Final extension	72°C	10 min	1

Primers for targeting vector 1 (TV1) cloning and Southern blot DNA probes

Primer	Sequence	gDNA *Npr2* locus
5´ Southern blot probe		
Npr2flx_5'S_UP	5´-CTTGCACTAAATCTGTTTCC-3´	23411->23430
Npr2flx_5'S_RP	5´-AAGGGATAGGCGGAGATAC-3´	24342->24360
PCR product length 950 bp		
3´ Southern blot probe		
Npr2flx_3'S_UP	5´-TCGAGGAATGGGCTTCCTAG-3´	32812->32831
Npr2flx_3'S_RP	5´-AGGAAAGCTGCACAATAAG-3´	33743->33761
PCR product length 950 bp		
A-arm for subclone subcloning into pDTA		
SC_A_UP	5´-GGGGTCGACGTGCCTTGTAGTTCGATGC-3´	24361->24379
SC_A_RP	5´-CCCAAGCTTGGACTTGAGGCTTCCATGAG-3´	24541->24660
PCR product length 318 bp		
B-arm for subclone subcloning into pDTA		
SC_B_UP	5´-GGGAAGCTTACGGGGGAGGTCAAAACAAG-3´	32512->32531
SC_B_RP	5´-CCCACTAGTATTAGCCAGGCTGAAGAGG-3´	32793->32811
PCR product length 318 bp		
Subcloning loxP1 5´-arm into pBlu[loxP-FRT-Neo-FRT-loxP]		
loxP1_5A_UP_E1	5´-GGGCTCGAGGGAAGGTGGTACCAGCATATTG-3´	25537->25558

loxP1_5A_RP_H3	5´-CCCAAGCTTGAAAAGGAAAGCAGCTGAGAC-3´	26016->26036
PCR product length 518 bp		
Subcloning loxP1 3´-arm into pBlu[loxP-FRT-Neo-FRT-loxP]		
loxP1_3A_UP_N1	5´-GGGGCGGCCGCTTCCACCAAAGCCAACTTCC-3´	26037->26056
loxP1_3A_RP_S1	5´-CCCGAGCTCTGTGAAGCCCACGATGTCAC-3´	26217->26236
PCR product length 220 bp		
Subcloning loxP2 5´-arm into pBlu[loxP-FRT-Neo-FRT-loxP]		
loxP2_5A_UP_E1	5´-GGGGAATTCGGAGAGACGGTTCAGGCGG-3´	26168->26186
loxP2_5A_RP_P1	5´-CCCCTGCAGATATCAGGAAGCCTGGGAGCC-3´	26646->26664
PCR product length 517 bp		
Subcloning loxP2 3´-arm into pBlu[loxP-FRT-Neo-FRT-loxP]		
loxP2_3A_UP_N1	5´-GGGGCGGCCGCCACGAGCTTTAGTCCCTTC-3´	26665->26683
loxP2_3A_RP_N1	5´-CCCGCGGCCGCATTTACGCCCAAGGGCAAG-3´	26845->26864
PCR product length 221 bp		

Table 4

Primers for targeting vector 2 (TV2) cloning and Southern blot DNA probe

Primer	Sequence	gDNA *Npr2* locus
5´ Southern blot probe(2)		
Npr2flx_5'S2_UP	5´-GTGGGTTTCTTGGACTGGC-3´	19801->19819
Npr2flx_5'S2_RP	5´-TCCCCTCTTCCAGGCTAGAG-3´	20781->20800
PCR product length 1000 bp		
A2-arm for subclone subcloning into pDTA		
SC_A2_UP	5´-GTCGACGGTGGCAGTTGCAGCTTC-3´	21038->21056
SC_A2_RP	5´-CTTAAGTGCAAGGGTCTATCATTAC-3´	21319->21337
PCR product length 311 bp		
B2-arm for subclone subcloning into pDTA		
SC_B2_UP	5´-GTCGACGGGGGAGGTCAAAACAAG-3´	32512->32531
SC_B2_RP	5´-ACTAGTATTAGCCAGGCTGAAGAGG-3´	32793->32811
PCR product length 310 bp		

Table 5

4.1.10 Homologous recombination in *E.coli*

Cloning of the gene targeting vector was based on homologous recombination in *E. coli* using the mobile recombination system mini-λ (Court et al., 2003). For this recombineering method, non-replicating circular phage DNA is integrated into the bacterial chromosome and replicated during cell division. Beyond that, the defective mini-λ-Tet prophage can be excised and transferred into other bacterial host cells. The mini-λ recombination system is based on expression of the phage genes *exo*, *bet*, and *gam*, under control of a temperature-sensitive CI-repressor (Yu et al., 2000). Finally, the

temperature-sensitive derepression of the mini-λ recombination system mediates the insertion of DNA fragments flanked by homology arms into defined target DNA.

In this study the mobile recombination system mini-λ was used for the integration of Npr2 locus DNA into the pDTA vector. For this purpose, the mini-λ-Tet construct was obtained from the bacterial strain DY380 and transferred into DH10B bacteria. DY380 bacteria were grown at 32°C in the presence of 12.5 µg/ml tetracycline and the mini-λ DNA circles were excised by incubation at 42°C for 20 min. 500 ng of purified mini-λ plasmid were electroporated into DH10B bacteria carrying BAC clone DNA and positively selected by treatment with 12.5 µg/ml tetracycline and 12.5 µg/ml chloramphenicol. The mini-λ mediated homologous recombination was then induced by heating to 42°C for 15 min. Other homologous recombinations which were required for the gene targeting vector cloning were directly initiated in the bacterial strain DY380. The operating principle of the mini-λ mediated homologous recombination remained the same. DY380 bacteria carrying target DNA were always grown at 32°C in the presence of appropriate antibiotics. Before the electroporation with linearized DNA fragments flanked by homology arms, the mini-λ recombination function was unrepressed by temperature control. For this, DY380 bacteria were incubation at 42°C for 15 min, immediately chilled on ice for 10 min, made electro-competent, and stored at -80°C until used.

4.1.11 Confirmation of functional Flp and Cre target sites

Both *E.coli* strains, EL250 and EL350, were in general grown at 32°C without antibiotic selection. Expression of the flippase or Cre-recombinase gene was induced by activation of the arabinose-inducible promoter pBAD. For this, 2.5 ml of overnight bacterial culture were transferred into 50 ml LB medium and grown with orbital shaking to an OD_{600} of around 0.4. Solute arabinose (10 % (w/v)) was added to a final concentration of 0.1 % and incubated for 1 hour at 32°C. Bacteria were made electro-competent and were electroporated with 250 ng of the gene targeting vector. After positive selection on agar plates (32°C, 100 µg/ml ampicillin), isolated plasmid DNA was analyzed by restriction digest and sequence analysis.

4.1.12 DNA sequence analysis of gene targeting vector

Table 6 outlines the oligonucleotides which were used for the DNA sequence analysis of the complete Npr2 targeting vector. The respective binding site and elongation direction is stated. Targeting vector 2 (TV2) was screened by two additional oligonucleotides due to its sequence extension.

Primers for DNA sequence analysis of the Npr2 targeting vector

Primer	Sequence	Targeting vector
TV1 (11.6kb)		
T7	5´-TAATACGACTCACTATAGGG-3´	626…645 →
SC_A_UP	5´-GGGGTCGACGTGCCTTGTAGTTCGATGC-3´	1789…1807 →
SC_A_RP	5´-CCCAAGCTTGGACTTGAGGCTTCCATGAG-3´	2069…2088 ←
loxP1_5A_UP_E1	5´-GGGCTCGAGGGAAGGTGGTACCAGCATATTG-3´	2965…2986 →
loxP1_3A_UP_N1	5´-GGGGCGGCCGCTTCCACCAAAGCCAACTTCC-3´	3568…3587 →
loxP2_3A_UP_N1	5´-GGGGCGGCCGCCACGAGCTTTAGTCCCTTC-3´	6193…6211 →
loxP2_3A_RP_N1	5´-CCCGCGGCCGCATTTACGCCCAAGGGCAAG-3´	6373…6392 ←
T3	5´-ATTAACCCTCACTAAAGGGA-3´	12417…12436 ←
TV2 (15kb)		
SC_A2_UP	5´-GTCGACGGTGGCAGTTGCAGCTTC-3´	1783…1801 →
SC_A2_RP	5´-CTTAAGTGCAAGGGTCTATCATTAC-3´	2064…2084 ←

Table 6

4.2 Mouse embryonic stem cell culture and establishing the floxed Npr2 mouse model

The targeting vector carrying the recombinant DNA was introduced into the genome of embryonic stem cells by homologous recombination. Handling of the ES cell culture in order to generate the transgenic Npr2 mouse line was based on *Laboratory protocols for conditional gene targeting* (Torres and Kühn, 1997) and *Manipulating the Mouse Embryo: a Laboratory Manual* (Nagy et al., 2003). The experimental procedures are schematically illustrated in Figure 8 and described in the following chapters.

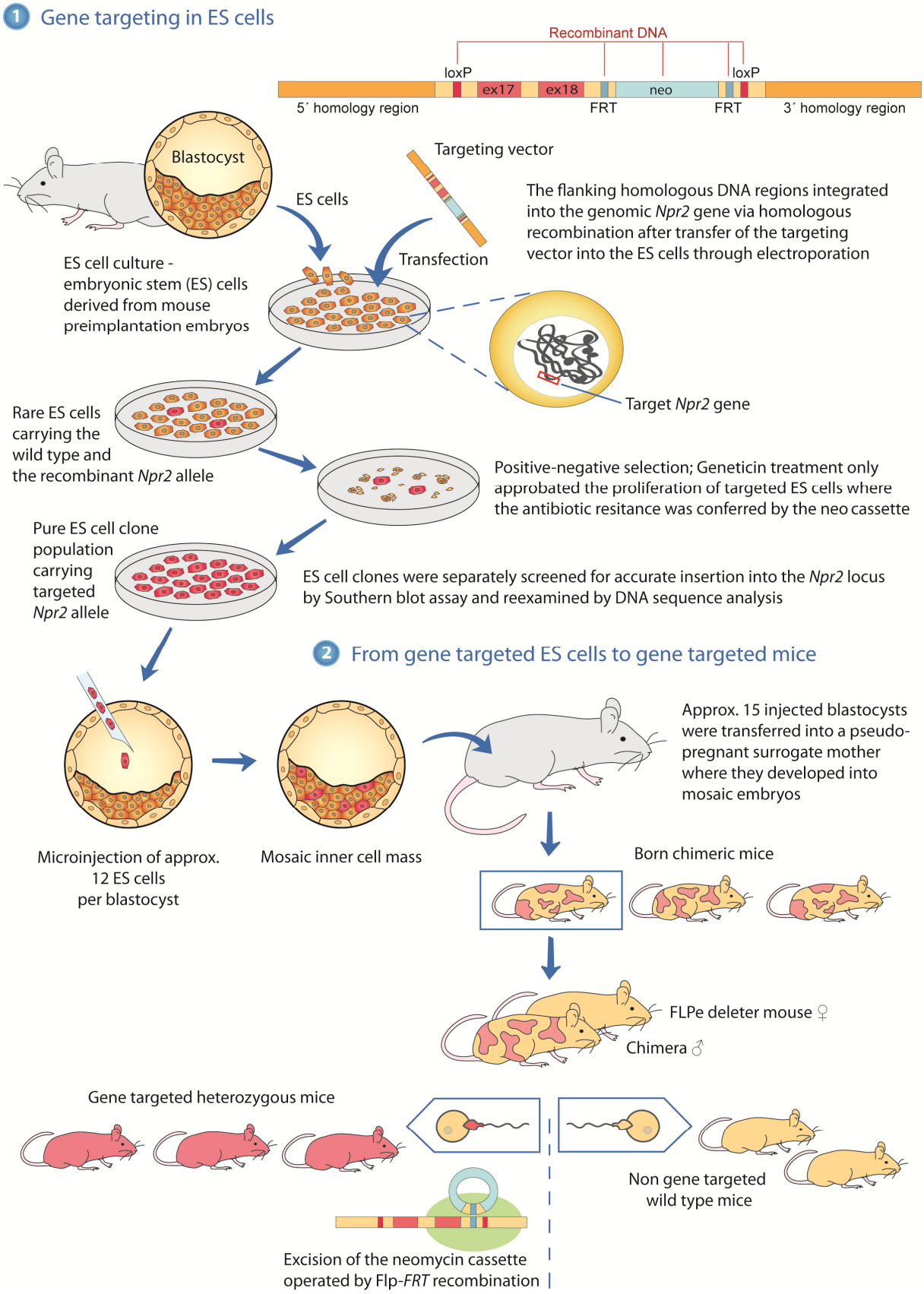

Figure 8: Outline of experimental workflow for generation of the transgenic Npr2 mouse strain.

4.2.1 Culturing of feeder cells

Mouse embryonic fibroblast (MEF) cells were used as feeder cells to support and maintain pluripotent stem cells in an undifferentiated state. The MEF cells were isolated from 13 to 15 days postcoitum mouse embryos deriving from mouse strains containing a *Neo* expression cassette. The embryos were dissociated and trypsinized to produce single-cell suspension. Fibroblast cells obtained from one embryo (passage P0) were seeded onto a 15 cm cell culture dish. The cells were grown changing the feeder medium every second day and split at a ratio of 1:4 up to passage P4, while cells in passage P1 to P3 were frozen in between. To split the feeder cells, they were washed twice with 1xPBS, trypsinized in 3ml trypsin-EDTA and incubated for 4 min at 37°C. After adding feeder medium, centrifugation at 150 g for 4 min and removal of the supernatant, the pellet was resuspended in feeder medium and seeded onto four 15 cm cell culture dishes. To freeze the feeder cells, they were resuspended after trypsinization in 5 ml freezing medium containing glycerol and DMSO and frozen at -80°C in 1 ml aliquots. MEF cells were treated with mitomycin C to inactivate the mitosis of the feeder cells. By the time the MEF cells stopped to overgrow 15 cm cell culture dishes within 2 days, confluent cells were incubated with mitomycin C at a final concentration of 10 µg/ml for 2 hours at 37°C and frozen at -80°C for later use as feeders for ES cell culture. Thawed MEF cells were seeded with a density of 50000 cells/cm^2. The feeder layer was suitable for about one week.

4.2.2 Culturing of ES cells

The ES cell lines were cultured on feeder cell layers in ES cell medium containing Leukemia Inhibitory Factor (LIF) to prevent the differentiation of the cells. All culture incubations were performed in a humidified 37℃, 5% CO_2 incubator. ES cell medium was daily changed at the minimum. ES cells were usually split in a 2-day cycle at a ratio of 1:2 or 1:3. ES cells formed a non-confluent cell culture with well-rounded and sharp-bordered ES cell clones. Freezing, thawing and splitting procedure was executed in accordance with the feeder cell handling except for using always ES cell medium instead of feeder medium.

4.2.3 Electroporation of ES cells

Before electroporation, the targeting vector DNA was linearized by overnight digestion with restriction enzyme *Pac*I and purified afterwards by either phenol-chloroform-isoamyl extraction followed by sodium acetate-ethanol precipitation (Sambrook and W Russell, 2001) or agarose gel extraction (Invisorb Fragment CleanUP). Advantage of the latter was the removal of the pDTA vector backbone during agarose gel electrophoresis. DNA was dissolved in salt-free, nuclease-free water and the concentration was adjusted to 1 µg/µl using a spectrophotometer. Nicely rounded ES cells of one 10 cm feeder dish were prepared per electroporation. The cells were once washed with 1x PBS, trypsinized with 1.2 ml trypsin-EDTA for 4 min at 37°C, centrifuged at 150 g for 4 min and resuspended thoroughly in 10ml ES cell medium. 10µl of the resuspension was applied to a Neubauer cell counting chamber to determine the cell count per milliliter. After another centrifugation step, the cell pellet was resuspended in 1x PBS to a final concentration of 10^7 ES cells/800 µl. 25-45 µg of DNA and 780 µl o the prepared ES cell suspension were gently mixed per electroporation. The mixture was transferred to an electroporation cuvette with 0.2 cm gap width and then electroporated with one pulse at 280 V and 500 µF. After an immediate cooling step on ice for 10 min, the electroporated cells were transferred into 20 ml ES cell medium, centrifuged and resuspended in 6 ml ES cell medium. Finally, the ES cells were equally divided and seeded onto three 10 cm feeder dishes filled with 8 ml fresh ES cell medium.

4.2.4 Selection of geneticin resistant clones

ES cells were grown for the first 2 days after electroporation in ES cell medium without geneticin (G418). ES cells (E14.1, R1, and $SV129_{(TCF)}$ ES cell line) were selected in the presence of 400 µg/ml geneticin from the third day onwards. ES cell line AB2.1 was treated with 250 µg/ml geneticin only. While most of the emerging ES cell clones died of antibiotic treatment, G418-resistant ES cell clones remained healthy showing round and sharp borders. At day eight after electroporation, the ES cells were gently washed with pre-warmed 1x PBS followed by refilling the 10 cm dishes with 5 ml 1x PBS. Single ES clones were picked under the microscope using a pipette adjusted to 25 µl and were subsequently transferred into single wells of a 96-well plate. 30 µl trypsin-EDTA was

added and incubated for 4 min at 37°C. 100 µl ES cell medium supplemented with geneticin was added to stop the trypsinization. ES cell clones were singularized by pipetting twenty times up and down using an 8-multichannel pipette and were transferred to a new 96-well feeder plate with 100 µl ES cell medium. After 2-3 days with daily medium change (250 µl per well), the separated ES cell clones were again split and transferred to a new 96-well feeder plate. After further 2-3 days, the fully multiplied ES cell clones were finally split into one 96-well feeder plate and two 96-well gelatin plates which were prepared by an one-hour incubation with 0.1% (v/v) gelatin solution. ES cell clones from the 96-well feeder plate were frozen after 2 days of growing. The cells were trypsinized, singularized in 100 µl ES freezing medium, wrapped in papers, placed in a Styrofoam box and stored at -80°C for 2-3 months. Meanwhile, the cells from the two 96-well gelatin plates were overgrown for about 5 days to extract the DNA which was required for Southern blot analysis.

4.2.5 Extraction of genomic ES cell DNA

The genomic DNA from ES cell clones grown in 96-well gelatin plates was extracted using the following procedure. Volumes are represented for one well.

1. *Cells were washed twice with 100 µl 1x PBS.*
2. *50 µl ES lysis buffer containing proteinase K (final conc. 200 µg/ml) was added.*
3. *Top of the plate was sealed with parafilm.*
4. *Overnight incubation at 55°C in humidity chamber.*
5. *140 µl of pre-chilled 3M sodium acetate was added.*
6. *Overnight incubation at 4°C.*
7. *96-well plates were centrifuged at 750 g for 20 min.*
8. *Supernatant was discarded by gentle overturning of the plate.*
9. *DNA precipitate was washed three times by adding 150 µl ice-cold 70% ethanol, dried and stored at RT in a dark place.*

In the later stages of ES cell culturing, DNA was extracted from expanded ES cell clones grown on 6-well plates. For this, the cells of one well were trypsinized in 1.2 ml trypsin-EDTA, centrifuged in 1x PBS and resuspended in 300 µl ES lysis buffer supplemented with proteinase K (final conc. 200 µg/ml). After gentle shaking overnight at 55°C, the

DNA was purified by phenol-chloroform-isoamyl extraction and sodium acetate-ethanol precipitation (Sambrook and W Russell, 2001).

4.2.6 Southern blot analysis of homologous recombination

To screen for the correct locus-specific recombination of the targeting vector into the genomic DNA, the ES cell DNA was digested generating two distinct DNA fragments which are recognized by radioactively labeled DNA probes. DNA from 96-well plates was digested in 45 µl of a 5 ml reaction mastermix containing 0.5 ml 10x restriction enzyme buffer, 25 µl RNase A (10 mg/ml), 0.15 ml restriction enzyme (3000 U), and 4.325 ml salt-free, nuclease-free water. Genomic DNA (20 µg) from a 6-well or liver extraction was digested in 60 µl reaction mixture containing 6 µl 10x restriction enzyme buffer, 0.3 µl RNase A (10 mg/ml), and 3 µl restriction enzyme (60 U) which was filled up to 60 µl with salt-free, nuclease-free water. Both DNA digestions were carried out overnight at 37°C with gentle shaking. The digested DNA was mixed with DNA loading buffer and either 30 µl of 96-well sample DNA or 60 µl of 6-well or liver sample DNA was loaded onto a 500 ml 1% agarose gel without ethidium bromide. 15 µl of 1kb DNA ladder were loaded as size control and the electrophoresis was carried out overnight at 25 V in the horizontal Maxigel M system (Peqlab) filled with 2 liter 1x TAE buffer. The next day, the agarose gel was prepared for the DNA capillary transfer onto the nylon Hybond N+ membrane.

Blotting

1. *The gel was transferred to a melamin basin filled with 300 ml ddH_2O.*
2. *15 µl of ethidium bromide were added and incubated with gentle shaking for 30 min.*
3. *The gel was photographed using the Gel Doc system.*
4. *Two washing steps were performed with ddH_2O; each for 15 min.*
5. *DNA depurination in 250 ml 250 mM HCl for 8 min.*
6. *The Gel was shortly washed twice with ddH_2O.*
7. *DNA denaturation in 250 ml 0.5 M NaOH and 1 M NaCl; 2x 15 min.*
8. *During step seven, the nylon Hybond N+ membrane (25x20 cm) and three Whatman paper (26x21 cm) were cut into shape and equilibrated first with ddH_2O and then with 10x SSC buffer.*

9. *The gel was equilibrated with 20x SSC buffer for 5min and placed upside down on a new gel tray.*
10. *Capillary transfer assembly (from bottom to top): gel tray > gel > membrane > 3 Whatman paper > one pack of paper towels divided into two level stacks > glass plate*
11. *The blotting construction was placed upside down on the table and ballasted with a weight (about 500 gram).*
12. *The DNA transfer was carried out overnight at room temperature.*
13. *The membrane was washed twice for 5 min in 2x SSC buffer and dried on Whatman paper.*
14. *Genomic DNA was cross-linked using UV-light irradiation; UV crosslinker intensity was set to 1250.*
15. *The membrane was stored at room temperature in the dark (e.g. drawer).*

DNA detection by ^{32}P-radiolabeled probes

To prepare the DNA probes for radiolabeling, 5 µg of pBluescript II SK+ plasmid DNA carrying the respective target sequence were digested with *Hin*dIII and *Eco*RI. DNA fragments were separated by agarose gel electrophoresis, purified by gel extraction and the concentration was determined using the spectrophotometer. The 3´ probe and 5´ probe had both a final fragment size of 962 bp whereas the second 5´ probe(2) measured 1012 bp. The Prime-It Random Primer Labeling Kit from Stratagene and radiolabeled ^{32}P-dCTPs, which were freshly purchased on the day of use, were used for the ^{32}P-radiolabeling of the DNA fragments.

1. *Dehydrated reaction mixture supplied with the kit was dissolved in 40 µl ddH_2O.*
2. *DNA was added to a final volume of 42 µl and a final concentration of 50 ng/µl; transferred to 1.5 ml screw-cap tube.*
3. *10 µl of sheared genomic mouse DNA (1 µg/µl) was prepared in another 1.5 ml screw-cap tube.*

Next steps were performed in the isotope laboratory.

4. *DNA in the 42 µl reaction mixture was denatured for 10 min at 95°C.*
5. *5 µl ^{32}P-dCTP and subsequently 3 µl Magenta polymerase were added to the hot DNA reaction mixture.*
6. *Incubation for 10 min at 37°C in a heating block.*
7. *2 µl Stop mix was added immediately.*
8. *G-50 spin column was centrifuged at 200 g for 2 min to remove the solution in the column.*

9. *Complete reaction mixture (52 µl) was applied onto the dried G-50 spin column; placed into the screw-cap tube with genomic DNA and centrifuged at 200 g for 2 min.*
10. *1 ml Church buffer pre-warmed at 65°C was added to the 62 µl DNA reaction mixture and was denatured at 95°C for 10 min.*
11. *Incubation at 65°C for 60-120 min in the hybridization oven.*
12. *Hybridization glass bottle (35x300 mm) was filled with 7 ml Church buffer pre-warmed at 65°C.*
13. *Nylon membrane with cross-linked DNA was shortly soaked in water and transferred to the wall of the hybridization glass bottle using a 20 ml serological pipette and avoiding air bubbles; DNA side of the membrane was showing inwards.*
14. *Pre-hybridization of the membrane for 1 hour at 65°C rotating in the hybridization oven.*
15. *Complete DNA probe solution from step 11 was added to the membrane and incubated overnight at 65°C rotating in the hybridization oven.*
16. *Hybridization solution was decanted; the membrane was washed with 10 ml Southern washing buffer I for 10 min and afterwards with 10 ml Southern washing buffer II for 20 min; both washing steps were performed in the hybridization glass bottle rotating in the hybridization oven at 68°C.*
17. *Membrane was transferred to a lockable plastic box and consecutively washed with 200 ml Southern washing buffer II, III, IV, and V; each washing step was performed in a shaking water bath at 68°C for 10 min; radioactivity of the membrane was lowered to room background radioactivity (1 Bq/cm^2) measured by contamination monitor.*
18. *Membrane was placed upside-down on cling film, covered with a layer of Whatman paper and overhead transparency; everything was wrapped up using the cling film.*
19. *Wrapped membrane was put onto one sheet of Amersham Hyperfilm MP in a film cassette in the dark room; DNA side facing towards the Hyperfilm.*
20. *Incubation for 7-10 days at -80°C; afterwards cassette was thawed at room temperature; film was developed in the developing machine in the dark room.*

4.2.7 Long-range PCR analysis of homologous recombination

Long-range PCR analysis of the homologous recombination was performed as an alternative for Southern blot analysis. *TaKaRa LA Taq* polymerase from Takara Shuzo Corporation was used for the PCR amplification to prove the locus-specific integration of the floxed Npr2 targeting construct. Genomic DNA to be examined was obtained from either ES cell clones, tail cuts or liver tissue. Reaction mixture, PCR program and applied oligonucleotides are subsequently listed. The heterozygous presence of recombinant

DNA was also reviewed by triplex PCR analysis but without giving information about the Npr2 locus integration. For that, the PCR protocol was executed with reduced dNTP concentration (200 µM) and lowered elongation time (2 min).

Pipetting scheme

Components	50 µl reaction	Final conc.
sterile ddH_2O	28.5 µl	N/A
10x LA Buffer II (Mg^{2+} free)	5 µl	1x
$MgCl_2$ (25 mM)	5 µl	2.5 mM
dNTP Mix (2.5 mM each)	8 µl	1600 µM
Primer for (50 µM)	0.5 µl	0.5 µM
Primer rev (50 µM)	0.5 µl	0.5 µM
TaKaRa LA Taq (5 U/µl)	0.5 µl	2.5 Units
Genomic DNA	2 µl	500 ng

PCR cycling protocol

Step	Temperature	Duration	Cycles
Initial denaturation	94°C	1 min	1
Denature	98°C	10 sec	30
Anneal	60°C	20 sec	
Extent	68°C	8 min	
Final extension	72°C	10 min	1

Long-range PCR primer for targeted Npr2 allele

Primer	Sequence	bp	Product size
Long-rang PCR			
Neo forward	5´-GGGTTATTGTCTCATGAGCGG-3´	21	rec **7000 bp**
External reverse	5´-TCCTGTGCACTTTCTGGTCA-3´	20	
Triplex PCR			
Ex18 forward	5´-CCTGCTTTGATGCCATTATCG-3´	21	wt **500 bp** rec **1414 bp**
Neo forward	5´-GGGTTATTGTCTCATGAGCGG-3´	21	
DS loxP2 reverse	5´-CTGCAACAACCAAAGCTCAG-3´	20	

4.2.8 Blastocyst injection and generation of chimeras

After initial Southern blot analysis, ES cell clones carrying the correct homologous recombination were unfrozen from the stored 96-well feeder plates, centrifuged and resuspended in ES cell medium and seeded onto a new 96-well feeder plate. ES cell medium which was supplemented with 400 µg/ml geneticin (G418) was daily exchanged to preserve the selection pressure. ES cell clones were gradually expanded until they grew on 6-well feeder plates. ES cell backup samples were frozen and stored at -80°C after each cell splitting step. Rescreened ES clones were finally prepared for the blastocyst injection. For this, ES cell aliquots frozen from a 6-well feeder plate were seeded onto a new 6-well feeder plate, cultured in the absence of G418 and finally split onto a 6-well gelatin plate with a ratio of around 1:3. Knowing the day of the injection, ES cells were seeded at least three days in advance with slightly diversified dilutions in order to select perfectly shaped ES cells for the blastocyst injection. The selected ES cells were washed, trypsinized and resuspended in 2 ml ES cell medium. The cell suspension was immediately plated onto a 12-well plate and incubated for 45 min at 37°C to roughly separate the fibroblasts from the embryonic stem cells. The ES cell medium containing most of the feeder cells was gently aspirated. The adherent ES cells were resuspended in 300 µl ES cell medium, transferred to a cryovial, placed on ice and delivered quickly to the Transgene Core Facility. Around 12 ES cells were microinjected per prepared blastocyst. Blastocysts were obtained from hormone-treated C57Bl/6 female mice. About 15 injected blastocysts were finally transferred into a pseudo-pregnant surrogate mother. Blastocyst injections were performed by the Transgene Core Facility of the Max Delbrück Center for Molecular Medicine.

4.2.9 Germline transmission and Neo-cassette removal

Born chimeric male mice were breed with Flpe-deleter female mice for germline transmission and excision of the *Neo* cassette at the same time. The coat color of newborn mice did not give any reference to successful germline transmission because the genetic background of the Flpe-deleter strain was not C57Bl/6. The entire offspring was therefore examined by PCR genotyping.

4.2.10 Genomic DNA purification

Genomic DNA from mice was obtained by several methods depending on the subsequent use. Genomic DNA from liver tissue was isolated using the Genomic DNA Buffer Set, Proteinase K, RNase A, and Genomic-tip 500/G from Qiagen according to the manufacturer´s recommended protocol. For standard genotyping, tail cuts were directly lyzed in 200 µl DirectPCR Lysis Reagent (Peqlab) supplemented by 0.2 mg/ml Proteinase K (Roche) and the genomic DNA was used without purification. In case of DNA sequence analysis, genomic DNA was purified using the High Pure PCR Template Preparation Kit from Roche in accordance to the manufacturer´s protocol.

4.3 Mouse genotyping protocols

Polymerase chain reactions were carried out to determine the genotype of individual transgenic mice using distinct pairs of oligonucleotides. Genomic DNA templates were obtained by lysis of tail biopsies. The tail biopsies were lyzed using 200 µl DirectPCR Lysis Reagent (Peqlab) together with 0.2 mg/ml Proteinase K (Roche). The samples were incubated in the thermomixer overnight at 55°C. The Proteinase K activity was afterwards heat-inactivated at 85°C for 45 minutes before PCR amplification. The *Taq* DNA Polymerase from Invitrogen and corresponding buffers were used for all PCR reactions. The general annealing temperature of 59°C and the extension time of 1 minute worked for each genotyping protocol. In case of the multiplex-PCR, the water quantity was adjusted to the enlarged volume of oligonucleotides. The respective pair of primers and the resulting DNA band sizes are listed in the genotyping primer table for each mouse line to be genotyped (Table 7). Band sizes are specified for the wild-type allele (wt) and for the transgenic allele (rec). Results of the PCR amplification were visualized by gel electrophoresis using 2.5 % (w/v) agarose gels and 1kb DNA ladder as control.

Pipetting scheme

Components	25 µl reaction	Final conc.
sterile ddH_2O	18.275 µl	N/A
10x PCR Buffer	2.5 µl	1x
$MgCl_2$ (50 mM)	1.5 µl	3 mM
dNTPs (10 mM each)	0.125 µl	200 µM
Primer for (50 µM)	0.2 µl	0.4 µM
Primer rev (50 µM)	0.2 µl	0.4 µM
Taq (5 U/µl)	0.2 µl	1 Unit
Template DNA	2 µl	≤ 500 ng

PCR cycling protocol

Step	Temperature	Duration	Cycles
Initial denaturation	94°C	3 min	1
Denature	94°C	30 sec	35
Anneal	59°C	30 sec	
Extent	72°C	1 min	
Final extension	72°C	5 min	1

Genotyping primers

Primer	Sequence	bp	Product size
Floxed Npr2 allele (loxP1 site)			
Npr2 loxP1-1	5´-GCCACTTTTGCACCCGGATG-3´	20	wt **231 bp**
Npr2 loxP1-2	5´-GTGACGCTGTCGAAGGCCTC-3´	20	rec **334 bp**
Floxed Npr2 allele (loxP2 site)			
Npr2 loxP2-1	5´-CCTGCTTTGATGCCATTATCG-3´	21	wt **506 bp**
Npr2 loxP2-2	5´-CTGCAACAACCAAAGCTCAG-3´	20	rec **684 bp**
Wnt1-Cre allele			
Wnt1_for	5´-AGCCCGGACCGACGATGAA-3´	19	rec **550 bp**
Wnt1_rev	5´-TAAGAGGCCTATAAGAGGCGG-3´	21	
Isl1-Cre allele			
Isl1-i[Cre] for	5´-CGAGTGATGAGGTTCGCAAG-3´	20	rec **312 bp**
Isl1-i[Cre] rev	5´-TTCACCGGCATCAACGTTTT-3´	20	
Thy1-YFP-H allele			
IL_oIMR0043	5´-GTAGGTGGAAATTGTAGCATCATCC -3´	25	
IL_oIMR0042	5´-CTACGCCACAGAATTGAAAGATCT-3´	24	wt **324 bp**
GFP_oIMR2416	5´-TCCTTGAAGAAGATGGTGCG-3´	20	rec **173 bp**
GFP_oIMR0872	5´-AAGTTCATCTGCACCACC-3´	18	
Flpe-deleter allele			
Flpe_for	5´-CTAATGTTGTGGGAAATTGGAGC -3´	23	rec **600 bp**
Flpe_rev	5´-CTCGAGGATAACTTGTTTATTGC -3´	23	

Table 7

4.3.1 Mouse lines

Mouse strain	Nomenclature	Genetic description	Provided by
Npr2-flox(1)	*Npr2*$^{tm3(hypo)Fgr}$	Exon 17 and exon 18 of the *Npr2* gene are flanked by *loxP* sites. Random silent point mutation leads to hypomorphic *Npr2* gene expression.	-
Npr2-flox(2)	*Npr2*$^{tm4(flox)Fgr}$	Exon 17 and exon 18 of the *Npr2* gene are flanked by two *loxP* sites; usable for conditional gene knockout generation.	-
Wnt1-Cre	*Tg(Wnt1-cre)*^{11Rth}	Cre-recombinase coding sequence controlled by upstream *Wnt1* promoter and downstream *Wnt1* enhancer (Danielian et al., 1998).	group of Prof. Dr. C. Birchmeier-Kohler
Isl1-Cre	*Isl1*$^{tm1(cre)Tmj}$	Cre-recombinase expression controlled by the *Isl1* promoter (Srinivas et al., 2001).	group of Prof. Dr. C. Birchmeier-Kohler
Thy1-YFP-H	*Tg(Thy1-YFP)*^{HJrs}	Integration of transgenic construct containing the *YFP* gene under direction of regulatory elements derived from mouse *Thy1* gene (Feng et al., 2000; Porrero et al., 2010).	group of Prof. Dr. R. Martini (University of Würzburg)
Flpe-deleter	*Tg(ACTFLPe)*^{9205Dym}	Variant of the *Saccharomyces cerevisiae FLP1* recombinase gene is expressed under the direction of human *ACTB* promoter (Dymecki and Tomasiewicz, 1998).	group of Prof. Dr. C. Birchmeier-Kohler

4.3.2 Cre-*loxP* recombination system

The Cre-*loxP* mechanism is based on two components, the Cre-recombinase and the *loxP* site, originally discovered in bacteriophage P1 (Sauer and Henderson, 1988; Sternberg and Hamilton, 1981). The Cre enzyme is a 38 kDa recombinase protein which mediates intra- and intermolecular site specific recombination between *loxP* sites during the viral live cycle. The *loxP* (locus of X-over P1) site is the target DNA site and consists of an asymmetric 8-bp spacer region, where recombination takes places, and two flanking 13-bp palindromic recognition regions. The distinct 34-bp *loxP* sequence, which was utilized in this study, was ATAACTTCGTATA-GCATACAT-TATACGAAGTTAT. The Cre-*loxP* recombination system is a standard procedure for genome manipulation in mammalian cell cultures and mice. Location and orientation of the *loxP* sites determine whether a deletion, inversion, or chromosomal translocation is induced by the recombination system (Nagy, 2000). In the case of the *loxP*-flanked (floxed) Npr2 mouse model generated in this thesis, both *loxP* sites are oriented in the same direction (cis

arrangement) causing the deletion of the floxed segment (exon 17 and exon 18). This inducible gene targeting enables the generation of conditional knockout mutants (Kühn et al., 1995). After cross-breeding with Cre expressing mouse strains which contain a transgene that expresses Cre directed by a tissue-specific (conditional) promoter, the floxed Npr2 mouse becomes an Npr2-cKO mutant.

4.4 Molecular cloning of mutant Npr2 and BioID constructs

The molecular cloning of Npr2 plasmid vectors used for the cGMP determination assay and the molecular cloning of Npr2 and cGKIα plasmid vectors used for the BioID assay is illustrated in the result section. The standard molecular technics being used are already outlined in the method section 4.1. The general principle was the PCR amplification of target DNA fragments with oligonucleotides attaching additional restriction sites. The restriction sites were used for DNA ligation causing the realignment of insert and vector DNA. Plasmid amplification and antibiotic-mediated selection was solely carried out using the bacterial strain DH5α. Single cloning steps were confirmed by restriction and sequence analysis. The following schemes outline the PCR reaction mixtures, the cycling programs and the cloning primers. The *Pfu* DNA polymerase was used for the cloning of the Npr2 plasmid vectors. DNA fragments of the BioID plasmid vectors were amplified using the Q5 High-Fidelity DNA Polymerase. Table 8 additionally displays the sequencing primers which were used for the sequence confirmation of Npr2 constructs.

Pipetting scheme

***Pfu* DNA Polymerase**			**Q5 High-Fidelity DNA Polymerase**		
Components	**50 µl reaction**	**Final conc.**	**Components**	**50 µl reaction**	**Final conc.**
nuclease-free H_2O	38 µl	N/A	nuclease-free H_2O	24.5 µl	N/A
10x Pfu Buffer with $MgSO_4$	5 µl	1x	5x Q5 Buffer	10 µl	1x
			5x Q5 Enhancer	10 µl	1x
dNTP Mix (2.5 mM each)	2 µl	400 µM	dNTP Mix (2.5 mM each)	2 µl	400 µM
Primer A (50 µM)	1 µl	1 µM	Primer A (50 µM)	0.5 µl	0.5 µM
Primer B (50 µM)	1 µl	1 µM	Primer B (50 µM)	0.5 µl	0.5 µM
Pfu Polymerase (2.5 U/µl)	1 µl	2.5 Units	Q5 High-Fidelity (2 U/µl)	0.5 µl	1 Unit
Plasmid DNA	2 µl	10-100 ng	Plasmid DNA	2 µl	100-250 ng

PCR cycling protocol

	Pfu DNA Polymerase			Q5 High-Fidelity DNA Polymerase		
Step	**Temperature**	**Duration**	**Cycles**	**Temperature**	**Duration**	**Cycles**
Initial denaturation	95°C	3 min	1	98°C	30 sec	1
Denature	95°C	30 sec	35	98°C	10 sec	35
Anneal	58°C	30 sec		58°C	30 sec	
Extent	72°C	2 min/kb		72°C	30 sec/kb	
Final extension	72°C	10 min	1	72°C	2 min	1

Primers for Npr2 mutant and pIRES2-mCherry vector cloning

Primer	Sequence	bp
mCherryBstXI_for	5´-CGGCCACAACCATGGTGAGCAAGG-3´	24
mCherryXbaI_rev	5´-GATTATGATCTAGAGTCGCGGCC-3´	23
SP6_for	5´-ATTTAGGTGACACTATAG-3´	18
T7_rev	5´-TAATACGACTCACTATAGGG-3´	20
Npr2_KHD[494]_rev	5´-AATGCGCCATAGCATGCTAGCC-3´	22
Npr2_KHD[545]_rev	5´-TCCCTTGAAGTGACCGGTG-3´	19
Npr2_KHD[784]_for	5´-GGCTTCATTCGCCGGTTTAAC-3´	21
Npr2_GC[824]_rev	5´-GGGGCGGCCGCTTATAGATAGGCCTGTGTGCG-3´	32

Primers for BioID construct cloning

Primer	Sequence	bp
BioNcGKI_for	5´-CCGCGGCCGCCAAGCGAACTGGAGGAA-3´	27
BioNcGKI_rev	5´-CCGGATCCTTTACTGGAGCAGCA-3´	23
BioCNpr2_for	5´-CCGAATTCGCCATGGCACTGCCATCC-3´	26
BioCNpr2_rev	5´-CCGAATTCCAGGAGTCCGGGAGG-3´	23

Primers for Npr2 CDS sequence analysis

Primer	Sequence	bp
Npr2_SQ_5´1	5´-CCCTGCAGGGCAGCAACC-3´	18
Npr2_SQ_5´2	5´-CCTTTGACTTGGACGACC-3´	18
Npr2_SQ_5´3	5´-ACCGGACGACAGCCATGC -3´	18

Table 8

4.4.1 Site-directed mutagenesis

The amino acid substitution in the coding DNA sequence of the Npr2 protein was performed by using QuikChange II XL Site-Directed Mutagenesis Kit from Stratagene in full accordance to the manufacturer protocol. The required point mutations were integrated by mutagenic primer-directed replication of both plasmid strands using *PfuUltra* high-fidelity DNA polymerase. The nucleotide substitutions were placed in the middle of two opposed primers with 10-15 bases of the correct sequence on both sides. Primers were purified by fast polynucleotide liquid chromatography (FPLC) during production. 10 ng of pCMV-Sport6-Npr2 (8064 bp) expression vector was applied to the PCR amplification. The restriction enzyme *Dpn*I which is specific for methylated and hemi-methylated DNA was used to digest the parental plasmid template and to select for mutation-containing synthesized DNA. 2 µl of the nicked vector DNA was mixed with 45 µl XL10-Gold ultracompetent cells and 2 µl XL10-Gold β-mercaptoethanol mixes. After 30 minutes incubation on ice, the plasmid transformation was induced by heat-pulse in a 42°C water bath for 30 second. After further 2 minutes on ice, 0.5 ml preheated (42°C) NZY^+ broth was added and incubated at 37°C for 1 hour with shaking at 250 rpm. 250 µl of the transformation reaction was plated on a LB-ampicillin agar plate and incubated overnight at 37°C. The plasmid vector of single bacteria colonies was purified per plasmid DNA mini-preparation and sequenced using Npr2 sequencing primer Npr2_SQ_5´2. Altogether, three independent mutagenesis steps were required for the glutamic acid substitutions and two steps for the alanine exchanges.

Pipetting scheme

Components	50 µl reaction	Final conc.
nuclease-free H_2O	X µl	N/A
10x reaction buffer	5 µl	1x
QuikSolution reagent	3 µl	N/A
dNTP Mix	1 µl	N/A
Primer A (50 µM)	0.17-0.23 µl	125 ng
Primer B (50 µM)	0.17-0.23 µl	125 ng
PfuUltra HF DNA polymerase (2.5 U/µl)	1 µl	2.5 Units
Plasmid dsDNA	1 µl	10 ng

PCR cycling protocol

Step	Temperature	Duration	Cycles
Initial denaturation	95°C	1 min	1
Denature	95°C	50 sec	18
Anneal	60°C	50 sec	
Extent	68°C	8.5 min	
Final extension	68°C	7 min	1

Primers for site-directed mutagenesis

Primer	Sequence	bp
KHD_Ala_1_for	5´-GGTGCAGGCGCTCGCCTGGCGCTGGCGCTGCGGG-3´	34
KHD_Ala_1_rev	5´-CCCGCAGCGCCAGCGCCAGGCGAGCGCCTGCACC-3´	34
KHD_Ala_2_for	5´-GCTGCGGGGATCCGCTTACGGCGCGCTCATGACAGC-3´	36
KHD_Ala_2_rev	5´-GCTGTCATGAGCGCGCCGTAAGCGGATCCCCGCAGC-3´	36
KHD_Glu_1_for	5´-CACAAGGGTGCAGGCGAGCGCCTGACGCTGTCG-3´	33
KHD_Glu_1_rev	5´-CGACAGCGTCAGGCGCTCGCCTGCACCCTTGTG-3´	33
KHD_Glu_2_for	5´-GCAGGCGAGCGCCTGGAGCTGGAGCTGCGGGGATCCAG-3´	38
KHD_Glu_2_rev	5´-CTGGATCCCCGCAGCTCCAGCTCCAGGCGCTCGCCTGC-3´	38
KHD_Glu_3_for	5´-TGGAGCTGCGGGGATCCGAGTACGGCGAGCTCATGACAGCCCATG-3´	45
KHD_Glu_3_rev	5´-CATGGGCTGTCATGAGCTCGCCGTACTCGGATCCCCGCAGCTCCA-3´	45
Npr2_SQ_5´2	5´-CCTTTGACTTGGACGACC-3´	18

4.5 HEK293 and F11 Cell culture

HEK 293 cells are primordially generated by transformation of human embryonic kidney cell cultures with sheared adenovirus 5 DNA (Graham et al., 1977). The cells were cultured in supplemented DMEM cell culture medium at 37°C under 5 % CO_2 in tissue culture flasks. At 100 % confluence cells were split using enzyme-free dissociation buffer (EDTA/PBS) for 5-10 min and centrifugation at 150 g for 4 min. 10 % of harvested cells were seeded onto the same surface area as before.

The F11 cell line is the somatic cell hybrid of rat embryonic dorsal root ganglion (DRG) cells and the mouse neuroblastoma cell line N18TG2. The line retains rat and mouse chromosomes and synthesizes rat and mouse isoenzymes (Platika et al., 1985). F11 cells were grown in Ham´s F-12 medium, supplemented with 15 % fetal bovine serum (FBS), 1x HAT (sodium hypoxanthine, aminopterin, and thymidine) supplement, and 1x antibiotic-antimycotic (penicillin/streptomycin) at 37°C under 5 % CO_2 in tissue culture

flasks. At 70-80 % confluence cells were split using enzyme-free dissociation buffer (EDTA/PBS) for 10-15 min and centrifugation at 150 g for 4 min. 30 % of harvested cells were seeded onto the same surface area as before.

4.5.1 Plasmid DNA transfection in cell culture

At 70-80 % confluence, HEK293 and F11 cells were transfected with supercoiled plasmid DNA using Lipofectamine 2000 DNA Transfection Reagent according to manufacturer´s protocol (Invitrogen). Starvation medium Opti-MEM and predefined plasmid DNA concentrations were used as recommended. For the transfection, cells were incubated with the DNA-lipid complex in Opti-MEM medium for 4 hours followed by medium change. The climax of plasmid DNA expression was assumed to develop 48 hours later.

4.6 Western blot analysis

The concentration of protein samples were roughly estimated using spectrophotometry. For that, the absorbance at 280 nm was compared between protein solution and buffer control solution without protein. Absorbance coefficient for protein mixture (measured values were divided by 1.25) was used to calculate the final concentration (mg/ml). For immunoblot analysis, total cell lysates or fractionated protein samples were mixed with Laemmli SDS/PAGE sample buffer and boiled for 5 min at 95°C. In the Western blot, the protein samples were electrophoresed using a stacking and a running SDS-gel (composition is shown in the SDS-gel preparation Table 9) and running buffer supplemented with SDS (final conc. 0.1 %). The electrophoresis was performed at 100 V for 5 min followed by 200 V for 60 min. Separated proteins were transferred to nitrocellulose sheets which were then incubated with antibody sera. The protein transfer was carried out for 60 min at 100 V using the wet electro-blotting system from Bio-Rad and ice-cold transfer buffer. After rapid staining of protein bands using Ponceau S solution, the nitrocellulose membrane was blocked by Western blocking buffer for 2 hour at room temperature. After overnight incubation at 4°C with a primary antibody diluted in the blocking buffer, the membrane was washed in the Western washing buffer for 25min, renewing the buffer 5 times. The nitrocellulose membrane was finally incubated with HRP-conjugated secondary antibody diluted in blocking buffer for 2 hours at room temperature. The Chemiluminescent reagent (Thermo Scientific), the

ChemiDoc system and the Quantity One software (Bio-Rad) were used for signal detection. In the case of the alkaline phosphatase conjugated secondary antibody, the nitrocellulose membrane was incubated in alkaline phosphate substrate solution containing nitro blue tetrazolium (NBT) and 5-bromo-4-chloro-3-indolyl phosphate (BCIP) until the appearance of purple-blue protein bands. More precisely, the washed membrane was first equilibrated for 5 min with substrate buffer for alkaline phosphatase and then incubated in fresh staining solution for 15-30 min. To stop the staining reaction, the membrane was washed three times with water.

SDS-gel preparation

Components (in order of use)	10 % running SDS-gel	4 % stacking SDS-gel
ddH_2O	2.8 ml	3.7 ml
1M Tris-HCl pH 8.8	3.75 ml	-
1M Tris-HCl pH 6.8	-	625 µl
10 % SDS solution	100 µl	50 µl
30 % Acrylamide/Bis-acrylamide (37,5:1)	3.3 ml	650 µl
10 % Ammonium persulfate	50 µl	25 µl
TEMED	5 µl	5 µl

Table 9

4.7 Immunocytochemistry

Immunocytochemistry was carried out to validate the expression of the Npr2 and BioID constructs in either HEK293 cells or F11 cells. Glass coverslips were sterilized with 70 % ethanol, briefly flamed and precoated with poly-D-lysine (100 µg/ml) for 30 min or more at room temperature. The coverslips were washed with sterile water and allowed to dry. HEK293 or F11 cells were dissociated using enzyme-free PBS/EDTA dissociation buffer for 5-10 min at 37°C, centrifuged at 150 g for 4 min and resuspended in 1 ml DMEM cell culture medium. The cell number was determined for 10 µl cell suspension using the TC10 Automated Cell Counter with trypan blue staining. 0.4x106 HEK293 cells and 0.6x106 F11 cells were seeded per well of a 6-well cell culture plate. On the day of transfection, cell density was 50-70 % confluent. The plasmid transfection was performed using Lipofectamine 2000 reagent according to manufacturer`s protocol. After 36-48 hours, the coverslips were washed twice with pre-warmed PBS buffer and treated with the following steps:

1. *Cells were fixed at 4°C for 15 min with 4 % formaldehyde/DMEM.*
2. *Cells were fixed at 4°C for 10 min with 4 % formaldehyde/PBS.*
3. *Two washing steps with PBS buffer; each for 1 min.*
4. *Cell membrane was optionally perforated using 0.05 % TritonX-100/PBS for 10 min.*
5. *Three washing steps with PBS buffer; each for 3 min.*
6. *Incubation with blocking solution (0.1 % BSA in PBS buffer) for 30 min at room temperature.*
7. *Incubation with primary antibody dissolved in blocking solution; overnight at 4°C.*
8. *Three washing steps with PBS buffer; each for 3 min.*
9. *Incubation with secondary antibody dissolved in blocking solution; 2 hours at room temperature in the dark.*
10. *Four washing steps with PBS buffer; each for 5 min.*
11. *DAPI staining; incubation with 300 nM DAPI (4',6-diamidino-2-phenylindole) in PBS for 5 min; dipping into water for a few times.*
12. *Coverslips were mounted onto object slides using Mowiol; dried overnight in the dark.*

4.8 Silver staining

Silver staining of acrylamide gels was performed in accordance with standard protocol (Ansorge, 1985). The solution volume for each step and gel was 30 ml. The acrylamide gels were gently shaken during incubation steps.

1. *Gel Fix Solution (50% (v/v) MeOH, 12% (v/v) TCA, 2% (w/v) $CuCl_2$) for 20 min.*
2. *Solution A (10% (v/v) EtOH, 5% (v/v) acetic acid) for 10 min.*
3. *0.01% (w/v) $KMnO_4$ for 10 min.*
4. *Solution A for 2x 5 min.*
5. *10% EtOH for 10 min.*
6. *ddH_2O for 10 min.*
7. *0.2% $AgNO_3$ for 10 min.*
8. *ddH_2O dip for 20 sec.*
9. *10% K_2CO_3 for 1 min.*
10. *Developer (2% K_2CO_3, 0.01% Formaldehyde) for 3-10 min.*
11. *Solution A for 10 min.*
12. *ddH_2O for 5 min.*

As a last point, the gels were dried between two porous cellophane foils at 85°C for 45 min using vacuum gel dryer.

4.9 cGMP determination in HEK293 cells

The cGMP concentration level in CNP-stimulated and non-stimulated HEK293 cells were determined using the Amersham cGMP Enzyme Immunoassay Biotrak (EIA) System from GE Healthcare. The procedure was strictly following the manufacturer´s recommended protocol number four. The 96-well plate loaded with samples and control samples for the standard curve was analyzed by a microplate reader model 3550 (Bio-Rad).

4.10 BioID assay

The nearest neighbor analysis of the promiscuous biotin ligase fusion proteins was adapted from the initial delineation of the BioID assay (Roux et al., 2012). F11 cells were cultured in 15 cm cell culture dishes for the proximity-dependent biotinylation assay (BioID). At 70-80 % confluence, cells were transfected using Lipofectamine 2000 DNA Transfection Reagent with some minor variations to standard protocol. 16 µg plasmid DNA and 30 µl Lipofectamine 2000 were mixed with 0.5 ml Opti-MEM Reduced Serum Medium, respectively. The 1 ml DNA-lipid complex was added to 14 ml Opti-MEM submitted in the 15 cm cell culture dish and was incubated at 37°C for 4 hours followed by 20 ml F12 medium change. After 48 hours, the F12 medium was exchanged by 19 ml fresh F12 medium. 1 ml solute (+)-biotin stock solution (1mM) was added achieving a final concentration of 50 µM. The 1mM (+)-biotin stock solution was freshly prepared by dissolving 1.22 mg (+)-biotin per milliliter in sterile water and 15 min heating at 80°C. After 16 hours of biotin incubation, the plates were washed twice with pre-warmed PBS buffer and F11 cells were harvested with enzyme-free EDTA/PBS dissociation buffer, centrifuged at 150 g for 4 min and dissolved in 1.5 ml BioID lysis buffer (150 mM NaCl, 50 mM Tris, 5 mM EDTA, 10 µM leupeptin hemisulfate salt, 10 µM pepstatin A, 10 µM aprotinin, 0.1 µM PMSF, and pH adjusted to 7.4). Subsequent procedure steps were carried out on ice or at 4°C. Cells were disrupted by sonication using ultrasonic water bath for 30 min and a cellular fractionation was performed as listed below.

1. *Lysed cells were centrifuged at 700 g for 10 min.*
2. *Pellet was discarded; supernatant was transferred to new 1.5 ml tube.*

3. *Ultra-centrifugation at 100,000 g for 15 min.*
4. *Supernatant (CF = cytosolic fraction) was transferred to new 1.5 ml tube and stored on ice.*
5. *Pellet was solubilized in 1 ml 1 % CHAPS/PBS and protease inhibitor mix (Membrane fraction buffer); incubation on ice for 20 min.*
6. *Ultra-centrifugation at 100,000 g for 15 min.*
7. *Supernatant (MF = membrane fraction) was transferred to new 1.5 ml tube and stored on ice; pellet was discarded.*

Before affinity purification of biotinylated proteins using Streptavidin Agarose resin (Thermo Scientific), detergent sodium dodecyl sulfate was added to both the cytosolic fraction sample and the membrane fraction sample with a final concentration of 0.1 % (v/v) SDS. Protein samples were pre-incubated on the laboratory rotating wheel at 4°C for 30 min. 50 µl of the streptavidin agarose beads were added to the cytosolic fraction sample and 30 µl to the membrane fraction sample. The biotin-streptavidin binding was induced by overnight incubation on the rotating wheel at 4°C. The following day, the agarose beads were gently washed five times by repeated centrifugation at 500 g for 5 min, discarding the supernatant and resolubilization in F11 lysis buffer without detergents. Finally, the resin-bound proteins were purified by boiling in 1x Laemmli sample buffer at 95°C for 5 min. The purified proteins were additionally separated from the agarose beads by transfer onto an Ultrafree-MC centrifugal filter tube (0.45 µm) and centrifugation at 7000 g for 5 min. Cytosolic fraction agarose beads were mixed with 110 µl 1x Laemmli sample buffer and membrane fraction agarose beads with 70 µl buffer. Approximately 2 % of the affinity purified protein samples were used for immunoblot analysis as well as silver staining. Three independent biological replicates were produced for each sample and control condition.

4.11 Mass spectrometry

Protein determination of the BioID protein samples was performed by the MS core facility of the Max Delbrück Center for Molecular Medicine using LC-MS-based (liquid chromatography-mass spectrometry) label-free protein quantification. Peptide sequences were aligned against a rat proteome database for protein identification. The statistical analysis and calculation of the data was carried out using the free software programming language R.

4.12 Reverse transcription polymerase chain reaction (RT-PCR)

The RT-PCR was performed to qualitatively detect the gene expression of distinct tissues and cell cultures. The total RNA from either liver, DRGs or embryonic stem cells was purified using the RNeasy Mini Kit from Qiagen. Additional used material like pipette tips and reaction tubes were treated with Diethylpyrocarbonate (DEPC) to inactivate ribonucleases. Up to 25 mg tissue material and 4 x 10^6 cells were respectively lyzed per sample. The released RNA was bound to the RNeasy spin column, repeatedly washed and finally eluted with 30 µl RNase-free water. All procedure and centrifugation steps were performed at room temperature and in accordance to the manufacturer protocol. The subsequent transcription of purified RNA into complementary DNA was accomplished by using SuperScript II Reverse Transcriptase (Invitrogen) and oligo(dT)$_{12\text{-}18}$ as template-primer. The inserted quantity of RNA was equalized for the samples to be compared. The resulting cDNA was inserted as template DNA into the ordinary PCR reaction. Taq DNA polymerase from Invitrogen was used for the qualitative analyses of Npr2 gene expression in animals and ES cell culture. FastGene Taq DNA polymerase (Nippon Genetics) was used to attest the gene expression in dorsal root ganglia of specifically purified proteins of the BioID approach. The protocol for cDNA transcription, the pipetting schemes and PCR cycling protocols, and applied pairs of oligonucleotides are listed below.

cDNA transcription from purified RNA

Components and steps	20 µl reaction
oligo(dT)$_{12\text{-}18}$ (0.5 mg/ml)	1 µl
1 - 4* µg of total RNA	x µl (max. 10 µl)
dNTPs (10 mM each)	1 µl
ddH_2O	to 12 µl
65°C for 5 min; fast chill down on ice and add:	
5x First-Strand Buffer	4 µl
0.1 M DTT	2 µl
RNaseOUT (40 U/µl)	1 µl
Incubate at 42°C for 2 min and add:	
SuperScript II RT (200 U/µl)	1 µl
Incubate at 42°C for 50 min	
Inactivate by heating at 70°C for 15 min	

***varying quantity of applied total RNA**

Pipetting scheme

Invitrogen Taq			FastGene Taq		
Components	**50 µl reaction**	**Final conc.**	**Components**	**25 µl reaction**	**Final conc.**
ddH_2O	38.55 µl	N/A	ddH_2O	19.275 µl	N/A
10x Buffer	5 µl	1x	10x Buffer	2.5 µl	1x
$MgCl_2$ (50 mM)	3 µl	3 mM	$MgCl_2$ (25 mM)	1.5 µl	3 mM
dNTPs (10 mM each)	0.25 µl	200 µM	dNTPs (10 mM each)	0.125 µl	200 µM
Primer A (50 µM)	0.4 µl	0.4 µM	Primer A (50 µM)	0.2 µl	0.4 µM
Primer B (50 µM)	0.4 µl	0.4 µM	Primer B (50 µM)	0.2 µl	0.4 µM
Invitrogen Taq (5 U/µl)	0.4 µl	2 Unit	FastGene Taq (5 U/µl)	0.2 µl	1 Unit
Template cDNA	2 µl	200-300 ng	Template cDNA	1 µl	~75 ng

PCR cycling protocol

	Invitrogen Taq			FastGene Taq		
Step	**Temperature**	**Duration**	**Cycles**	**Temperature**	**Duration**	**Cycles**
Initial denaturation	94°C	3 min	1	95°C	3 min	1
Denature	94°C	30 sec	35	95°C	30 sec	35
Anneal	58°C	30 sec		58°C	30 sec	
Extent	72°C	2 min		72°C	45 sec	
Final extension	72°C	10 min	1	72°C	10 min	1

RT-PCR primer for *Npr2* gene expression analysis

Primer	Sequence	bp
Npr2_Ex13_for	5´-GATCAACTGCTGAACCGGACG-3´	21
Npr2_Ex17_rev	5´-ATGGGGGTGCTCTCAGCTGAC-3´	21
Npr2_Ex22_rev	5´-GCTCTCCCAAGAGCCAGTAAG-3´	21

RT-PCR primer for BioID candidate gene expression analysis

Primer	Sequence	bp
Reticulon-4		
RT Rtn4 for	5´-TCAGATGAAGGCCACCCATT-3´	20
RT Rtn4 rev	5´-GATCTATCTGCGCCTGATGC-3´	20
G kinase-anchoring protein 1		
RT Gkap1 for	5´-CTCACAGAGCACAACGGAAC-3´	20
RT Gkap1 rev	5´-CATCTCTCCCTCCTGAAGCA-3´	20
Ataxin-2-like protein		
RT Atxn2l for	5´-GCCCCGTACTCATTCAACAC-3´	20
RT Atxn2l rev	5´-CTGTGGGTTGTAGGGGATGT-3´	20

Primer	Sequence	bp
Coronin-1C		
RT Coro1c for	5´-ATTGTGGCGGAGAAGGAGAA-3´	20
RT Coro1c rev	5´-GGCTCGCACTTTCTCTCATG-3´	20
Cortactin		
RT Cttn for	5´-GCAAAGGAGAGAGAGCAGGA-3´	20
RT Cttn rev	5´-CAGGAGCCTCTGTAGTCTCG-3´	20
WASH complex subunit FAM21		
RT Fam21 for	5´-CCCAAGAGCAGAGGATCACA-3´	20
RT Fam21 rev	5´-TGTCTTGATGGCTGTCAGGT -3´	20
Serine/threonine-protein phosphatase 2A 65 kDa regulatory subunit A		
RT Ppp2r1a for	5´-AGTGTCCTGAAGTCCGACTG-3´	20
RT Ppp2r1a rev	5´-CCACTCCTTCCCGAACTTCT-3´	20
Cytoskeleton-associated protein 5		
RT Ckap5 for	5´-AGAGAACACTAAGGAGGGCC-3´	20
RT Ckap5 rev	5´-AGATGGCCCCACTTCTTCTC-3´	20
GTPase-activating protein RAB7		
RT Tbc1d15 for	5´-GGCAAAGCACTATGGCTTCA-3´	20
RT Tbc1d15 rev	5´-ACAAGGGCTGCCAACATTTT-3´	20
Ribosomal protein S6 kinase alpha-1		
RT Rps6ka1 for	5´-CGGACTCCTCATGACACCTT-3´	20
RT Rps6ka1 rev	5´-CTTGGCTGTCTCTGAAACCG-3´	20
Dihydropyrimidinase-related protein 2		
RT Dpysl2 for	5´-ACCATCTCTGCCAAGACACA-3´	20
RT Dpysl2 rev	5´-GCAGGGGATGTCTTAGCTGA-3´	20
Afadin		
RT Mllt4 for	5´-ACAGTTGGAAGAGATGCGGA-3´	20
RT Mllt4 rev	5´-GGGGAGAGGACCTGTGTTTT-3´	20
Nuclear migration protein nudC		
RT Nudc for	5´-AAGTCAAGGTGGAGGAGAGC-3´	20
RT Nudc rev	5´-GGACTTCTGCCTCTGGTCAT-3´	20
Septin-9		
RT Sept9 for	5´-AGGAGTTTGATGAGGACGCA-3´	20
RT Sept9 rev	5´-GCATGTGCGTCCTGATAAGG-3´	20
Dihydropyrimidinase-related protein 1		
RT Crmp1 for	5´-AAGCCATTCCCAGAGCATCT-3´	20
RT Crmp1 rev	5´-AAGTTGGACTGGTGGAGGTT-3´	20
A-kinase anchor protein 12		
RT Akap12 for	5´-TTGCACGTACAGAAACAGCC-3´	20
RT Akap12 rev	5´-CTTTGGTCCGTTGGTGTCTG-3´	20
Synapsin-2		
RT Syn2 for	5´-TGAAATGTTTGGTGGCCTGG-3´	20
RT Syn2 rev	5´-GGCTGTTGGGTGGTTAAAGG-3´	20
Actin-related protein 2/3 complex subunit 4		
RT Arpc4 for	5´-AGGCTCCATCAACTCTGTCC-3´	20
RT Arpc4 rev	5´-GCATTGACCGACAGCTTCAT-3´	20

Primer	Sequence	bp
Ras-related protein Rab-5C		
RT Rab5c for	5´-ACGGGCTAAGAATTGGGTGA-3´	20
RT Rab5c rev	5´-TTCTGGGGCTCATTCTTGGG-3´	20
Talin-1; Talin-2		
RT Tln1-2 for	5´-TGTGACTGAGCTCATCCAGG-3´	20
RT Tln1-2 rev	5´-GGACTTGGCAGCTTCTAGGA-3´	20
Talin-1		
RT Tln1 for	5´-CCGACTGGCCTCACAAGCCAAGCCT-3´	25
RT Tln1 rev	5´-GGCAGGTGGCTCTGGGGAACAGAAG-3´	25
Kindlin-3		
RT Kind3 for	5´-AGCTGTCTCTGCTGCGTGCTC-3´	21
RT Kind3 rev	5´-ATACCTTGCTGCATGAGGCAC -3´	21
Actin beta		
RT ActinB for	5´-CGTGGGCCGCCCTAGGCACCA-3´	21
RT ActinB rev	5´-CTTAGGGTTCAGGGGGGC-3´	18
GAPDH (Glyceraldehyde-3-phosphate dehydrogenase)		
RT Gapdh for	5´-GAGCTGAACGGGAAGCTCAC-3´	20
RT Gapdh rev	5´-ACCTGGTCCTCAGTGTAGCC-3´	20

4.13 Spinal cord preparation

The entire spinal cord of adolescent mice (postnatal day 14 up to postnatal day 21) was prepared to analyze the axon bifurcation of DRG neurons. Sensory neurons were labeled by the expression of yellow fluorescent protein directed by the promoter of the *Thy1* gene (Porrero et al., 2010). After decapitation of the animal, the complete vertebral column was extracted and fixed with dissecting needles onto a silicone cell culture dish filled with ice-cold 1x PBS buffer. The spinal cord was laid open by successively cutting the vertebra bodies alternating right and left starting from cervical segments using a spring scissors. Dorsal parts of the vertebral column were steadily removed until the sacral segments were reached. By using the sharp edge of tweezers, the spinal cord was carefully detached from the ganglia, transferred into a 15 ml screw-cap tube and fixed by incubation on ice for 4 hours in 4 % PFA solution. The fixed spinal cord was placed between two object slides with 1x PBS buffer and stored overnight at 4°C in the dark. The next day, the LSM710 confocal microscope was used to record Z-stack images.

4.14 Plantar Test (Hargreaves' Method)

The Plantar Test enables the researcher to discern a peripherally mediated response to thermal stimulation in the unrestrained mouse. The test was performed directly referring to the Hargreaves´ Method (Hargreaves et al., 1988). The experimental animals were placed into separate compartments. After an acclimation period of one hour, a light beam source was positioned under the glass floor directly radiating beneath the hind paw. The beam of light was exclusively pointed to the ball of the foot avoiding the tiptoes. A trial was commenced by depressing a pedal which turned on the light source and started a digital solid state timer. In so doing, the idle intensity was increased from 5 % to 30 % of the maximal luminous intensity. The mouse responded with paw withdrawal to the acute pain perception. At this very moment, a renewed push of the pedal stopped the reaction time counter. The withdrawal latency was measured to the nearest second decimal. 25 measurements were carried out per day and animal. One course of the experiment involved three trial days each with one day break in between. One previous training day was executed without data collection to familiarize the animals with the experimental setting and procedure. To avoid learning and adaptive behavior, two weeks were never measured consecutively.

5. RESULTS

5.1 Generation of a floxed Npr2 mouse line

Since constitutive Npr2 or CNP knockout mice having sensory axon bifurcation errors are dwarfs due to impaired endochondral ossification, the generation of a conditional knockout mouse is mandatory to perform behavioral or physiological tests in order to clarify whether the axonal bifurcation of sensory axons has an impact on the processing of sensory information. For this aim, a targeting vector based on genomic DNA of the mouse locus of Npr2 was generated containing exons 17 and 18 of the *Npr2* gene flanked by two equally aligned *loxP* sites. The receptor guanylyl cyclase Npr2 was chosen as gene target due to its central role within the cGMP signaling cascade. After integration of the targeting vector into embryonic stem cells by homologous recombination and subsequent generation of chimeric mice using blastocyst injection, germline positive transgenic animals were used to establish a floxed Npr2 mouse line. A floxed Npr2 mouse model should allow us to inactivate Npr2 preferentially in neurons of dorsal root ganglia or cranial sensory ganglia and should therefore avoid body size restrictions caused by Npr2 or CNP-dependent bone growth. A conditional Npr2 knockout mouse should allow us to perform a variety of behavioral or physiological tests.

5.1.1 Cloning strategy for generation of the targeting vector

The targeting construct for the floxed Npr2 mouse model was generated by the use of a BAC clone and mini-λ-mediated genomic engineering (Copeland et al. 2001; Court DL et al. 2003). To identify a BAC clone which could be utilized as a genomic DNA template of Npr2 for the following cloning steps, a sequence alignment between the gene locus of mouse Npr2 and an appropriate BAC library was performed using Ensembl browser data. The selected BAC clone bMQ331a20 carries the Npr2 gene locus on the backbone vector pBACe3.6 and was generated from 129S7/AB2.2 ES cell DNA (Figure 9).

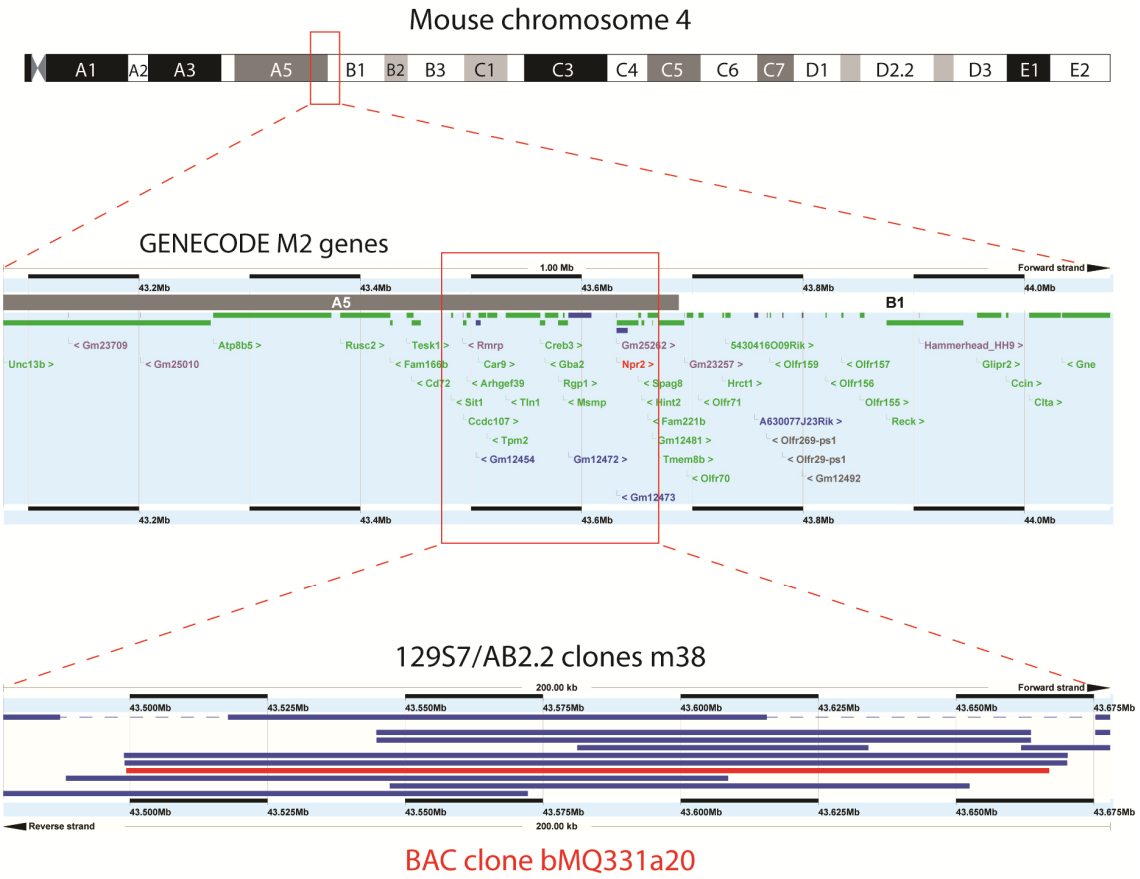

Figure 9: BAC clone localization within Npr2 gene locus. Ensembl browser data (Mus musculus version 75 (GRCm38)) illustrates the Npr2 gene locus on mouse chromosome 4 (4:43.631.935-43.651.244) together with several aligned 129S7/AB2.2 BAC clones (blue lines). The bMQ331a20 BAC clone (red line) selected for generation of the targeting vector is localized at 4:43.499.367-43.666.888 and is based on a pBACe3.6 backbone. (http://www.ensembl.org)

5.1.2 Subcloning of the Npr2 gene locus

Subcloning of the DNA fragment of the Npr2 gene locus was performed using the mobile lambda Red recombination system (mini-λ). BAC clone bMQ331a20 and mini-λ DNA was consecutively transferred into the bacterial strain DH10B by electroporation. At the same time, a pDTA vector was constructed with two homology arms corresponding to the genomic DNA sequence of Npr2 exon 13 and exon 22 (Figure 10). The pDTA vector was linearized between these homology arms and introduced into the DH10B strain which carried the BAC clone and mini-λ DNA. Proteins expressed by the defective lambda prophage guided the homologous recombination of genomic DNA into the pDTA vector. After positive selection with ampicillin, the accurate insertion of genomic DNA from exon 13 to exon 22 was verified by restriction enzyme digestion. The pDTA vector with the subcloned Npr2 fragment was introduced into the bacterial strain DY380 for

the next recombineering steps. DNA sequencing and analysis was carried out to exclude any errors in the coding sequence of Npr2.

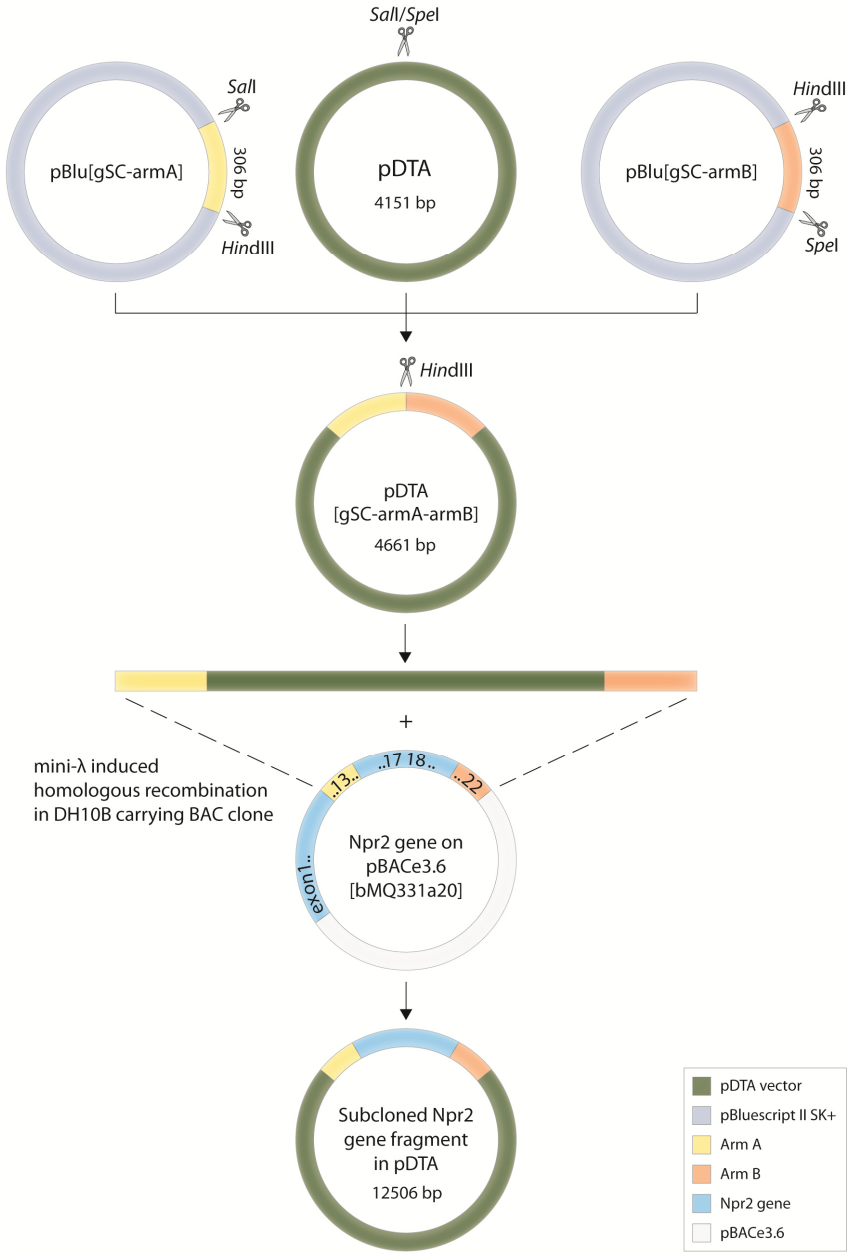

Figure 10: Generation of the genomic Npr2 subclone. A gene fragment including the genomic sequence of mouse Npr2 from exon 13 to exon 22 was subcloned into the pDTA vector. First, two homology arms (A and B), both 306 nucleotides long and pre-cloned in pBluescript II SK+ vectors, were inserted in the pDTA vector by a triple sticky end ligation using the cleavage sites of restriction enzymes *Sal*I, *Hin*dIII, and *Spe*I. The resulting plasmid pDTA[gSC-armA-armB] (4661 bp) was linearized between A and B by *Hin*dIII and electroporated in DH10B bacteria which were before provided with mini-λ DNA and the Npr2 gene on BAC clone bMQ331a20. The mini-λ DNA which was integrated into the bacterial chromosome as a defective prophage promoted the homologous recombination by the lambda Red recombination system. The resulting pDTA plasmid containing the subcloned Npr2 gene fragment had a length of 12524 bp.

5.1.3 Cloning of the first mini-targeting vector and recombination into the genomic subclone

Single cloning steps of the first mini-targeting vector and its recombination with the genomic subclone are illustrated in Figure 11. The purpose of this vector was insertion of a *loxP* site between exon 16 and exon 17. In brief, the mini-targeting vector was based on the pHW025 plasmid generated by Dr. Hagen Wende containing a *FRT*-flanked neomycin cassette surrounded by two *loxP* sites. This *loxP*-flanked neomycin cassette was provided with two homology arms, 5´ and 3´ homology arm, corresponding to the genomic Npr2 DNA between exon 16 and exon 17. For this purpose, two BAC amplification products were primarily cloned into the pBluescript II SK+ plasmid by blunt end ligation and afterwards successively subcloned into the pHW025 plasmid using sticky end restriction enzymes. The linearized mini-targeting vector was inserted into the genomic Npr2 subclone by homologous recombination after electroporation into DY380 bacteria providing the temperature-sensitive lambda Red recombination system and the pDTA vector carrying the subcloned Npr2 fragment. The subsequent removal of the *loxP*-flanked neomycin cassette was achieved by arabinose-induced activation of Cre-recombinase activity resulting in the excision of the sequence between the two identical *loxP* sites after electroporation into bacterial strain EL350. Every ligation and recombination step was followed by antibiotic selection, control digestion and sequence analysis. The final genomic subclone carrying one *loxP* site upstream of exon 17 was transferred into the DY380 strain for the following recombination steps.

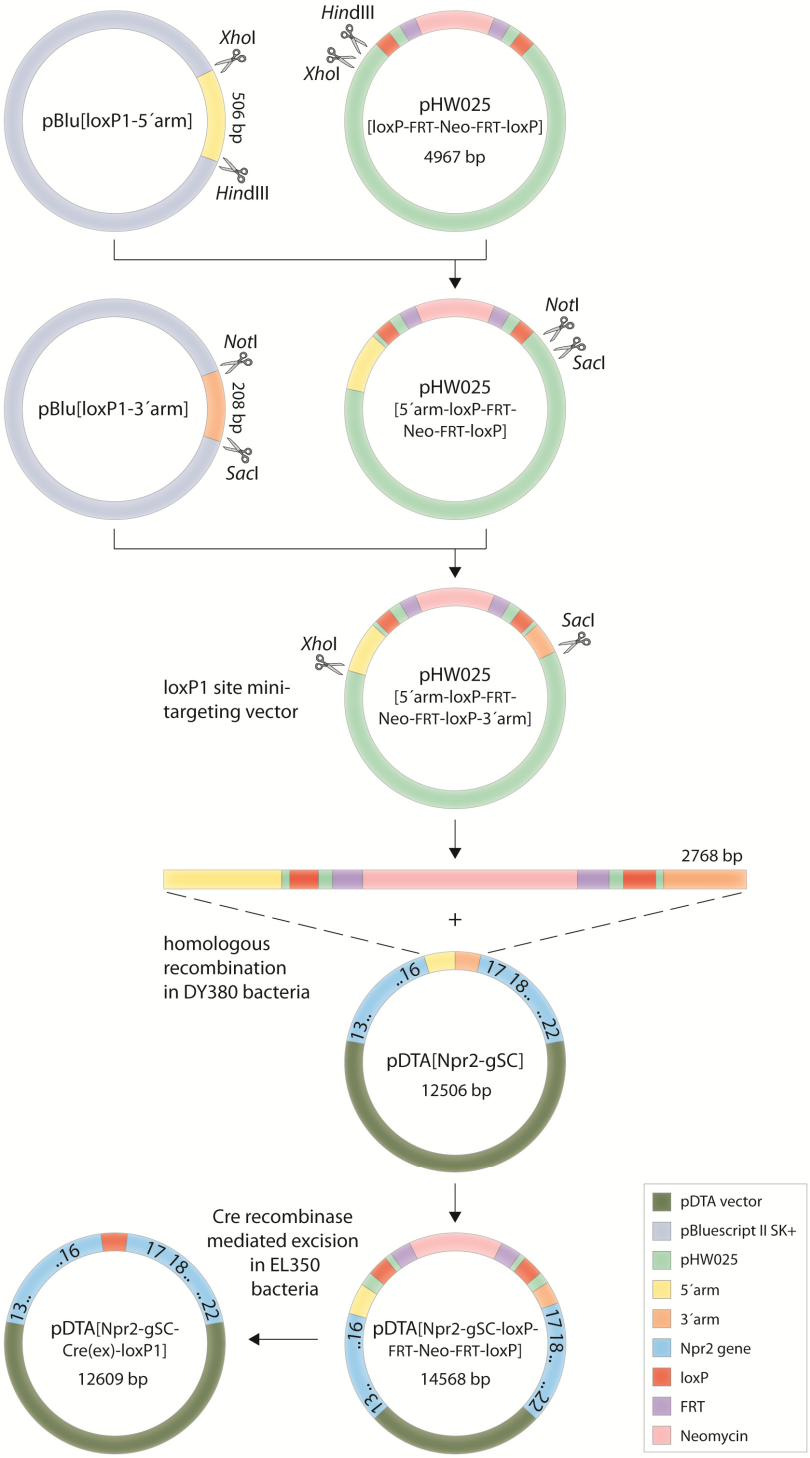

Figure 11: Cloning strategy for the first mini-targeting vector resulted in loxP1 site integration between Npr2 exon 16 and exon 17. The first mini-targeting vector is based on the pHW025[loxP-FRT-Neo-FRT-loxP] plasmid which contains a FRT-flanked neomycin cassette flanked by two loxP sites. Two homology arms were cloned upstream and downstream of the loxP-FRT-Neo-FRT-loxP site in order to transfer this pHW025 plasmid fragment into the genomic Npr2 subclone. First, the 5´arm (506 bp) was inserted by sticky end ligation using the cleavage sites of the restriction enzymes *Hin*dIII and *Xho*I, followed by the cloning of the 3´arm (208 bp) into pHW025[5´arm-loxP-FRT-Neo-FRT-loxP] via sticky end ligation using the restriction enzymes *Not*I and *Sac*I. The resulting mini-targeting vector pHW025[5´arm-loxP-FRT-Neo-FRT-loxP-3´arm] (5642 bp) was linearized by the restriction enzymes *Xho*I and *Sac*I. The purified 5´arm-loxP-FRT-Neo-FRT-loxP-3´arm fragment (2768 bp) was then electroporated into heat shock induced DY380

bacteria which were before provided with the genomic subclone pDTA[Npr2-gSC] (12506 bp). The activated recombination proteins *exo*, *bet* and *gam* of the defective λ prophage promoted homologous recombination between exon 16 and exon 17. Sequence analysis confirmed the correctness of the genomic subclone which was then transformed into electro-competent EL350 bacteria. Cre-recombinase activity resulted then in the excision of the FRT-flanked neomycin cassette between the two directly orientated loxP sites leaving only one loxP site. The genetically modified genomic Npr2 subclone pDTA[Npr2-gSC-Cre(ex)-loxP1] (12609 bp) carrying the loxP1 site upstream of exon 17 was re-introduced into DY380 bacteria by electroporation for the next round of recombination.

5.1.4 Cloning of the second mini-targeting vector and recombination into the genomic subclone

Single cloning steps of the second mini-targeting vector and its recombination into the genomic subclone which carried already one *loxP* site upstream of exon 17 are illustrated in Figure 12. This vector was generated to enable the integration of a *FRT*-flanked neomycin cassette together with a 3´ *loxP* site between exon 18 and exon 19. The second mini-targeting vector was based on the pHW025 plasmid containing a *FRT*-flanked neomycin cassette surrounded by two *loxP* sites. This time the two homology arms corresponding to the genomic Npr2 DNA between exons 18 and 19 were placed between the 5´ *loxP* and *FRT* site and downstream of the 3´ *loxP* site. For that, two BAC amplification products were first cloned into the pBluescript II SK+ plasmid by blunt end ligation and afterwards subcloned into the pHW025 plasmid using sticky end restriction enzymes. After linearization, this second mini-targeting vector was integrated into the second genomic Npr2 subclone by homologous recombination mediated by the temperature-sensitive lambda Red recombination system of DY380 bacteria. Every ligation and recombination step was followed by antibiotic selection, control digestion and sequence verification. The conclusively created plasmid vector was used as targeting vector for blastocyst injection. The first targeting vector was composed of two homology regions covering Npr2 exon 13 up to exon 16 at the 5´ end and exon 19 up to exon 22 at the 3´ end. In addition to it, exon 17 and exon 18 were now flanked by two *loxP* sites and the *FRT*-flanked neomycin cassette was placed between exon 18 and the downstream *loxP* site.

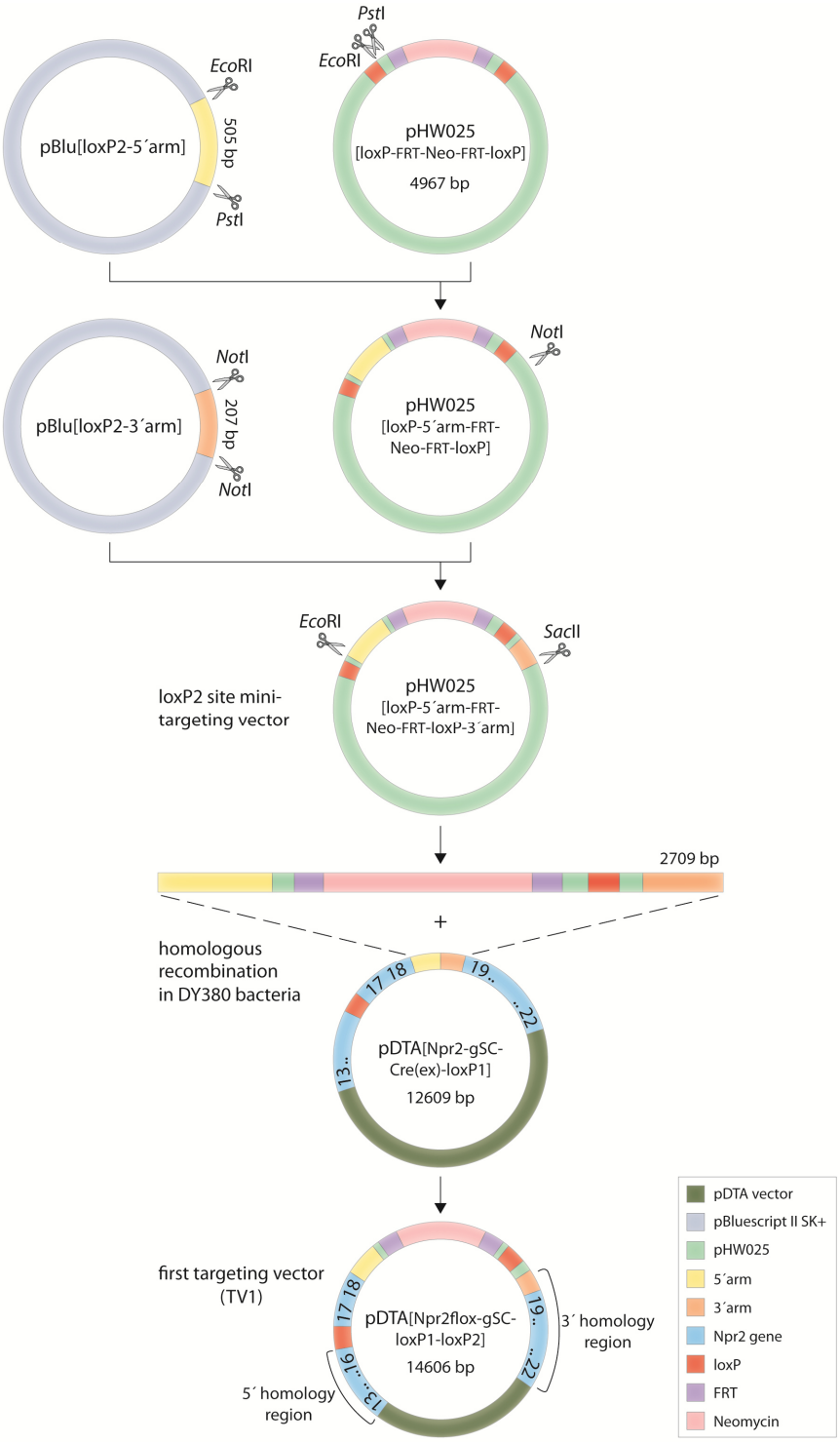

Figure 12: Cloning strategy for the second mini-targeting vector resulted in FRT-Neo-FRT-loxP2 site integration between Npr2 exon 18 and exon 19. The second mini-targeting vector based on the pHW025[loxP-FRT-Neo-FRT-loxP] plasmid which contains a FRT-flanked neomycin cassette flanked by two loxP sites. Here, the 5´ homology arm was cloned between the first loxP site and the FRT-flanked neomycin cassette, while the 3´ homology arm was placed behind the second loxP site in order to transfer this pHW025 plasmid fragment into the genomic Npr2 subclone. First, the 5´arm (505 bp) was subcloned by sticky end ligation using the cleavage sites of the restriction enzymes *Eco*RI and *Pst*I, followed by the insertion of the 3´arm (207 bp) into pHW025[loxP-5´arm-FRT-Neo-FRT-loxP] per sticky end ligation using

the restriction enzyme *Not*I. The resulting mini-targeting vector pHW025[loxP-5´arm-FRT-Neo-FRT-loxP-3´arm] (5673 bp) was linearized by the restriction enzymes *Eco*RI and *Sac*II. The purified 5´arm-FRT-Neo-FRT-loxP-3´arm fragment (2706 bp) was electroporated into heat shock induced DY380 bacteria which were provided with the priorly modified genomic Npr2 subclone pDTA[Npr2-gSC-Cre(ex)-loxP1] (12609 bp) carrying the loxP1 site upstream of exon 17. The activated recombination proteins *exo*, *bet* and *gam* of the defective λ prophage promote the homologous recombination between exon 18 and exon 19. The resulting pDTA[Npr2flox-gSC-loxP1-loxP2] plasmid (14606 bp) served as our first targeting vector used for embryonic stem cell electroporation after amplification in DH10B bacteria, sequence analysis and functional test of the recombination sites.

5.1.5 Functional test of the Flp-*FRT* and Cre-*loxP* recombination of the target vector

To test the functionality of *FRT* and *loxP* sites, the targeting vector was introduced into bacterial strains expressing either flippase or Cre-recombinase (Figure 13). The precise removal of the *FRT*-flanked neomycin cassette induced by flippase-mediated recombination between two identical *FRT* sites was monitored after transformation into EL250 bacteria which carry an arabinose-inducible *flpe* gene. Subsequently, efficient excision of the floxed sequence containing exons 17 and 18 was confirmed by transformation into the bacterial strain EL350 carrying an arabinose-inducible *cre* gene. Control digestions and DNA sequence analysis verified that recombination proceeds properly in both cases.

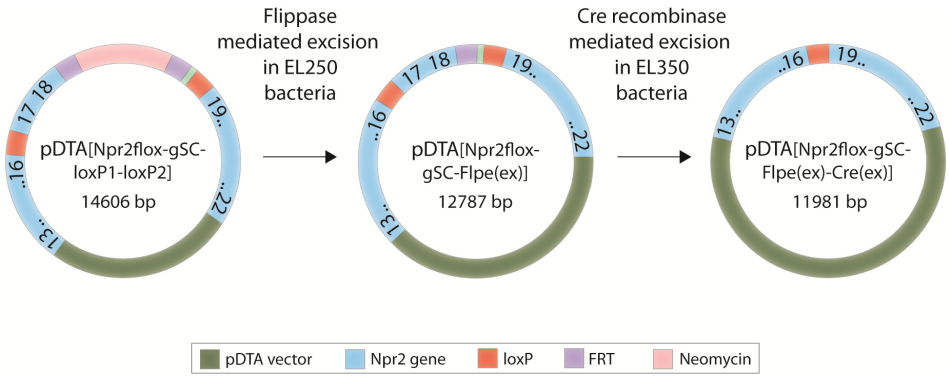

Figure 13: Functional test of the FRT and loxP recombination sites in appropriate bacterial strain systems. The first targeting vector pDTA[Npr2flox-gSC-loxP1-loxP2] (14606 bp) was transformed in EL250 bacteria containing the *flpe* gene. In EL250 bacteria, the expressed flippase protein mediated the recombination between the two identical FRT sites causing excision of the neomycin cassette and retention of one FRT site. The resultant pDTA[Npr2flox-gSC-Flpe(ex)] plasmid (12787 bp) was in turn electroporated into EL350 bacteria to monitor the accurate removal of the floxed exon 17 and exon 18 by the Cre/loxP system. Exon 16 is subsequently followed by exon 19 in the final recombinant genomic Npr2 subclone pDTA[Npr2flox-gSC-Flpe(ex)-Cre(ex)] (11981 bp). Restriction and sequence analysis verified the accuracy of the initiated recombinations.

5.1.6 Homologous recombination in embryonic stem (ES) cells

To generate ES cell clones which carry the engineered Npr2 allele, the Npr2-flox targeting vector was introduced into E14.1 ES cells by electroporation. Because of a higher genetic similarity with the genomic BAC clone DNA derived from 129S7/AB2.2 ES cells, the targeting vector was additionally electroporated into the ES cell line AB2.1. Before, the targeting vector was linearized by restriction enzyme *Pac*I producing an 11.7 kb fragment (Figure 14). Electroporated ES cells that had incorporated the targeting vector were positively selected with geneticin (G418) treatment. Correct and locus-specific insertion of the targeting vector into the genome of ES cell clones was identified via Southern blot analysis using two probes located outside the targeting vector and genomic DNA digested by restriction enzymes. The primary screen applying the 5´ probe detected only one positive clone out of 2016 tested E14.1 ES cell clones. Together with 384 negatively tested AB2.1 ES cell clones; this gave a recombination efficiency of 0.04 %. Later, a rescreen with 3´ probe and 5´ probe confirmed the accurate integration of the targeting vector into the ES cell genome (primary screen and rescreen of the positive ES clone are shown in Figure 14).

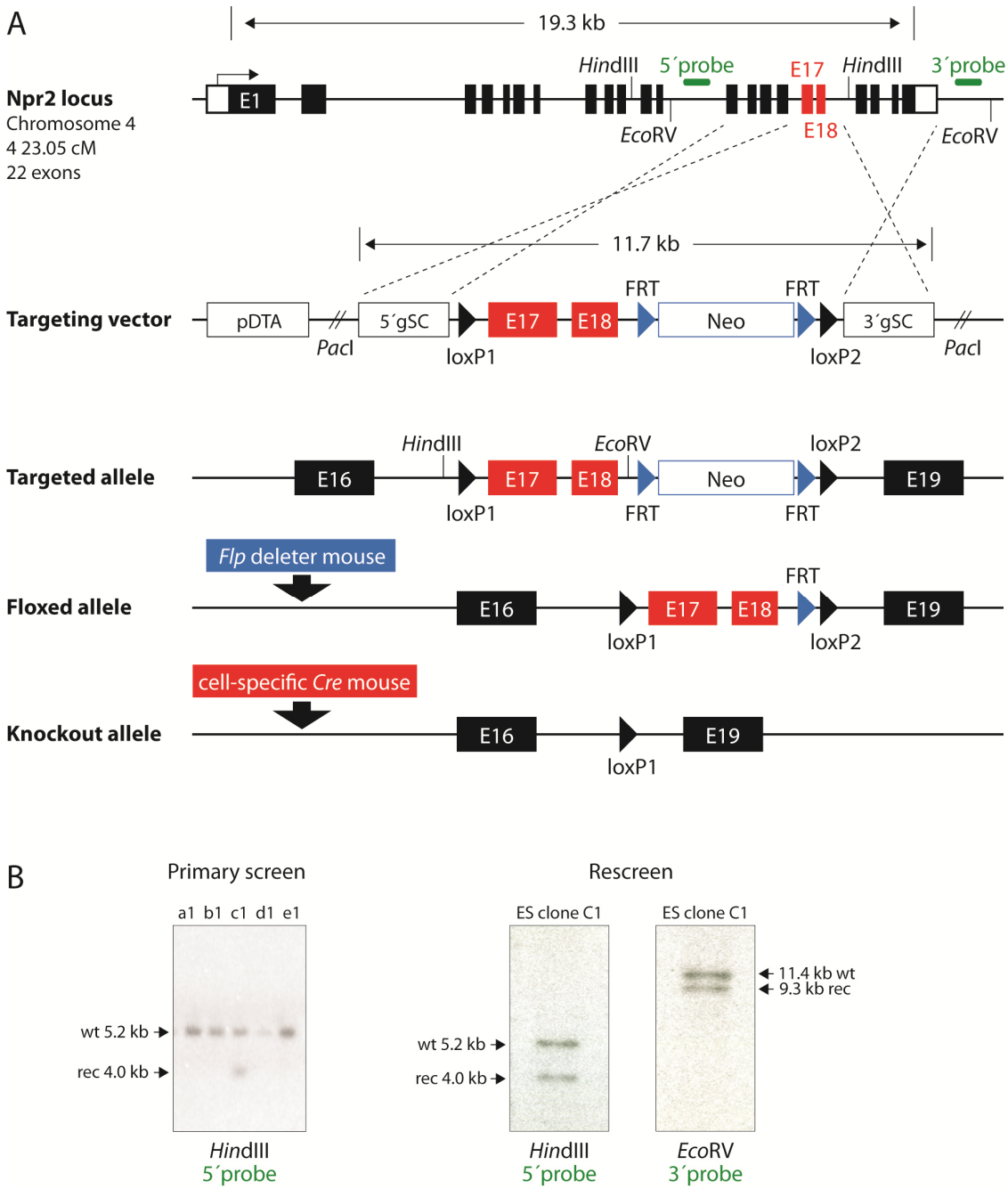

Figure 14: Strategy for the generation of the floxed Npr2 mouse model. (A) The illustration shows the targeting vector integration into the Npr2 locus by homologous recombination of the 5´ and 3´ homology regions. Before being introduced into ES cells, the targeting vector was linearized using restriction enzyme *Pac*I. Blastocyst injection with positive ES cell clone resulted in chimeric mice carrying the targeted allele. Crossbreeding with Flpe-deleter mice induced the excision of the neomycin selection cassette flanked by FRT sites presumed that the offspring was germline positive. The final floxed Npr2 allele features exon 17 and exon 18 surrounded by two loxP sites. The generation of the conditional Npr2 knockout mouse can now be induced by crossbreeding with a specific Cre-recombinase mouse line resulting in cell-specific lack of exon 17 and exon 18. (B) Confirmation of locus-specific homologous recombination by Southern blot analysis. The primary screen was performed with the external 5´ DNA probe to discriminate between wild-type (wt) and targeted Npr2 allele (rec) after *Hin*dIII digestion of genomic DNA. The novel *Hin*dIII restriction site introduced by the recombinant DNA of the targeting vector resulted in different sized fragment bands. ES clone C1 was the first clone out of 2400 screened ES clones which demonstrated the targeted Npr2 allele at 4 kb. The Southern blot rescreen confirmed the first result

of the 5´ DNA probe and verified the locus-specific recombination at the 3´ end in terms of the 3´ DNA probe and *Eco*RV digestion.

5.1.7 Blastocyst injection, chimera production and germline transmission

In order to produce chimeric mice, the confirmed positive ES cell clone was injected into C57Bl/6 blastocysts and implanted into pseudopregnant surrogate mother animals by the Transgene Core Facility of the Max Delbrück Center for Molecular Medicine (results shown in Table 10). Due to the 129/Ola background of E14.1 ES cells coding for white coat color, the generated male chimeras displayed patches of bright colored coat (Figure 15). To induce germline transmission of the targeted Npr2 allele and to simultaneously remove the *FRT*-flanked neomycin cassette, male chimeras were mated with Flpe-deleter females. Because this crossing was conducted with a mouse on another genetic background than C57Bl/6, the conventional coat color identification could not be used as selection criterion and only direct genomic DNA testing could clarify the positive germline transmission and *Neo* cassette excision. Two PCR based genotyping strategies were designed using primer constellations targeting the 5´ or 3´ *loxP* site to discriminate between wild-type and the floxed Npr2 allele by PCR (Figure 15). Four heterozygous germline positive animals were born and used to establish the floxed Npr2 mouse line. Figure 15 exemplarily illustrates genotyping results from wild-type, heterozygous and homozygous offspring.

ES cell line	targeting vector	# of tested ES cell clones	# of positive clones	# of surrogate mothers	offspring	# of chimeras (male)	germline transmission
E14.1	TV1 (11.7 kb)	2016	1	2	6	2	4 x
AB2.1	TV1 (11.7 kb)	384	0	-	-	-	-

Table 10: Generation process of the Npr2-flox transgenic mouse line. The number of ES cell clones tested by Southern blot analysis, the number of positive clones with homologous recombination, the number of pseudopregnant embryo recipients provided with injected blastocysts, the corresponding numbers of the entire offspring and male chimera after blastocyst injection and finally the number of positive germline transmission are presented for each ES cell line, individually.

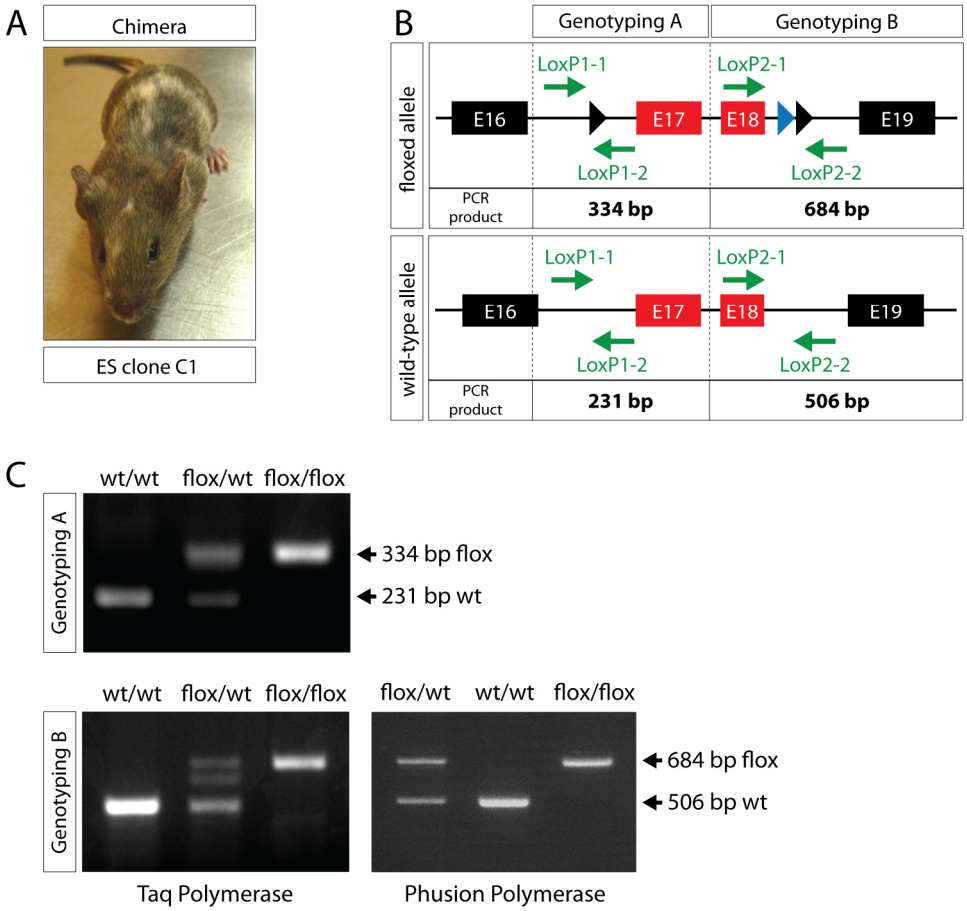

Figure 15: Genotyping strategy for the floxed Npr2 allele. (A) Photograph of chimeric male mouse which generated germline positive offspring based on ES cell clone C1. (B) The scheme illustrates the two strategies used for genotyping (A and B) with particular primer constellation for the floxed Npr2 allele and the Npr2 wild-type allele. Genotyping approach A utilizes the 5´ loxP site (loxP1) resulting in a wild-type band of 231 bp and a transgenic band of 334 bp. The two primers of genotyping reaction B bind next to the 3´ loxP site (loxP2) and the remaining FRT site resulting in a wild-type band of 506 bp and a transgenic band of 684 bp. (C) Exemplary results of PCR-genotyping reactions from animals which are wild-type, heterozygous or homozygous for the Npr2-flox allele. A double band periodically appeared for the floxed Npr2 allele (see the heterozygous genotype in genotyping B using Taq polymerase). DNA sequence analysis revealed the lower band as a fragmentary piece of the correct sequence. The usage of a proof-reading polymerase such as Phusion polymerase entirely prevented the occurrence of a double band.

5.1.8 A hypomorphic splice site mutation in the first generated Npr2-flox mouse line affects bone growth

Animals which carried the floxed Npr2 allele in combination with an allele of the conventional Npr2 knockout developed the abnormal bone growth phenotype as observed previously in constitutive Npr2 knockout mice. This unambiguous bone phenotype led to the assumption that the floxed Npr2 allele, instead of expressing the wild-type Npr2 protein, operates as Npr2 knockout allele. Detailed genomic DNA sequence analysis of the floxed Npr2 allele revealed two single point mutations at the end of exon 17 and the beginning of exon 18 (Figure 16). Both point mutations were silent mutations causing no alteration of the amino acid sequence. Since the functionality of Npr2 was not affected by an amino acid exchange, the general transcriptional regulation and the modification of the emerging pre-messenger RNA were tested for any deviation from the wild-type. For this purpose, a RT-PCR strategy was designed which amplified PCR products covering the processed Npr2 mRNA from exon 13 to exon 22 (Figure 16). mRNA isolated from liver tissue was transcribed into complementary DNA. The comparison of wild-type, heterozygous and homozygous Npr2-flox mice revealed an mRNA splicing defect leading to a smaller sized mRNA transcript. DNA sequence analysis demonstrated the complete absence of exon 18 in the smaller fragment. In addition, quantification of the RT-PCR results illustrated that heterozygous Npr2-flox$^{wt/flox}$ mice express 72 % of wild-type mRNA and 28 % of Npr2Δexon18 mRNA while homozygous Npr2-flox$^{flox/flox}$ mice express still 15 % of wild-type mRNA and 85 % of Npr2Δexon18 mRNA. This implies that the splice site mutation which caused a non-functional splice variant of Npr2 has an incomplete penetrance. The result was a hypomorphic Npr2 loss-of-function where the function of the *Npr2* gene was reduced but not completely lost. The first generated Npr2-flox mouse line containing the splice site mutation was termed Npr2-flox(1). Due to a lack of high quality antibodies to Npr2, a decreased level of Npr2 protein in the Npr2-flox(1) mouse could not be demonstrated.

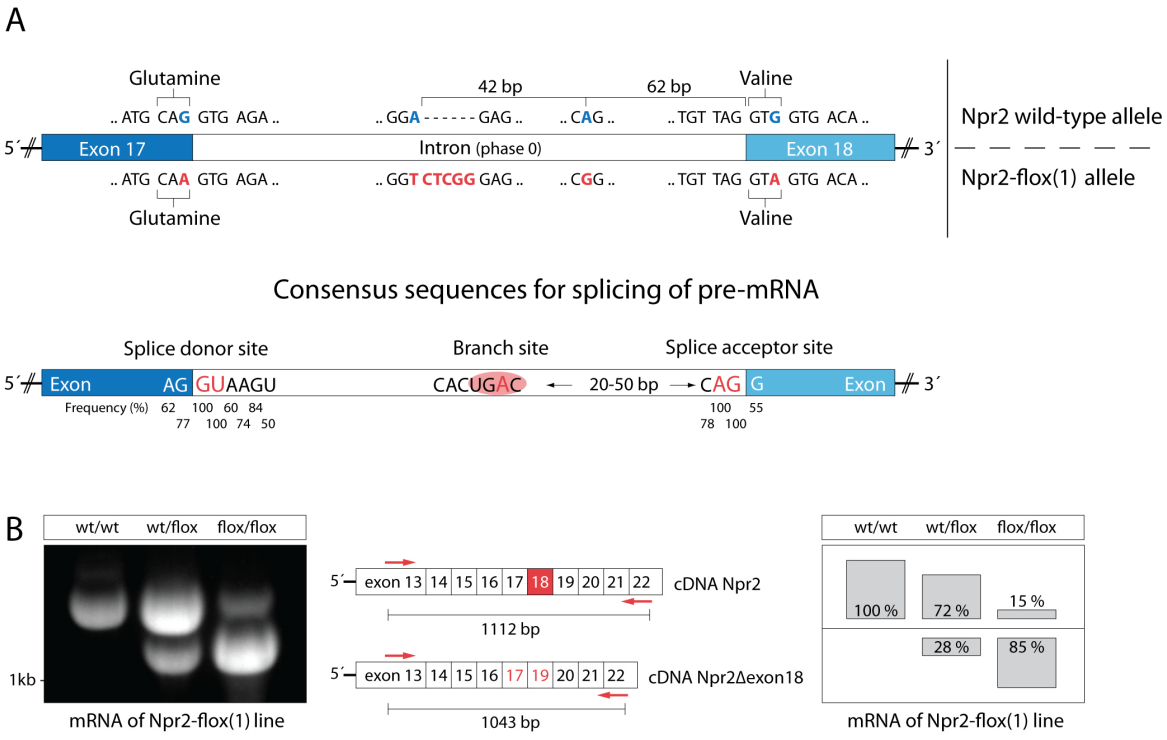
A
Glutamine
42 bp
62 bp
Valine
.. ATG CAG GTG AGA ..
.. GGA - - - - - GAG ..
.. CAG ..
.. TGT TAG GTG GTG ACA ..
5´
Exon 17
Intron (phase 0)
Exon 18
3´
Npr2 wild-type allele
.. ATG CAA GTG AGA ..
.. GGT CTCGG GAG ..
.. CGG ..
.. TGT TAG GTA GTG ACA ..
Npr2-flox(1) allele
Glutamine
Valine
Consensus sequences for splicing of pre-mRNA
Splice donor site
Branch site
Splice acceptor site
5´
Exon
AG GUAAGU
CACUGAC
20-50 bp
CAG G
Exon
3´
Frequency (%) 62 100 60 84
77 100 74 50
100 55
78 100
B
wt/wt wt/flox flox/flox
1kb
mRNA of Npr2-flox(1) line
5´
exon 13 14 15 16 17 18 19 20 21 22
cDNA Npr2
1112 bp
5´
exon 13 14 15 16 17 19 20 21 22
cDNA Npr2Δexon18
1043 bp
wt/wt wt/flox flox/flox
100 %
72 %
15 %
28 %
85 %
mRNA of Npr2-flox(1) line
C
Splice site mutation in the hypomorphic Npr2-flox(1) mouse line
5´
GU
A
AG GTA
GU
A
AG GTG
3´
Exon 17
Intron 17
Exon 18
Intron 18
Exon 19
The spliceosome B-complex recognizes the defined splice acceptor site
U1
U4
U6
U2
U5
UG
A
AG
Exon 17
Exon 18
A
17
18
19
Spliced exons
15 %
of processed Npr2 mRNA
5´
GU
A
AG GTA
GU
A
AG GTG
3´
Exon 17
Intron 17
Exon 18
Intron 18
Exon 19
The spliceosome B-complex skips the defined splice acceptor site
U1
U4
U6
U2
U5
UG
A
AG
Exon 17
Exon 19
Exon 18
FRT
loxP2
A
17
19
Mis-spliced exons
85 %
of processed Npr2 mRNA

Figure 16: Sequence analysis of genomic DNA revealed two silent point mutations as possible reason for the bone phenotype attested in the first generated Npr2-flox(1) mouse line. (A) Sequence analysis of the genomic DNA of the Npr2-flox(1) allele revealed two new silent point mutations at the border of exon 17 and exon 18. Already known point mutation and multiple nucleotide insertion in the intron derived from the BAC clone DNA template are also highlighted (nucleotide mutations are shown in red). Comparison with the consensus sequence of pre-mRNA splicing demonstrates that the key nucleotides of both splice sites and the branch site are unmodified. However, the G→A exchange at the end of exon 17, where Guanine is conserved in 77 % of all cases, mutates the consensus sequence of the splice donor site (Nissim-Rafinia and Kerem, 2002). (B) Agarose gel electrophoresis displays the diversification of Npr2 pre-mRNA splicing by reference to cDNA amplification. The RT-PCR was performed using cDNAs as templates which were reverse transcribed from mRNA purified from the livers of wild-type, heterozygous or homozygous littermates. Opposed oligonucleotides were placed in exon 13 and exon 22 for PCR amplification. DNA sequence analysis revealed that the smaller band lacks the sequence for exon 18, whereas the upper band corresponds to the wild-type open reading frame of Npr2. Both mRNA variants were expressed by animals of either heterozygous or homozygous genotype. The quantification of the RT-PCR illustrates the ratio between the wild-type mRNA and the Npr2Δexon18 mRNA. The recombinant Npr2 allele, which obviously contains a splice site mutation, can still express 15 % of wild-type Npr2 mRNA. (C) Hypothetical model for induced alternative splicing in the Npr2-flox(1) allele. In 15 % of the cases the spliceosome B-complex recognizes the determined splice acceptor site at the border of exon 18 inducing the lariat formation between splice donor site and branch site and resulting in accurate excision of the intermediary intron. The same molecular mechanism works for the next exon-intron border leading to proper exon concatenation. In 85 % of the cases the spliceosome B-complex skips the determined splice acceptor site at the border of exon 18 caused by the G→A point mutation. Instead the spliceosome recognizes the subsequent splice acceptor site at the border of exon 19 inducing a lariat formation which includes exon 18 and both flanking introns leading to the mis-spliced exon concatenation revealed by DNA sequence analysis.

Since the strict consensus sequences of the splice donor, acceptor and branch sites were not affected by the single point mutations, the question of the causal relationship could be clarified only hypothetically. In 85 percent of the cases, the spliceosome misrecognized and skipped the splice acceptor site at the beginning of exon 18 due to the point mutation of the third nucleotide causing exon 18 to be part of a newly emerging intron between exon 17 and exon 19. The hypothetical mRNA splicing model of the Npr2-flox(1) allele is illustrated in Figure 16. The loss of exon 18 in 85 % of the expressed Npr2 mRNA severely affected the process of chondral ossification. Mice with the Npr2-flox(1)$^{flox/flox}$ genotype suffer from dwarfism characterized by a decrease in tail length, body size and weight combined with hydrocephaly and short snout (Figure 17). The observed bone phenotype symptomatically corresponds to the bone phenotypes already described for several Npr2 loss-of-function mutations. Besides dwarfism, homozygous mice suffer from premature mortality causing the early death before weaning of approximately 50 percent of the newborn animals. Furthermore, only 57 % of homozygous females were fertile and the average litter size was significantly reduced to 4 pups per litter (Figure 26).

Figure 17: Bone phenotype attested in our first Npr2-flox mouse line. The size comparison shows two male littermates at postnatal day 35. The underdeveloped Npr2-flox(1)$^{flox/flox}$ mouse reveals a stumpy tail and reduced body length in relation to the Npr2-flox(1)$^{(wt/wt)}$ sibling. The shortened tail measures only 60 % and the body 80 % of the wild-type control. The Npr2-flox(1)$^{flox/flox}$ mouse suffers from the bone phenotype that is based on dysfunctional chondrocyte ossification and which is already described for multiple Npr2 loss-of-function mutations.

5.1.9 Axon bifurcation at the dorsal root entry zone of the hypomorphic Npr2-flox(1) mouse is not impaired

Cross-breeding with the Thy1-YFP-H mouse reporter line enabled the visualization of axonal outgrowth in only a small number of sensory neurons by the transgenic expression of yellow fluorescence protein under control of the *Thy1* promoter. Dissections of Npr2-flox(1)$^{flox/flox}$;Thy1-YFP-H^{+} mice at several postnatal stages uniformly demonstrated unmodified axon bifurcation (Figure 18). Despite the fact that mice homozygous for the Npr2-flox(1) allele displayed abnormal bone growth, the axonal bifurcation of sensory neurons at the dorsal root entry zone was not affected. Considering that 15 % of expressed wild-type mRNA was sufficient for the proper axon bifurcation, conditional Npr2 knockout mutants were generated using cell- and stage-specific Cre mouse lines in order to prevent axon bifurcation. For this purpose, the DRG-specific expression of Cre-recombinase promoted by the Isl1-Cre or Wnt1-Cre mouse line at early embryonic stages were combined with the homozygous hypomorphic Npr2-flox(1) allele. The Npr2-flox(1)$^{flox/flox}$;Thy1-YFP-H^{+};Isl1-Cre^{+} mice exhibited no

neuroanatomical abnormality with respect to axon bifurcation (Figure 18). In contrast, conditional inactivation of Npr2 using the Wnt1-Cre driver mouse line which also expresses Cre-recombinase in sensory neurons at early embryonic stages caused impaired bifurcation (Figure 19). The removal of *loxP*-flanked exons 17 and 18 mediated by the Cre-recombinase in Npr2-flox(1)$^{flox/flox}$;Thy1-YFP-H^{+};Wnt1-Cre^{+} transformed the hypomorphic floxed allele into a complete knockout allele. As a result, all axons of the sensory neurons turned either in rostral or caudal direction at the dorsal root entry zone. Using the Wnt1-Cre driver mouse it was possible to induce the lack of axon bifurcation in the Npr2-flox(1) mouse indicating that the Cre-*loxP* mediated inactivation of Npr2 from the floxed Npr2 allele works.

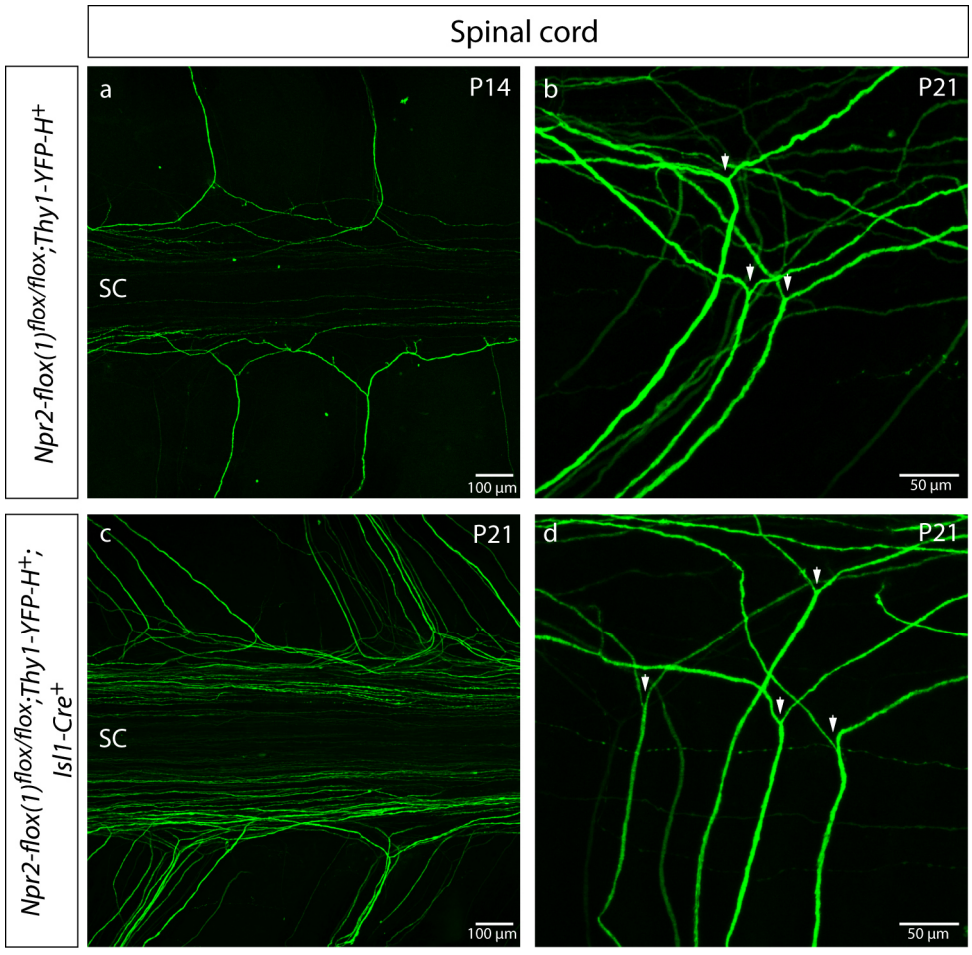

Figure 18: Unmodified axon bifurcation at the dorsal root entry zone in homozygous Npr2-flox(1)$^{flox/flox}$ mice and Npr2-flox(1)$^{flox/flox}$ mice expressing Cre-recombinase regulated by *Isl1* promoter. Crossbreeding with the Thy1-YFP-H mouse line made it possible to visualize axonal outgrowth of individual sensory neurons. YFP (Yellow Fluorescent Protein) is expressed at high levels in motor and sensory neurons. Approximately 10 to 30 % of sensory neurons are labeled in the dorsal root ganglia (Feng et al., 2000). Experimental animals were dissected at postnatal day 14 or 21. All pictures are Z-stack images obtained by confocal microscopy showing the spinal cord and attached DRGs from a dorsal view. (a) Four sensory

neurons bifurcate at dorsal root entry zone of the spinal cord (SC). (b) Close-up view displays bifurcation (white arrows) of several sensory neurons deriving from the same DRG. (c, d) The Npr2-flox(1)$^{flox/flox}$;Isl1-Cre^{+} genotype demonstrated regular axon bifurcation of sensory neurons such as the Npr2-flox(1)$^{flox/flox}$ genotype.

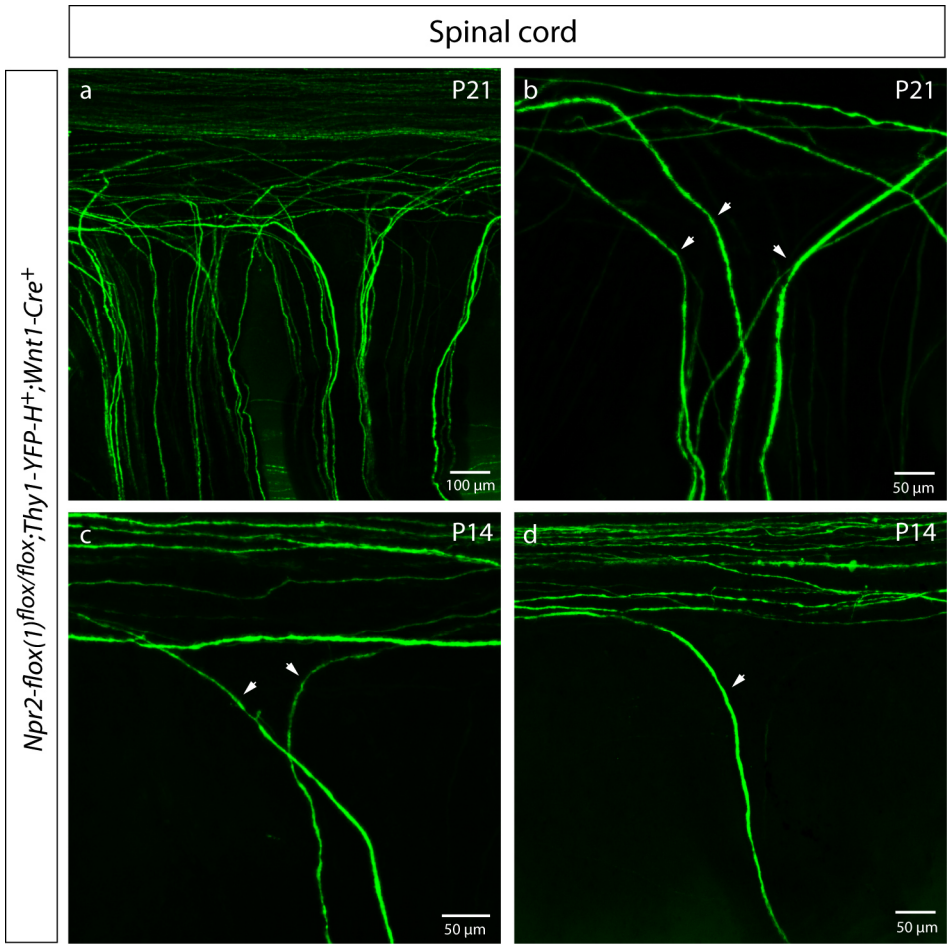

Figure 19: Impaired axon bifurcation at the dorsal root entry zone in homozygous Npr2-flox(1) mice expressing Cre-recombinase under control of *Wnt1* promoter. Crossbreeding with the Thy1-YFP-H mouse line made it possible to visualize axonal outgrowth of individual sensory neurons. Mice were dissected at postnatal day 14 or 21. Z-stack images were obtained by confocal microscope showing sensory neurons entering the dorsal root entry zone from a dorsal view. (a) Unilateral image of sensory neurons which turn either in caudal or rostral direction after entering the DREZ. (b, c, d) Close-up view of non-bifurcating sensory axons. The assumed points of axonal bifurcation are indicated by white arrows.

5.1.10 Second attempt for the generation of a floxed Npr2 allele

Because the hypomorphic Npr2-flox(1) mouse carrying the splice site mutation did not meet the expectations, a second attempt was made to produce an errorless floxed Npr2 mouse line. In addition, the first targeting vector was recloned and modified to improve the extremely inefficient recombination rate of the previous homologous recombination in embryonic stem cells. The cloning strategy for the second targeting vector is illustrated in Figure 20. In brief, the first targeting vector was provided with a new 5´ homology arm containing exon 8 of Npr2. After homologous recombination with the genomic subclone, the second targeting vector possessed a larger 5´ homology region extended by 3324 bp. The temperature-sensitive lambda Red recombination system of DY380 bacteria was again utilized to induce the homologous recombination. Every ligation and recombination step was followed by antibiotic selection, control digestion and sequence analysis. The extended targeting vector fragment used for ES electroporation measured 15 kb instead of 11.7 kb and it revealed an enhanced recombination rate of approximately 7 % on average during the upcoming ES cell recombinations.

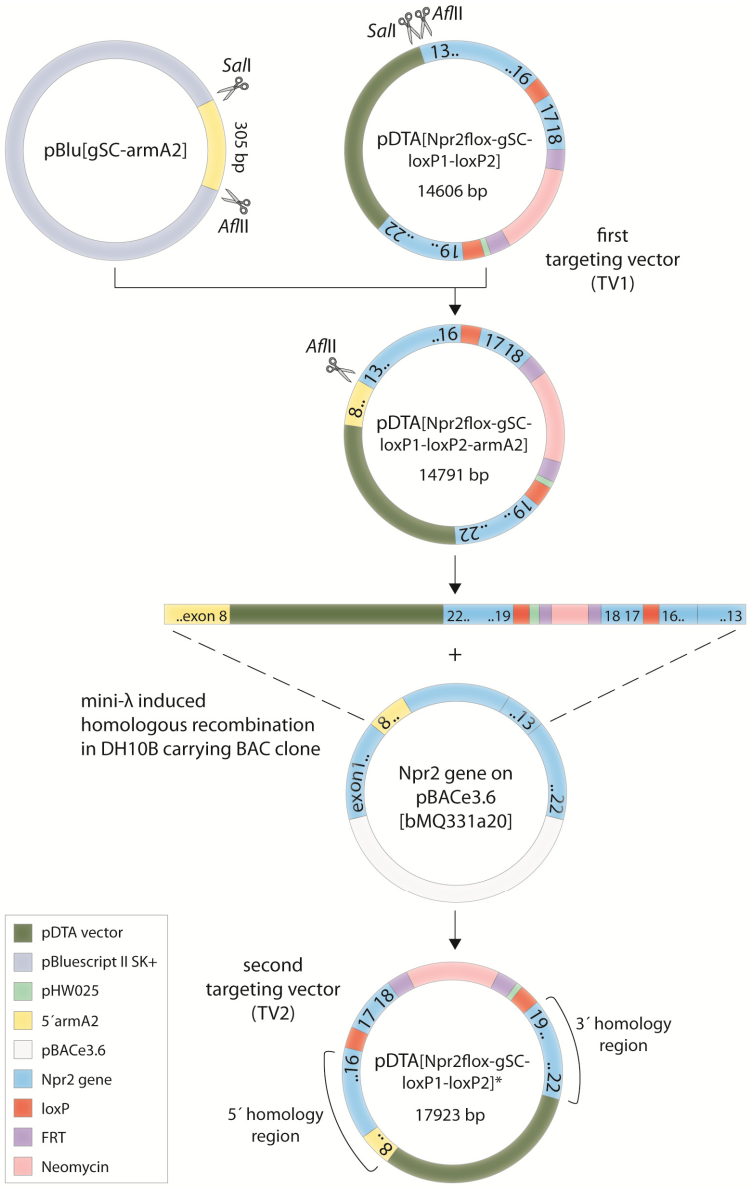

Figure 20: Cloning strategy for an extended targeting floxed Npr2 vector. Since the recombination rate of the first targeting vector pDTA[Npr2flox-gSC-loxP1-loxP2] (14606 bp) in embryonic stem cells emerged to be insufficient, the extension of the 5´ homology region causing a general vector enlargement was designed to improve the recombination performance. After linearization by the restriction enzyme *Pac*I, the first targeting vector in total measured 11678 bp containing a 1676 bp long 5´ homology region and a 6147 bp long 3´ homology region for homologous recombination into the genome of ES cells. A further upstream localized 5´ homology arm (arm A2) targeting exon 8 was subcloned in front of exon 13 with the aid of restriction enzymes *Sal*I and *Afl*II. The in this way modified first targeting vector pDTA[Npr2flox-gSC-loxP1-loxP2-armA2] was linearized by *Afl*II and subsequently electroporated into DH10B bacteria carrying the Npr2 BAC clone as well as the mini-λ recombination system. The induced homologous recombination created the second targeting vector pDTA[Npr2flox-gSC-loxP1-loxP2]* (17923 bp) which exhibits a prolonged 5´ homology region spanning from exon 8 to exon 16. After linearization by *Pac*I, the second targeting vector in total measured 14995 bp containing a 4999 bp long 5´ homology region and the same 6147 bp long 3´ homology region as before. The application of the second targeting vector actually enhanced the recombination rate significantly. While only 0.04 % of ES clones, which were transformed with the first targeting vector, were screened to be positive, the second targeting vector was capable to obtain a recombination rate of about 7 % at an average.

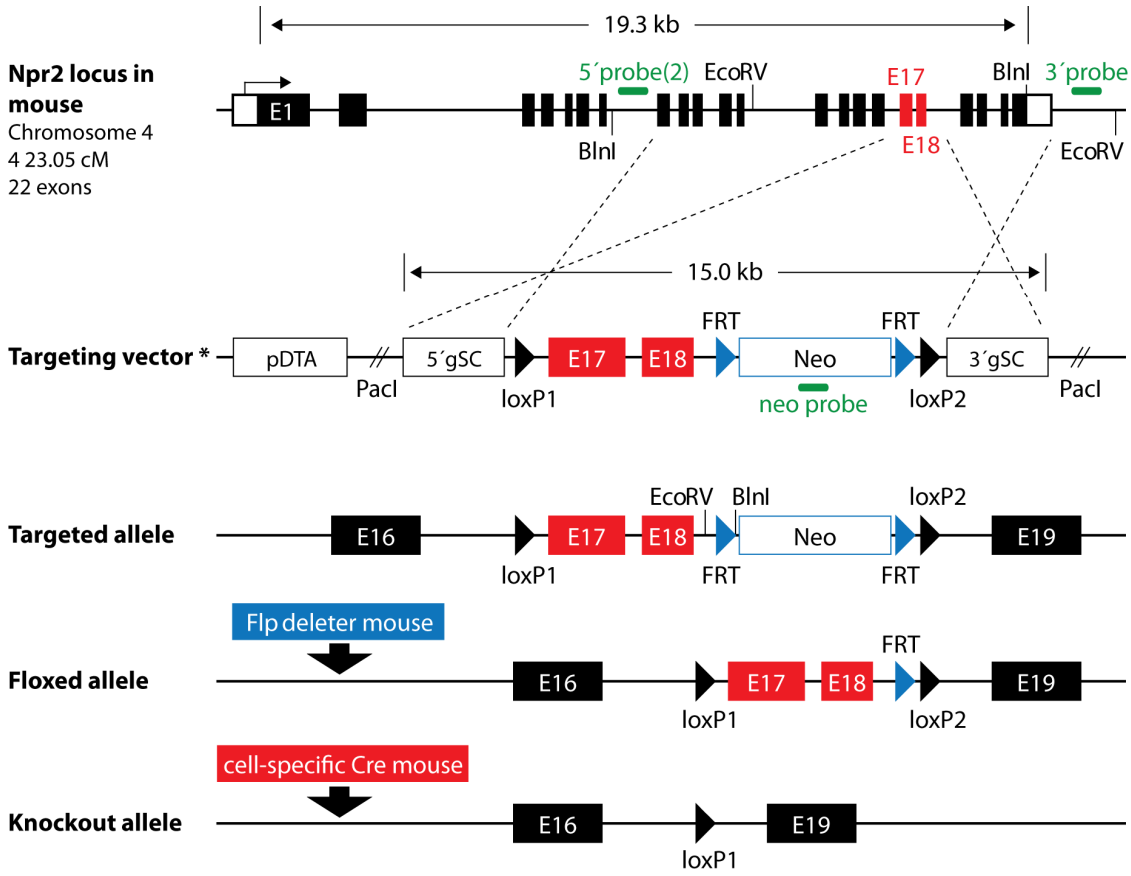

Figure 21: Strategy for generation of the Npr2-flox mouse line applying the extended Npr2 gene targeting vector 2 (TV2). The illustration shows the targeting vector integration into the Npr2 locus via homologous recombination of the extended 5´ homology and unmodified 3´ homology region. The Southern blot analysis of locus-specific recombination at the 5´ region was adjusted using 5´ DNA probe(2) and restriction enzyme *Bln*I. Flippase activity in the transgenic animal results in the floxed Npr2 allele. Cell-specific Cre-recombinase activity mediated by distinct Cre driver mouse lines leads to the conditional Npr2 knockout allele.

5.1.11 Homologous recombination in R1 and SV129$_{(TCF)}$ ES cell lines

Four attempts of blastocyst injection using positive E14.1 ES cell clones resulted neither in reproductive chimeric mice nor germline transmission. Since an increased number of independent ES cell projects at our institute experienced difficulties using the E14.1 ES cell line efficiently, two new ES cell lines, R1 and SV129$_{(TCF)}$, were cultivated for targeting vector electroporation. It was hoped that the usage of new ES cell lines could promote the germline transmission efficiency. The R1 cell line which is derived from F1 hybrid embryos after 129X1/SvJ x 129S1 mouse strain crossing was already scientifically established and commercially available. The SV129$_{(TCF)}$ cell line was exclusively produced by the Transgene Core Facility (TCF) of the Max Delbrück Center for Molecular Medicine. The source of the SV129$_{(TCF)}$ cell line were embryonic stem cells obtained from F1 hybrid

embryos after mating between C57BL/6NCrl males and 129s2/SvPasCrl females (both mouse lines originated from Charles River). Before electroporation, the second targeting vector was linearized with restriction enzyme *Pac*I producing a 15 kb fragment. The general genetic strategy for the floxed Npr2 mouse generation was the same as in the previous attempt. Only the detection strategy of the Southern blot analysis to verify the correct homologous recombination was adjusted due to the prolongation of the 5´ homology region from exon 13 to exon 8 of the genomic Npr2 DNA (Figure 21). ES cells that had inserted the targeting vector were positively selected with geneticin (G418) treatment. The primary screen using the external 5´ DNA probe(2) in combination with *Bln*I digestion detected 19 primary positive clones out of 248 tested R1 ES cell clones and 9 primary positive clones out of 136 tested $SV129_{(TCF)}$ ES cell clones. Twelve ES cell clones were selected and further tested for the correct locus-specific homologous recombination of the targeting vector. In addition to Southern blot analysis, two PCR strategies were designed as an alternative proof of positive homologous recombination. This was necessary because of reappearing technical issues with the Southern blot method. In this way, two positive ES cell clones for each cell line were strongly confirmed and subsequently injected into blastocysts. The presented results only account the two ES cell clones which finally led to germline transmission. The primary screens of both clones showed the recombinant band at 7.3 kb and the positive rescreen with the *neo* probe indicated no multi-insertion (Figure 22). Triplex PCR was used to verify the general presence of the targeted Npr2 allele and proved the heterozygous genotype of both ES cell clones (Figure 22). A long-range PCR was specifically designed to confirm the locus-specific homologous recombination of the targeting vector by using an external reverse primer in combination with an internal forward primer binding within the neomycin cassette of the targeted Npr2 allele. The DNA band at 7000 bp which was amplified for both ES cell clones demonstrated the accurate locus-specific vector integration (Figure 22). Conclusively, the absence of splice site mutations and sequence accuracy was verified via complete DNA sequence analysis.

5.1.12 Blastocyst injection, chimera production and germline transmission based on R1 and SV129$_{(TCF)}$ ES cell lines

In order to produce chimeric mice, the two positive ES cell clones were separately injected into multiple C57Bl/6 blastocysts and implanted into pseudopregnant surrogate mothers by the Transgene Core Facility (results shown in Table 11). The blastocyst implantations of the R1 ES cell clone produced eleven male chimeras whereas only two male chimeras were born after applying the SV129$_{(TCF)}$ ES cell clone. The male chimeras were directly mated with Flpe-deleter females to induce germline transmission and eliminate the *FRT*-flanked neomycin cassette. PCR genotyping of the entire offspring was performed to clarify positive germline transmission and *Neo* cassette excision. In summary, 7 % of the F1 generation based on the R1 clone and 34 % of the F1 generation derived from the SV129$_{(TCF)}$ clone were germline positive. In the process, only one animal of the germline positive progeny missed the flippase induced *Neo* cassette excision. Genomic DNA and complementary DNA obtained from liver tissue of heterozygous F1 generation mice with either R1 or SV129 genetic background were successfully tested for errorless DNA sequence and correct pre-mRNA splicing (data not shown). The F1 generation derived from the SV129$_{(TCF)}$ ES cell clone was chiefly used for the establishing of the transgenic mouse line during further breeding. The mouse line originated from the R1 clone was instead kept as backup offering an independent genetic background. At the same time, both floxed Npr2 mouse strains were back-crossed with C57BL/6N mice in order to achieve a pure genetic background. Currently, the backcrossing has reached the F5 generation and will ideally be continued until F10 generation.

ES cell line	targeting vector	# of tested ES cell clones	# of positive clones	# of surrogate mothers	offspring	# of chimeras (male)	germline transmission
R1	TV2 (15 kb)	248	19	2	20	11	7 x
SV129 (TCF)	TV2 (15 kb)	136	9	2	4	2	18 x

Table 11: Generation of the floxed Npr2 mouse line using ES cell line R1 and SV129$_{(TCF)}$. The number of ES cell clones tested by Southern blot analysis, the number of positive clones with correct homologous recombination, the number of surrogate mother animals used for blastocyst injection, the number of the offspring and male chimera, and the number of positive germline transmission are represented for each ES cell line.

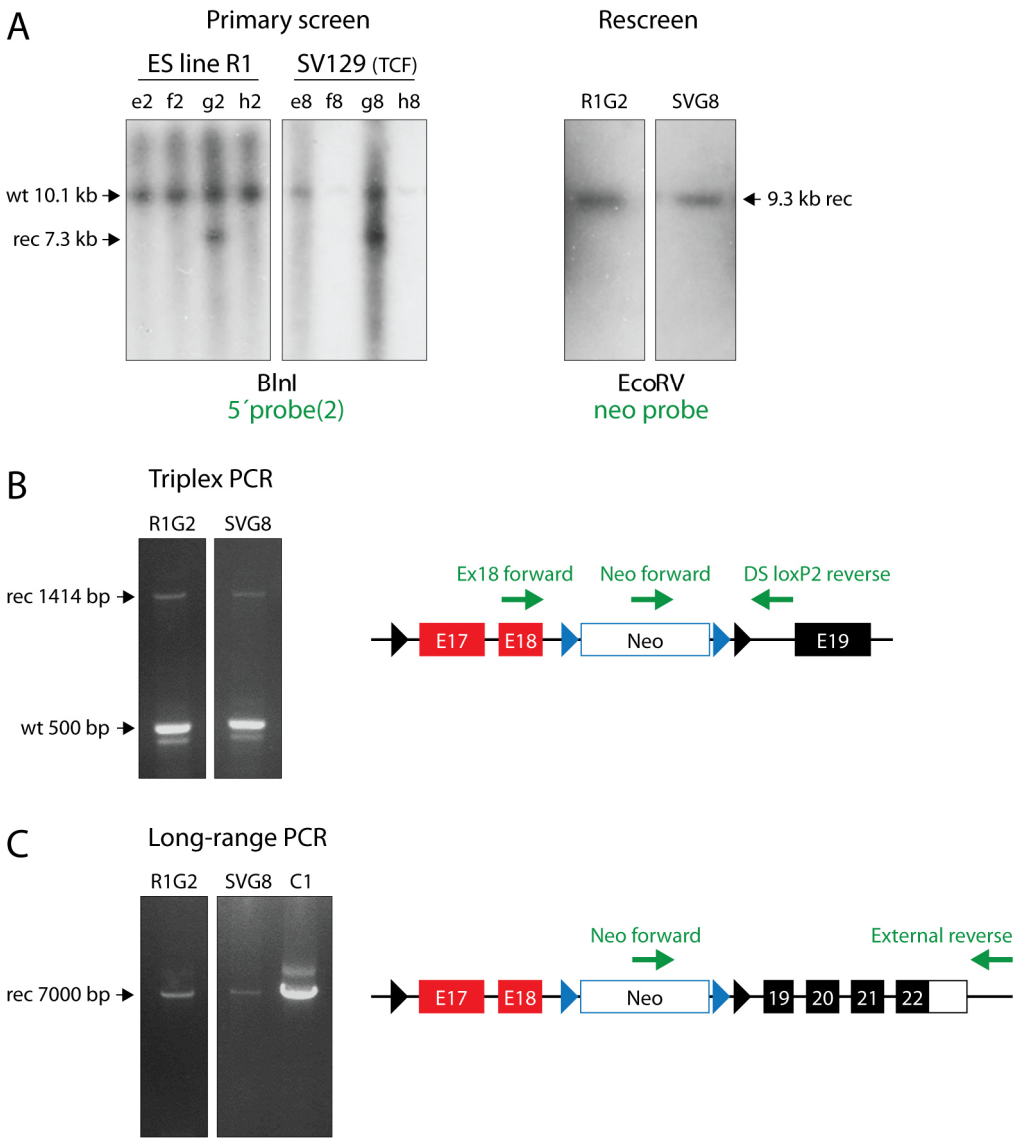

Figure 22: Verification of recombinant ES cell clones through Southern blot analysis, triplex PCR and long-range PCR for the embryonic stem cell line R1 and SV129(TCF). The depicted results represent only the two ES cell clones (R1G2 and SVG8) which were used for blastocyst injection. (A) The primary Southern blot screens applying 5´ probe(2) in combination with *Bln*I digestion revealed a band at 7.3 kb for around 7 % of the screened embryonic stem cell clones. Re-screens were done with the *neo* probe detecting the neomycin cassette upon *Eco*RV digestion. The band at 9.3 kb proved the integration of the targeting vector. (B) The triplex PCR (binding strategy of the oligonucleotides shown in the graph) confirmed the heterozygous genotype of both ES cell clones. Primer Ex18-forward and DSloxP2-reverse amplified a 500 base pairs piece of DNA in case of the Npr2 wild-type allele. Parallel, primer Neo-forward and DSloxP2-reverse revealed a band at 1414 bp. (C) The long-range PCR was performed to certify the locus-specific recombination. Primer "External-reverse" was designed to bind outside of the homologous recombination region of the targeted Npr2 allele. Primer "External-reverse" and "Neo-forward" produce a 7000 bp DNA band in case of the recombinant allele. ES cell clones R1G2 and SVG8 demonstrated correct genomic localization of the recombinant DNA. ES cell clone C1 was used as positive control; recombinant (rec); wild-type (wt).

5.1.13 Prevention of the bone phenotype in the Npr2-flox mouse line

The first litter of the new floxed Npr2 mouse strain consisting of wild-type, heterozygous and homozygous littermates showed no noticeable divergences related to body size, body weight or tail length. Especially, the absence of abnormal bone growth in homozygous Npr2-flox(2) mice provided clear indication of an unmodified and fully functional natriuretic peptide receptor 2 expressed by the floxed Npr2 allele. Figure 24 representatively illustrates the size comparison between a homozygous floxed Npr2 mutant and a wild-type littermate at postnatal stage 40. Long-term body size and body weight recording of several genotypes was carried out to verify whether the floxed Npr2 allele affects the chondral ossification or the physical development in general (Figure 23). Simultaneously, the influence of the Wnt1-Cre induced conditional Npr2 knockout allele was tested for potential physical changes. Homozygous mice of the hypomorphic Npr2 mouse strain, Npr2-flox(1)$^{flox/flox}$, were included in the study as control for the bone growth phenotype caused by the Npr2 loss-of-function. All mice were measured on a five day basis starting at postnatal day one and over a period of 70 days. Female and male mice were separately analyzed. The study demonstrated similar increases in body size and body weight for wild-type, heterozygous and homozygous Npr2-flox(2) mice irrespective of whether carrying the Wnt1-Cre allele or not. Figure 25 exemplarily illustrates that neither the homozygous Npr2-flox(2) mouse nor the Wnt1-Cre induced Npr2-cKO mouse suffered from dwarfism which was demonstrated by size comparison with Npr2 wild-type and Npr2 null mice. The growth delay of hypomorphic Npr2 mouse mutants which was manifested after the third postnatal week resulted in a final body size reduction of 20 % and a body weight reduction of 30 % on average demonstrating an increase in body size in relation to the global Npr2 Knockouts, which measure approximately 60 % of wild-type body size (Tamura et al., 2004). In particular, the contrast between hypomorphic Npr2-flox(1)$^{flox/flox}$ mutants and Npr2-flox(2)$^{flox/flox}$ mice confirmed that the new floxed Npr2 mouse model did not result in a dwarfed phenotype. No gender-specific discrimination was recorded.

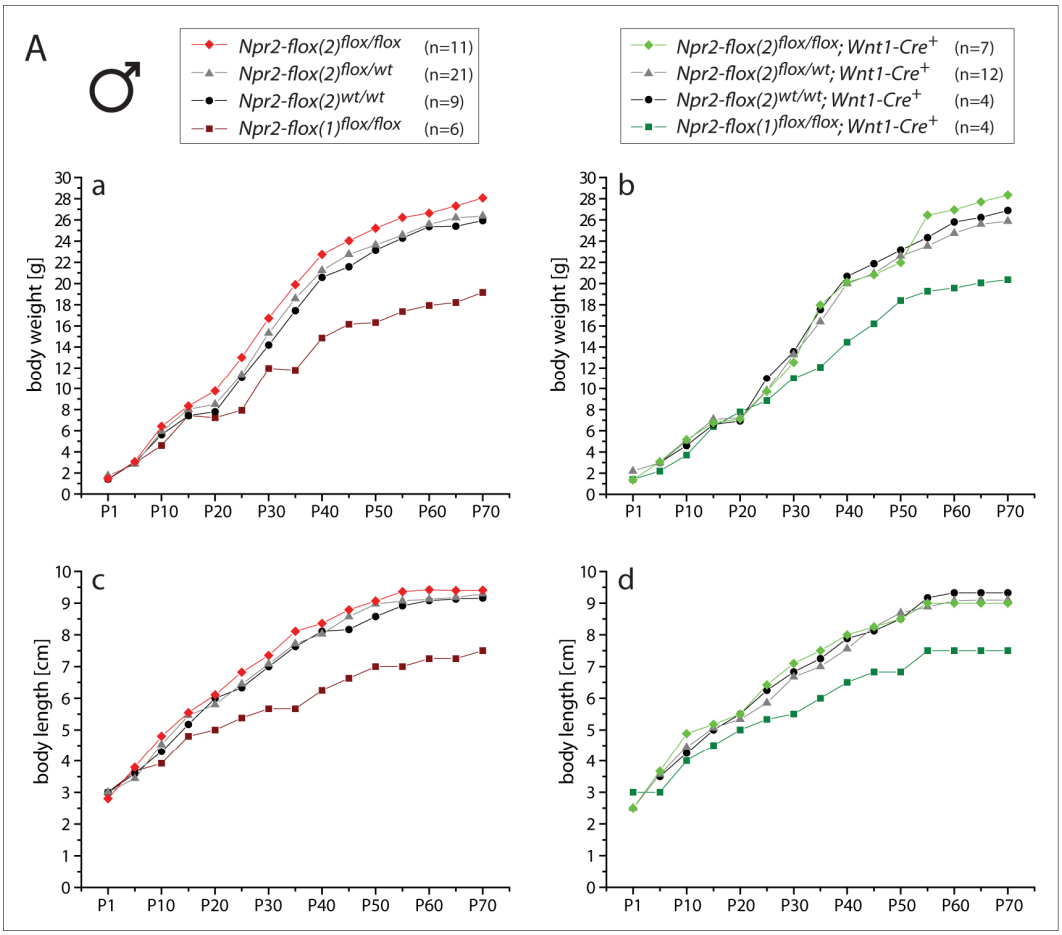
A
♂
Npr2-flox(2)flox/flox (n=11)
Npr2-flox(2)flox/wt (n=21)
Npr2-flox(2)wt/wt (n=9)
Npr2-flox(1)flox/flox (n=6)
Npr2-flox(2)flox/flox; Wnt1-Cre+ (n=7)
Npr2-flox(2)flox/wt; Wnt1-Cre+ (n=12)
Npr2-flox(2)wt/wt; Wnt1-Cre+ (n=4)
Npr2-flox(1)flox/flox; Wnt1-Cre+ (n=4)
a
b
c
d
body weight [g]
body length [cm]
P1 P10 P20 P30 P40 P50 P60 P70

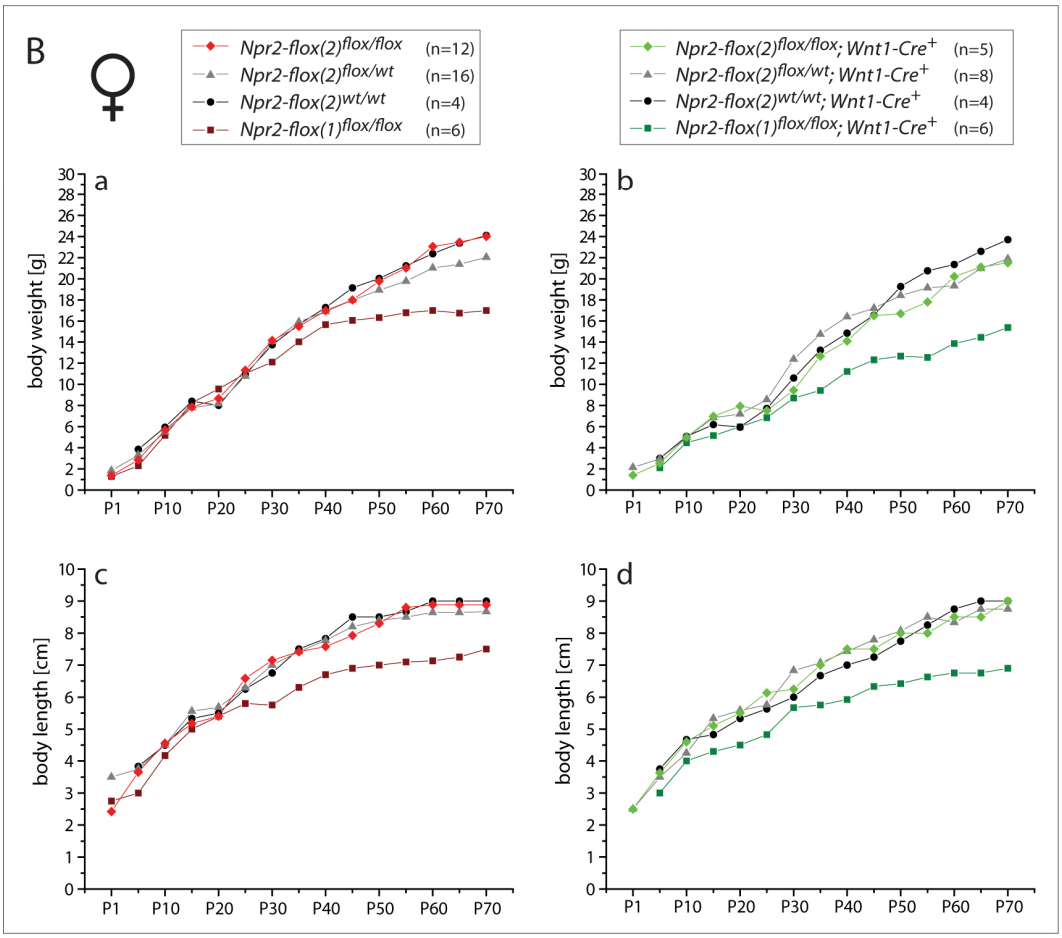
B
♀
Npr2-flox(2)flox/flox (n=12)
Npr2-flox(2)flox/wt (n=16)
Npr2-flox(2)wt/wt (n=4)
Npr2-flox(1)flox/flox (n=6)
Npr2-flox(2)flox/flox; Wnt1-Cre+ (n=5)
Npr2-flox(2)flox/wt; Wnt1-Cre+ (n=8)
Npr2-flox(2)wt/wt; Wnt1-Cre+ (n=4)
Npr2-flox(1)flox/flox; Wnt1-Cre+ (n=6)
a
b
c
d
body weight [g]
body length [cm]
P1 P10 P20 P30 P40 P50 P60 P70

Figure 23: Illustration of growth development of floxed Npr2 mouse strains over a period of 70 days after birth. Body length (body length measured from the nose to beginning of the tail) and body weight was recorded every five days. (A) Growth progression considering only male mice. Graph a and c illustrate the data of wild-type, heterozygous and homozygous Npr2-flox(2) animals along with homozygous Npr2-flox(1) mice which were used as control for the bone phenotype. Graph b and d display the results of the identical floxed Npr2 genotypes crossbred with Wnt1-Cre. No significant growth delay was recorded within the Npr2-flox(2) mouse strain whether or not Wnt1-Cre was crossbred. Npr2-flox(1)$^{flox/flox}$ mice suffering from dwarfism began to reveal their distinct developmental disorder around postnatal day 20. Crossbreeding with Wnt1-Cre did not induce any further significant changes in growth development. (B) Growth progression considering only female mice. The growth rate ratio of female experimental animals considering the specific genotypes is identical to the results of male animals.

Figure 24: Growth of homozygous Npr2-flox(2) mice. Neither body length, nor body weight, nor tail length is evidently changed in the Npr2-flox(2)$^{flox/flox}$ mutant compared to the wild-type littermate at postnatal day 40.

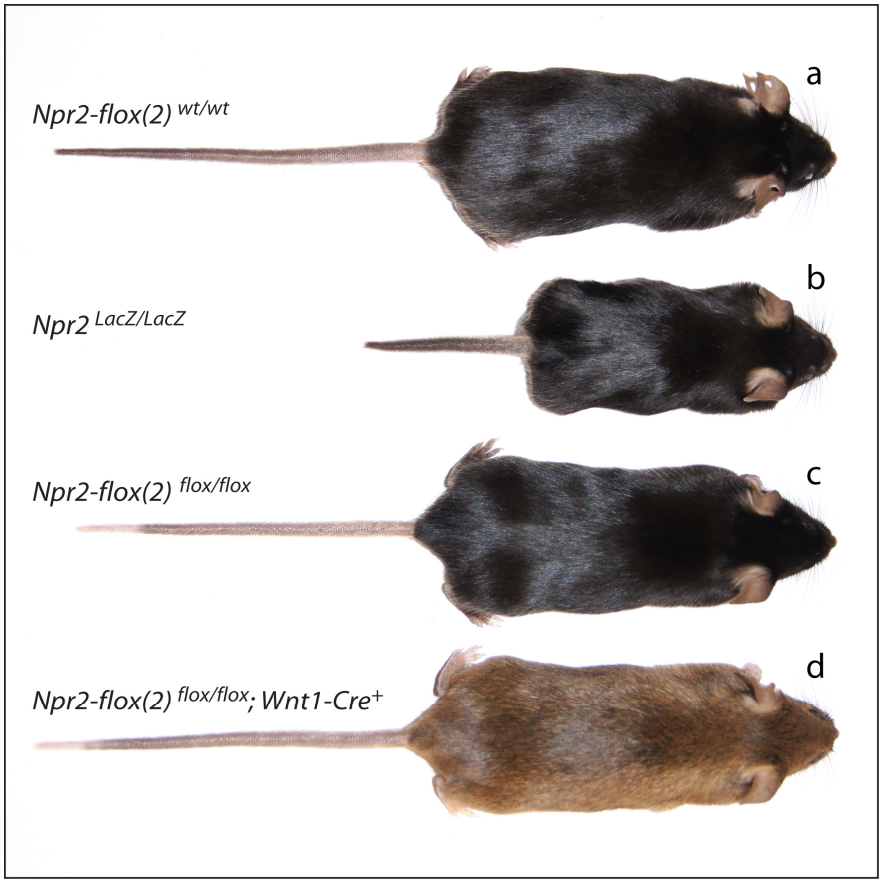

Figure 25: The Wnt1-Cre induced conditional Npr2 knockout mouse prevents the Npr2-related impaired endochondral ossification. Male mice were photographed at postnatal day 85. (a) Wild-type control animal; (b) Npr2(LacZ/LacZ) mouse which is a Npr2 null mouse generated by Dr. Ter-Avetisyan shows the full manifestation of the Npr2-related dwarf phenotype; (c) Homozygous Npr2-flox(2)$^{flox/flox}$ mouse and (d) Wnt1-Cre induced Npr2-cKO mouse Npr2-flox(2)$^{flox/flox}$;Wnt1-Cre^{+} demonstrate normal bone development and no size difference compared to the wild-type control.

5.1.14 Verification of normal fertility and longevity in the Npr2-flox(2) mouse line

Because the hypomorphic Npr2 mouse line suffered from reduced fertility, small litter size, and premature mortality, the floxed Npr2 mouse line was assessed for these pathological phenotypes. The evaluation of breeding data revealed that the mean litter size of heterozygous and homozygous mating of the floxed Npr2 mouse strain was almost identical (Figure 26). The average number of newborn mice was around eight per litter which corresponds to the value cited in the literature for wild-type animals. Furthermore, all mated homozygous Npr2-flox(2) female and male mice were fertile and able to procreate. In summary, no negative effect on the fertility was caused by the floxed Npr2 allele.

To clarify the question of enhanced premature mortality, the survival was evaluated based on data from the body length and weight study. The survival rate diagram illustrates the deceases of particular Npr2-flox genotypes over a period of 70 days (Figure 27). Homozygous mice of the hypomorphic Npr2-flox(1) mouse strain were included as control for the premature mortality caused by Npr2 loss-of-function. 50 % of Npr2-flox(1)$^{flox/flox}$ mice and 40 % of Npr2-flox(1)$^{flox/flox}$;Wnt1-Cre^{+} mice deceased during the first 4 weeks of life. Whereas wild-type and heterozygous Npr2-flox(2) genotypes showed no prominent reduction of the survival rate, homozygous Npr2-flox(2) mice carrying the Wnt1-Cre allele suffered from severe premature mortality. 42 % of the conditional Npr2 knockout mutants deceased before the recording period was finished. Even so, no animal prematurely died during the first 4 weeks of life. However, the homozygous Npr2-flox(2) genotype itself showed absolutely no decrease of the survival rate. While the new floxed Npr2 allele prevented premature mortality, the Wnt1-Cre induced Npr2 knockout allele of the conditional knockout mutant provoked a similar death rate as recorded for the Npr2 hypomorph but with a significant delayed starting time.

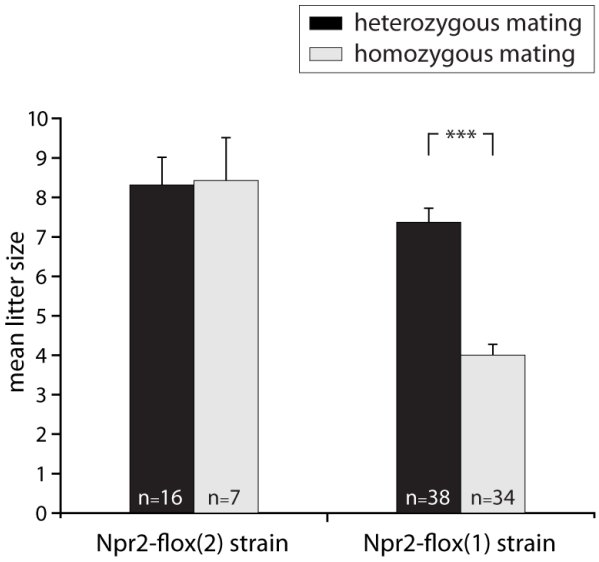

Figure 26: Litter sizes comparing the mating of heterozygous and homozygous animals. The Npr2-flox(2) mouse line showed similar litter sizes for both mating types which correspond to standard wild-type litter sizes. The hypomorphic Npr2-flox(1) strain carrying the splice site mutation demonstrated severe reduction of newborn pups in the case of homozygous mating. Furthermore, 43 per cent of the female Npr2-flox(1)$^{flox/flox}$ mice which have been used for the breeding suffered from infertility. The number of offspring was statistically significant reduced by almost one half to 4 animals per litter (t test, ***$p < 0.001$).

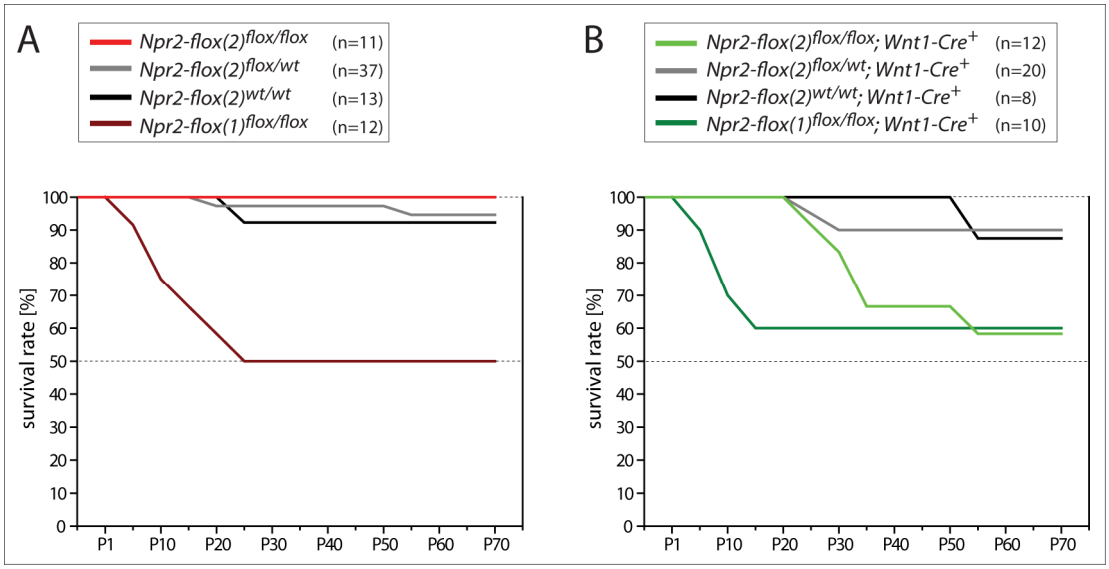

Figure 27: Survival rate of floxed Npr2 mouse strains with and without Wnt1-Cre interbreeding. (A) Wild-type, heterozygous and homozygous Npr2-flox(2) mice showed no conspicuous premature mortality over a period of 70 days after birth. Homozygous Npr2-flox(1)$^{flox/flox}$ mice carrying the splice site mutation demonstrated a continuously decreasing survival rate starting shortly after birth. Half of the Npr2-flox(1)$^{flox/flox}$ mice deceased until postnatal day 25. (B) Survival rate diagram likening the same Npr2-flox genotypes as before now crossed with Wnt1-Cre, respectively. Animals with Npr2-flox(2)$^{flox/flox}$;Wnt1-Cre^{+} genotype demonstrated continuously increased premature mortality beginning with postnatal day 25. When the recording period was finished, the survival rate was below 60 %. Wild-type and heterozygous Npr2-flox(2) strain mice were not appreciably affected. Npr2-flox(1)$^{flox/flox}$;Wnt1-Cre^{+} animals showed no rising premature mortality compared with Npr2-flox(1)$^{flox/flox}$ control animals. Data of male and female animals are combined in these graphs.

5.1.15 Further phenotype characterization of the conditional Npr2 knockout correlating with premature mortality

Due to premature death of Wnt1-Cre induced conditional Npr2 knockout mutants, further phenotypic characterizations were performed. Afflicted animals suffered from weight stagnation up to weight loss. In addition to it, deteriorating lethargy, extreme fatigue, and food rejection was recorded shortly before exitus. Dissection of several Npr2-flox(2)$^{flox/flox}$;Wnt1-Cre^{+} animals which suffered from malnutrition revealed prominent intestinal disturbances (Figure 28). Particularly striking were the strongly blood-circulated inflammation of the proximal small intestine and the non-natural accumulation of gas in the distal part of the small intestine. However, the degree of the enteric phenotype showed varying characteristics for individual animals.

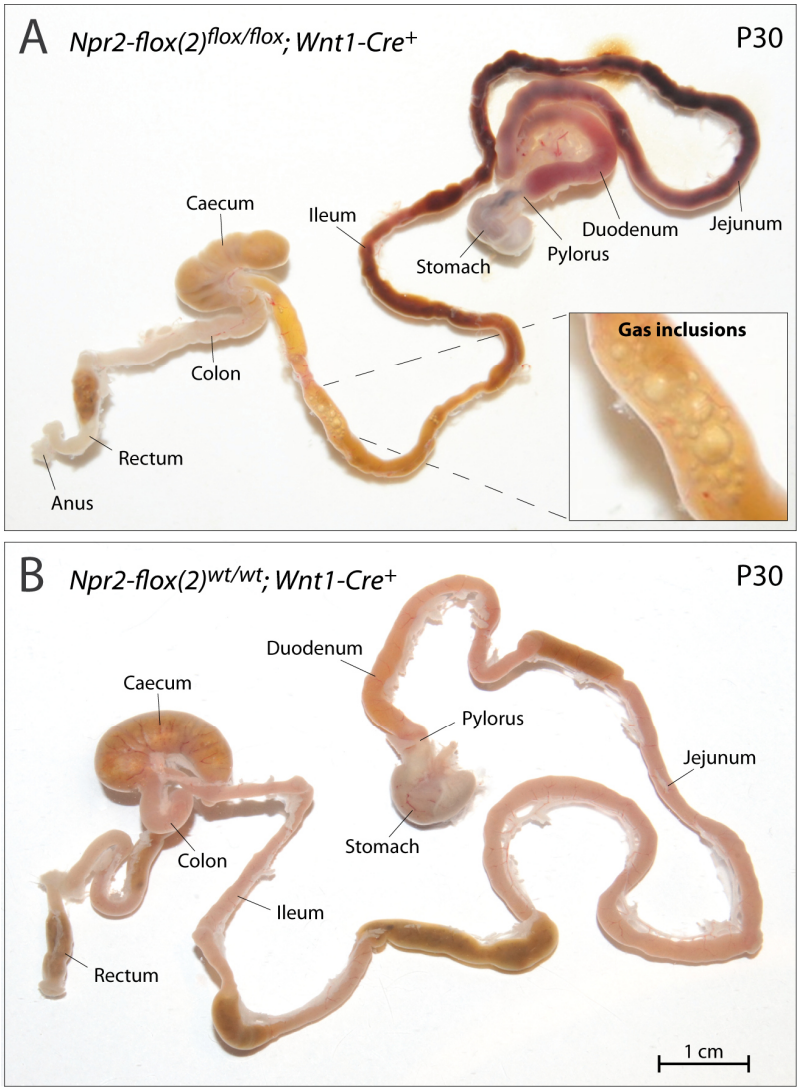

Figure 28: Illustration of intestinal disturbance found in Npr2-flox(2)$^{flox/flox}$;Wnt1-Cre^{+} mice. (A) Preparation of the gastrointestinal tract of an Npr2-flox(2)$^{flox/flox}$;Wnt1-Cre^{+} mouse at postnatal day 30 shows evidence of severe intestinal disorders. Strongly blood-circulated inflammation of the duodenum extends far into the jejunum associated with unnaturally mis-colored feces in the proximal part of the gastrointestinal tract. The end part of the ileum exhibits accumulation of gas (magnified section). Physical development and nutritional level of mice showing the intestinal phenotype were inferior in comparison to control littermates. (B) Preparation of an Npr2-flox(2)$^{wt/wt}$;Wnt1-Cre^{+} control animal at postnatal day 30 shows a healthy gastrointestinal tract. Physical development and nutritional level of the control mouse showed no abnormalities.

Another premature mortality associated phenotype was the malformation of the mandibular incisors (Figure 29). This dental phenotype was already previously ascertained for a number of homozygous mice of the hypomorphic floxed Npr2 mouse strain where it correlated with premature death as well. The non-natural prolongation of the mandibular incisors started after the second postnatal week and was therefore

utilized as pre-indication for the physical manifestation of the pathological phenotypes. Tooth clipping and providing of softened nourishments sufficiently in advance as a countermeasure alleviated the consecutive symptoms significantly. The medical condition was fully recovered for half of the affected animals by this treatment. Without this treatment, around 40 % of the Wnt1-Cre induced conditional Npr2 knockout mutants suffered from premature mortality, whereas the remaining 60 % showed absolutely no physical difference compared to wild-type animals.

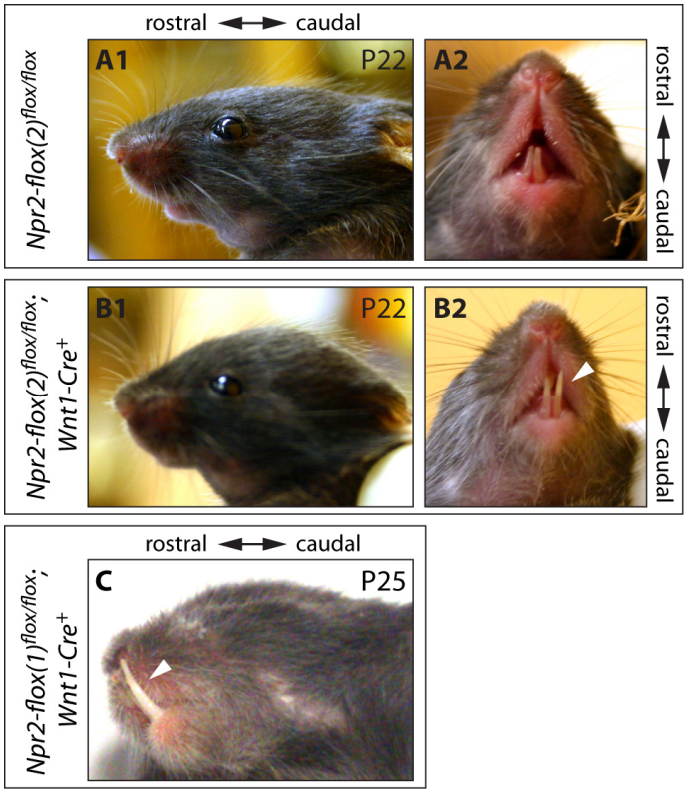

Figure 29: Malformation of incisor teeth in Npr2-flox(2)$^{flox/flox}$;Wnt1-Cre^{+} mice. (A1) Profile view and (A2) front view of homozygous Npr2-flox(2)$^{flox/flox}$ mouse showing no aberration of mandibular incisors. (B1) Profile view and (B2) front view of Npr2-flox(2)$^{flox/flox}$;Wnt1-Cre^{+} mouse displaying unnaturally elongated mandibular incisors (arrow). The slightly shortened snout in picture B1 is presumably a side effect of a delayed development caused by a general lack of nourishment. Typical indications for the Npr2-mediated bone phenotype such as snub nose, caudal skull enlargement, and stumpy tail are not present in the animal with the dental phenotype. Both mice are female littermates photographed at postnatal day 22. (C) Deceased Npr2-flox(1)$^{flox/flox}$;Wnt1-Cre^{+} mouse showing heavily extended mandibular incisors (arrow). Severe malformation of incisor teeth was already documented for Npr2-flox(1)$^{flox/flox}$ mice independently from crossbreeding with the Wnt1-Cre mouse line. It has not been determined whether the dental phenotype is caused by missing attrition or by impaired tooth morphogenesis. The dental phenotype has incomplete penetrance but correlates with premature mortality.

5.1.16 Axon bifurcation at the dorsal root entry zone of the Npr2-flox(2) mouse line

The axon bifurcation of sensory neurons was analyzed in the Npr2-flox mouse and the conditional Npr2 knockout mouse considering Npr2 expression. To prove protein expression of Npr2 in dorsal root ganglia of Npr2-flox mice and Wnt1-Cre induced conditional Npr2 knockout mice, an immunoblotting test was performed using 40 DRGs that were prepared from mouse embryos at embryonic day 13 for each genotype (Figure 30). After cell homogenization and membrane fractionation, the receptor protein was detected by using a guinea pig antibody against the extracellular domain of Npr2. The homozygous Npr2-flox sample showed the Npr2-specific double band at around 130 kDa. The Wnt1-Cre induced conditional Npr2 knockout sample exhibited no detectable Npr2 protein band at all. Although the expectation was that the sizes of the receptor protein expressed by the conditional knockout allele will be reduced by 4 to 5 kDa due to the Cre-recombinase mediated excision of exons 17 and 18 of Npr2. However, the floxed Npr2 allele ensured the expression of the wild-type receptor protein whereas the conditional Npr2 knockout allele caused an entire absence of the Npr2 protein.

Npr2-flox(2)$^{flox/flox}$ and Npr2-flox(2)$^{flox/flox}$;Wnt1-Cre^{+} mice were tested for axonal branching at the dorsal root entry zone. DiI-labeling of DRG neurons was carried out in whole mount preparations of the spinal cord at embryonic day 12.5 by Dr. H. Schmidt (Figure 30). By using the lipophilic tracer 1,1'-dioctadecyl-3,3,3',3'-tetramethylindocarbocyanine perchlorate (DiI) as a diffusive staining, the trajectories of only a small number of sensory neurons growing into the dorsal root entry zone were labeled for analysis. In homozygous floxed Npr2 embryos, the axonal outgrowth of sensory neurons bifurcated at the dorsal root entry zone. The axon bifurcation of Npr2-flox(2)$^{flox/flox}$;Wnt1-Cre^{+} embryos, in turn, was impaired causing the sensory axons to turn either in rostral or caudal direction. Results of the Western blot and analysis of axon bifurcation proved that the Npr2-flox(2) mouse is suitable to create a conditional Npr2 knockout mouse. The Cre-recombinase activity controlled by the *Wnt1* promoter in homozygous Npr2-flox mice results in ablation of Npr2 expression in DRGs early enough to cause impaired axon bifurcation by prevention of Npr2-mediated cGMP signaling. On

the contrary, the homozygous Npr2-flox mouse expresses the wild-type receptor protein in DRGs allowing proper axon bifurcation of sensory neurons in the spinal cord.

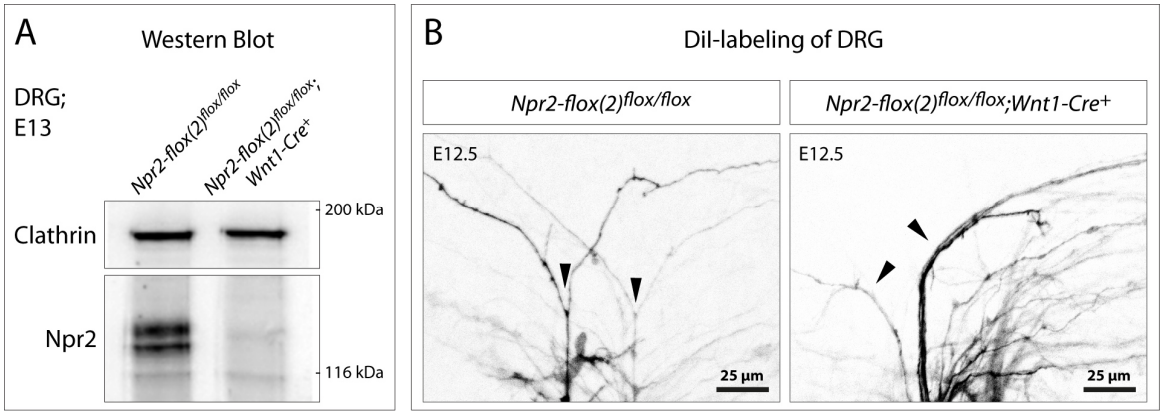

Figure 30: Examination of Npr2 protein expression and sensory axon bifurcation at the dorsal root entry zone comparing Npr2-flox(2)$^{flox/flox}$ genotype with Npr2-flox(2)$^{flox/flox}$;Wnt1-Cre^{+} genotype of the Npr2-cKO. (A) Western blot analysis of the membrane fraction of dorsal root ganglia prepared at embryonic day 13. The Npr2 protein is demonstrated by a GP-α-Npr2 antibody. M-α-Clathrin heavy chain is used as loading control. The unmodified floxed Npr2 allele ensures the expression of Npr2 at embryonic day 13 demonstrated by the specific Npr2 double band at 125 kDa. In contrast, the floxed Npr2 allele missing exon 17 and exon 18 after *Wnt1* promoted Cre-recombinase activity reveals an entire lack of Npr2 protein expression. (B) DiI-labeling of dorsal root ganglia prepared at embryonic day 12.5 in order to trace the bifurcation phenotype at the dorsal root entry zone. Axons of sensory neurons of Npr2-flox(2)$^{flox/flox}$ mice bifurcate at the dorsal root entry zone corresponding to wild-type bifurcation. In contrast, Npr2-flox(2)$^{flox/flox}$;Wnt1-Cre^{+} mice revealed a lack of bifurcation where the sensory axons turn either in rostral or caudal direction according to conventional Npr2 knockout mutants.

5.1.17 Conditional Npr2 knockout mutants revealed a reduced sensitivity in the Hargreaves Test

After confirming a normal bone growth phenotype and the inducibility of impaired axon bifurcation in the floxed Npr2 mouse line, the Hargreaves Test was performed to ask whether the absence of axon bifurcation affects sensory perception. However, the breeding of an appropriate number of experimental animals was aggravated by the premature mortality of Npr2-flox(2)$^{flox/flox}$;Wnt1-Cre^{+} mice. All tested mice showed normal development of bone growth, normal physical health condition, and normal life expectancy. Eight even-aged mice without gender-based differentiation were analyzed for each genotype. After an acclimatization period, the response time of the withdrawal reaction induced by heat stimulation at the bottom of the hind paw was daily measured 25 times per animal over a period of 3 consecutive days. The performed Hargreaves Test compared eight Npr2-flox(2)$^{flox/flox}$ control animals with eight Npr2-flox(2)$^{flox/flox}$;Wnt1-

Cre+ conditional Npr2 knockout animals. The conditional Npr2 knockout mutants without axonal bifurcation consistently demonstrated sensory hyposensitivity in relation to the control animals (Figure 31). While the mean latency time of control animals was around 5 seconds, the conditional knockout animals averagely needed 2 seconds more to response to the heat stimulus. The extended withdrawal latency time of the conditional Npr2 knockout was statistically significant for the tested animals.

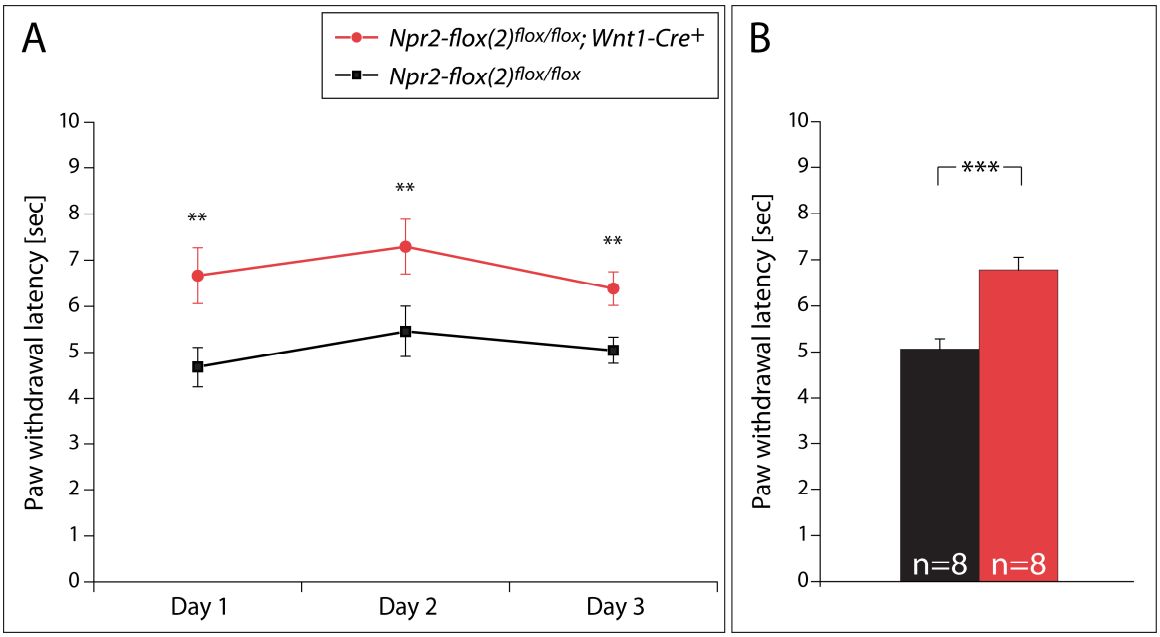

Figure 31: Plantar Test (Hargreaves´ Method) comparing conditional Npr2 knockout mice carrying the Wnt1-Cre allele with Npr2-flox control animals. (A) Graphical representation of the Hargreaves Test results over a period of 3 consecutive trial days with 25 measurements per day and experimental animal. 8 conditional knockout and 8 control littermates were tested at the age of 8 weeks. The mean hind paw withdrawal latency of Npr2-flox(2)$^{flox/flox}$;Wnt1-Cre^{+}conditional knockout animals (red) was extended compared to Npr2-flox(2)$^{flox/flox}$ control animals (black) over the total experiment time. (B) Summarized test results revealed a mean response time for the Npr2-flox(2)$^{flox/flox}$;Wnt1-Cre^{+} conditional knockout genotype which is increased by 2 seconds in comparison to the Npr2-flox(2)$^{flox/flox}$ control genotype (u test, ***$p < 0.001$). The Hargreaves Test was performed with idle value of 5 % and stimulus value of 50 % of the maximum intensity. Error bars were calculated by standard error of the mean. The Shapiro-Wilk test revealed no normal distribution of individual data records. As a result, the determination of statistical significance was evaluated by Mann-Whitney U test.

5.2 Regulation of the guanylyl cyclase activity of Npr2

Since the outgrowing axons of sensory neurons bifurcate only one time at the dorsal root entry zone, the conversion of GTP to cGMP by the Npr2 receptor needs to be a non-recurring signaling event for each individual axon which is most likely tightly regulated. Although not much is known about the deactivation of the CNP-Npr2-cGKI signaling cascade *in vivo*, three conceivable scenarios were debated whereby the cGMP signaling could be switched off. In this context, scavenger receptor Npr3 could decrease the cGMP production by removing ligand CNP. Or, the cGMP could be directly degraded by phosphodiesterases or alternatively the receptor itself could regulate its own activation status. However, previous genetic analysis in our group demonstrated that the scavenger receptor as well as the phosphodiesterase 2a (PDE2a) are not essential for the bifurcation suggesting that Npr2 itself may be an important determinant for the regulation of the intracellular cGMP level. Earlier biochemical studies investigating the regulation of the enzymatic activity of Npr2 showed that the Npr2 homodimer is highly phosphorylated at five residues (Ser-513, Thr-516, Ser-518, Ser-523, and Ser-526) in the so-called kinase homology domain (KHD) in absence of the ligand CNP (Potter et al., 1998). To study how phosphorylation and dephosphorylation of the kinase homology domain affects the guanylyl cyclase activity of Npr2, five diverse receptor mutants were cloned and analyzed for cGMP production after CNP stimulation. Two Npr2 proteins were constructed containing amino acid substitutions in order to mimic either a constitutively phosphorylated or a constitutively dephosphorylated receptor protein. Furthermore, two receptor mutants lacking the complete or nearly the complete KHD and a control receptor protein without the guanylyl cyclase domain were cloned.

5.2.1 Cloning of diverse Npr2 receptor mutants

To identify the receptor protein expression in living cells after plasmid transfection, the recombinant protein expression was linked to the expression of mCherry using the internal ribosome entry site (IRES) of a bicistronic plasmid vector. The monomeric mCherry fluorophore was selected due to its superior photostability, brightness and non-cytotoxicity (Shaner et al., 2005). The complete cloning strategy and domain structure of the Npr2 mutants are explicitly illustrated in Figure 32.

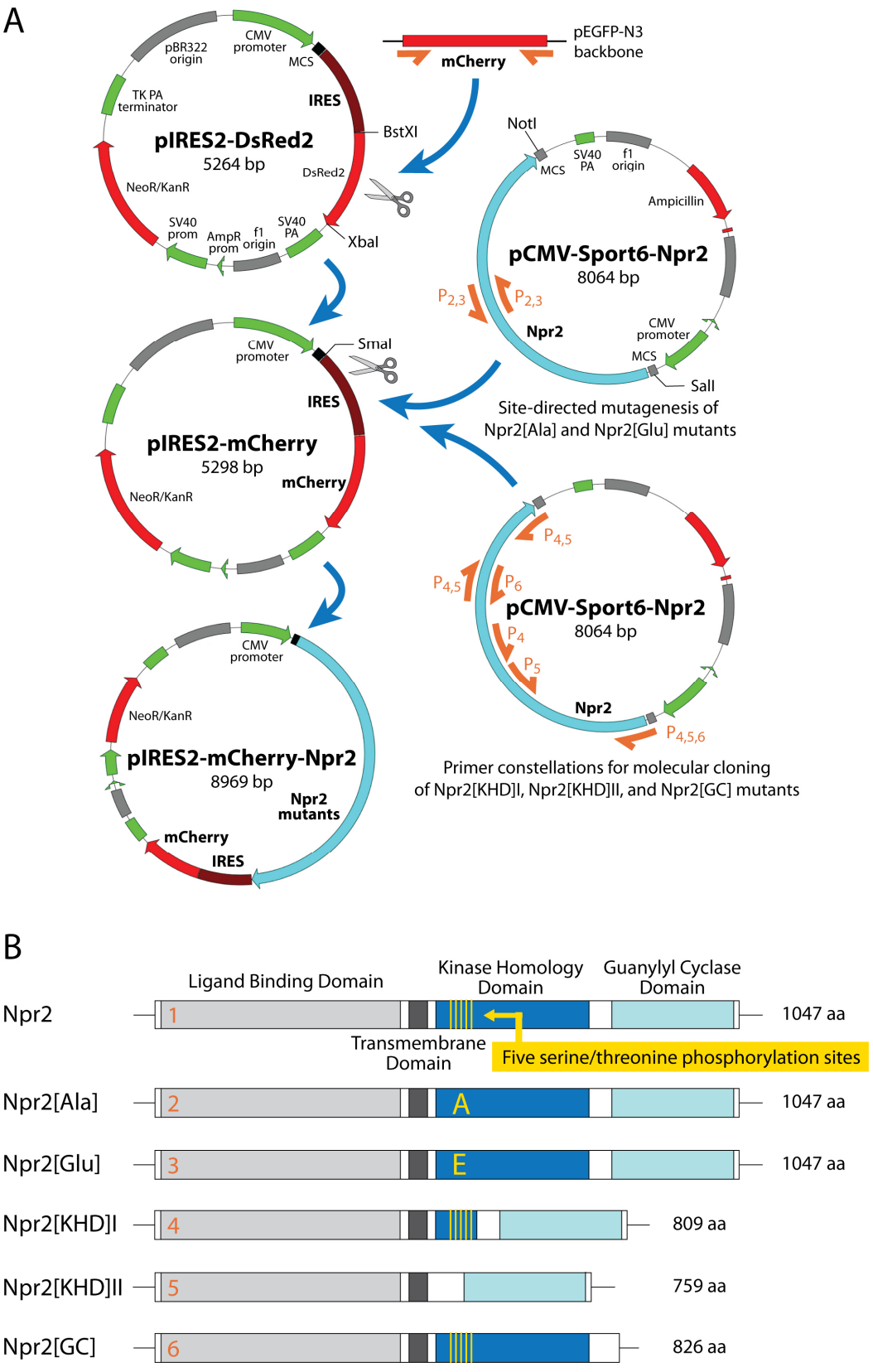

Figure 32: Plasmid cloning strategy for mutated Npr2 receptor proteins. All recombinant Npr2 constructs were cloned into a bicistronic plasmid vector to be linked to mCherry co-expression. (A) The DsRed2 fluorescent protein of the commercially available plasmid vector pIRES2-dsRed2 (Clonetech) was replaced by mCherry using the cleavage sites of restriction enzyme *Bst*XI and *Xba*I. The mCherry expression

sequence was obtained from a carrier plasmid with pEGFP-N3 backbone by PCR amplification. The oligonucleotides were placed at the start and stop codon of the mCherry open reading frame and additionally equipped with the cleavage sites of restriction enzyme *Bst*XI or *Xba*I, respectively. The Npr2 mutants as well as the Npr2 wild-type sequence were cloned into the multiple cloning sites of the pIRES2-mCherry plasmid with the aid of restriction enzyme *Sma*I and blunt end ligation. For this, every particular Npr2 expression sequence was excised by restriction enzyme *Sal*I and *Not*I and afterwards prepared for blunt end ligation by filling in the receded 3´ ends using the Klenow fragment. A pCMV-Sport6 plasmid carrying the Npr2 expression sequence was the source for the Npr2 protein. Almost complementary oligonucleotides were used to induce amino acid substitutions during site-directed mutagenesis. Several pairs of oligonucleotides were used to amplify Npr2 sections which were recombined as Npr2 deletion mutants by DNA ligation. The positioning within the pCMV-Sport6-Npr2 of all applied primer constellations used for cloning is schematically illustrated (orange arrows) and numerically assigned to the particular Npr2 mutant in section B. (B) (1) The wild-type Npr2 protein contained all functional receptor domains. (2, 3) The Npr2[Ala] and Npr2[Glu] proteins were generated by the use of site-directed mutagenesis. In the process, five amino acids, four serine residues and one threonine residue, which are part of the kinase homology domain, were replaced by either alanine or glutamic acid. (4) The Npr2[ΔKHD]I protein lacked most of the kinase homology domain except for the five phosphorylation sites. The protein sequence between amino acid 545 and amino acid 784 was therefore excised. (5) The Npr2[ΔKHD]II protein was cloned without the complete kinase homology domain and the five phosphorylation sites. In this case, the protein sequence between amino acid 494 and amino acid 784 was abolished. (6) The Npr2[ΔGC] protein contained no catalytic guanylyl cyclase domain at all. The amino acid 825 of the Npr2 open reading frame was therefore substituted by a new stop codon leading to the expression of an abbreviated Npr2 molecule.

In brief, the pCMV-Sport6-Npr2 plasmid vector containing the coding DNA sequence of Npr2 was used as source vector either for the site-directed mutagenesis to induce amino acid substitution at the five phosphorylation sites or for the amplification of particular Npr2 sections which were recombined by DNA ligation to generate three different Npr2 deletion mutants. The wild-type and the mutated Npr2 coding DNA sequences were cloned into the multiple cloning site of the bicistronic expression vector pIRES2-mCherry using blunt end ligation. Apart from the particular protein coding sequence, every Npr2 expression sequence was complemented by leader sequence, trailer sequence and polyadenylation signal of the wild-type Npr2 mRNA. Each cloning step was checked for its accuracy using restriction and sequence analysis. The amino acid substitutions that permanently determined the phosphorylation status of the five phosphorylation sites of the kinase homology domain were integrated with the aid of the QuikChange II XL Site-Directed Mutagenesis Kit from Stratagene. The nucleotide triplet code was modified by multiple amplification steps of the entire pCMV-Sport6-Npr2 vector using oligonucleotides which were almost complementary to the phosphorylation site sequence except for specific mismatches (Figure 33). As a consequence, Serine-513, Threonine-516, Serine-518, Serine-523, and Serine-526 were substituted either by

alanine or glutamic acid and the wild-type amino acid sequence was transcribed from SRLTLSLRGSSYGS either into ARLALALRGSAYGA or ERLELELRGSEYGE.

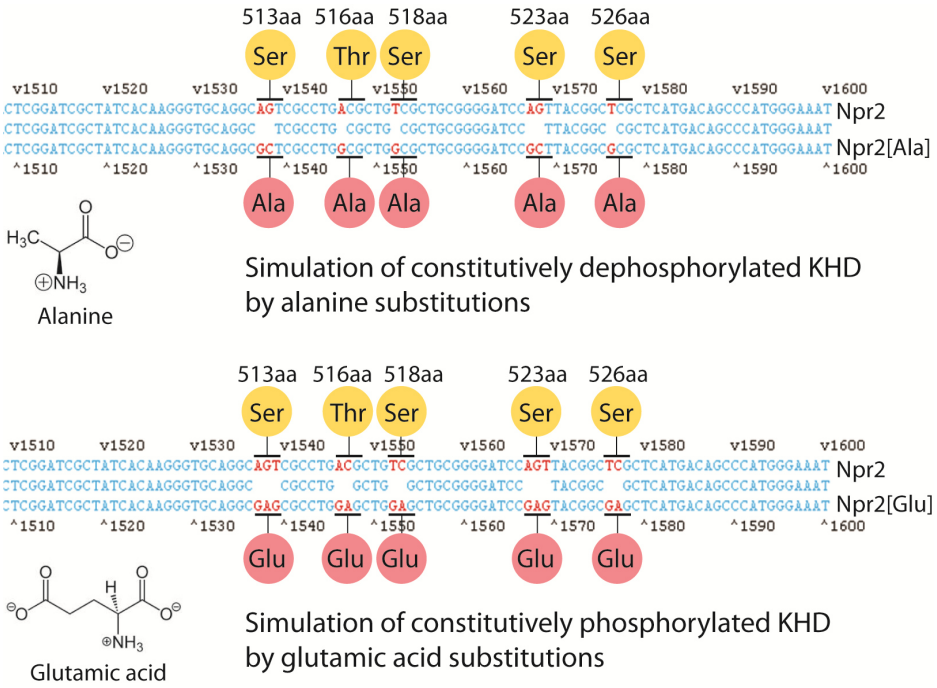

Figure 33: Alanine and glutamic acid substitution at the five phosphorylation sites of the Npr2 kinase homology domain. Codons of amino acid 513, 516, 518, 523, and 526 were changed with the aid of the QuikChange II XL Site-Directed Mutagenesis Kit from Stratagene. The specific sequence modification which was required for recoding the native triplet code is highlighted in red. In order to express a receptor protein which is constitutively dephosphorylated, the serine and threonine amino acids were substituted by alanine which is lacking the hydroxyl group necessary for the phosphorylation. The glutamic acid substitution, on the other hand, mimics a constitutively phosphorylated receptor protein by its chemical similarity to phosphoserine and phosphothreonine.

Naturally, serine and threonine are potentially phosphorylated at their hydroxyl group and converted into phosphoserine and phosphothreonine. The introduced alanine substitutions inhibited the general phosphorylation capability by lacking the necessary hydroxyl group leading to a constitutively dephosphorylated receptor protein. The principle of phosphomimetics was conversely applied to mimic a constitutively phosphorylated Npr2 protein. Thereby, glutamate, anion of glutamic acid, simulates a non-reversible negative charge and the chemical structure of phosphoserine and phosphothreonine. Alanine mutant (Npr2[Ala]) and glutamic acid mutant (Npr2[Glu]) had an unchanged protein length of 1047 amino acids equal to the Npr2 wild-type protein (Npr2). Kinase homology domain mutant Npr2[KHD]I, measuring 809 amino acids, lacked nearly the complete KHD sequence between amino acid 545 and 784

except for the five phosphorylation sites. Kinase homology domain mutant Npr2[KHD]II, measuring only 759 amino acids, was constructed without the complete KHD sequence between amino acid 494 and 784 including the five phosphorylation sites. Guanylyl cyclase domain mutant (Npr2[GC], measuring 826 amino acids, was cloned with a premature stop codon at amino acid 825 leading to chain stop and elimination of the guanylyl cyclase domain in the expressed Npr2 protein.

5.2.2 Expression of Npr2 receptor mutants in HEK293 cells

The efficient and errorless expression of the Npr2 receptor mutants was validated by western blot analysis and immunocytochemistry. Two days after lipofectamine-mediated transfection in HEK293 cells, total cell lysate samples were tested for Npr2 protein expression using the polyclonal antibody PGCB-201AP (FabGennix) and the self-produced polyclonal antibody Rb-α-Npr2. Apart from that the results of both antibodies were supportive and complementary; the use of Rb-α-Npr2 was inevitable to visualize the expression of Npr2[ΔGC] due to the fact that the epitope of PGCB-201AP is exclusively restricted to the guanylyl cyclase domain. Expression and predicted protein size of all Npr2 receptor proteins was correctly attested (Figure 34). The control samples, which were untransfected HEK293 cells and HEK293 cells transfected with the empty pIRES2-mCherry plasmid vector, showed no detectable Npr2 protein expression. As expected, the wild-type Npr2 protein and both amino acid substitution mutants, Npr2[Ala] and Npr2[Glu], were visualized at around 125 kDa showing the distinctive N-linked glycosylation related double band of Npr2 in western blotting. The expressed Npr2 deletion mutants, Npr2[ΔKHD]I, Npr2[ΔKHD]II, and Npr2[ΔGC], demonstrated protein sizes between approximately 100 kDa and 110 kDa due to their abbreviated amino acid sequences. Whereas Npr2[ΔKHD]I and Npr2[ΔGC] maintained the N-linked glycosylation double band, the second kinase homology domain mutant, Npr2[ΔKHD]II, showed only a more prominent lower band. The immunocytochemical analysis of transfected HEK293 cells attested the co-expression of the Npr2 proteins and the mCherry fluorescent protein. Staining with the PGCB-201AP antibody and an Alexa Fluor 488 Goat α–Rabbit IgG showed the Npr2 proteins to be primarily localized at the cell membrane. Simultaneously, the endogenous red fluorescence verified the mCherry

expression in the same transfected HEK293 cells. The results of the wild-type pIRES2-mCherry-Npr2 plasmid vector are representatively pictured in Figure 34.

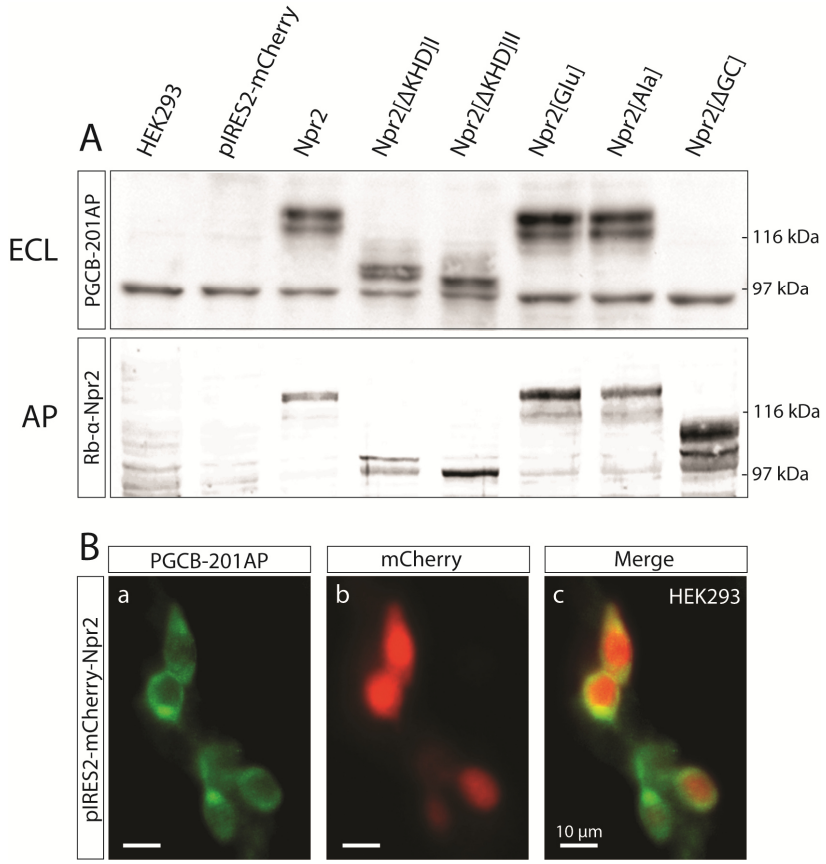

Figure 34: Npr2 protein expression of pIRES-mCherry-Npr2 plasmids in HEK293 cells. (A) Western blot analysis of transfected HEK293 cell lysates using the polyclonal antibody PGCB-201AP (FabGennix) in combination with ECL detection and the polyclonal antibody Rb-α-Npr2 directed to the extracellular region of Npr2 combined with AP staining. An untransfected HEK293 cell sample and cells transfected with the empty pIRES2-mCherry vector without Npr2 expression sequence were applied as control. All expressed Npr2 proteins were correctly detected with their predicted band sizes. (B) Immunocytochemical analysis of the Npr2 protein expression in correlation with the endogenous mCherry expression mediated by the bicistronic plasmid vector. Only the result of the wild-type pIRES2-mCherry-Npr2 plasmid transfection is exemplarily represented (a) The expression of the Npr2 protein in HEK293 cells was verified by the primary PGCB-201AP antibody and an Alexa Fluor 488 Goat α–Rabbit IgG. (b) The simultaneous expression of the fluorophore mCherry was detected by strong red emission signal at 610 nm (c) The image overlay illustrates the co-expression of mCherry and Npr2.

5.2.3 Determination of the guanylyl cyclase activity of Npr2 receptor mutants in HEK293 cells

The lipofectamine transfected HEK293 cell cultures reached transfection rates of roughly 30 percent. Therefore, in order to generate a homogeneous transfected cell culture, FACSorting was carried out on the basis of the expressed mCherry fluorescence of transfected cells. The cell sorting was performed by the FACS Core Facility of the Max Delbrück Center for Molecular Medicine using a FACSAria II cell sorter. After an additional day of cultivation, 125000 almost homogeneous transfected cells per sample were incubated with 0.5 µM CNP (Calbiochem) or with control solution for 15 minutes at 37°C. Approximately 95 percent of the harvested cells were alive as shown by trypan blue dye staining (Bio-Rad). The cGMP levels of stimulated and non-stimulated transfected cell samples were determined by the cGMP "Direct Biotrak Enzyme Immunoassay System" (GE Healthcare) in accordance to protocol four of the user manual. The cGMP level of one single cell sample was absolutely determined with the help of the calibration curve and duplicate determination. The results of the cGMP measurement are comparatively illustrated in Figure 35. Since HEK293 cells have no endogenous Npr2 expression, the untransfected cell samples did not respond to the CNP stimulation and the cGMP concentration remained stationary comparing unstimulated sample to stimulated sample. This procedural control assured that other observed CNP-induced cGMP elevations were exclusively restricted to the Npr2 activity. Comparison of stimulated and unstimulated samples of the wild-type Npr2 plasmid vector confirmed the operating principle of the Npr2-mediated cGMP signaling cascade where ligand CNP activates Npr2 causing cGMP generation. Here, the cGMP concentration was increased by around 5 times after 15-minute CNP stimulation. The inducibility of the guanylyl cyclase activity of Npr2[Glu], mimicking a permanent phosphorylated receptor protein, was roughly the same as shown for the Npr2 wild-type protein. The cGMP concentration of Npr2[Glu] samples was increased by around 3 times after CNP stimulation whereas the basic activity was slightly higher as for the Npr2 wild-type protein. Although the cGMP level of Npr2[Ala], mimicking a permanent dephosphorylated receptor protein, was increased twice by CNP stimulation, the maximum cGMP level of the stimulated samples reached not even half of the maximum cGMP levels of wild-type Npr2 or

Npr2[Glu] indicating that the guanylyl cyclase activity of Npr2[Ala] is impeded by constitutive dephosphorylation of the KHD.

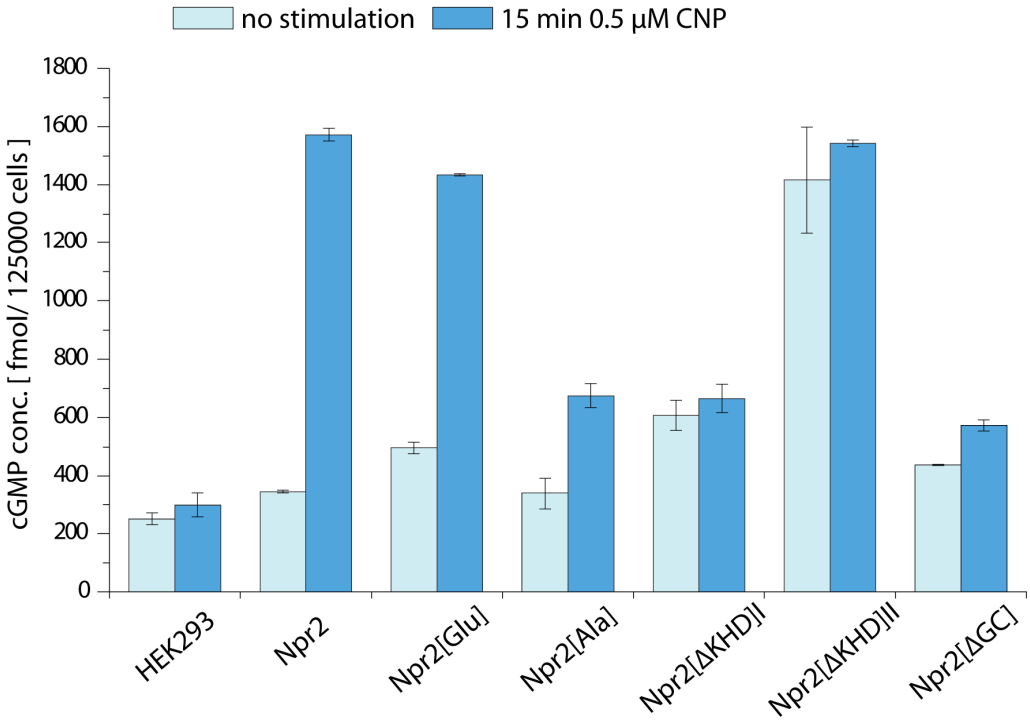

Figure 35: Determination of the cGMP concentration produced by the Npr2 mutants after CNP stimulation. Lipofectamine transfected HEK293 cell samples were enriched by Fluorescence-activated-Cell-sorting using the co-expression of mCherry to gain a pure plasmid vector expressing cell population. After an additional day of cultivation, 125000 cells per double determination were stimulated with 0.5 µM CNP for 15 minutes at 37°C (blue). The unstimulated control cells were treated with HBSS (Hank´s Balanced Salt Solution) instead of CNP (light blue). Phosphodiesterase activity was blocked by IBMX (3-isobutyl-1-methylxanthine) during stimulation. Immediately afterwards, the cytosolic cGMP concentration was measured using the cGMP Direct Biotrak Enzyme Immunoassay System (Protocol 4) from GE Healthcare. Three independent stimulated samples and three independent non-stimulated samples were determined by double determination for the untransfected control (HEK293), the Npr2 wild-type expression (Npr2), the constitutively phosphorylated Npr2 mutant (Npr2[Glu]), and the constitutively dephosphorylated Npr2 mutant (Npr2[Ala]). Only two stimulated and two non-stimulated samples were calculated by double determination for the guanylyl cyclase missing Npr2 mutant (Npr2[ΔGC]) and both kinase homology domain deletion mutants (Npr2[ΔKHD]I, Npr2[ΔKHD]II).

The kinase homology domain mutant Npr2[ΔKHD]I containing the five phosphorylation sites did not respond to the CNP stimulation, but showed a slightly increased basic activity. The Npr2[ΔKHD]II mutant lacking the complete kinase homology domain including the phosphorylation sites was constitutively activated regardless of CNP stimulation. The cGMP level of unstimulated Npr2[ΔKHD]II reached the level of stimulated wild-type Npr2 and Npr2[Glu] samples. Finally, the absence of the guanylyl cyclase domain in the Npr2[GC] control mutant prevented the generation of cGMP

completely. Npr2[GC] did not respond to CNP stimulation. Using the cGMP levels of Npr2[GC] as control for the guanylyl cyclase inactivity, a baseline at around 600 (fmol/125000 cells) can be set for the actual receptor activity. In conclusion, only wild-type Npr2 and constitutively phosphorylated Npr2[Glu] have clearly demonstrated to be activated whereas Npr2[ΔKHD]II was constitutively active. Taken together, CNP stimulated increase of cGMP levels requires phosphorylation at the five phosphorylation sites in the KHD segment of Npr2. Constitutive dephosphorylation of the KHD impede the activation of the guanylyl cyclase. In case of the five phosphorylation sites lacking the rest of the KHD sequence, the guanylyl cyclase activity is also blocked indicating that the complete KHD segment, not only the five phosphorylation sites, contributes to the activation of the enzymatic activity of Npr2. In contrast, complete removal of the KHD domain results in a constitutively active Npr2.

5.3 Interactome analysis of Npr2 and cGKIα based on proximity-dependent biotin identification (BioID)

My previous experiments indicated that the phosphorylation of serine and threonine residues in the KHD domain is essential for the generation of cGMP by Npr2. This result also implies an interaction of Npr2 with other intracellular signaling cascades that affect the phosphorylation status of Npr2. Therefore, to identify potential interaction partner of Npr2 a new technique for proximity-dependent labeling of proteins in eukaryotic cells was adapted. Furthermore, to identify downstream phosphorylation targets of cGKIα which convey the Npr2-mediated cGMP signaling necessary for axon bifurcation, cGKIα was also tested by proximity-dependent biotin identification (BioID). The BioID approach was first introduced by Kyle J. Roux and is based on fusion of the promiscuous prokaryotic biotin protein ligase BirA* to a protein of interest (Roux et al. 2012). Expression of the fusion protein in mammalian cells leads to proximity-dependent biotinylation of near-neighbor proteins which can be isolated by affinity capture and identified by western blot or mass spectrometry. In this method, one takes advantages of an amino acid substitution (R118G) found in the biotin protein ligase mutant called BirA*. The natural biotinylation by wild-type BirA is a two-step process. In the first step, biotinoyl-5´-AMP (bioAMP) is formed from biotin and ATP. In the second step, the activated biotin is retained within the BirA active site until it reacts with a specific lysine residue of the biotin acceptor tag sequence in substrate proteins. However, BirA* demonstrates an affinity for bioAMP two orders of magnitude less than the wild-type enzyme. As a result, the loose bioAMP readily reacts with primary amines regardless of the biotin acceptor tag sequence causing promiscuous protein biotinylation. The biotin-streptavidin affinity known as strongest noncovalent biological interaction is utilized for the affinity capture of biotinylated proteins. Both the receptor Npr2 and the kinase cGKIα were designed as BirA* fusion protein and expressed in F11 cells. The complete strategy for the BioID approach is schematically illustrated in Figure 36 showing the Npr2-BirA* and BirA*-cGKIα fusion proteins.

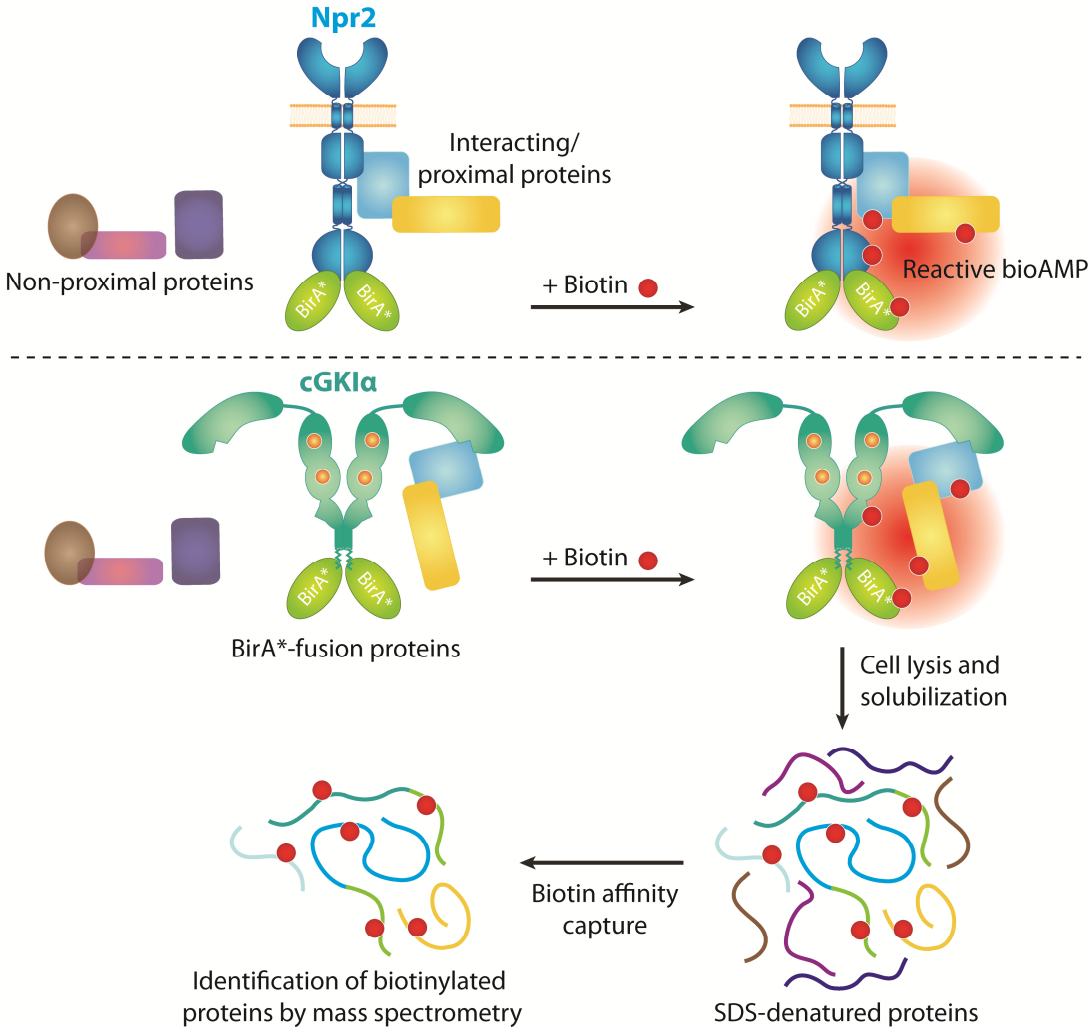

Figure 36: Schematic representation of the proximity-dependent biotin identification (BioID). The approach was conceptualized on the basis of a promiscuous *Escherichia coli* biotin protein ligase (BirA*) which was fused either to the C-terminal part of Npr2 or to the N-terminal part of cGKIα. In both cases, the biotin ligase induces proximity-dependent biotinylation of proteins (reactive bioAMP) that are near-neighbors of the fusion proteins whereas non-proximal proteins are not labeled with biotin. In my application of BioID to identify potentially interacting proteins the two fusion proteins were expressed in separate F11 cell cultures and incubated with 50 µM (+)-biotin for 16 hours. After cell lysis and fractionation under mild conditions, biotinylated proteins were affinity purified with streptavidin-conjugated beads for subsequent identification by mass spectrometry. (Adapted from (Roux et al., 2012)).

5.3.1 Cloning of Npr2-BirA* and BirA*-cGKIα expression vectors

The commercially available pcDNA3.1-MCS-BirA(R118G)-HA vector was used as basis for the cloning of an Npr2-BirA* fusion protein expression vector. Because the focus was on protein-protein interaction in the cytosol, the biotin protein ligase was fused to the C-terminal end of the transmembrane Npr2 receptor. For this purpose, the complete functional cDNA of Npr2 except for the final stop codon was obtained from a pCMV-Sport6-Npr2 expression vector by PCR amplification and introduced into the multiple

cloning site of the pcDNA3.1-MCS-BirA(R118G)-HA vector using the cleavage site of restriction enzyme *Eco*RI along with sticky end DNA ligation.

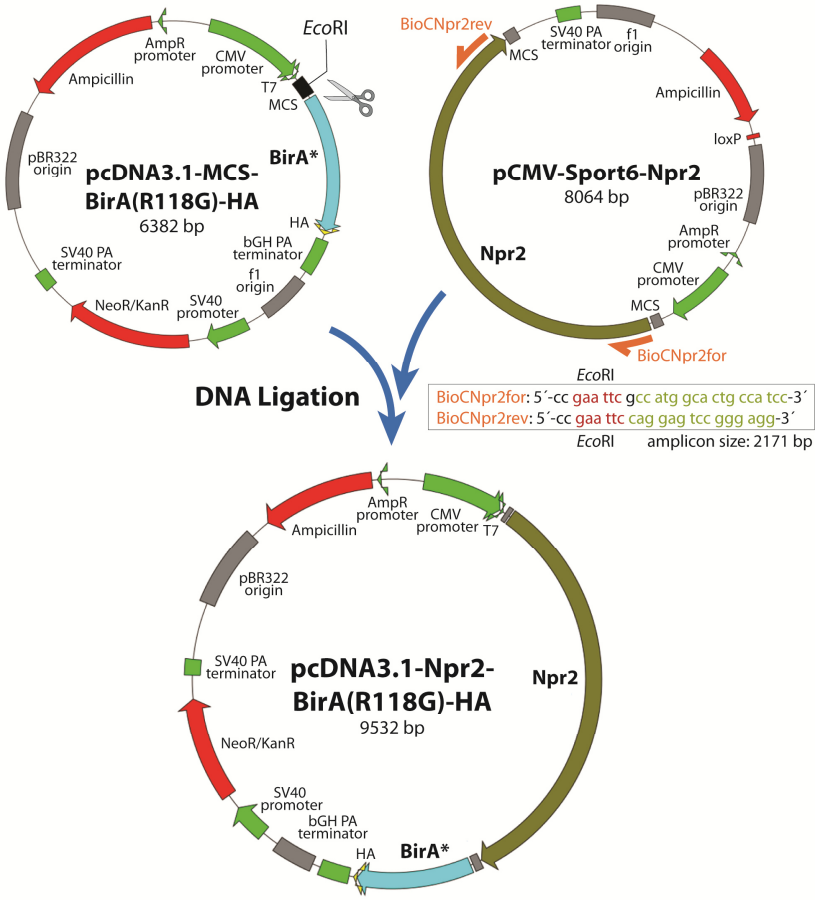

Figure 37: Molecular cloning strategy for the Npr2-BirA* expression vector. Two oligonucleotides were designed to amplify the complementary DNA of Npr2 from the pCMV-Sport6-Npr2 plasmid. The resulting PCR amplicon covered the complete open reading frame of Npr2 except for the final stop codon and was additionally flanked by two novelly attached *Eco*RI restriction sites. The cleavage site of *Eco*RI was then used for DNA ligation into the multiple cloning site (MCS) of the commercial pcDNA3.1-MCS-BirA(R118G)-HA vector considering the same reading frame as well as for the biotin ligase. The generated vector pcDNA3.1-Npr2-BirA(R118G)-HA expresses the Npr2-BirA* fusion protein (approx. 152 kDa) with supplementary N-terminal HA-tag under the cytomegalovirus promoter.

After transformation into DH5α bacteria and positive ampicillin selection, restriction and sequence analysis revealed correctly ligated plasmids. The final vector had a size of 9532 bp. The cloning strategy for the pcDNA3.1-Npr2-BirA(R118G)-HA vector is illustrated in detail in Figure 37. The cloning strategy for the BirA*-cGKIα expression vector was based on the commercially available pcDNA3.1-mycBioID vector. In this case, the biotin protein ligase was fused to the N-terminal end in order to have no effect on the active site of the cGKIα which has to interact with the phosphorylation targets. The entire cDNA of the

cGKIα except for the start codon was obtained from a pBluescriptIIKS(+)-cGKIα expression vector by PCR amplification and introduced into the multiple cloning site of the pcDNA3.1-mycBioID vector using the cleavage sites of the restriction enzymes *Not*I and *Bam*HI along with sticky end DNA ligation. After transformation into DH5α bacteria and positive ampicillin selection, the restriction and sequence analysis revealed correctly ligated plasmid vectors. The final vector had a size of 8521 bp. The strategy for the pcDNA3.1-mycBioID-cGKIα vector is illustrated in Figure 38.

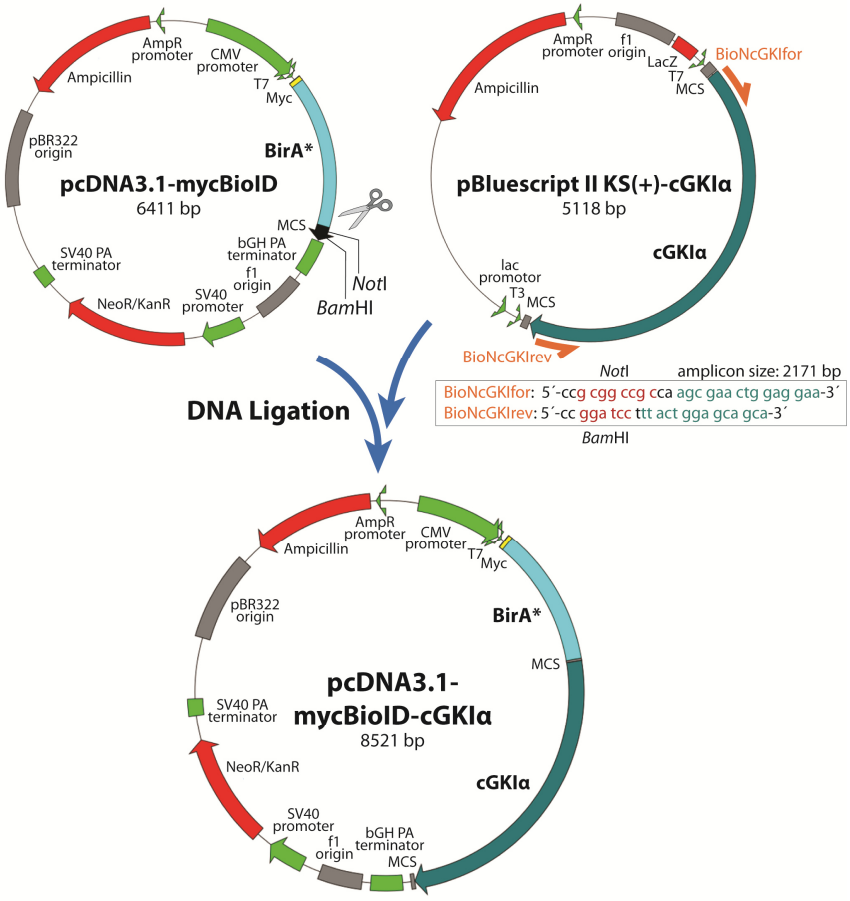

Figure 38: Molecular cloning strategy for the BirA*-cGKIα expression vector. Two oligonucleotides were designed to amplify the cGKIα cDNA from the pBluescript II KS(+)-cGKIα plasmid. The resulting PCR amplicon covered the complete open reading frame of cGKIα except for the start stop codon and was additionally flanked by two novelly attached *Not*I and *Bam*HI restriction sites. The cleavage sites of *Not*I and *Bam*HI were then used for integration into the multiple cloning site (MCS) of the commercial pcDNA3.1-mycBioID vector considering the same reading frame as well as for the biotin ligase. The new vector pcDNA3.1-mycBioID-cGKIα expresses the BirA*-cGKIα fusion protein (approx. 111 kDa) with an additional C-terminal Myc-tag under the cytomegalovirus promoter.

5.3.2 Verification of the Npr2-BirA* and BirA*-cGKIα fusion protein expression in F11 cells

The F11 cell line is a fusion product of the mouse neuroblastoma cell line N18TG-2 with embryonic dorsal root ganglion neurons from the rat and should therefore provide an artificial *in vitro* cell system which resembles the expression profile of DRG neurons. The expression of both fusion proteins in F11 cells was attested by immunocytochemistry 48 hours after plasmid transfection. The expression of the BirA*-cGKIα fusion protein was proven for single transfected cells due to its plasmid-mediated overexpression which strongly overlaid the background signal of the endogenous expressed cGKIα (Figure 39). The immunocytochemic detection of Npr2 which is not endogenously expressed in F11 cells revealed an efficient expression of the fusion protein, too. Western blot analysis of biotin treated F11 cells transfected either with pcDNA3.1-mycBioID-cGKIα or pcDNA3.1-Npr2-BirA(R118G)-HA confirmed the efficient and accurate expression of both fusion proteins. After fractionation, entire cell lysate samples as well as eluate samples obtained by purification with streptavidin-conjugated beads were tested with the same antibodies applied for the immunocytochemistry. The recombinant cGKIα fusion protein which has a theoretically calculated size of 111 kDa was detected in the cytosolic and membrane fractions of the cell lysate sample as well as the eluate sample (Figure 39). Results of the latter, showing that the BirA*-cGKIα proteins were biotinylated, proved the dimerization of single BirA*-cGKIα molecules due to their reciprocal biotinylation. The double band at 75 kDa which is specific for the endogenous cGKIα protein was detected in both fractionated cell lysate samples but not in the cytosolic eluate sample and only the upper band slightly in the membrane fraction. The fact that mainly the BirA*-cGKIα proteins were captured by biotin-streptavidin purification indicated that the dimerization preferably proceeded between recombinant fusion proteins among themselves. The obviously insufficient affinity capture of the cytosolic fraction was later substantially improved by changes in the composition of the lysis buffer permitting cell lysis under gentle conditions. The recombinant Npr2 fusion protein which has a theoretically calculated size of 152 kDa was primarily detected in the membrane fractions of the cell lysate sample and the eluate sample (Figure 39). Consequently, the Npr2-BirA* proteins were correctly anchored in the membrane. In addition, the efficient

biotin-streptavidin purification of Npr2-BirA* proteins caused by reciprocal biotinylation revealed the dimerization of single Npr2-BirA* molecules which is essential for an operative receptor. No endogenous Npr2 was attested due to the lack of expression in the F11 cell line.

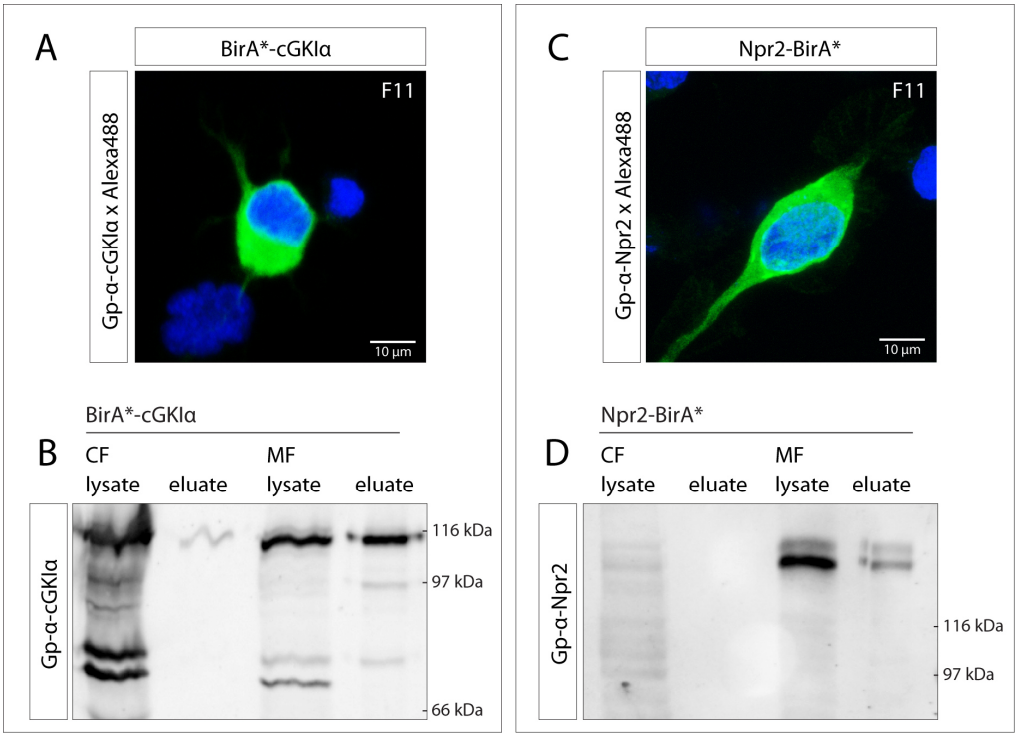

Figure 39: Immunocytochemistry and Western blot validation of recombinant protein expression in F11 cells. (A) Immunocytochemistry using a guinea pig-α-cGKIα antibody and DAPI-staining demonstrated the BirA*-cGKIα expression in F11 cells 48 hours after plasmid transfection by Lipofectamine reagent. The emission of the Alexa Fluor 488 conjugated secondary antibody revealed an efficient plasmid expression. BirA*-cGKIα was localized in the cytosol. (B) Same antibody exposed the endogenous cGKIα double band at 75 kDa as well as the recombinant cGKIα fusion protein band at 111 kDa by immunoblot analysis. Both were detected in the cytosolic fraction (CF) and the membrane fraction (MF). The lysate samples included all proteins after cell lysis. The eluate samples contained all proteins which were purified by streptavidin-mediated affinity capture after BirA* induced biotinylation. (C) Immunocytochemistry using a guinea pig-α-Npr2 antibody and DAPI-staining displayed efficient expression of Npr2-BirA* in F11 cells after 48 hours. Npr2-BirA* was localized in the cytosol and at the cell membrane. (D) The recombinant Npr2 protein was detected at 152 kDa by Western blot analysis using the guinea pig-α-Npr2 antibody, primarily in the membrane protein fraction and only slightly in the cytosolic fraction. Endogenous Npr2 protein was unverifiable since the receptor is not expressed in F11 cells. The lysate samples included all proteins after cell lysis. The eluate samples contained all proteins which were purified by streptavidin affinity capture after BirA* induced biotinylation.

5.3.3 Verification of proximity-dependent biotinylation induced by Npr2-BirA* and BirA*-cGKIα fusion proteins

Before the mass spectrometry, the degree of inducible biotinylation and the efficiency of the biotinylation-dependent purification were maximized and adjusted. 48 hours after transfection, Npr2-BirA* and BirA*-cGKIα transfected F11 cells together with untransfected control cells were treated with 50 µM biotin over a period of 16 hours causing the proximity-dependent biotinylation mediated by BirA*. After cell lysis and fractionation, the protein lysates were incubated with streptavidin-conjugated beads in order to bind all biotinylated proteins. The subsequent heat-induced elution with SDS containing sample buffer purified the biotinylated proteins by disruption of the biotin-streptavidin binding. The western blot analysis using streptavidin-HRP conjugate revealed a range of sample-specific protein bands (Figure 40). The band pattern of the untransfected cell samples was indicative for unspecifically bound and non-biotinylated proteins. The most important internal control to prove accurate biotinylation and efficient purification was the exclusive detection of biotinylated cGKIα fusion proteins at 111 kDa for the BirA*-cGKIα samples and the exclusive detection of biotinylated Npr2 fusion proteins at 152 kDa for the Npr2-BirA* samples. While the BirA*-cGKIα protein was strongly attested in both subcellular fractions, the Npr2-BirA* protein could be visualized slightly and only for the membrane fraction. The complementary silver staining revealed the complete protein quantity after affinity capture (Figure 40). 2 % of the cytosolic lysate and 4 % of the membrane protein lysate were applied per lane. Both recombinant fusion proteins and distinct protein bands were again detected. The silver staining showed a large number of unspecific proteins for every sample possibly dragged along the purification step.

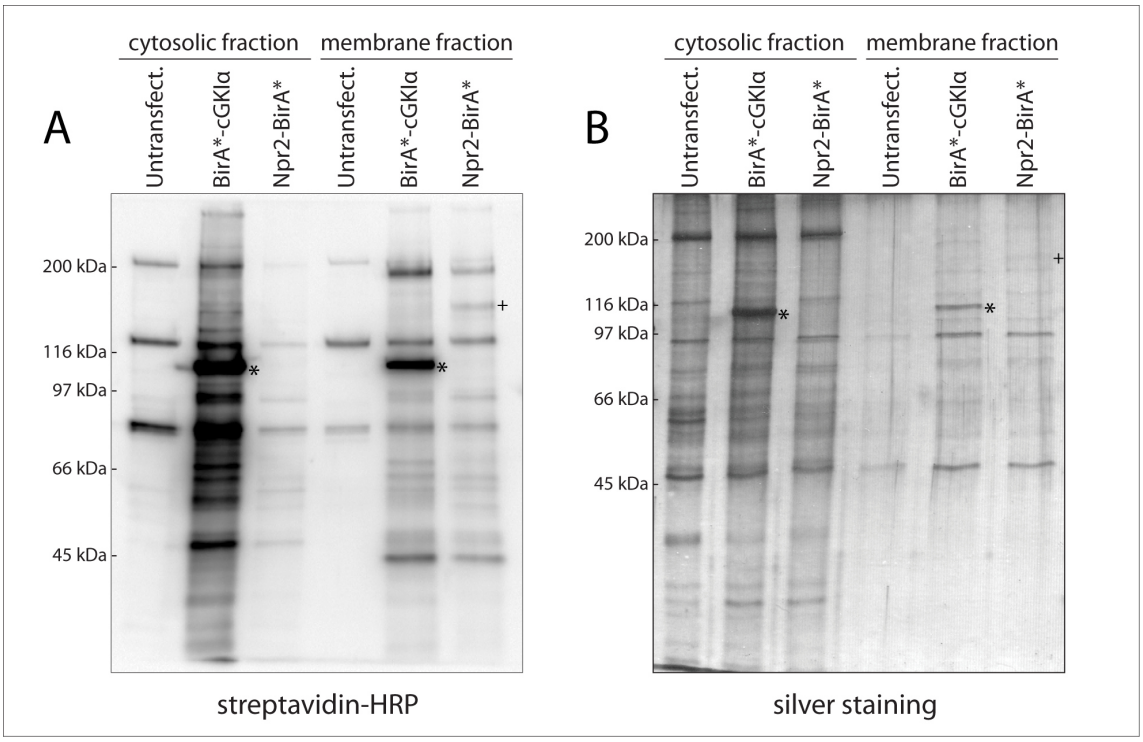

Figure 40: Western blot and silver staining analysis of affinity purified protein samples before MS-analysis. (A) Western blot analysis with horseradish peroxidase associated streptavidin to visualize biotin-bound proteins. The cytosolic fraction and membrane fraction were obtained from the same cell source per particular sample condition. 2.5 % of the total cytosolic sample and 3.5 % of the solubilized membrane proteins were applied respectively. In both fractionations, the untransfected F11 cell sample revealed unspecifically purified proteins. The BirA*-cGKIα samples showed a distinct banding pattern with increased biotinylation rate in the cytosolic fraction. The recombinant cGKIα fusion protein (*) was detected in either cases at 111 kDa serving as positive control due to its self-biotinylation. The Npr2-BirA* samples showed a decreased quantity of biotinylated proteins compared to BirA*-cGKIα samples with tendentially more biotin-bound proteins in the membrane fraction. The Npr2 fusion protein ($^{+}$) appears only in the membrane fraction at 152 kDa which in turn is the positive control for the Npr2-BirA* samples. (B) Silver stain analysis illustrated the complete protein quantity after purification. Without streptavidin-mediated enhanced chemiluminescence, all non-biotinylated, unspecific proteins, which have been dragged along the purification step, were now visualized. Especially, the untransfected cytosolic sample now showed an amplified banding pattern. In general, the protein yield of the cytosolic fractions was significantly higher compared to the membrane fractions.

5.3.4 Mass spectrometric analysis of proximity-dependent biotinylated proteins

Three biological replicates for each test condition were prepared for MS-analysis. Details about the sample preparation are given in the Methods section. In brief, untransfected as well as Npr2-BirA* or BirA*-cGKIα transfected F11 cells were treated with 50 µM biotin over a period of 16 hours to cause the proximity-dependent biotinylation mediated by BirA*. After cell lysis, cell fractionation, and affinity purification using streptavidin-conjugated beads, all protein samples were reviewed for efficient

biotinylation before MS-analysis by Western blot analysis using streptavidin-HRP and silver stain analysis. The quantitative proteomic analysis using label-free quantification (LFQ) was performed by Dr. Oliver Popp from the MS core facility at the Max Delbrück Center for Molecular Medicine in Berlin. Single detected peptides were aligned with a protein database of *rattus norvegicus*. A total of 821 protein species were attested for all protein samples together. Figure 41 illustrates the number of proteins that were detected per congeneric protein samples in relation to their mean LFQ intensity. These results were consistent with the findings of the western blot analysis using streptavidin-HRP conjugate or the silver staining. Irrespective of the type of sample, the number of proteins and their absolute LFQ intensity was significantly increased in the cytosolic fraction compared to the membrane fraction. The BirA*-cGKIα transfected F11 cell samples exhibited the highest quantity of proteins while a balance was nearly maintained between untransfected F11 cell samples and Npr2-BirA* transfected F11 cell samples.

Figure 41: Histograms of LFQ intensities. The summarizing graphs illustrate the number of proteins that were detected per congeneric protein samples in relation to their mean LFQ intensity. A total of 821 diverse protein species were attested. Three biological replicates were measured; (CF) cytosolic fraction; (MF) membrane fraction; (UN) untransfected F11 cell sample; (B6) BirA*-cGKIα transfected F11 cell sample; (C7) Npr2-BirA* transfected F11 cell sample.

To narrow down putative candidates that participated in protein-protein interactions, the mass spectrometry results were evaluated from a qualitative point of view while the LFQ intensity was only secondarily considered. The selection process consequently relied on the comparison between the three types of protein samples and a process of elimination. Whereas the untransfected F11 cell samples served as negative control for the Npr2-BirA* and the BirA*-cGKIα transfected F11 cell samples, the latter two were mutually exclusive. First and foremost, all proteins which were also positive in the untransfected samples were excluded due to their unspecific and biotinylation-independent purification. The residual proteins were screened for candidates which were exclusively detected either in Npr2-BirA* or in BirA*-cGKIα samples along with the mandatory verification to be found in every of the three biological replicates. In the tabular summary, the identified proteins are registered in descending order referring to their LFQ intensities and with respect to the particular cell sample and cellular fraction (Table 12-15). The detection of the Npr2 receptor in all Npr2-BirA* samples as well as the detection of the cGKIα kinase in all BirA*-cGKIα samples served as internal positive control and as scale for the relative degree of potential protein interaction or protein proximity. Another positive control for the BirA*-cGKIα fusion protein interaction was the G kinase-anchoring protein 1 which is known to interact with cGKIα by guiding the kinase to the membrane. In general, very few proteins were identified in the membrane fractions, whereas distinctly more proteins were found in the cytosolic fractions. To further delineate the proteins of the BirA*-cGKIα samples, only proteins were taken into account which contain a predicted phosphorylation site of cGKIα (K/R-K/R-X-S/T). Since phosphorylation targets of cGKIα are of main interest, the presence of a cGKIα phosphorylation site is required in interacting proteins. Thereby, eight proteins were excluded. In addition, proteins were listed which were tested three times positive for both the BirA*-cGKIα and the Npr2-BirA* fusion protein. Interestingly, a variety of all discovered proteins belonged to the cytoskeleton network and had mainly a neuronal relation. 20 of the BioID-revealed proteins were further analyzed by RT-PCR in order to demonstrate that the potential protein-protein interaction could generally have relevance *in vivo*. All of them were found to be expressed in dorsal root ganglia neurons at embryonic day 12.5. The attested proteins are labeled with red asterisks in the tabular summaries and the results of the RT-PCR are shown in Figure 42. In the case of

the identified Talin-1 protein, the usage of two distinct RT-PCR primer pairs revealed Talin-2 as the probably detected protein. Since only Talin-2 is expressed in DRGs at an early stage, the incorrect classification of the MS-analysis could be potentially caused by a high level of sequence similarity between Talin-1 and Talin-2.

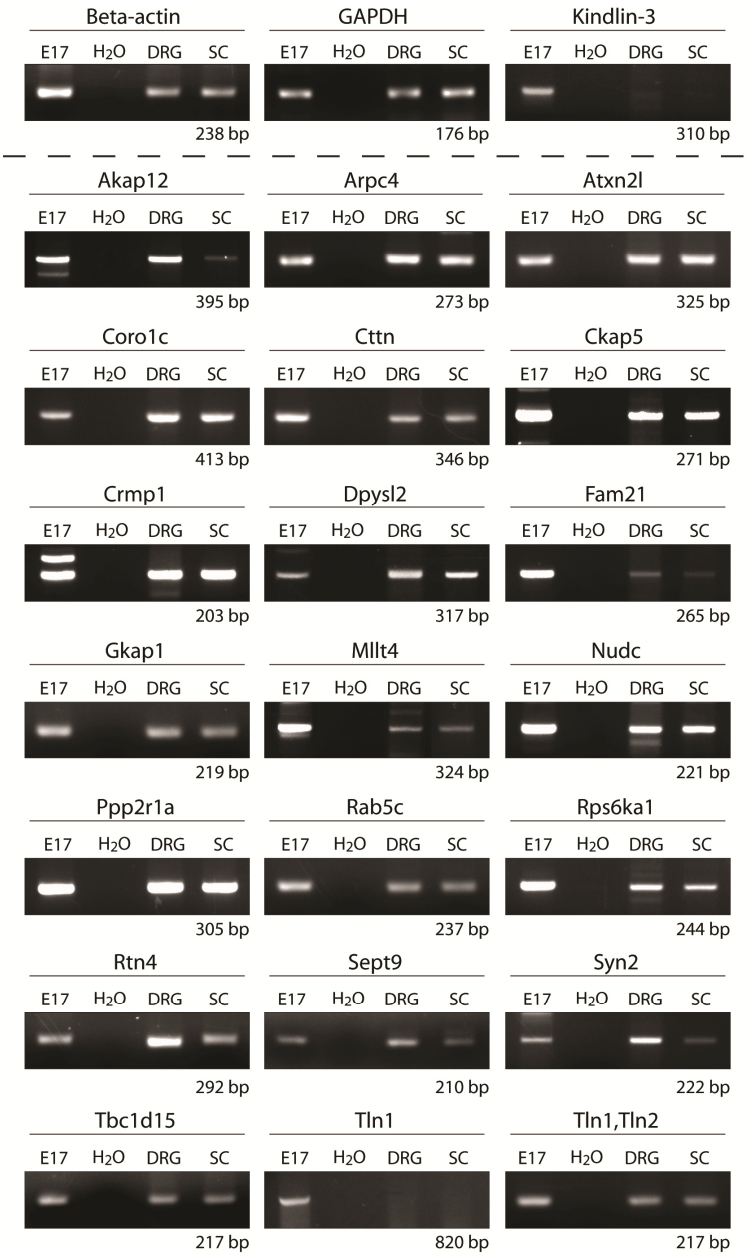

Figure 42: RT-PCR gene expression analysis in DRGs of proteins identified by BioID assay and MS-analysis. The same template cDNAs were used for every reaction; (E17) whole embryo at stage E17 as expression control; (H_2O) water control; (DRG) dorsal root ganglia at E12.5; (SC) spinal cord at E12.5. 1.2 µg of mRNA isolated from DRG or SC samples (both development stage E12.5) were reversely transcribed into cDNA which served as a template for RT-PCR analysis permitting a semi-quantitative interpretation. The housekeeping genes *beta-actin* and *GAPDH* were included to contrast the basal expression. Kindlin-3 which is not expressed either in DRGs or spinal cord served as negative control.

Specific proteins for BirA*-cGKIα (cytosolic fraction)									
Protein name	**Gene**	**MW (kDa)**	**Amino acids**	**Intensity**	**BirA*-cGKIα/ Untransf. p-value**	**BirA*-cGKIα/ Npr2-BirA* p-value**	**Phospho-rylation motifs**	**Relative to cGKIα**	**Function**
cGKIα	Prkg1	51.9	459, 762	9.22E+10	0.070	0.070	-	-	endogenous and recombinant cGKIα (positive control)
cGKIα fragment	D4AAY2	10.6	89	5.88E+09	0.101	0.101	2x	1 : 15.7	cGKIα fragment (proteolysis product)
Cortactin	Cttn *	56.9	509	7.14E+08	0.024	0.024	1x	1 : 129	related to actin filament modeling/ target of the Focal adhesion kinase 1 (FAK1)
Host cell factor 1	Hcfc1	209.2	2034	4.42E+08	0.043	0.043	1x	1 : 209	involved in control of the cell cycle
Ataxin-2-like protein	Atxn2l *	113.1	1074	2.44E+08	0.002	0.002	2x	1 : 378	unknown function/ associated with a complex group of neurodegenerative disorders
Dihydropyrimidinase-related protein 2	Dpysl2 *	62.3	572	2.15E+08	0.054	0.054	2x	1 : 429	necessary for signaling by class 3 semaphorins and cytoskeleton remodeling/ phosphorylation (Thr-514) by GSK3β abolishes tubulin-binding
Coronin	Coro1c *	53.2	474	2.08E+08	0.025	0.025	1x	1 : 443	binds F-actin/ highly enriched in F-actin-rich areas
Nucleoprotein TPR	Tpr	267.3	2360	2.03E+08	0.050	0.050	4x	1 : 454	component of the nuclear pore complex/ required for the trafficking across the nuclear envelope
Ribosomal protein S6 kinase	Rps6ka1 *	24.3	211	1.68E+08	0.005	0.005	6x	1 : 549	serine/threonine-protein kinase that acts downstream of MAPK/ERK pathway (MAPK1/ERK2 and MAPK3/ERK1)
GTPase-activating protein RAB7	Tbc1d15 *	76.7	670	1.67E+08	0.013	0.013	1x	1 : 552	acts as a GTPase activating protein for RAB7A/ associated with sensory neuropathy (CMT2B)/ RAB7A controls neurite outgrowth signaling of NTRK1/TRKA
Cytoskeleton-associated protein 5	Ckap5 *	189.9	1718	1.55E+08	0.031	0.031	2x	1 : 595	binds the plus end of microtubules and regulates their dynamics and organization/ promotes cytoplasmic microtubule nucleation and elongation/ interacts with Lis1
Serine/threonine-protein phosphatase 2A	Ppp2r1a *	65.3	589	1.41E+08	0.001	0.001	1x	1 : 654	serine/threonine-protein phosphatase 2A 65 kDa regulatory subunit A alpha isoform/ constant regulatory subunit of protein phosphatase 2
G kinase-anchoring protein 1	Gkap1 *	41.9	366	1.30E+08	0.002	0.002	0x	1 : 709	cGMP-dependent protein kinase-anchoring protein of 42 kDa/ interacts with cGKIα (positive control)
Nuclear pore complex protein Nup54	Nup54	55.7	510	8.58E+07	0.008	0.008	1x	1 : 1075	component of the nuclear pore complex, a complex required for the trafficking across the nuclear membrane
Nuclear pore complex protein Nup124	Nup214	211.4	2067	8.15E+07	0.019	0.019	1x	1 : 1131	involved in the import of substrates across the nuclear pore complex
Cyclin-G-associated kinase	Gak	138.4	1256	7.99E+07	0.038	0.038	1x	1 : 1154	involved in the uncoating of clathrin-coated vesicles
Signal recognition particle subunit SRP68	Srp68	65.9	587	6.56E+07	0.004	0.004	2x	1 : 1405	signal-recognition-particle assembly has a crucial role in targeting secretory proteins to the rough endoplasmic reticulum membrane
Eukaryotic translation initiation factor 3 subunit D	Eif3d	64.0	548	6.11E+07	0.007	0.007	1x	1 : 1509	component of the eukaryotic translation initiation factor 3 (eIF-3) complex
WASH complex subunit FAM21	Fam21 *	136.2	1246	4.42E+07	0.073	0.073	6x	1 : 2086	complex present at the surface of endosomes/ recruits and activates the Arp2/3 complex to induce actin polymerization

Table 12: Tabular summary of mass spectrometrically detected proteins which were exclusively attested in the cytosolic fraction of BirA*-cGKIα samples. Descending order of the proteins is determined by the entire intensity measured during three experimental replicates. P-value calculation compares distribution of the protein intensity in the BirA*-cGKIα samples with the distribution in untransfected samples or Npr2-BirA* samples. Ratio of potential protein-protein interaction is listed considering intensity ratio between the cGKIα fusion protein and purified proteins. Known protein functions were obtained using the Swiss-Prot section of the UniProt Knowledgebase (http://www.uniprot.org). Red asterisks indicate proteins which were confirmed by RT-PCR to be expressed in DRGs at E12.5. The number of predicted phosphorylation sites of cGKIα (K/R-K/R-X-S/T) is given for each protein.

Specific proteins for Npr2-BirA* (cytosolic fraction)								
Protein name	**Gene**	**MW (kDa)**	**Amino acids**	**Intensity**	**Npr2-BirA*/ Untransf. p-value**	**Npr2-BirA*/ BirA*-cGKIα p-value**	**Relative to Npr2**	**Function**
Natriuretic peptide receptor 2	Npr2	114.4	1022	1.05E+09	0.231	0.231	-	recombinant Npr2 (positive control)
Histone H1.4	Hist1h1e	22.0	219	2.25E+08	0.162	0.162	1 : 4.7	necessary for condensation of nucleosome chains into higher-order structured fibers
A-kinase anchor protein 12	Akap12 *	170.2	1582	1.91E+08	0.170	0.170	1 : 5.5	anchoring protein mediating the subcellular compartmentation of protein kinase A (PKA) and protein kinase C (PKC)
Synapsin-2	Syn2 *	52.5	479	1.65E+08	0.032	0.032	1 : 6.4	neuronal phosphoprotein that coats synaptic vesicles/ binds to the cytoskeleton/ believed to contribute to the regulation of neurotransmitter release
Nucleolin	Ncl	61.7	569	1.58E+08	0.073	0.073	1 : 6.6	nucleolin is the major nucleolar protein of growing eukaryotic cells
Splicing factor U2AF 65 kDa subunit	U2af2	53.5	475	1.54E+08	0.043	0.043	1 : 6.8	required for splicing of pre-mRNA and for export of mRNA out of the nucleus
Junction plakoglobin	Jup	81.8	745	1.18E+08	0.359	0.359	1 : 8.9	common junctional plaque protein/ can replace beta-catenin in E-cadherin-catenin adhesion complexes to couple cadherins to the actin cytoskeleton
Proteasome activator complex subunit 1	Psme1	28.6	249	6.87E+07	0.006	0.006	1 : 15	PA28 activator complex enhances the generation of class I binding peptides by altering the cleavage pattern of the proteasome
Actin-related protein 2/3 complex subunit 4	Arpc4 *	19.7	168	6.62E+07	0.032	0.032	1 : 16	functions as actin-binding component of the Arp2/3 complex which is involved in regulation of actin polymerization
Ras-related protein Rab-11A	Rab11a	24.4	216	5.15E+07	0.187	0.187	1 : 20	small GTPases Rab are key regulators of intracellular membrane trafficking
Peroxiredoxin-4	Prdx4	31.0	273	4.88E+07	0.205	0.205	1 : 22	regulates the activation of NF-kappa-B in the cytosol
Upf1 fragment (1124aa)	F1LY19	43.1	391	4.68E+07	0.004	0.004	1 : 22	RNA-dependent helicase and ATPase/ required for nonsense-mediated mRNA decay
Ras-related protein Rab-5C	Rab5c *	23.4	216	4.41E+07	0.200	0.200	1 : 24	contributes to the regulation of filopodia extension/ KO of Rab5a decreases cancer cell motility and invasion through integrin-mediated signaling pathway
F1LXC8; F1LX65; F1LXC9; F1LXC6	-	58.8	529	3.90E+07	0.289	0.289	1 : 27	unkown protein with 51% identity with Epiplakin/ which belongs to the plakin or cytolinker family
Kinesin light chain 2	Klc2	66.9	605	3.61E+07	0.017	0.017	1 : 29	microtubule-associated force-producing protein/ plays a role in organelle transport
Annexin A6	Anxa6	75.2	667	2.83E+07	0.220	0.220	1 : 37	may regulate the release of Calcium ions from intracellular stores
Superkiller viralicidic activity 2-like 2	Skiv2l2	86.8	764	2.04E+07	0.126	0.126	1 : 52	involved in pre-mRNA splicing
Nuclear pore complex protein Nup160	Nup160	155.6	1380	1.44E+07	0.091	0.091	1 : 73	involved in poly(A)+ RNA transport

Table 13: Tabular summary of proteins which were exclusively detected in the cytosolic fraction of Npr2-BirA* samples. Descending order of proteins is aligned to the cumulative intensity measured during three independent biological replicates. P-value calculation is based on the distribution of protein intensity comparing the Npr2-BirA* samples either with the untransfected or BirA*-cGKIα samples. The relation between the intensity of Npr2 fusions protein and purified protein provides information about the probability of protein-protein proximity. The Swiss-Prot section of the UniProt Knowledgebase has been source for known protein functions **(http://www.uniprot.org).** Red asterisks indicate proteins which were confirmed by RT-PCR to be expressed in DRGs at E12.5.

A Specific proteins for BirA*-cGKIα (membrane fraction)

Protein name	Gene	MW (kDa)	Amino acids	Intensity	BirA*-cGKIα/ Untransf. p-value	BirA*-cGKIα/ Npr2-BirA* p-value	Phospho-rylation motifs	Relative to cGKIα	Function
cGKIα	Prkg1	51.9	459	1.59E+10	0.082	0.082	-	-	endogenous and recombinant cGKIα (positive control)
cGKIα fragment	D4AAY2	10.6	89	6.82E+08	0.094	0.094	2x	1 : 23	cGKIα fragment (proteolysis product)
Guanine nucleotide-binding protein G(s) subunit alpha isoforms short	Gnas	45.7	394	4.57E+08	0.070	0.070	0x	1 : 35	binds keratan sulfate (KS) chains/ KS chains are large molecules which absorb mechanical shock
NADPH-cytochrome P450 reductase	Por	77.0	678	2.62E+08	0.049	0.049	0x	1 : 61	membrane-bound enzyme required for electron transfer to cytochrome P450 in the endoplasmic reticulum

B Specific proteins for Npr2-BirA* (membrane fraction)

Protein name	Gene	MW (kDa)	Amino acids	Intensity	Npr2-BirA*/ Untransf. p-value	Npr2-BirA*/ BirA*-cGKIα p-value	Relative to Npr2	Function
Natriuretic peptide receptor 2	Npr2	114.4	1022	8.14E+08	0.231	0.231	-	recombinant Npr2 (positive control)
ADP/ATP translocase 1	Slc25a4	32.9	298	1.41E+08	0.065	0.065	1 : 5.8	catalyzes the exchange of cytoplasmic ADP with mitochondrial ATP across the mitochondrial inner membrane/ belongs to the mitochondrial carrier family
Reticulon-4	Rtn4 *	114.0	1045	1.30E+08	0.189	0.189	1 : 6.3	developmental neurite growth regulatory factor/ negative regulation of axon-axon adhesion and growth/ facilitator of neurite branching

Table 14: Compilation of proteins which were exclusively identified in the membrane fraction of either the BirA*-cGKIα samples (A) or the Npr2-BirA*samples (B). Listing and statistical calculation are in accordance with the previous charts for cytosolic fractions. Red asterisks indicate proteins which were confirmed by RT-PCR to be expressed in DRGs at embryonic day 12.5. **Protein functions have been outlined on the basis of the Swiss-Prot section of the UniProt Knowledgebase (http://www.uniprot.org).**

Specific proteins for BirA*-cGKIα and Npr2-BirA* (cytosolic fraction)												
Protein name	**Gene**	**MW (kDa)**	**Amino acids**	**Intensity cGKIα samples**	**Intensity Npr2 samples**	**BirA*-cGKIα/ Untransf. p-value**	**Npr2-BirA*/ Untransf. p-value**	**BirA*-cGKIα/ Npr2-BirA* p-value**	**Phospho-rylation motifs**	**Relative to cGKIα**	**Relative to Npr2**	**Function**
cGKIα	Prkg1	51.9	459	9.22E+10	-	0.070	-	0.070	-	-	-	endogenous and recombinant cGKIα (positive control)
Natriuretic peptide receptor 2	Npr2	114.4	1022	-	1.05E+09	-	0.232	0.232	-	-	-	recombinant Npr2 (positive control)
Coatomer subunit gamma	Copg2	55.1	490	9.22E+08	4.41E+08	0.062	0.061	0.174	1x	1 : 100	1 : 2.4	cytosolic protein complex/ reversibly associates with Golgi non-clathrin-coated vesicles
Afadin	Mllt4 *	189.0	1663	4.04E+08	1.82E+08	0.089	0.097	0.222	2x	1 : 228	1 : 5.8	nectin- and actin-filament-binding protein/ connects nectin to the actin cytoskeleton
Arginine-tRNA ligase, cytoplasmic	Rars	75.8	660	3.95E+08	1.72E+08	0.072	0.019	0.179	1x	1 : 233	1 : 6.1	catalyzes the attachment of specific amino acids to cognate tRNAs during protein synthesis
Nuclear migration protein nudC	Nudc *	38.4	332	3.17E+08	4.55E+08	0.105	0.122	0.550	1x	1 : 290	1 : 2.3	NudC associates with Lis1 and the dynein motor at the leading pole of neurons
ADP-ribosylation factor 4	Arf4	20.4	180	3.01E+08	3.23E+08	0.005	0.051	0.798	0x	1 : 306	1 : 3.3	plays a role in vesicular trafficking/ activator of phospholipase D
Ankyrin repeat domain-containing protein 17	Ankrd17	169.3	1589	2.73E+08	1.38E+08	0.018	0.019	0.046	3x	1 : 338	1 : 7.6	detected in DRGs (E17.5)/ plays a role in protein folding/ does not belong to cytoskeletal proteins
Septin-9	Sept9 *	38.5	333	2.71E+08	1.21E+08	0.095	0.078	0.233	1x	1 : 340	1 : 8.7	filament-forming cytoskeletal GTPase/ strong expression in DRGs (E9.5) / interacts with ARHGEF18
Dihydropyrimidinase-related protein 1	Crmp1 *	62.2	572	2.48E+08	2.13E+08	0.057	0.100	0.727	0x	1 : 371	1 : 4.9	necessary for signaling by class 3 semaphorins/ subsequent remodeling of the cytoskeleton
Talin-1	Tln1 *	269.7	2541	2.44E+08	1.15E+08	0.022	0.007	0.064	4x	1 : 378	1 : 9.1	high molecular weight cytoskeletal protein/ interacts with PTK2/FAK1/ only talin-2 is expressed in DRGs
Coatomer subunit delta	Arcn1	57.2	511	2.28E+08	1.69E+08	0.065	0.030	0.454	2x	1 : 404	1 : 6.2	coatomer complex/ required for budding from the Golgi membranes
Ubiquitin-like modifier-activating enzyme 1	Uba1	117.8	1058	1.68E+08	1.24E+08	0.036	0.023	0.324	2x	1 : 549	1 : 8.5	activates ubiquitin by first adenylating its C-terminal glycine residue with ATP
60S ribosomal protein L38	Rpl38	8.3	70	1.64E+08	1.52E+08	0.000	0.013	0.576	0x	1 : 562	1 : 6.9	ribosomal protein/ component of the 60S subunit (L38E family)
E3 SUMO-protein ligase RanBP2 Ran-binding protein 2	Ranbp2	341.0	3055	1.55E+08	8.80E+07	0.007	0.034	0.037	3x	1 : 594	1 : 12	involved in protein modification and sumoylation/ component of the nuclear export pathway
Eukaryotic translation initiation factor 3 subunit F	Eif3f	38.0	361	1.48E+08	9.73E+07	0.047	0.035	0.273	1x	1 : 623	1 : 11	required for several steps in the initiation of protein synthesis/ positive regulator of Notch signaling
Cytoplasmic dynein 1 heavy chain 1	Dync1h1	532.3	4644	1.42E+08	1.02E+08	0.005	0.010	0.045	9x	1 : 649	1 : 10	cytoplasmic dynein 1/ motor for intracellular retrograde motility of vesicles and organelles along microtubules
Acetyl-CoA carboxylase 2	Acacb	259.6	2316	1.27E+08	1.13E+08	0.050	0.024	0.710	4x	1 : 726	1 : 9.3	may be involved in the regulation of fatty acid oxidation or the provision of malonyl-CoA
Spectrin alpha chain, non-erythrocytic 1	Sptan1	284.6	2472	1.10E+08	1.05E+08	0.005	0.001	0.586	3x	1 : 838	1 : 10	candidate for the calcium-dependent movement of the cytoskeleton at the membrane

Table 15: Compilation of proteins which were concurrently attested in the cytosolic fractions of both biotin ligase fusion proteins. Total intensity, relative intensity, and statistical significance is separately presented for BirA*-cGKIα and Npr2-BirA* in accordance with the previous charts for cytosolic fractions. Red asterisks indicate proteins which were confirmed by RT-PCR to be expressed in dorsal root ganglia at embryonic day 12.5. Protein functions have been outlined on the basis of the Swiss-Prot section of the UniProt Knowledgebase (http://www.uniprot.org). The number of predicted phosphorylation sites of cGKIα (K/R-K/R-X-S/T) is given for each protein.

6. DISCUSSION

6.1 Generation of a floxed Npr2 mouse

The generation of a floxed Npr2 mouse was mandatory to create a conditional Npr2 knockout mouse in which the ablation of Npr2 expression is restricted to the sensory system in order to prevent the Npr2-related dwarf phenotype. It was intended to use this mouse model in behavioral studies to clarify whether the impaired axon bifurcation of sensory neurons found in Npr2-deficient mice causes a modification in sensory perception which would indicate that proper axon bifurcation at the dorsal root entry zone is necessary for regular processing of sensory stimuli. The Npr2-flox mouse model was designed with two *loxP* sites flanking exons 17 and 18 of Npr2 to inhibit the guanylyl cyclase activity of the expressed receptor protein. However, the first generated Npr2-flox mouse (Npr2-flox(1)) revealed a hypomorphic phenotype most likely caused by decreased Npr2 expression due to a splice site mutation. While sensory axons in the hypomorphic Npr2-flox(1) mouse bifurcate, the dwarf phenotype and premature mortality was not prevented and the mouse model was not qualified for behavioral studies.

Another Npr2 gene targeting vector was created with extended 5´ homology region to improve the inefficient ES cell recombination rate of the first cloned targeting vector. Following this, the Npr2-flox mouse was generated based on ES cell line R1 as well as ES cell line $SV129_{(TCF)}$. These Npr2-flox(2) mouse models were free of genetic mutations. The Npr2-flox(2) allele encodes for Npr2 wild-type protein resulting in regular axon bifurcation of sensory neurons and regular bone development. Generation of a conditional Npr2 knockout mouse, in which the axon bifurcation is impaired and the dwarf phenotype is prevented, was possible using the Wnt1-Cre driver mouse line. Nevertheless, approximately one-half of the Npr2-flox(2)$^{flox/flox}$; Wnt1-Cre^{+} mice deceased prematurely. Furthermore, most of the affected Npr2-cKO animals revealed retarded physical development, overgrowth of incisors, and an intestinal disorder. The other half of the Npr2-flox(2)$^{flox/flox}$; Wnt1-Cre^{+} mice showed none of these adverse phenotypes. All Npr2-cKO animals were heterozygous for the Wnt1-Cre allele.

A plantar test (Hargreaves´ method) was performed comparing Npr2-flox(2)$^{flox/flox}$ and healthy Npr2-flox(2)$^{flox/flox}$;Wnt1-Cre^{+} mice which revealed that the paw withdrawal

latency of Npr2-cKO mice is significantly increased. This result demonstrated for the first time that the axon bifurcation of sensory neurons at the dorsal root entry zone of the spinal cord plays a role for regular sensory perception.

6.1.1 The hypomorphic Npr2-flox(1) mouse model

The results of the first attempt to generate a conditional Npr2 mouse mutant did not meet the expectations. The homozygous genotype of the Npr2-flox(1) mouse demonstrated roughly the same bone phenotype which is characteristic for Npr2 and CNP null mice. Therefore, it was concluded that the recombinant floxed Npr2 allele mistakenly induces a full gene knockout even before crossbreeding with Cre driver mouse lines. A closer study of the genetic locus revealed two silent point mutations located at the intron-exon border of both *loxP*-flanked Npr2 exons. The origin of these mutations could not be precisely explained. The mutations were introduced either during gene targeting vector cloning and bacterial amplification or during ES cell cultivation. Since the single point mutations are not located in the 5´ homology or 3´ homology region of the gene targeting vector, the recombination process itself can be excluded as origin for the nucleotide substitutions. The correct sequence of the Npr2 gene targeting vector was verified by sequence analysis and a glycerol stock was stored at -80°C. In contrast, the ES cell clone which was used for the blastocyst injection was screened positive for both mutations. Unfortunately, the initial sequence analysis of the ES cell clone focused only on the accuracy of the *loxP* and *FRT* target sites. Even though the point mutations were only attested in the ES cell clone and the hypomorphic Npr2-flox(1) mouse, it appears more likely that the mutations were introduced by the genetically more unstable bacterial DNA amplification rather than during ES cell cultivation. The errorless gene targeting vector was amplified several times to obtain enough DNA material which was required for the numerous ES cell electroporations.

Analysis of Npr2 gene expression at the RNA level indicated that the RNA splicing machinery is affected by the silent point mutations causing an alternatively spliced mRNA strand of Npr2 lacking exactly the sequence of exon 18. However, the recognition of the splice donor site and splice acceptor site is not consistently misguided. Semi-quantitative RT-PCR comparison of wild-type mRNA and alternatively spliced mRNA of Npr2 expressed by homozygous Npr2-flox(1) mice revealed that the Npr2-flox(1) allele

encodes for around 15 percent of wild-type mRNA and around 85 percent of alternatively spliced mRNA. It can be assumed that an Npr2 protein based on an mRNA template missing exon 18 leads to a non-functional receptor protein, due to the fact that a single amino acid exchange in exon 18 has been shown to prevent the entire enzymatic activity of the guanylyl cyclase (Tsuji and Kunieda, 2005). As a result, the splice site mutation causes a hypomorphic allele mutation causing the partial loss of the Npr2 gene activity. Interestingly, this reduced Npr2 gene activity in the hypomorphic Npr2 mouse mutant resulted in an altered phenotype pattern compared to the conventional Npr2 knockout mouse, indicating that development and function of distinct cellular tissues depend on different expression levels of the Npr2 receptor protein. While female fertility in homozygous knockout mice is completely prevented (Kiyosu et al., 2012), at least around half of the hypomorphic Npr2 mice are able to reproduce even though the litter size is significantly reduced. However, the reduced *Npr2* gene activity cannot prevent the disproportionate dwarfism and the premature mortality found for the complete loss of gene expression (Chusho et al., 2001). Counter-intuitively, the hypomorphic Npr2 mutants show accurate sensory axon bifurcation at the dorsal root entry zone, indicating that the bifurcation machinery of DRG neurons is more stable in terms of a strikingly decreased *Npr2* gene activity. 15 percent of the regular Npr2 gene expression is still sufficient for an adequate cGMP production which can induce growth cone splitting. This is in line with observations on double heterozygosity of Npr2-deficient and cGKIα-deficient mice (Schmidt et al., 2007). In summary, the unintentionally generated hypomorphic Npr2 mouse represents an Npr2-related dwarfed mouse model with regular development of sensory axon branching pattern which is in conformity with wild-type animals.

The hypomorphic Npr2-flox(1) mouse was used to prove the functional principle of the floxed Npr2 allele. Despite the splice site mutation, conditional Npr2 knockout mice were generated successfully. Cross-breeding with the Wnt1-Cre driver mouse line leads to the intended lack of sensory axon bifurcation, in contrast usage of the Isl1-Cre driver mouse line did not produce an effect on the axonal branching of sensory neurons. This observation was unexpected because both directed Cre-recombinase expressions were thought to induce impaired axon bifurcation in DRG neurons during early embryonic stages. Lineage-tracing experiments have shown that the Wnt1/β-catenin signaling

pathway is a key factor for the sensory fate of pluripotent neural crest cells which migrate from the roof plate of the neural tube to become DRG neurons (Lee et al., 2004; Zirlinger et al., 2002). The LIM-homeodomain factor Isl1 is involved in the transition from sensory neurogenesis to subtype specification of DRG neurons. Gene knockout studies have shown that the *Isl1* gene activity is essential for the expression of nociceptive markers, like TrkA and Runx1, and proprioceptive markers, like TrkC and Runx3 (Sun et al., 2008). In summary, these data indicate, that the Wnt1-Cre activity is initiated before the Isl1-Cre activity during the embryonic neurogenesis of primary sensory neurons. Considering that the precise time point of the Cre-recombinase expression is crucial for the timely disruption of the Npr2 allele to prevent the axon bifurcation, it seems likely that the Cre enzyme activity controlled by the *Isl1* promoter is not introduced on time in order to affect the axonal branching of sensory neurons.

6.1.2 The Npr2-flox(2) mouse model

Prolongation of the recombination site at the 5´-end of the recloned gene targeting vector enabled considerably higher recombination rates in the ES cell culture compared to the first cloned gene targeting vector. This result is in line with previous studies analyzing ideal parameter settings for an efficient gene targeting frequency in ES cells. It was shown that the gene targeting efficiency is increased by at least 200 times associated with an increase of the homologous sequence from 1.3 to 6.8 kb indicating that the length of target homology is a critical factor (Hasty et al., 1991). In the case of the *Npr2* gene targeting vector, the extension of the homologous sequence from 1.6 to 6.0 kb enhanced the gene targeting frequency by factor 175. These data explain why around 2400 individual ES cell clones had to be screened in order to detect one positive ES cell clone in the beginning. While the R1 ES cell line showed a clear advantage for the recombination efficiency and the generation of chimeric animals, the $SV129_{(TCF)}$ line was superior for the germline transmission. The floxed Npr2 mouse model was finally generated based on both ES cell lines carrying the transgenic Npr2 allele. Prior DNA sequence and mRNA expression analysis of the ES cell clones guaranteed the prevention of the splice site mutation and the hypomorphic phenotype. The floxed Npr2 allele expressed a fully functional receptor protein. Floxed Npr2 mice with homozygous genotype did not show any kind of known Npr2-related phenotype. The heterozygous

and homozygous transgenic animals were in full conformity with wild-type animals in terms of bone growth, female fertility, longevity, and axon bifurcation of sensory neurons.

To analyze whether Cre-recombinase activity can cause the generation of an Npr2 knockout allele, the floxed Npr2 mouse was crossbred with the Wnt1-Cre driver line. As shown before, Cre-recombinase expression directed by the *Wnt1* promoter can specifically disrupt the *Npr2* gene activity leading to impaired growth cone splitting at the dorsal root entry zone. At the same time, the conditional Npr2 knockout (Npr2-cKO) mutant is not affected by dysfunctional endochondral ossification and develops a normally proportioned bone structure. This indicates that Cre/*loxP*-mediated recombination of the floxed Npr2 mouse model operates properly in order to induce the cell-specific loss-of-function of the Npr2 receptor protein. Closer study of the protein expression in DRG neurons reveals that the Npr2 protein is no longer detectable in case of the Npr2-cKO genotype. The genomic deletion of the two *loxP*-flanked exons, namely exon 17 and exon 18, was originally intended to lead to the expression of an enzymatically inactive Npr2 receptor protein lacking the central sequence of the guanylyl cyclase domain. However, it turned out that exon 17 is an asymmetrical exon which causes a framing error when it is removed. The conjunction of exon 16 and exon 19 of the conditional Npr2 knockout allele derived from the floxed Npr2 allele leads to a frame shift introducing a premature stop codon. The resulting aberrant protein structure is most likely not accurately folded by molecular chaperones and subsequently directed to the ubiquitin-proteasome system for destruction (Imai et al., 2003). As a result, the cell-specific Cre activity entirely eliminates the Npr2 expression in the target tissue of the floxed Npr2 mouse model. Nevertheless, it is now possible to create an Npr2-cKO mutant which is well suited for behavioral studies to analyze the consequence of deficient axonal branching at the DREZ independent from the bone phenotype.

6.1.3 Generation of conditional Npr2 knockout mice causes intestinal disorders, abnormal incisors size, and premature death

Breeding of a sufficient number of experimental animals for behavioral studies concerning sensory perception is hampered by unexpected side effects which exclusively occur in conditional Npr2 knockout animals carrying the Wnt1-Cre allele. While homozygous floxed Npr2 mice show a wild-type phenotype, around half of the Npr2-cKO mice derived from the same litter have a significantly higher premature mortality rate. Affected animals show overgrowth of incisors, proportioned growth retardation probably caused by malnourishment, and physical weakness as well as lethargy shortly before death. Everything points to the fact that the food ingestion is severely disturbed resulting in premature death most likely due to starvation of affected mice. Interestingly, previous studies have already created the link between a gastrointestinal tract disorder and the cause of death provoked by Npr2 loss-of-function (Sogawa et al., 2010, 2013). It was demonstrated that the CNP-Npr2-signaling defect found in the short-limb dwarfism (slw) mouse leads to intestinal distention and milk retention in the stomach which presumably causes death before weaning. Further analysis has revealed that the circular muscle cells of the pylorus and the large intestine do not respond any more to CNP stimulation in slw/slw mice. Moreover, it was shown that the CNP-induced cGMP signaling is distributed in neuronal tissue in the gastrointestinal tract (Sogawa et al., 2010). More detailed studies have suggested that the CNP-Npr2-mediated cGMP production affects the gastrointestinal smooth muscle relaxation in the pylorus, colon, and rectum which contributes to gastric emptying. Furthermore, the Npr2 receptor has been found to be highly expressed in nerve fibers, blood vessels, and smooth muscle cells of the gastrointestinal tract (Sogawa et al., 2013). Since the preparation of moribund Npr2-cKO mice revealed an obvious intestinal phenotype, it is reasonable to assume that the Cre activity directed by the *Wnt1* promoter induced the Npr2 knockout allele in cell populations which belong to the gastrointestinal tract. The intestinal inflammation and restrained digestive gases indicate that the intestinal motility of the conditional Npr2 knockout animal could be disturbed as well. If one considers that progenitor cells of the neural crest migrate extensively to give rise to most of the peripheral nervous system, including enteric, sympathetic, parasympathetic, and dorsal

root ganglia, as well as to the craniofacial skeleton and smooth muscles, it is most likely that the early Cre activity, which is induced directly after the neural crest delamination, could cause the Npr2 loss-of-function in all of the above-mentioned cellular tissues (Hu et al., 2014). Since Npr2 is expressed in neuronal and muscular cell populations of the digestive tract, it cannot be clarified whether the intestinal disorder of the conditional Npr2 knockout is related to a shutdown of the receptor expression in the enteric nervous system or the smooth muscle cells of the gastrointestinal tract (Sogawa et al., 2013). Data obtained from developmental assessments of the enteric nervous system have additionally shown that the Wnt1-Cre driver line can be used to generate conditional knockout mutants of distinct neuronal cell populations of the enteric nervous system (Lake and Heuckeroth, 2013). By using the *Wnt1*-directed Cre expression in combination with several floxed genes, it was possible to induce disrupted pattering of the enteric ganglia and the fiber network, reduction in neuronal density, and colonization failures of enteric neural crest derived cells (Fuchs et al., 2009; Hendershot et al., 2007; Zehir et al., 2010). In accordance with the literature, it is most likely that Cre-recombinase activity controlled by the *Wnt1* promoter induces the ablation of Npr2 expression in migrating neural crest cells before their sensory lineage. As a result, another NCC-derived cell population, apart from sensory DRG neurons, could be affected by impaired Npr2 activity causing the gastrointestinal disorder and premature death. Further analysis of the intestinal motility and tissue structure could provide detailed information about the role which Npr2 expression in both the enteric nervous system and the intestinal smooth muscles plays for the motorial and secretory activity of the lower digestive tract. Associated with distinctive Cre-driver mouse lines, the floxed Npr2 mouse model could be used to generate conditional Npr2 knockout mutants which target either neuronal or smooth muscle cells of the gastrointestinal tract.

Surprisingly, the dental phenotype of malformed incisors partly observed in the Wnt1-Cre induced Npr2-cKO mouse as well as the hypomorphic Npr2 mouse has never been reported before in any study analyzing conventional Npr2 knockout mice like the *cn/cn*, *slw/slw*, or *pwe/pwe* mouse (Geister et al., 2013; del Marco, 1981; Sogawa et al., 2007; Tsuji and Kunieda, 2005). Even though these studies mainly focus either on skeletal growth of the achondroplastic mouse model or on oocyte meiotic arrest, a physical abnormality like the overgrowth of incisors should have been noticed. As yet, the reason

for this discrepancy is a matter of speculation. However, three eventualities can be considered to be the origin of the dental phenotype, if one takes into account that migratory multipotent neural crest cells could be affected by the Cre activity before they are differentiating into smooth muscle and neuronal cells of the gastrointestinal tract or into craniofacial ganglia neurons and craniofacial bone cells (Hu et al., 2014). (1) The Npr2-mediated gastrointestinal tract disorder could simply prevent the usage and subsequent attrition of the teeth by causing food refusal. (2) The sensory perception of craniofacial ganglia neurons innervating the masseter muscles could be disturbed due to impaired axon bifurcation causing anatomically incorrect jaw movements and less attrition of the teeth. (3) Despite that the main endochondral ossification of the limbs is not altered, Npr2-negative neural crest derived bone cells which normally shape large parts of the craniofacial skeleton could induce a partial bone phenotype again causing anatomically incorrect jaw movements and less attrition of the teeth. To identify the leading contributor of the dental phenotype, closer monitoring of the precise phenotype occurrence is required comparing individual Npr2-related genotypes in respect of prevalence and degree of severity. For that reason, the floxed Npr2 mouse could be used in combination with distinct Cre driver mouse lines to induce the cell-specific Npr2 loss-of-function shortly after the subtype differentiation of neural crest cells in order to target distinct cellular tissues, such as the enteric nervous system or the intestinal smooth muscle cells.

Another important issue concerning unexpected Npr2-related phenotypes in the Wnt1-Cre induced Npr2-cKO mutant is the absolute death rate which is similar to that of the hypomorphic Npr2 mouse and the Npr2 knockout mice although the time of death is clearly postponed by a few weeks. In the literature, dwarfed Npr2 knockout animals have been reported to decease within the first three weeks of life which is consistent with results for the dwarfed hypomorphic Npr2 knockout mouse (Sogawa et al., 2010). This could indicate that the Npr2-related bone phenotype, which is prevented in the longer living Npr2-cKO mouse, is not necessarily the cause of death but has an additional negative effect on the premature mortality. At this point, the question arises, why half of the conditional Npr2 knockout mice are affected by early death whereas the remaining animals show absolutely no indication for any physical change or for a shorter life span. Previous studies have shown that even isogenic organisms with the same

genotype in the same environment can develop distinctive phenotypes on the basis of epigenetic modulation (Vogt et al., 2008). In the mouse, it has been shown that widespread alterations in DNA methylation can cause variances in cell proliferation and maturation by guiding transcriptional changes (Sim et al., 2014). In particular, distinct epigenetic contributions during neural crest development causing variable expressivity of phenotypes have been described in detail (Hu et al., 2014). Furthermore, numerous studies have addressed strain-dependent phenotype variability in genetically engineered knockout mice. It was shown that the genetic background onto which the gene-targeted allele is placed can cause completely different phenotypes, variations in the penetrance of phenotypes, and variable expressivity of the phenotypes (Doetschman, 2009; Sanford et al., 2001). Furthermore, study of standardized inbred mouse strains demonstrated a pivotal metabolic, hematologic, and biochemical difference between these inbred strains causing genetic background-dependent phenotypes (Champy et al., 2008). Considering the genetic diversity of the conditional Npr2 knockout animals due to the SV129 background derived from the injected embryonic stem cell, the C57BL/6 background derived from the blastocysts, and the subsequent crossbreeding with the Flpe-deleter and Wnt1-Cre mouse line, it is highly presumable that the individual DNA methylation and genetic background of every animal could play an important role for the penetrance and variable expressivity of the Npr2-related phenotypes. In around 50 percent of the Npr2-cKO mice, it seems as if the Npr2 gene defect can be fully compensated by the slightly different regulation of metabolic processes. The polyphenism of the Npr2-cKO mutant only applies to the intestinal disorder, overgrowth of incisors, and premature mortality. The lack of Npr2 expression, on the contrary, showed complete penetrance for the impaired axon bifurcation and the disproportioned dwarfism without variable expressivity of these phenotypes. In summary, the floxed Npr2 mouse model is qualified for the generation of conditional Npr2 knockout mutants, although the distinct crossbreeding with the Wnt1-Cre driver mouse line caused adverse effects.

6.1.4 Sensory hyposensitivity provoked by impaired axon bifurcation in Npr2-flox(2)$^{flox/flox}$;Wnt1-Cre^{+} mice

Even though the breeding of conditional Npr2 knockout mutants based on Wnt1-Cre was interfered by the premature mortality, it was possible to obtain a sufficient number of appropriate animals in order to perform behavioral studies. The results of the Hargreaves´ test showed for the first time that the lack of sensory axon bifurcation is associated with a functional effect *in vivo*. Conditional Npr2 knockout mice containing impaired axon bifurcation revealed a significantly increased latency to harmful heat stimulation. This sensory hyposensitivity of the Npr2-cKO mutant indicates that the pain threshold, which is the minimum intensity of the heat stimulus that is perceived as painful, is elevated which could be caused by a reduced neural innervation of the dorsal horn. The result of the behavioral test is in accordance with previous functional studies analyzing the lack of bifurcation by patch-clamp recording. Patch-clamp recordings have demonstrated that the frequency of synaptic events after capsaicin application in interneurons, which are connected downstream of the sensory DRG neurons, is significantly reduced in the case of the bifurcation error (Schmidt et al., 2007, 2009). Furthermore, it has been shown that the interstitial branching of collaterals from the primary stem axons remains unaffected in the Npr2 knockout while the ingrowing sensory axons turn either in rostral or in caudal direction (Schmidt et al., 2007). However, the total number of collaterals, which grow deeper into the spinal cord, must be reduced by about half due to the bifurcation error which bisects the number of primary stem axons elongating along the dorsal roof plate. Considering the results of the electrophysical and behavioral study, it can be postulated that a decreased number of synaptic connections is formed between primary and secondary neurons in the event of disturbed axonal T-branching at the dorsal root entry zone.

The observed Npr2-related loss in sensory perception could be explained as follows: While the sensory perception of the thermal stimuli in the periphery and the axonal transmission along the nociceptive Aδ-fibers is not adversely affected in the Npr2-cKO mutant, the totality of the stimulus information gets halved at the dorsal root entry zone. The random turning of the sensory stem axon in dorsal or caudal direction causes the reduced number of collaterals and the lower synaptic connectivity with the

interneuronal circuitry leading to a quantitative reduction of the perceived action potentials which are accumulated by the second order neurons. Considering that the network of the interneurons is unmodified in the Npr2-cKO mutant, it can be assumed that a higher sensory input for the same nociceptor is required to exceed the stated threshold in order to permit the onward stimulus conduction and processing. In accordance with the extended latency of the withdrawal reaction, non-bifurcated sensory neurons need to fire more action potentials to induce the motor response of the spinal reflex arc. However, it cannot be clarified whether only the direct control of motor neurons in the spinal cord or also the ascending pain pathway of the neospinothalamic tract which connects to the brain is affected by the impaired axon bifurcation.

In order to correctly interpret the obtained results, it has to be mentioned that a recent study focusing on an Npr2-related bifurcation error in the auditory system has revealed a slightly increased threshold in acoustic brain stem response but no indication for a behavioral-modifying effect. It has been shown that the mutant mice can hear even with the bifurcation deficit (Lu et al., 2014). This could indicate that the Npr2-induced axon bifurcation of primary neurons does not necessarily have the same function for every sensory system. Further comparative behavioral studies of distinct sensory bifurcation errors could finally provide detailed information about the precise function of the Npr2-induced bifurcation in the peripheral nervous system.

6.1.5 Outlook: which Cre driver mouse line could be appropriate for selective inactivation of Npr2 in sensory neurons?

Since the breeding of Npr2-cKO mice using the Wnt1-Cre mouse line is heavily restricted by premature mortality, it would be beneficial to use alternative Cre driver mouse lines in future behavioral experiments. In the course of this, the conditional Cre expression needs to be specifically initiated in sensory DRG neurons around embryonic day 8. Impaired axon bifurcation can only be induced, if the homozygous floxed Npr2 allele is transformed into the Npr2 knockout allele before sensory neurons enter the dorsal root entry zone starting at embryonic day 9.5 (Schmidt et al., 2007, 2009). On the contrary, an early Cre activity could again affect additional neural crest-derived cell tissue as seen in the Wnt1-Cre induced Npr2-cKO mutant. The cell-specific Cre expression has to be

localized outside of bone tissues throughout all stages of development to prevent the dysfunctional endochondral ossification. Coexisting overlaps of Cre and Npr2 expression in other tissues and at other developmental stages have to be preventively reviewed for unexpected phenotypes. So far, it is intended to use the TrkA-IRES-Cre ($Ntrk1^{tm1(cre)Lfr}$) and TrkC-IRES-Cre ($Ntrk3^{tm1(cre)Lfr}$) driver mouse lines for the generation of conditional Npr2 knockout mice. Upcoming behavioral studies based on the Cre-recombinase activity directed by the transcription pattern of the neurotrophic tyrosine kinase receptor type 1 (TrkA) and type 3 (TrkC), would allow to discriminate between distinct subtypes of sensory neurons in the DRG. While the TrkA expression is restricted to nociceptive sensory neurons, the expression of TrkB and TrkC is believed to define mechanosensitive and proprioceptive neurons (Huang et al., 1999). In general, the examination of Npr2-cKO mutants derived from dissimilar Cre driver mouse lines causing the same axon bifurcation phenotype would increase the reliability of congruent results. Furthermore, appropriate control animals have to be selected. It must be taken into consideration that cGMP signaling by itself has been shown to influence the perception of noninflammatory acute pain. In rats, determination of the analgesia nociception index in the tail flick test showed that antinociception is dependent on stress-induced cGMP activity (Carvalho et al., 2014). Pretreatment with the guanylyl cyclase inhibitor 1H-[1,2,4] oxadiazolo [4,3-a] quinoxaline-1-one blocked the painkilling effect induced by acute stress. Prior to this, multiple studies pointed out that the HO-CO-cGMP pathway, which is composed of the enzyme heme oxygenase (HO) that produces endogenous carbon monoxide (CO) and stimulates the formation of cGMP, plays a key phasic antinociceptive role in modulating physiological processes such as thermoregulation and nociception (Carvalho et al., 2011; Nascimento and Branco, 2007; Steiner et al., 2003). Although no direct reference has yet been made to the cGMP signaling of the particular guanylyl cyclase B, it is essential to clarify whether the sensory signal transmission of Npr2-cKO mice is exclusively altered by impaired axon branching. For this purpose, the conditional gene deletion has to take place once the growth cone has split and the neuronal connectivity of sensory neurons has been developed. Only if the structurally unmodified neuronal circuit lacking the enzymatic activity of Npr2 shows no sensory differences compared to the wild-type, an influence on the neuronal signal conduction by Npr2-mediated cGMP signaling can be excluded. Suitable Cre driver mouse lines, in

order to target peripheral sensory neurons at later embryonic stages, would be the Advillin-Cre or the TRPV1-Cre driver line. The *Advillin* gene encodes for an actin regulatory/binding protein involved in neuronal outgrowth and stress response of peripheral sensory neurons which is strongly expressed in dorsal root ganglia and trigeminal ganglia at embryonic stages E14.5 to E16.5 and in the adult animal (Zurborg et al., 2011). The capsaicin receptor TRPV1, which provides the sensation of heat and pain in nociceptive sensory neurons, is expressed in dorsal root ganglia from embryonic stage E14.5 until adult life stages (Diez-Roux et al., 2011; Elg et al., 2007). In both cases, behavioral tests would determine whether the Npr2 receptor expression at a later stage contributes to pain transmission regardless of the structural organization of the sensory circuitry.

6.1.6 Outlook: which behavioral tests might be performed with Npr2-cKO mice to explore physiological deficits upon axon bifurcation?

The conditional Npr2 knockout mouse model was primarily generated to clarify whether an impaired T-branching of primary sensory neurons can adversely affect conduction and processing of sensory stimuli causing anomalous mouse behavior. So far, the nociception assay, which demonstrated reduced pain perception in Npr2-cKO animals, gave a first indication for a sensory modulation disorder caused by the absence of axon bifurcation. To verify whether this observation can be transferred to other sensory perception systems, further behavioral studies have to be performed. Beyond that, the analysis of distinct sensory perception capabilities will determine whether the degree of sensory degradation is consistent for all perception processes or if it differs from case to case. The intended behavioral tests will focus on the different subpopulations of the sensory DRG neurons with respect to nociception, mechanoreception, and proprioception, respectively. Considering the variety of Npr2-mediated phenotypes, equal preconditions for all experimental animals, including conditional Npr2 knockout and control mice, have to be guaranteed before extensive test series can be started. The conformity of physical development, physical condition, and gross sensory motor skills needs to be validated. The latter will be monitored using the rotarod performance test (Jones and Roberts, 1968) in order to exclude prominent movement disorders that could

interfere with the reliability of subsequent behavioral testing. Since further analysis of acute pain sensitivity is required to confirm the results of the Hargreaves´ test, the spinal reflex pain will be measured using variants of the tail-flick test. Hot water and cold water immersion tail-flick tests could quantify the latency for the mouse to withdraw the tail when plunged into a beaker of water maintained at 52.5°C or in ice water, respectively (Gonzales-Rios et al., 1986; Pizziketti et al., 1985). The tail flick tests and the Hargreaves´ test provide information about the polysynaptic spinal reflex arc where peripheral nociceptors conduct noxious stimuli towards interneurons that are directly connected with motor neurons causing the withdrawal reflex. In contrast, the hot-plate test measures a reflex that is modulated by circuitry in the spinal cord as well as in the brain (Bannon and Malmberg, 2007; O'Callaghan and Holtzman, 1975). Comparing Npr2-cKO mice in both test procedures could furthermore clarify whether the minor innervation of the dorsal horn and the reduced connectivity with pain transmission neurons can be compensated and adjusted by the supraspinal circuitry of the brain. The assessment of pain, which can be manipulated by descending modulation coming from the thalamus and the brainstem, has been reported to be modified diversely, comparing between tail-flick test and hot-plate test (Pick et al., 1991). In addition to the acute pain perception, the formalin test could demonstrate, if the lack of axon bifurcation also affects persistent inflammatory pain perception (Bannon and Malmberg, 2007; Dubuisson and Dennis, 1977). Additional behavioral testing will focus on cutaneous mechanoreceptors which belong to another subset of sensory neuron of the dorsal root ganglion. In this context, a differentiation will be made between noxious and innocuous mechanosensation. Von Frey filaments will measure the withdrawal threshold to mechanical stimulation regarding painful touch sensation (Kwan et al., 2006; Pitcher et al., 1999). Additionally, the mechanosensitivity of low-threshold mechanoreceptors involved in the innocuous touch sensation could be determined using a tactile acuity test based on the MoTil system (Wetzel et al., 2007).

The aforementioned behavioural tests will determine the precise degree of sensory degradation caused by impaired axon bifurcation. Less collateral projections can transmit peripheral stimuli leading to an increased perception threshold. In order to investigate whether the T-shaped projection of sensory neurons within the spinal cord is also required to ensure a precise sensory mapping of peripheral stimuli, behavioral tests

could be performed that focus on complex neuromuscular motor activity regarding proprioception. Proprioception is a multicomponent sensory system for the sensation of the body position composed of various types of peripheral receptors like neuromuscular and neurotendinous spindles, Meissner and Pacinian corpuscles, Ruffini endings, and Merkel disks (Johnson et al., 2008). At conscious and unconscious levels, major sensory afferent pathways carry information about static limb position and limb movement (kinesthesia) from the spinal cord up to the sensory cortex where peripheral areas are represented in somatotopic and modality-based organization (Johnson et al., 2008; Niu et al., 2013; Schweizer et al., 2008). The analysis of conditional Npr2 knockout mice might be able to demonstrate that the point-for-point correspondence between periphery and sensory cortex is accessorily affected by appropriate T-shaped projections of sensory neurons. In that case, the bifurcation of afferent neurons would shape a kind of premature and preceded sensory map which contributes to the final somatotopic refinement in the brain. The assumption that the Npr2-related axon bifurcation of primary neurons could play a crucial role for the development of correct wiring diagrams in the spinal cord and the brain has recently been emphasized by connectivity analysis of the auditory system. It was shown that the bifurcation error of spiral ganglion neurons, which naturally bifurcate and subsequently branch into both the anteroventral cochlear nucleus and the posteroventral and dorsal cochlear nuclei, leads to a blurred tonotopic organization of the central auditory circuits (Lu et al., 2014).

So far, three types of behavioral tests are being considered to verify this hypothesis by attesting sensory ataxia in Npr2-cKO mice. The balance-beam test could give first indication for abnormal balance and motor coordination (Carter et al., 1999). Furthermore, computer-controlled analysis of the footprint pattern could precisely quantify the degree of ataxia and gait abnormalities (Carter et al., 2001; Cheret et al., 2013). Finally, an elaborated goal-directed reaching assay, which monitors skilled forelimb movements, could evaluate the precision of fine motor skills evident in reach, grasp and object manipulation (Azim et al., 2014). Particularly, the last test procedure is based on voluntary complex motion sequences that require the accurate sensory representation of environment and body position and will prove whether the lack of sensory axon bifurcation could be a potential source of degraded or modified motor performance. The assumption that primary afferents develop a precise somatotopic

map in the spinal cord is supported by studies showing that spinal multisensory circuits receive topographically ordered information and that the dorsal horn of the spinal cord seems to be a highly adaptive brain-body interface (Granmo et al., 2008; Levinsson et al., 2002). The skin areas of individual digits, which were labeled with cholera toxin operating as anterograde axonal tracer, have been shown to form distinct termination fields in the spinal cord with highly conserved shape, volume, and location (Conte et al., 2009; Granmo et al., 2008). Detailed examination of these termination fields using the same technique could be extremely helpful to interpret the physiological effects caused by impaired bifurcation.

Considering the fact that axonal branching depending on the CNP-Npr2-cGKIα cascade has been also proven for all cranial sensory ganglia neurons, behavioral tests could be additionally performed with focus on cranial sensory ganglia instead of dorsal root ganglia (Ter-Avetisyan et al., 2014). An appropriate and extensively described sensory system would be the rodent whisker-to-barrel pathway where tactile information derived from vibrissa follicles is transmitted to the whiskers-specific barrel cortex (Erzurumlu and Gaspar, 2012; Wu et al., 2011). Here, the Npr2 expressing primary sensory neurons of the trigeminal ganglion, which convey an inverted face map to the rostral principal nucleus and the caudal spinal nucleus, bifurcate before they innervate the brainstem trigeminal nuclei (Erzurumlu et al., 2010; Ter-Avetisyan et al., 2014). In summary, the analysis of the trigeminal circuit in the brain as well as the sensory motor circuits in the spinal cord could reveal the conceptual and functional nature of the sensory axon bifurcation at the brainstem trigeminal nuclei or at the dorsal root entry zone and could explain, why the nervous system picked out a T-shaped representation for the sensory perception of external stimuli.

6.2 Regulation of Npr2-mediated cGMP signaling in sensory axon bifurcation

The detailed *in vivo* regulation of the Npr2-mediated cGMP signaling cascade contributing to the implementation of axonal growth cone splitting and the involved downstream targets of the cGKIα are currently a matter of speculation. Therefore, one part of my thesis was focused on *in vitro* studies aiming for a better understanding of the CNP-Npr2-cGKIα cascade in the nervous system. The axonal bifurcation of sensory neurons at the dorsal root entry zone is a definite and non-recurring process. Whereas turning and elongation of the stem axon in caudal or rostral direction as well as the formation of collaterals is not affected in mutants of the CNP-Npr2-cGKIα signaling pathway, growth cone splitting critically depends on the proper activity of the CNP-Npr2-cGKIα cascade (Schmidt et al., 2002, 2007, 2009). Considering that no further axon branches are formed directly after the bifurcation event, it can be assumed that the Npr2-mediated cGMP signaling is under tight control. cGMP signaling most likely operates in a transient and locally restricted manner causing a locally restricted rearrangement of cytoskeletal structures within the growth cone whereas other parts proceed with axonal elongation. On account of previous examinations, the receptor ligand CNP itself can be excluded as restricting regulatory factor of the cGMP signaling cascade. C-type natriuretic peptide is secreted from the dorsal part of the spinal cord during the period when axon bifurcation of primary DRG neurons occurs (Schmidt et al., 2009). In other tissues, receptor-mediated degradation, degradation by extracellular proteases, and secretion of the natriuretic peptides into body fluids has been reported to contribute to the rapid clearance of natriuretic peptides (Potter, 2011a). Especially, receptor-mediated clearance of natriuretic peptides by binding to the scavenger receptor Npr3 has been demonstrated to play a predominant role in the resolution of the availability of natriuretic peptides (Cohen et al., 1996; Maack et al., 1987). However, analysis of Npr3 knockout mice did not reveal similar levels of failed axon bifurcation at the dorsal root entry zone as observed in CNP mutant mice (Dr. H. Schmidt, personal communication) indicating that increased amounts of CNP due to the absence of the clearance receptor have no deleterious effects on the bifurcation of sensory axons. As a result, the enzymatic activity of the Npr2 receptor has to be regulated by another

intracellular pathway or intramolecular mechanism. In this thesis, by analysis of cGMP levels generated by different Npr2 receptor mutants it was shown that the phosphorylation status of the kinase homology domain of Npr2 provides a main regulatory element for receptor activity which is in agreement with previously published data (Potter and Hunter, 1998). In addition, the subsequent nearest neighbor analysis of Npr2 and cGKIα based on the promiscuous biotin ligase BirA* revealed potential protein interaction candidates for the cGMP signaling cascade.

6.2.1 The phosphorylation state of the kinase homology domain regulates Npr2 activity

The quantitative analysis of cGMP levels in HEK293 cells expressing different recombinant Npr2 variants verified the regulatory role of the kinase homology domain in terms of the catalytic receptor activity. In accordance with previous studies, the results confirmed that the phosphorylation status of the five phosphorylation sites (Ser-513, Thr-516, Ser-518, Ser-523, and Ser-526) within the kinase homology domain is mandatory for the enzymatic activity of the cGMP producing guanylyl cyclase domain (Potter and Hunter, 1998). Alanine substitutions at the five phosphorylation sites which mimic a constitutively dephosphorylated receptor protein were capable of preventing CNP-induced cGMP production by Npr2. In contrast, glutamic acid residues at the same five phosphorylation sites which mimic a constitutively phosphorylated receptor protein were capable of maintaining the receptor capacity to be activated by CNP and to generate cGMP. Considering previous biochemical studies of Npr2 which have demonstrated that exposure to CNP results in a time-dependent dephosphorylation and desensitization of the receptor (Potter, 1998), the following activation mechanism of the particular guanylyl cyclase B can be postulated (Figure 43). The inactive Npr2 dimer needs to be phosphorylated at the kinase homology domain in order to bind to the C-type natriuretic peptide at the extracellular ligand binding domain. CNP binding leads to a conformational change of the receptor protein causing an intermolecular realignment of the two guanylyl cyclase domains subsequently introducing the conversion of guanosine triphosphate into cyclic guanosine monophosphate (Potter et al., 2006). The catalytically active receptor gets dephosphorylated over time and, as a consequence, the activity of the guanylyl cyclase domain ceases. The hypothesis of the conformational

modulation mediated by the kinase homology domain is corroborated by the cGMP determination results of the second KHD deletion mutant. The deletion of the entire KHD domain resulted in an Npr2 receptor protein which was constantly active regardless of CNP stimulation. This additionally indicates that the kinase homology domain plays a key role for the intramolecular regulation of the guanylyl cyclase domain through structural rearrangement.

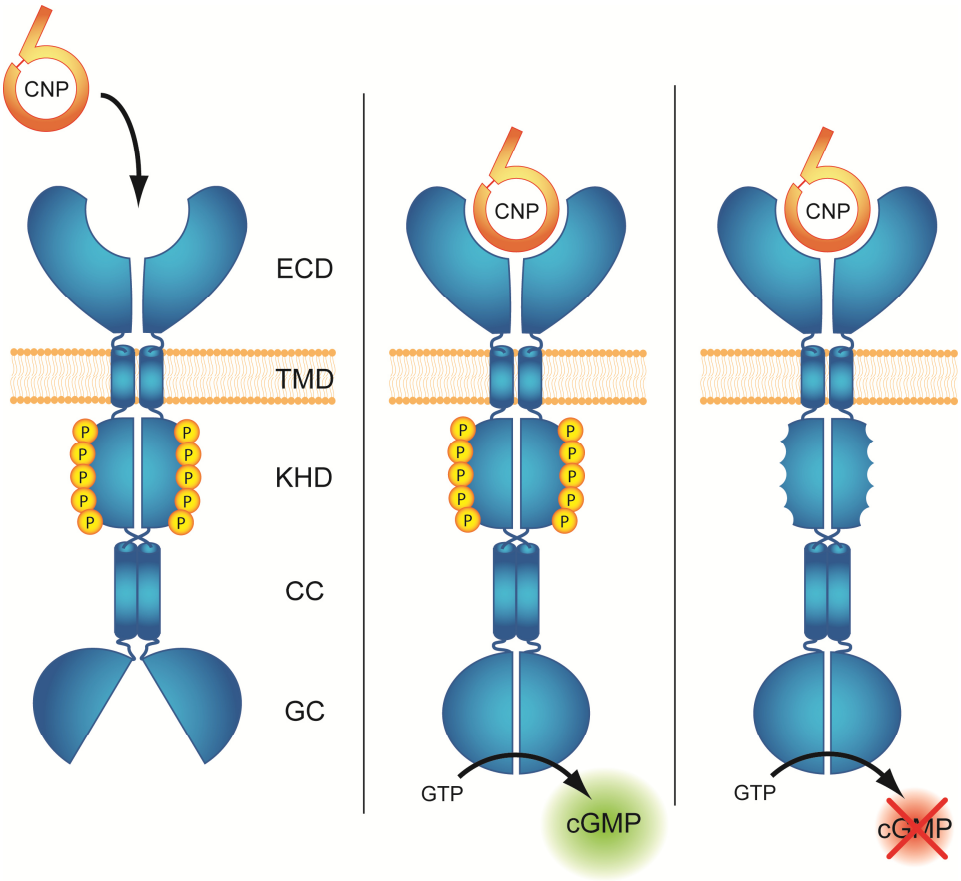

Figure 43: The activity of the receptor guanylyl cyclase Npr2 depends on the phosphorylation state of the kinase homology domain. cGMP measurements indicated that the Npr2 receptor dimer needs to be phosphorylated at the KHD domain in order to be activated by the ligand CNP. Only in a phosphorylated state and after binding of CNP, the guanylyl cyclase domain of Npr2 becomes catalytically active and converts GTP into cGMP. A dephosphorylated state of the KHD domain results in an inactive guanylyl cyclase domain irrespective of CNP stimulation. (CNP) C-type natriuretic peptide, (ECD) extracellular ligand binding domain, (TMD) transmembrane domain, (KHD) kinase homology domain, (CC) coiled coil domain, (GC) guanylyl cyclase domain.

In summary, the phosphorylation state of the Npr2 kinase homology domain controls the receptor activation and the receptor desensitization. The general relevance of the kinase homology domain for the Npr2 regulation is additionally supported by an *in vivo*

study in humans where a homozygous missense mutation L658F in the KHD of Npr2 was found to cause acromesomelic dysplasia, type Maroteaux (Hachiya et al., 2007).

The question arises, how the phosphorylation and dephosphorylation of the Npr2 receptor is mediated. Several candidates for interaction between signaling pathways, so called molecular cross-talk, are discussed in the literature to be involved in the Npr2 regulation, primarily with respect to non-neuronal systems. *In vitro*, it was shown that vasoactive peptides, such as vasopressin, endothelin, and angiotensin II, inhibit CNP-dependent cGMP elevation by activating protein kinase C (PKC) (Potter and Hunter, 2000). PKC-dependent dephosphorylation of the kinase homology domain at Ser-523 was postulated to provide a potential molecular explanation for how pressor hormones can indirectly influence the cGMP signaling by desensitizing the Npr2 receptor. Furthermore, it was demonstrated in NIH3T3 fibroblasts and A10 vascular smooth muscle cells that the receptor dephosphorylation and desensitization is linked to an elevated intracellular calcium concentration and that the sphingosine-1-phosphate signaling pathway can prevent the receptor activation (Abbey-Hosch et al., 2004; Potthast et al., 2004). While Vasopressin-dependent, PKC-dependent, and calcium-dependent inhibition of the Npr2 activity was observed in multiple cell types, the cellular factor which directly interacts with Npr2 is still unknown (Abbey and Potter, 2002; Abbey-Hosch et al., 2005). However, the axon bifurcation analysis of endothelin knockout mice revealed accurate branching of DRG neurons at the dorsal root entry zone (data not shown). Also, no calcium elevation could be detected in dissociated DRG neurons stimulated with CNP (Dr. H. Schmidt, personal communication). Both results indicate that neither pressor hormone nor calcium signaling are relevant for the *in vivo* Npr2 receptor regulation in the nervous system and that different Npr2 regulation mechanisms might be present in distinct tissues. Furthermore, a negative feedback regulation of the receptor activity directly mediated by the cGMP activated cGKIα kinase is rather improbable. Studies of the Npr2 related natriuretic peptide receptor 1 (Npr1) have demonstrated that the cyclase activity and the phosphorylation state of Npr1 is not regulated by cGKIα (Bryan et al., 2006). Another study provided recently an *in vivo* link between the Semaphorin 1a receptor plexin A and the catalytic activity of the Drosophila receptor guanylyl cyclase Gyc76C which shows a high structural similarity to the Npr2 receptor in mammals (Chak and Kolodkin, 2014). In contrast, Npr2-mediated

cGMP signaling can be regulated by the activity of cGMP-dependent phosphodiesterases irrespective of the receptor phosphorylation. It was demonstrated that the decrease of Npr2-mediated cGMP signaling during the meiotic cell cycle arrest in mammalian oocytes is regulated through a process that requires the activity of phosphoprotein phosphatase family members and phosphodiesterase PDE5 (Egbert et al., 2014). Thereby, the cyclic nucleotide phosphodiesterase catalyzes cGMP hydrolysis causing degradation of the Npr2-mediated cGMP elevation. However, axon bifurcation analysis of phosphodiesterase 2A (PDE2A) knockout mice, which is the major PDE in DRGs, showed no lack of bifurcation or uncontrolled multiple branches of DRG neurons at the dorsal root entry zone (Dr. H. Schmidt, personal communication). Although the exact mechanism of Npr2 regulation in the nervous system is still a matter of speculation, the activity-dependent cGMP determination assay has revealed that the phosphorylation sites of the kinase homology domain play an important role for the receptor activation. Looking at previous studies, a regulatory cross-talk between the CNP-Npr2-cGKIα cascade and other signaling pathways could be assumed.

6.2.2 Biotin ligase BirA*-dependent proximity analysis of Npr2 and cGKIα

The proximity-dependent biotin identification (BioID) labeling assay was performed to reveal proteins that interact either with Npr2 or cGKIα. Particularly, it was attempted to detect a protein kinase or a phosphoprotein phosphatase which could regulate the phosphorylation status of Npr2 as well as downstream phosphorylation targets of cGKIα which are linked to the cytoskeleton.

Mass spectrometric analysis of three independent biological replicates identified several biotinylated proteins which were specific either for the Npr2-BirA* fusion protein or the BirA*-cGKIα fusion protein (data are shown in Table 12-15). Although the biotin ligase BirA*-dependent labeling assay was first introduced in 2012 (Roux et al., 2012), several protein complex and protein interaction studies have already used this method, e.g. to screen for components of the mammalian nuclear lamina (Roux et al., 2012), the cell junction complexes (Van Itallie et al., 2013, 2014; Steed et al., 2014), the centrosomes (Comartin et al., 2013; Firat-Karalar et al., 2014), and could identify kinase-phosphatase interaction involved in the Hippo signaling pathway (Couzens et al., 2013). Even though

the biotin labeling by BirA* has been shown to detect weak or transient interactions in living cells, it is only an estimation of proximity and not evidence for physical interaction. A recent study by Kyle J. Roux and colleagues has determined the biotinylation radius with approximately 10 nm whereby the degree of biotinylation is linearly increased with the proximity to the biotin ligase (Kim et al., 2014). As a consequence, a higher degree of biotinylation reflects a higher probability of actual interaction with the fusion protein. In general, the results of the BioID assay in this thesis have to be considered as first indication for potential protein-protein interaction which have to be confirmed in future experiments.

Unfortunately, neither a protein serine/threonine kinase nor a protein serine/threonine phosphatase were found to be in the proximity of the Npr2 receptor which would have revealed a potential interaction partner for the phosphorylation sites of the kinase homology domain mediating the receptor activation or desensitization. Interestingly, the A-kinase anchor protein 12 (AKAP12, also termed gravin) was highly biotinylated by the Npr2-BirA* fusion protein in the cytosolic fraction. AKAP12 is an anchoring protein that is mainly associated with the subcellular compartmentation of protein kinase A (PKA) and protein kinase C (PKC). Even though PKA and PKC were not attested, AKAP12 might play a role for Npr2-mediated cGMP signaling cascade. Previous studies have linked AKAP12 to the actin-cytoskeleton reorganization and have demonstrated that it can directly bind to the beta 2-adrenergic receptor providing a mobile scaffold during the receptor desensitization (Akakura and Gelman, 2012; Fan et al., 2001; Havekes et al., 2012).

The BioID assay of the BirA*-cGKIα fusion protein was intended to reveal potential phosphorylation targets of the cGMP-dependent protein kinase I alpha regulating cytoskeletal structures downstream of the CNP-Npr2-cGKIα cascade. Surprisingly, known proteins which are phosphorylated by cGKIα in dorsal root ganglia were not detected. Both Mena (mammalian enabled Ena/VASP family member) and VASP (Vasodilator stimulated phosphoprotein) have been shown to be phosphorylated in CNP stimulated DRG material (Schäffer, 2006; Stonkute, 2010). However, an impaired axon bifurcation of DRG neurons was neither found for VASP knockout mice nor Mena/VASP double knockout mice (Stonkute, 2010). The direct protein-protein interaction between cGKIα and Mena/VASP could also not be verified by the biotin labeling assay in F11 cells. The

identified protein with the highest degree of BirA*-cGKIα fusion protein-dependent biotinylation was cortactin (cortical actin binding protein) which is reported to contribute to the organization of the actin cytoskeleton and cell structure. This is particularly interesting because it was recently shown that a dynamin-1 and cortactin ring complex mechanically stabilizes F-actin bundles in growth cone filopodia (Yamada et al., 2013). Due to its cGKIα kinase phosphorylation motif (KKQT) at threonine 401, cortactin could be a new phosphorylation target for the cGKIα.

The main critical aspect of the BioID assay is the artificial system which is provided by biotin labeling in F11 cells. Even though the F11 cell line was generated from rat embryonic dorsal root ganglion neurons and the mouse neuroblastoma cell line N18TG2 for the identification of gene products that characterize individual and small subsets of DRG neurons (Platika et al., 1985), the distinct gene regulation, signal transduction, and cytoskeleton structure of the growth cone during the axon bifurcation of sensory neurons is not imitated by the F11 cell culture. Therefore, the gene expression of 20 identified proteins was reviewed in DRG at embryonic day 12.5 by RT-PCR considering the general possibility of an *in vivo* protein interaction which could be involved in the process of axon bifurcation. All of the tested genes are expressed simultaneously with the CNP-Npr2-cGKIα cascade in sensory neurons. Further experiments have to be conducted to verify whether and how one of these proteins might play a role for the bifurcation process. *In vitro* phosphorylation studies such as yeast two-hybrid screening, could confirm the kinase-substrate specificity between cGKIα and the respective protein of interest (Fields and Song, 1989). Given that appropriate antibodies are available, the subcellular localization of putative protein-protein interactions could be examined at single-molecule resolution in both cell culture and tissue by using the proximity ligation assay (*in situ* PLA) based on rolling circle amplification and fluorescent probes (Söderberg et al., 2006). Furthermore, antibodies which can reveal the phosphorylation state of the antigen by showing a slight size shift in mass in western blot analysis could demonstrate the relationship between the activity of the CNP-Npr2-cGKIα cascade and the phosphorylation of the target protein. For that, DRG material stimulated with CNP or cGMP has to be analyzed in comparison with unstimulated controls by immunoblotting. In any case, whether the protein is involved in the regulation of the cGMP signaling cascade or the cGKIα-dependent rearrangement of the growth cone cytoskeleton will be

gained only by analysis of axon bifurcation at the dorsal root entry zone of knockdown mouse mutants.

7. REFERENCE LIST

Abbey, S.E., and Potter, L.R. (2002). Vasopressin-dependent inhibition of the C-type natriuretic peptide receptor, NPR-B/GC-B, requires elevated intracellular calcium concentrations. J. Biol. Chem. *277*, 42423–42430.

Abbey-Hosch, S.E., Cody, A.N., and Potter, L.R. (2004). Sphingosine-1-phosphate inhibits C-type natriuretic peptide activation of guanylyl cyclase B (GC-B/NPR-B). Hypertension *43*, 1103–1109.

Abbey-Hosch, S.E., Smirnov, D., and Potter, L.R. (2005). Differential regulation of NPR-B/GC-B by protein kinase c and calcium. Biochem. Pharmacol. *70*, 686–694.

Akakura, S., and Gelman, I.H. (2012). Pivotal role of AKAP12 in the regulation of cellular adhesion dynamics: control of cytoskeletal architecture, cell migration, and mitogenic signaling. J. Signal Transduct. *2012*, 1–7.

Van den Akker, F., Zhang, X., Miyagi, M., Huo, X., Misono, K.S., and Yee, V.C. (2000). Structure of the dimerized hormone-binding domain of a guanylyl-cyclase-coupled receptor. Nature *406*, 101–104.

Amano, N., Mukai, T., Ito, Y., Narumi, S., Tanaka, T., Yokoya, S., Ogata, T., and Hasegawa, T. (2014). Identification and functional characterization of two novel NPR2 mutations in Japanese patients with short stature. J. Clin. Endocrinol. Metab. jc2013–jc3525.

Ansorge, W. (1985). Fast and sensitive detection of protein and DNA bands by treatment with potassium permanganate. J. Biochem. Biophys. Methods *11*, 13–20.

Appler, J.M., and Goodrich, L. V. (2011). Connecting the ear to the brain: Molecular mechanisms of auditory circuit assembly. Prog. Neurobiol. *93*, 488–508.

Azim, E., Jiang, J., Alstermark, B., and Jessell, T.M. (2014). Skilled reaching relies on a V2a propriospinal internal copy circuit. Nature *508*, 357–363.

Bannon, A.W., and Malmberg, A.B. (2007). Models of nociception: hot-plate, tail-flick, and formalin tests in rodents. Curr. Protoc. Neurosci. *Chapter 8*, Unit 8.9.

Barnes, A.P., and Polleux, F. (2009). Establishment of axon-dendrite polarity in developing neurons. Annu. Rev. Neurosci. *32*, 347–381.

Barnes, S.H., Price, S.R., Wentzel, C., and Guthrie, S.C. (2010). Cadherin-7 and cadherin-6B differentially regulate the growth, branching and guidance of cranial motor axons. Development *137*, 805–814.

Bartels, C.F., Bükülmez, H., Padayatti, P., Rhee, D.K., van Ravenswaaij-Arts, C., Pauli, R.M., Mundlos, S., Chitayat, D., Shih, L.-Y., Al-Gazali, L.I., et al. (2004). Mutations in the transmembrane natriuretic peptide receptor NPR-B impair skeletal growth and cause acromesomelic dysplasia, type Maroteaux. Am. J. Hum. Genet. *75*, 27–34.

Basbaum, A.I., Bautista, D.M., Scherrer, G., and Julius, D. (2009). Cellular and Molecular Mechanisms of Pain. Cell *139*, 267–284.

Bäumner, D., and Nawrath, H. (1995). Effects of inhibitors of cGMP-dependent protein kinase in atrial heart and aortic smooth muscle from rats. Eur. J. Pharmacol. *273*, 295–298.

Bertrand, N., Castro, D.S., and Guillemot, F. (2002). Proneural genes and the specification of neural cell types. Nat. Rev. Neurosci. *3*, 517–530.

Bocciardi, R., Giorda, R., Buttgereit, J., Gimelli, S., Divizia, M.T., Beri, S., Garofalo, S., Tavella, S., Lerone, M., Zuffardi, O., et al. (2007). Overexpression of the C-type natriuretic peptide (CNP) is associated with overgrowth and bone anomalies in an individual with balanced t(2;7) translocation.

Bodmer, D., Levine-Wilkinson, S., Richmond, A., Hirsh, S., and Kuruvilla, R. (2009). Wnt5a mediates nerve growth factor-dependent axonal branching and growth in developing sympathetic neurons. J. Neurosci. *29*, 7569–7581.

Bryan, P.M., Smirnov, D., Smolenski, A., Feil, S., Feil, R., Hofmann, F., Lohmann, S., and Potter, L.R. (2006). A sensitive method for determining the phosphorylation status of natriuretic peptide receptors: cGK-Ialpha does not regulate NPR-A. Biochemistry *45*, 1295–1303.

Cantallops, I., Haas, K., and Cline, H.T. (2000). Postsynaptic CPG15 promotes synaptic maturation and presynaptic axon arbor elaboration in vivo. Nat. Neurosci. *3*, 1004–1011.

Carter, R.J., Lione, L.A., Humby, T., Mangiarini, L., Mahal, A., Bates, G.P., Dunnett, S.B., and Morton, A.J. (1999). Characterization of progressive motor deficits in mice transgenic for the human Huntington's disease mutation. J. Neurosci. *19*, 3248–3257.

Carter, R.J., Morton, J., and Dunnett, S.B. (2001). Motor coordination and balance in rodents. Curr. Protoc. Neurosci. *Chapter 8*, Unit 8.12.

Carvalho, P.G., Branco, L.G.S., and Leite-Panissi, C.R.A. (2011). Involvement of the heme oxygenase-carbon monoxide-cGMP pathway in the nociception induced by acute painful stimulus in rats. Brain Res. *1385*, 107–113.

Carvalho, P.G., Branco, L.G.S., and Leite-Panissi, C.R.A. (2014). Acute stress-induced antinociception is cGMP-dependent but heme oxygenase-independent. Braz J Med Biol Res *47*, 1057–1061.

Cavanaugh, D.J., Lee, H., Lo, L., Shields, S.D., Zylka, M.J., Basbaum, A.I., and Anderson, D.J. (2009). Distinct subsets of unmyelinated primary sensory fibers mediate behavioral responses to noxious thermal and mechanical stimuli. Proc. Natl. Acad. Sci. *106*, 11424–11424.

Chak, K., and Kolodkin, A.L. (2014). Function of the Drosophila receptor guanylyl cyclase Gyc76C in PlexA-mediated motor axon guidance. Development *141*, 136–147.

Champy, M.F., Selloum, M., Zeitler, V., Caradec, C., Jung, B., Rousseau, S., Pouilly, L., Sorg, T., and Auwerx, J. (2008). Genetic background determines metabolic phenotypes in the mouse. Mamm. Genome *19*, 318–331.

Charron, F., Stein, E., Jeong, J., McMahon, A.P., and Tessier-Lavigne, M. (2003). The morphogen sonic hedgehog is an axonal chemoattractant that collaborates with Netrin-1 in midline axon guidance. Cell *113*, 11–23.

Chen, A.I., de Nooij, J.C., and Jessell, T.M. (2006). Graded activity of transcription factor Runx3 specifies the laminar termination pattern of sensory axons in the developing spinal cord. Neuron *49*, 395–408.

Cheret, C., Willem, M., Fricker, F.R., Wende, H., Wulf-Goldenberg, A., Tahirovic, S., Nave, K.-A., Saftig, P., Haass, C., Garratt, A.N., et al. (2013). Bace1 and Neuregulin-1 cooperate to control formation and maintenance of muscle spindles. EMBO J. *32*, 2015–2028.

Chikuda, H., Kugimiya, F., Hoshi, K., Ikeda, T., Ogasawara, T., Shimoaka, T., Kawano, H., Kamekura, S., Tsuchida, A., Yokoi, N., et al. (2004). Cyclic GMP-dependent protein kinase II is a molecular switch from proliferation to hypertrophic differentiation of chondrocytes. Genes Dev. *18*, 2418–2429.

Chinkers, M., and Wilson, E.M. (1992). Ligand-independent oligomerization of natriuretic peptide receptors: Identification of heteromeric receptors and a dominant negative mutant. J. Biol. Chem. *267*, 18589–18597.

Chrisman, T.D., and Garbers, D.L. (1999). Reciprocal antagonism coordinates C-type natriuretic peptide and mitogen-signaling pathways in fibroblasts. J. Biol. Chem. *274*, 4293–4299.

Chusho, H., Tamura, N., Ogawa, Y., Yasoda, a, Suda, M., Miyazawa, T., Nakamura, K., Nakao, K., Kurihara, T., Komatsu, Y., et al. (2001). Dwarfism and early death in mice lacking C-type natriuretic peptide. Proc. Natl. Acad. Sci. U. S. A. *98*, 4016–4021.

Cohen, D., Koh, G.Y., Nikonova, L.N., Porter, J.G., and Maack, T. (1996). Molecular determinants of the clearance function of type C receptors of natriuretic peptides. J. Biol. Chem. *271*, 9863–9869.

Comartin, D., Gupta, G.D., Fussner, E., Coyaud, É., Hasegan, M., Archinti, M., Cheung, S.W.T., Pinchev, D., Lawo, S., Raught, B., et al. (2013). CEP120 and SPICE1 cooperate with CPAP in centriole elongation. Curr. Biol. *23*, 1360–1366.

Conte, W.L., Kamishina, H., and Reep, R.L. (2009). Multiple neuroanatomical tract-tracing using fluorescent Alexa Fluor conjugates of cholera toxin subunit B in rats. Nat. Protoc. *4*, 1157–1166.

Court, D.L., Swaminathan, S., Yu, D., Wilson, H., Baker, T., Bubunenko, M., Sawitzke, J., and Sharan, S.K. (2003). Mini-λ: a tractable system for chromosome and BAC engineering. Gene *315*, 63–69.

Couzens, A.L., Knight, J.D.R., Kean, M.J., Teo, G., Weiss, A., Dunham, W.H., Lin, Z.-Y., Bagshaw, R.D., Sicheri, F., Pawson, T., et al. (2013). Protein interaction network of the mammalian Hippo pathway reveals mechanisms of kinase-phosphatase interactions. Sci. Signal. *6*, rs15.

Danielian, P.S., Muccino, D., Rowitch, D.H., Michael, S.K., and McMahon, A.P. (1998). Modification of gene activity in mouse embryos in utero by a tamoxifen-inducible form of Cre recombinase. Curr. Biol. *8*, 1323–S2.

Dent, E.W., Tang, F., and Kalil, K. (2003). Axon guidance by growth cones and branches: common cytoskeletal and signaling mechanisms. Neuroscientist *9*, 343–353.

Dent, E.W., Barnes, A.M., Tang, F., and Kalil, K. (2004). Netrin-1 and semaphorin 3A promote or inhibit cortical axon branching, respectively, by reorganization of the cytoskeleton. J. Neurosci. *24*, 3002–3012.

Dent, E.W., Gupton, S.L., and Gertler, F.B. (2011). The growth cone cytoskeleton in axon outgrowth and guidance. Cold Spring Harb. Perspect. Biol. *3*.

Diez-Roux, G., Banfi, S., Sultan, M., Geffers, L., Anand, S., Rozado, D., Magen, A., Canidio, E., Pagani, M., Peluso, I., et al. (2011). A high-resolution anatomical atlas of the transcriptome in the mouse embryo. PLoS Biol. *9*, e1000582.

Doetschman, T. (2009). Influence of genetic background on genetically engineered mouse phenotypes. Methods Mol. Biol. *530*, 423–433.

Dotti, C.G., and Banker, G.A. (1987). Experimentally induced alteration in the polarity of developing neurons. Nature *330*, 254–256.

Le Douarin, N., and Kalcheim, C. (1999). The Neural Crest. Biomed. Rev. *2nd Editio*, 445.

Doyle, D.D., Upshaw-Earley, J., Bell, E.L., and Palfrey, H.C. (2002). Natriuretic peptide receptor-B in adult rat ventricle is predominantly confined to the nonmyocyte population. Am. J. Physiol. Heart Circ. Physiol. *282*, H2117–H2123.

Drewett, J.G., Fendly, B.M., Garbers, D.L., and Lowe, D.G. (1995). Natriuretic peptide receptor-B (guanylyl cyclase-B) mediates C-type natriuretic peptide relaxation of precontracted rat aorta. J. Biol. Chem. *270*, 4668–4674.

Dubuisson, D., and Dennis, S.G. (1977). The formalin test: a quantitative study of the analgesic effects of morphine, meperidine, and brain stem stimulation in rats and cats. Pain *4*, 161–174.

Duda, T., Goraczniak, R.M., Sitaramayya, A., and Sharma, R.K. (1993). Cloning and expression of an ATP-regulated human retina C-type natriuretic factor receptor guanylate cyclase. Biochemistry *32*, 1391–1395.

Duda, T., Yadav, P., and Sharma, R.K. (2011). Allosteric modification, the primary ATP activation mechanism of atrial natriuretic factor receptor guanylate cyclase. Biochemistry *50*, 1213–1225.

Dymecki, S.M., and Tomasiewicz, H. (1998). Using Flp-recombinase to characterize expansion of Wnt1-expressing neural progenitors in the mouse. Dev. Biol. *201*, 57–65.

Ebens, A., Brose, K., Leonardo, E.D., Hanson, M.G., Bladt, F., Birchmeier, C., Barres, B.A., and Tessier-Lavigne, M. (1996). Hepatocyte growth factor/scatter factor is an axonal chemoattractant and a neurotrophic factor for spinal motor neurons. Neuron *17*, 1157–1172.

Egbert, J.R., Shuhaibar, L.C., Edmund, A.B., Van Helden, D. a, Robinson, J.W., Uliasz, T.F., Baena, V., Geerts, A., Wunder, F., Potter, L.R., et al. (2014). Dephosphorylation and inactivation of NPR2 guanylyl cyclase in granulosa cells contributes to the LH-induced decrease in cGMP that causes resumption of meiosis in rat oocytes. Development *141*, 3594–3604.

Elg, S., Marmigere, F., Mattsson, J.P., and Ernfors, P. (2007). Cellular subtype distribution and developmental regulation of TRPC channel members in the mouse dorsal root ganglion. J. Comp. Neurol. *503*, 35–46.

Erzurumlu, R.S., and Gaspar, P. (2012). Development and critical period plasticity of the barrel cortex. Eur. J. Neurosci. *35*, 1540–1553.

Erzurumlu, R.S., and Killackey, H.P. (1983). Development of order in the rat trigeminal system. J. Comp. Neurol. *213*, 365–380.

Erzurumlu, R.S., Murakami, Y., and Rijli, F.M. (2010). Mapping the face in the somatosensory brainstem. Nat. Rev. Neurosci. *11*, 252–263.

Estrada, K., Krawczak, M., Schreiber, S., van Duijn, K., Stolk, L., van Meurs, J.B.J., Liu, F., Penninx, B.W.J.H., Smit, J.H., Vogelzangs, N., et al. (2009). A genome-wide association study of northwestern Europeans involves the C-type natriuretic peptide signaling pathway in the etiology of human height variation. Hum. Mol. Genet. *18*, 3516–3524.

Fan, G.F., Shumay, E., Wang, H.Y., and Malbon, C.C. (2001). The scaffold protein gravin (cAMP-dependent protein kinase-anchoring protein 250) binds the beta(2)-Adrenergic receptor via the receptor cytoplasmic Arg-329 to Leu-413 domain and provides a mobile scaffold during desensitization. J. Biol. Chem. *276*, 24005–24014.

Feil, R., Gappa, N., Rutz, M., Schlossmann, J., Rose, C.R., Konnerth, A., Brummer, S., Kuhbandner, S., and Hofmann, F. (2002). Functional reconstitution of vascular smooth muscle cells with cGMP-dependent protein kinase I isoforms. Circ Res *90*, 1080–1086.

Feng, G., Mellor, R.H., Bernstein, M., Keller-Peck, C., Nguyen, Q.T., Wallace, M., Nerbonne, J.M., Lichtman, J.W., and Sanes, J.R. (2000). Imaging neuronal subsets in transgenic mice expressing multiple spectral variants of GFP. Neuron *28*, 41–51.

Fenrick, R., Bouchard, N., McNicoll, N., and De Léan, A. (1997). Glycosylation of asparagine 24 of the natriuretic peptide receptor-B is crucial for the formation of a competent ligand binding domain. Mol. Cell. Biochem. *173*, 25–32.

Fields, S., and Song, O. (1989). A novel genetic system to detect protein-protein interactions. Nature *340*, 245–246.

Firat-Karalar, E.N., Rauniyar, N., Yates, J.R., and Stearns, T. (2014). Proximity interactions among centrosome components identify regulators of centriole duplication. Curr. Biol. *24*, 664–670.

Frank, E., and Sanes, J.R. (1991). Lineage of neurons and glia in chick dorsal root ganglia: analysis in vivo with a recombinant retrovirus. Development *111*, 895–908.

Fuchs, S., Herzog, D., Sumara, G., Büchmann-Møller, S., Civenni, G., Wu, X., Chrostek-Grashoff, A., Suter, U., Ricci, R., Relvas, J.B., et al. (2009). Stage-specific control of neural crest stem cell proliferation by the small Rho GTPases Cdc42 and Rac1. Cell Stem Cell *4*, 236–247.

Galimberti, I., Bednarek, E., Donato, F., and Caroni, P. (2010). EphA4 signaling in juveniles establishes topographic specificity of structural plasticity in the hippocampus. Neuron *65*, 627–642.

García-Castro, M.I., Marcelle, C., and Bronner-Fraser, M. (2002). Ectodermal Wnt function as a neural crest inducer. Science *297*, 848–851.

Geister, K. a, Brinkmeier, M.L., Hsieh, M., Faust, S.M., Karolyi, I.J., Perosky, J.E., Kozloff, K.M., Conti, M., and Camper, S. a (2013). A novel loss-of-function mutation in Npr2 clarifies primary role in female reproduction and reveals a potential therapy for acromesomelic dysplasia, Maroteaux type. Hum. Mol. Genet. *22*, 345–357.

Gianola, S., de Castro, F., and Rossi, F. (2009). Anosmin-1 stimulates outgrowth and branching of developing Purkinje axons. Neuroscience *158*, 570–584.

Gibson, D. a, and Ma, L. (2011). Developmental regulation of axon branching in the vertebrate nervous system. Development *138*, 183–195.

Gong, Q., Chen, H., and Farbman, A.I. (2009). Olfactory sensory axon growth and branching is influenced by sonic hedgehog. Dev. Dyn. *238*, 1768–1776.

Gonzales-Rios, F., Vlaiculescu, A., Ben Natan, L., Protais, P., and Costentin, J. (1986). Dissociated effects of apomorphine on various nociceptive responses in mice. J. Neural Transm. *67*, 87–103.

Graham, F.L., Smiley, J., Russell, W.C., and Nairn, R. (1977). Characteristics of a human cell line transformed by DNA from human adenovirus type 5. J. Gen. Virol. *36*, 59–74.

Granmo, M., Petersson, P., and Schouenborg, J. (2008). Action-based body maps in the spinal cord emerge from a transitory floating organization. J. Neurosci. *28*, 5494–5503.

Hachiya, R., Ohashi, Y., Kamei, Y., Suganami, T., Mochizuki, H., Mitsui, N., Saitoh, M., Sakuragi, M., Nishimura, G., Ohashi, H., et al. (2007). Intact kinase homology domain of natriuretic peptide receptor-B is essential for skeletal development. J. Clin. Endocrinol. Metab. *92*, 4009–4014.

Haneda, M., Kikkawa, R., Maeda, S., Togawa, M., Koya, D., Horide, N., Kajiwara, N., and Shigeta, Y. (1991). Dual mechanism of angiotensin II inhibits ANP-induced mesangial cGMP accumulation. Kidney Int. *40*, 188–194.

Hannema, S.E., van Duyvenvoorde, H. a, Premsler, T., Yang, R.-B., Mueller, T.D., Gassner, B., Oberwinkler, H., Roelfsema, F., Santen, G.W.E., Prickett, T., et al. (2013). An activating mutation in the kinase homology domain of the natriuretic peptide receptor-2 causes extremely tall stature without skeletal deformities. J. Clin. Endocrinol. Metab. 1–10.

Hargreaves, K., Dubner, R., Brown, F., Flores, C., and Joris, J. (1988). A new and sensitive method for measuring thermal nociception in cutaneous hyperalgesia. Pain *32*, 11.

Hasty, P., Rivera-Pérez, J., and Bradley, A. (1991). The length of homology required for gene targeting in embryonic stem cells. Mol. Cell. Biol. *11*, 5586–5591.

Hattori, D., Chen, Y., Matthews, B.J., Salwinski, L., Sabatti, C., Grueber, W.B., and Zipursky, S.L. (2009). Robust discrimination between self and non-self neurites requires thousands of Dscam1 isoforms. Nature *461*, 644–648.

Havekes, R., Canton, D. a, Park, A.J., Huang, T., Nie, T., Day, J.P., Guercio, L. a, Grimes, Q., Luczak, V., Gelman, I.H., et al. (2012). Gravin orchestrates protein kinase A and β2-adrenergic receptor signaling critical for synaptic plasticity and memory. J. Neurosci. *32*, 18137–18149.

Hendershot, T.J., Liu, H., Sarkar, A.A., Giovannucci, D.R., Clouthier, D.E., Abe, M., and Howard, M.J. (2007). Expression of Hand2 is sufficient for neurogenesis and cell type-specific gene expression in the enteric nervous system. Dev. Dyn. *236*, 93–105.

Hjerling-Leffler, J., Marmigère, F., Heglind, M., Cederberg, A., Koltzenburg, M., Enerbäck, S., and Ernfors, P. (2005). The boundary cap: a source of neural crest stem cells that generate multiple sensory neuron subtypes. Development *132*, 2623–2632.

Hofmann, F., Bernhard, D., Lukowski, R., and Weinmeister, P. (2009). cGMP regulated protein kinases (cGK). Handb. Exp. Pharmacol. 137–162.

Hu, N., Strobl-Mazzulla, P.H., and Bronner, M.E. (2014). Epigenetic regulation in neural crest development. Dev. Biol. *396*, 159–168.

Hu, Z.-L., Shi, M., Huang, Y., Zheng, M.-H., Pei, Z., Chen, J.-Y., Han, H., and Ding, Y.-Q. (2011). The role of the transcription factor Rbpj in the development of dorsal root ganglia. Neural Dev. *6*, 14.

Hume, A.N., Buttgereit, J., Al-Awadhi, A.M., Al-Suwaidi, S.S., John, A., Bader, M., Seabra, M.C., Al-Gazali, L., and Ali, B.R. (2009). Defective cellular trafficking of missense NPR-B mutants is the major mechanism underlying acromesomelic dysplasia-type Maroteaux. Hum. Mol. Genet. *18*, 267–277.

Hunt, P.J., Richards, A.M., Espiner, E.A., Nicholls, M.G., and Yandle, T.G. (1994). Bioactivity and metabolism of C-type natriuretic peptide in normal man. J. Clin. Endocrinol. Metab. *78*, 1428–1435.

Hutchins, B.I., and Kalil, K. (2008). Differential outgrowth of axons and their branches is regulated by localized calcium transients. J. Neurosci. *28*, 143–153.

Ikeya, M., Lee, S.M., Johnson, J.E., McMahon, A.P., and Takada, S. (1997). Wnt signalling required for expansion of neural crest and CNS progenitors. Nature *389*, 966–970.

Imai, J., Yashiroda, H., Maruya, M., Yahara, I., and Tanaka, K. (2003). Proteasomes and molecular chaperones. CELL CYCLE *2*, 585–589.

Van Itallie, C.M., Aponte, A., Tietgens, A.J., Gucek, M., Fredriksson, K., and Anderson, J.M. (2013). The N and C termini of ZO-1 are surrounded by distinct proteins and functional protein networks. J. Biol. Chem. *288*, 13775–13788.

Van Itallie, C.M., Tietgens, A.J., Aponte, A., Fredriksson, K., Fanning, A.S., Gucek, M., and Anderson, J.M. (2014). Biotin ligase tagging identifies proteins proximal to E-cadherin, including lipoma preferred partner, a regulator of epithelial cell-cell and cell-substrate adhesion. J. Cell Sci. *127*, 885–895.

Jiao, Y., Yan, J., Jiao, F., Yang, H., Donahue, L.R., Li, X., Roe, B. a, Stuart, J., and Gu, W. (2007). A single nucleotide mutation in Nppc is associated with a long bone abnormality in lbab mice. BMC Genet. *8*, 16.

Johnson, E.O., Babis, G.C., Soultanis, K.C., and Soucacos, P.N. (2008). Functional neuroanatomy of proprioception. J. Surg. Orthop. Adv. *17*, 159–164.

Jones, B.J., and Roberts, D.J. (1968). The quantiative measurement of motor inco-ordination in naive mice using an acelerating rotarod. J. Pharm. Pharmacol. *20*, 302–304.

Kake, T., Kitamura, H., Adachi, Y., Yoshioka, T., Watanabe, T., Matsushita, H., Fujii, T., Kondo, E., Tachibe, T., Kawase, Y., et al. (2009). Chronically elevated plasma C-type natriuretic peptide level stimulates skeletal growth in transgenic mice. Am. J. Physiol. Endocrinol. Metab. *297*, E1339–E1348.

Kalil, K., and Dent, E.W. (2013). Branch management: mechanisms of axon branching in the developing vertebrate CNS. Nat. Rev. Neurosci. *15*, 7–18.

Kasemeier-Kulesa, J.C., Kulesa, P.M., and Lefcort, F. (2005). Imaging neural crest cell dynamics during formation of dorsal root ganglia and sympathetic ganglia. Development *132*, 235–245.

Khan, S., Ali, R., Abbasi, S., Nawaz, M., Muhammad, N., and Ahmad, W. (2012). Novel mutations in natriuretic peptide receptor-2 gene underlie acromesomelic dysplasia, type maroteaux. BMC Med. Genet. *13*, 44.

Kim, D.I., Kc, B., Zhu, W., Motamedchaboki, K., Doye, V., and Roux, K.J. (2014). Probing nuclear pore complex architecture with proximity-dependent biotinylation. Proc. Natl. Acad. Sci. U. S. A. *111*, E2453–E2461.

Kishimoto, I., Tokudome, T., Horio, T., Soeki, T., Chusho, H., Nakao, K., and Kangawa, K. (2008). C-type natriuretic peptide is a Schwann cell-derived factor for development and function of sensory neurones. J. Neuroendocrinol. *20*, 1213–1223.

Kiyosu, C., Tsuji, T., Yamada, K., Kajita, S., and Kunieda, T. (2012). NPPC/NPR2 signaling is essential for oocyte meiotic arrest and cumulus oophorus formation during follicular development in the mouse ovary. Reproduction *144*, 187–193.

Koller, K.J., Lowe, D.G., Bennett, G.L., Minamino, N., Kangawa, K., Matsuo, H., and Goeddel, D. V (1991). Selective activation of the B natriuretic peptide receptor by C-type natriuretic peptide (CNP). Science *252*, 120–123.

Kolodkin, A.L., and Tessier-Lavigne, M. (2011). Mechanisms and molecules of neuronal wiring: a primer. Cold Spring Harb. Perspect. Biol. *3*.

Kramer, E.R., Knott, L., Su, F., Dessaud, E., Krull, C.E., Helmbacher, F., and Klein, R. (2006a). Cooperation between GDNF/Ret and ephrinA/EphA4 signals for motor-axon pathway selection in the limb. Neuron *50*, 35–47.

Kramer, I., Sigrist, M., de Nooij, J.C., Taniuchi, I., Jessell, T.M., and Arber, S. (2006b). A role for Runx transcription factor signaling in dorsal root ganglion sensory neuron diversification. Neuron *49*, 379–393.

Kühn, R., Schwenk, F., Aguet, M., and Rajewsky, K. (1995). Inducible Gene Targeting in Mice. Science *269*, 1427–1429.

Kwan, K.Y., Allchorne, A.J., Vollrath, M. a, Christensen, A.P., Zhang, D.-S., Woolf, C.J., and Corey, D.P. (2006). TRPA1 contributes to cold, mechanical, and chemical nociception but is not essential for hair-cell transduction. Neuron *50*, 277–289.

Lake, J.I., and Heuckeroth, R.O. (2013). Enteric nervous system development: migration, differentiation, and disease. Am. J. Physiol. Gastrointest. Liver Physiol. *305*, G1–G24.

Lee, H.-Y., Kléber, M., Hari, L., Brault, V., Suter, U., Taketo, M.M., Kemler, R., and Sommer, L. (2004). Instructive role of Wnt/beta-catenin in sensory fate specification in neural crest stem cells. Science *303*, 1020–1023.

Lentz, S.I., Knudson, C.M., Korsmeyer, S.J., and Snider, W.D. (1999). Neurotrophins support the development of diverse sensory axon morphologies. J. Neurosci. *19*, 1038–1048.

Levinsson, A., Holmberg, H., Broman, J., Zhang, M., and Schouenborg, J. (2002). Spinal sensorimotor transformation: relation between cutaneous somatotopy and a reflex network. J. Neurosci. *22*, 8170–8182.

Li, L., Rutlin, M., Abraira, V.E., Cassidy, C., Kus, L., Gong, S., Jankowski, M.P., Luo, W., Heintz, N., Koerber, H.R., et al. (2011). The functional organization of cutaneous low-threshold mechanosensory neurons. Cell *147*, 1615–1627.

López-Bendito, G., Cautinat, A., Sánchez, J.A., Bielle, F., Flames, N., Garratt, A.N., Talmage, D.A., Role, L.W., Charnay, P., Marín, O., et al. (2006). Tangential neuronal migration controls axon guidance: a role for Neuregulin-1 in thalamocortical axon navigation. Cell *125*, 127–142.

Lu, C.C., Cao, X.-J., Wright, S., Ma, L., Oertel, D., and Goodrich, L. V (2014). Mutation of npr2 leads to blurred tonotopic organization of central auditory circuits in mice. PLoS Genet. *10*, 1–16.

Ma, L., and Tessier-Lavigne, M. (2007). Dual branch-promoting and branch-repelling actions of Slit/Robo signaling on peripheral and central branches of developing sensory axons. J. Neurosci. *27*, 6843–6851.

Ma, Q., Fode, C., Guillemot, F., and Anderson, D.J. (1999). Neurogenin1 and neurogenin2 control two distinct waves of neurogenesis in developing dorsal root ganglia. Genes Dev. *13*, 1717–1728.

Maack, T., Suzuki, M., Almeida, F.A., Nussenzveig, D., Scarborough, R.M., McEnroe, G.A., and Lewicki, J.A. (1987). Physiological role of silent receptors of atrial natriuretic factor. Science *238*, 675–678.

Man, K., Kaplan, J., Damasio, H., and Damasio, A. (2013). Neural convergence and divergence in the mammalian cerebral cortex: From experimental neuroanatomy to functional neuroimaging. J. Comp. Neurol. *521*, 4097–4111.

Del Marco, A. (1981). Observations of growth plate development in achondroplastic (cn/cn) mice. Reprod. Nutr. Dev. *21*, 1025–1031.

Marler, K.J.M., Becker-Barroso, E., Martínez, A., Llovera, M., Wentzel, C., Poopalasundaram, S., Hindges, R., Soriano, E., Comella, J., and Drescher, U. (2008). A TrkB/EphrinA interaction controls retinal axon branching and synaptogenesis. J. Neurosci. *28*, 12700–12712.

Marmigère, F., Montelius, A., Wegner, M., Groner, Y., Reichardt, L.F., and Ernfors, P. (2006). The Runx1/AML1 transcription factor selectively regulates development and survival of TrkA nociceptive sensory neurons. Nat. Neurosci. *9*, 180–187.

Maro, G.S., Vermeren, M., Voiculescu, O., Melton, L., Cohen, J., Charnay, P., and Topilko, P. (2004). Neural crest boundary cap cells constitute a source of neuronal and glial cells of the PNS. Nat. Neurosci. *7*, 930–938.

Matsuda, S., Baluk, P., Shimizu, D., and Fujiwara, T. (1996). Dorsal root ganglion neuron development in chick and rat. Anat. Embryol. (Berl). *193*, 475–480.

Mears, S.C., and Frank, E. (1997). Formation of specific monosynaptic connections between muscle spindle afferents and motoneurons in the mouse. J. Neurosci. *17*, 3128–3135.

Mericq, V., Uyeda, J.A., Barnes, K.M., De Luca, F., and Baron, J. (2000). Regulation of fetal rat bone growth by C-type natriuretic peptide and cGMP. Pediatr. Res. *47*, 189–193.

Miura, K., Kim, O.-H., Lee, H.R., Namba, N., Michigami, T., Yoo, W.J., Choi, I.H., Ozono, K., and Cho, T.-J. (2014). Overgrowth syndrome associated with a gain-of-function mutation of the natriuretic peptide receptor 2 (NPR2) gene. Am. J. Med. Genet. A *164A*, 156–163.

Miyazawa, T., Ogawa, Y., Chusho, H., Yasoda, A., Tamura, N., Komatsu, Y., Pfeifer, A., Hofmann, F., and Nakao, K. (2002). Cyclic GMP-dependent protein kinase II plays a critical role in C-type natriuretic peptide-mediated endochondral ossification. Endocrinology *143*, 3604–3610.

Moncla, A., Missirian, C., Cacciagli, P., Balzamo, E., Legeai-Mallet, L., Jouve, J.-L., Chabrol, B., Le Merrer, M., Plessis, G., Villard, L., et al. (2007). A cluster of translocation breakpoints in 2q37 is associated with overexpression of NPPC in patients with a similar overgrowth phenotype. Hum. Mutat. *28*, 1183–1188.

Montelius, A., Marmigère, F., Baudet, C., Aquino, J.B., Enerbäck, S., and Ernfors, P. (2007). Emergence of the sensory nervous system as defined by Foxs1 expression. Differentiation. *75*, 404–417.

Nagase, M., Katafuchi, T., Hirose, S., and Fujita, T. (1997). Tissue distribution and localization of natriuretic peptide receptor subtypes in stroke-prone spontaneously hypertensive rats. J. Hypertens. *15*, 1235–1243.

Nagy, A. (2000). Cre recombinase: the universal reagent for genome tailoring. Genesis *26*, 99–109.

Nagy, A., Gertsenstein, M., and Vintersten, K. (2003). Manipulating the Mouse Embryo: A Laboratory Manual (Cold Spring Harbor Laboratory).

Nakagawa, S., and Takeichi, M. (1998). Neural crest emigration from the neural tube depends on regulated cadherin expression. Development *125*, 2963–2971.

Nascimento, C.G.O., and Branco, L.G.S. (2007). Role of the peripheral heme oxygenase-carbon monoxide pathway on the nociceptive response of rats to the formalin test: Evidence for a cGMP signaling pathway. Eur. J. Pharmacol. *556*, 55–61.

Nissim-Rafinia, M., and Kerem, B. (2002). Splicing regulation as a potential genetic modifier. Trends Genet. *18*, 123–127.

Niu, J., Ding, L., Li, J.J., Kim, H., Liu, J., Li, H., Moberly, A., Badea, T.C., Duncan, I.D., Son, Y.-J., et al. (2013). Modality-based organization of ascending somatosensory axons in the direct dorsal column pathway. J. Neurosci. *33*, 17691–17709.

O'Callaghan, J.P., and Holtzman, S.G. (1975). Quantification of the analgesic activity of narcotic antagonists by a modified hot-plate procedure. J. Pharmacol. Exp. Ther. *192*, 497–505.

O'Connor, R., and Tessier-Lavigne, M. (1999). Identification of maxillary factor, a maxillary process-derived chemoattractant for developing trigeminal sensory axons. Neuron *24*, 165–178.

O'Leary, D.D., Bicknese, A.R., De Carlos, J.A., Heffner, C.D., Koester, S.E., Kutka, L.J., and Terashima, T. (1990). Target selection by cortical axons: alternative mechanisms to establish axonal connections in the developing brain. Cold Spring Harb. Symp. Quant. Biol. *55*, 453–468.

Ogawa, H., Qiu, Y., Ogata, C.M., and Misono, K.S. (2004). Crystal structure of hormone-bound atrial natriuretic peptide receptor extracellular domain: rotation mechanism for transmembrane signal transduction. J. Biol. Chem. *279*, 28625–28631.

Ozaki, S., and Snider, W.D. (1997). Initial trajectories of sensory axons toward laminar targets in the developing mouse spinal cord. J. Comp. Neurol. *380*, 215–229.

Patel, T.D., Jackman, A., Rice, F.L., Kucera, J., and Snider, W.D. (2003). Development of sensory neurons in the absence of NGF/TrkA signaling in vivo. Neuron *37*, 183.

Pfeifer, A., Klatt, P., Massberg, S., Ny, L., Sausbier, M., Hirneiss, C., Wang, G.X., Korth, M., Aszódi, A., Andersson, K.E., et al. (1998). Defective smooth muscle regulation in cGMP kinase I-deficient mice. EMBO J. *17*, 3045–3051.

Pfeifer, A., Ruth, F., Dostmann, W., Sausbier, M., Klatt, F., and Hofmann, F. (1999). Structure and function of cGMP-dependent protein kinases. Rev Physiol Biochem Pharmacol.

Pick, C.G., Cheng, J., Paul, D., and Pasternak, G.W. (1991). Genetic influences in opioid analgesic sensitivity in mice. Brain Res. *566*, 295–298.

Pitcher, G.M., Ritchie, J., and Henry, J.L. (1999). Paw withdrawal threshold in the von Frey hair test is influenced by the surface on which the rat stands. J. Neurosci. Methods *87*, 185–193.

Pizziketti, R.J., Pressman, N.S., Geller, E.B., Cowan, A., and Adler, M.W. (1985). Rat cold water tail-flick: a novel analgesic test that distinguishes opioid agonists from mixed agonist-antagonists. Eur. J. Pharmacol. *119*, 23–29.

Platika, D., Boulos, M.H., Baizer, L., and Fishman, M.C. (1985). Neuronal traits of clonal cell lines derived by fusion of dorsal root ganglia neurons with neuroblastoma cells. Proc. Natl. Acad. Sci. *82*, 3499–3503.

Porrero, C., Rubio-Garrido, P., Avendaño, C., and Clascá, F. (2010). Mapping of fluorescent protein-expressing neurons and axon pathways in adult and developing Thy1-eYFP-H transgenic mice. Brain Res. *1345*, 59–72.

Potter, L.R. (1998). Phosphorylation-dependent regulation of the guanylyl cyclase-linked natriuretic peptide receptor B: dephosphorylation is a mechanism of desensitization. Biochemistry *37*, 2422–2429.

Potter, L.R. (2005). Domain analysis of human transmembrane guanylyl cyclase receptors: implications for regulation. Front. Biosci. *10*, 1205–1220.

Potter, L.R. (2011a). Natriuretic peptide metabolism, clearance and degradation. FEBS J. *278*, 1808–1817.

Potter, L.R. (2011b). Guanylyl cyclase structure, function and regulation. Cell. Signal. *23*, 1921–1926.

Potter, L.R. (2011c). Regulation and therapeutic targeting of peptide-activated receptor guanylyl cyclases. Pharmacol. Ther. *130*, 71–82.

Potter, L.R., and Hunter, T. (1998). Identification and characterization of the major phosphorylation sites of the B-type natriuretic peptide receptor. J. Biol. Chem. *273*, 15533–15539.

Potter, L.R., and Hunter, T. (2000). Activation of protein kinase C stimulates the dephosphorylation of natriuretic peptide receptor-B at a single serine residue: a possible mechanism of heterologous desensitization. J. Biol. Chem. *275*, 31099–31106.

Potter, L.R., and Hunter, T. (2001). Guanylyl cyclase-linked natriuretic peptide receptors: structure and regulation. J. Biol. Chem. *276*, 6057–6060.

Potter, L.R., Abbey-Hosch, S., and Dickey, D.M. (2006). Natriuretic peptides, their receptors, and cyclic guanosine monophosphate-dependent signaling functions. Endocr. Rev. *27*, 47–72.

Potter, L.R., Yoder, A.R., Flora, D.R., Antos, L.K., and Dickey, D.M. (2009). Natriuretic peptides: their structures, receptors, physiologic functions and therapeutic applications. Handb. Exp. Pharmacol. 341–366.

Potthast, R., Abbey-Hosch, S.E., Antos, L.K., Marchant, J.S., Kuhn, M., and Potter, L.R. (2004). Calcium-dependent dephosphorylation mediates the hyperosmotic and lysophosphatidic acid-dependent inhibition of natriuretic peptide receptor-B/guanylyl cyclase-B. J. Biol. Chem. *279*, 48513–48519.

Ralat, L.A., Guo, Q., Ren, M., Funke, T., Dickey, D.M., Potter, L.R., and Tang, W.-J. (2011). Insulin-degrading enzyme modulates the natriuretic peptide-mediated signaling response. J. Biol. Chem. *286*, 4670–4679.

Riddell, J.S., and Hadian, M. (2000). Interneurones in pathways from group II muscle afferents in the lower-lumbar segments of the feline spinal cord. J. Physiol. *522 Pt 1*, 109–123.

Robinson, J.W., and Potter, L.R. (2012). Guanylyl cyclases A and B are asymmetric dimers that are allosterically activated by ATP binding to the catalytic domain. Sci. Signal. *5*, ra65.

Robinson, J.W., Dickey, D.M., Miura, K., Michigami, T., Ozono, K., and Potter, L.R. (2013). A human skeletal overgrowth mutation increases maximal velocity and blocks desensitization of guanylyl cyclase-B. Bone *56*, 375–382.

Roux, K.J., Kim, D.I., Raida, M., and Burke, B. (2012). A promiscuous biotin ligase fusion protein identifies proximal and interacting proteins in mammalian cells. J. Cell Biol. *196*, 801–810.

Ruthazer, E.S., Akerman, C.J., and Cline, H.T. (2003). Control of axon branch dynamics by correlated activity in vivo. Science *301*, 66–70.

Salinas, P.C., and Zou, Y. (2008). Wnt signaling in neural circuit assembly. Annu. Rev. Neurosci. *31*, 339–358.

Sambrook, J., and W Russell, D. (2001). Molecular Cloning: A Laboratory Manual. Cold Spring Harb. Lab. Press. Cold Spring Harb. NY 999.

Sanford, L.P., Kallapur, S., Ormsby, I., and Doetschman, T. (2001). Influence of genetic background on knockout mouse phenotypes. Methods Mol. Biol. *158*, 217–225.

Sauer, B., and Henderson, N. (1988). Site-specific DNA recombination in mammalian cells by the Cre recombinase of bacteriophage P1. Proc. Natl. Acad. Sci. U. S. A. *85*, 5166–5170.

Schäffer, S. (2006). Investigations about the function of the cGMP-dependent kinase I alpha during the development of the nervous system. Diss. Submitt. to Dep. Biol. Chem. Pharm. Freie Univ. Berlin.

Schmidt, H., and Rathjen, F.G. (2010). Signalling mechanisms regulating axonal branching in vivo. Bioessays *32*, 977–985.

Schmidt, H., Werner, M., Heppenstall, P. a, Henning, M., Moré, M.I., Kühbandner, S., Lewin, G.R., Hofmann, F., Feil, R., and Rathjen, F.G. (2002). cGMP-mediated signaling via cGKIalpha is required for the guidance and connectivity of sensory axons. J. Cell Biol. *159*, 489–498.

Schmidt, H., Stonkute, A., Jüttner, R., Schäffer, S., Buttgereit, J., Feil, R., Hofmann, F., and Rathjen, F.G. (2007). The receptor guanylyl cyclase Npr2 is essential for sensory axon bifurcation within the spinal cord. J. Cell Biol. *179*, 331–340.

Schmidt, H., Stonkute, A., Jüttner, R., Koesling, D., Friebe, A., and Rathjen, F.G. (2009). C-type natriuretic peptide (CNP) is a bifurcation factor for sensory neurons. Proc. Natl. Acad. Sci. U. S. A. *106*, 16847–16852.

Schulz, S., Singh, S., Bellet, R. a, Singh, G., Tubb, D.J., Chin, H., and Garbers, D.L. (1989). The primary structure of a plasma membrane guanylate cyclase demonstrates diversity within this new receptor family. Cell *58*, 1155–1162.

Schweizer, R., Voit, D., and Frahm, J. (2008). Finger representations in human primary somatosensory cortex as revealed by high-resolution functional MRI of tactile stimulation. Neuroimage *42*, 28–35.

Scott, A., Hasegawa, H., Sakurai, K., Yaron, A., Cobb, J., and Wang, F. (2011). Transcription factor Shox2 is required for proper development of TrkB-expressing mechanosensory neurons. J. Neurosci. *31*, 6741–6749.

Serbedzija, G.N., Fraser, S.E., and Bronner-Fraser, M. (1990). Pathways of trunk neural crest cell migration in the mouse embryo as revealed by vital dye labelling. Development *108*, 605–612.

Shapiro, F., Barone, L., Johnson, A., and Flynn, E. (2014). The cn/cn dwarf mouse: Histomorphometric, ultrastructural, and radiographic study in mutants corresponding to human acromesomelic dysplasia Maroteaux type (AMDM). BMC Musculoskelet. Disord. *15*, 1–12.

Shirasaki, R., Lewcock, J.W., Lettieri, K., and Pfaff, S.L. (2006). FGF as a target-derived chemoattractant for developing motor axons genetically programmed by the LIM code. Neuron *50*, 841–853.

Silberberg, R., and Lesker, P. (1975). Skeletal growth and development of achondroplastic mice. Growth *39*, 17–33.

Sim, C.B., Ziemann, M., Kaspi, A., Harikrishnan, K.N., Ooi, J., Khurana, I., Chang, L., Hudson, J.E., El-Osta, A., and Porrello, E.R. (2014). Dynamic changes in the cardiac methylome during postnatal development. FASEB J. 1–15.

Söderberg, O., Gullberg, M., Jarvius, M., Ridderstråle, K., Leuchowius, K.-J., Jarvius, J., Wester, K., Hydbring, P., Bahram, F., Larsson, L.-G., et al. (2006). Direct observation of individual endogenous protein complexes in situ by proximity ligation. Nat. Methods *3*, 995–1000.

Sogawa, C., Tsuji, T., Shinkai, Y., Katayama, K., and Kunieda, T. (2007). Short-limbed dwarfism: slw is a new allele of Npr2 causing chondrodysplasia. J. Hered. *98*, 575–580.

Sogawa, C., Abe, A., Tsuji, T., Koizumi, M., Saga, T., and Kunieda, T. (2010). Gastrointestinal tract disorder in natriuretic peptide receptor B gene mutant mice. Am. J. Pathol. *177*, 822–828.

Sogawa, C., Wakizaka, H., Aung, W., Jin, Z.-H., Tsuji, A.B., Furukawa, T., Kunieda, T., and Saga, T. (2013). C-type natriuretic peptide specifically acts on the pylorus and large intestine in mouse gastrointestinal tract. Am. J. Pathol. *182*, 172–179.

Sogawa, C., Fujiwara, Y., Tsukamoto, S., Ishida, Y., Yoshii, Y., and Furukawa, T. (2014). Mutant phenotype analysis suggests potential roles for C-type natriuretic peptide receptor (NPR-B) in male mouse fertility. Reprod. Biol. Endocrinol. *12*, 1–6.

Srinivas, S., Watanabe, T., Lin, C.S., William, C.M., Tanabe, Y., Jessell, T.M., and Costantini, F. (2001). Cre reporter strains produced by targeted insertion of EYFP and ECFP into the ROSA26 locus. BMC Dev. Biol.

Steed, E., Elbediwy, A., Vacca, B., Dupasquier, S., Hemkemeyer, S.A., Suddason, T., Costa, A.C., Beaudry, J.B., Zihni, C., Gallagher, E., et al. (2014). MarvelD3 couples tight junctions to the MEKK1-JNK pathway to regulate cell behavior and survival. J. Cell Biol. *204*, 821–838.

Steiner, A. a., Reste, G., and Branco, L.G.S. (2003). Role of the brain heme oxygenase-carbon monoxide pathway in stress fever in rats. Neurosci. Lett. *341*, 193–196.

Sternberg, N., and Hamilton, D. (1981). Bacteriophage P1 site-specific recombination. J. Mol. Biol. *150*, 603–608.

Stonkute, A. (2010). cGMP signalling via CNP-Npr2-cGKI, and its role in axonal branching during embryonic development. Diss. Freie Univ. Berlin.

Stucky, C.L., and Lewin, G.R. (1999). Isolectin B(4)-positive and -negative nociceptors are functionally distinct. J. Neurosci. *19*, 6497–6505.

Sun, Y., Dykes, I.M., Liang, X., Eng, S.R., Evans, S.M., and Turner, E.E. (2008). A central role for Islet1 in sensory neuron development linking sensory and spinal gene regulatory programs. Nat. Neurosci. *11*, 1283–1293.

Szebenyi, G., Dent, E.W., Callaway, J.L., Seys, C., Lueth, H., and Kalil, K. (2001). Fibroblast growth factor-2 promotes axon branching of cortical neurons by influencing morphology and behavior of the primary growth cone. J. Neurosci. *21*, 3932–3941.

Tamás, G., Buhl, E.H., and Somogyi, P. (1997). Massive autaptic self-innervation of GABAergic neurons in cat visual cortex. J. Neurosci. *17*, 6352–6364.

Tamura, N., Doolittle, L.K., Hammer, R.E., Shelton, J.M., Richardson, J. a, and Garbers, D.L. (2004). Critical roles of the guanylyl cyclase B receptor in endochondral ossification and development of female reproductive organs. Proc. Natl. Acad. Sci. U. S. A. *101*, 17300–17305.

Tegeder, I., Del Turco, D., Schmidtko, A., Sausbier, M., Feil, R., Hofmann, F., Deller, T., Ruth, P., and Geisslinger, G. (2004). Reduced inflammatory hyperalgesia with preservation of acute thermal nociception in mice lacking cGMP-dependent protein kinase I. Proc. Natl. Acad. Sci. U. S. A. *101*, 3253–3257.

Ter-Avetisyan, G., Rathjen, F.G., and Schmidt, H. (2014). Bifurcation of Axons from Cranial Sensory Neurons Is Disabled in the Absence of Npr2-Induced cGMP Signaling. J. Neurosci. *34*, 737–747.

Tessier-Lavigne, M., and Goodman, C.S. (1996). The Molecular Biology of Axon Guidance. Science *274*, 1123–1133.

Tokudome, T., Horio, T., Soeki, T., Mori, K., Kishimoto, I., Suga, S., Yoshihara, F., Kawano, Y., Kohno, M., and Kangawa, K. (2004). Inhibitory effect of C-type natriuretic peptide (CNP) on cultured cardiac myocyte hypertrophy: interference between CNP and endothelin-1 signaling pathways. Endocrinology *145*, 2131–2140.

Torres, R., and Kühn, R. (1997). Laboratory Protocols for Conditional Gene Targeting (Oxford Uninversity Press).

Tsuji, T., and Kunieda, T. (2005). A loss-of-function mutation in natriuretic peptide receptor 2 (Npr2) gene is responsible for disproportionate dwarfism in cn/cn mouse. J. Biol. Chem. *280*, 14288–14292.

Vaandrager, A.B., Hogema, B.M., and De Jonge, H.R. (2005). Molecular properties and biological functions of cGMP-dependent protein kinase II. Front. Biosci. *10*, 2150–2164.

Vasques, G.A., Amano, N., Docko, A.J., Funari, M.F.A., Quedas, E.P.S., Nishi, M.Y., Arnhold, I.J.P., Hasegawa, T., and Jorge, A.A.L. (2013). Heterozygous mutations in natriuretic peptide receptor-B (NPR2) gene as a cause of short stature in patients initially classified as idiopathic short stature. J. Clin. Endocrinol. Metab. *98*, E1636–E1644.

Vogt, G., Huber, M., Thiemann, M., van den Boogaart, G., Schmitz, O.J., and Schubart, C.D. (2008). Production of different phenotypes from the same genotype in the same environment by developmental variation. J. Exp. Biol. *211*, 510–523.

Wall, M.E., Francis, S.H., Corbin, J.D., Grimes, K., Richie-Jannetta, R., Kotera, J., Macdonald, B.A., Gibson, R.R., and Trewhella, J. (2003). Mechanisms associated with cGMP binding and activation of cGMP-dependent protein kinase. Proc. Natl. Acad. Sci. U. S. A. *100*, 2380–2385.

Wang, K.H., Brose, K., Arnott, D., Kidd, T., Goodman, C.S., Henzel, W., and Tessier-Lavigne, M. (1999). Biochemical purification of a mammalian slit protein as a positive regulator of sensory axon elongation and branching. Cell *96*, 771–784.

Wang, Y., Kong, N., Li, N., Hao, X., Wei, K., Xiang, X., Xia, G., and Zhang, M. (2013). Epidermal growth factor receptor signaling-dependent calcium elevation in cumulus cells is required for NPR2 inhibition and meiotic resumption in mouse oocytes. Endocrinology *154*, 3401–3409.

Watanabe, Y., Nakajima, K., Shimamori, Y., and Fujimoto, Y. (1997). Comparison of the hydrolysis of the three types of natriuretic peptides by human kidney neutral endopeptidase 24.11. Biochem. Mol. Med. *61*, 47–51.

Wetzel, C., Hu, J., Riethmacher, D., Benckendorff, A., Harder, L., Eilers, A., Moshourab, R., Kozlenkov, A., Labuz, D., Caspani, O., et al. (2007). A stomatin-domain protein essential for touch sensation in the mouse. Nature *445*, 206–209.

Wickramasinghe, S.R., Alvania, R.S., Ramanan, N., Wood, J.N., Mandai, K., and Ginty, D.D. (2008). Serum response factor mediates NGF-dependent target innervation by embryonic DRG sensory neurons. Neuron *58*, 532–545.

Wikström, B., Hjerpe, A., Reinholt, F.P., and Engfeldt, B. (1986). Stereological studies on the epiphyseal growth cartilage and characterization of costal cartilage proteoglycans in the achondroplastic (cn/cn) mouse. Coll. Relat. Res. *6*, 279–293.

Wu, C.-S., Ballester Rosado, C.J., and Lu, H.-C. (2011). What can we get from “barrels”: the rodent barrel cortex as a model for studying the establishment of neural circuits. Eur. J. Neurosci. *34*, 1663–1676.

Yamada, H., Abe, T., Satoh, A., Okazaki, N., Tago, S., Kobayashi, K., Yoshida, Y., Oda, Y., Watanabe, M., Tomizawa, K., et al. (2013). Stabilization of actin bundles by a dynamin 1/cortactin ring complex is necessary for growth cone filopodia. J. Neurosci. *33*, 4514–4526.

Yasoda, A., Komatsu, Y., Chusho, H., Miyazawa, T., Ozasa, A., Miura, M., Kurihara, T., Rogi, T., Tanaka, S., Suda, M., et al. (2004). Overexpression of CNP in chondrocytes rescues achondroplasia through a MAPK-dependent pathway. Nat. Med. *10*, 80–86.

Yeung, V.T.F., Ho, S.K.S., Nicholls, M.G., and Cockram, C.S. (1996). Binding of CNP-22 and CNP-53 to cultured mouse astrocytes and effects on cyclic GMP. Peptides *17*, 101–106.

Yoder, A.R., Kruse, A.C., Earhart, C.A., Ohlendorf, D.H., and Potter, L.R. (2008). Reduced ability of C-type natriuretic peptide (CNP) to activate natriuretic peptide receptor B (NPR-B) causes dwarfism in lbab-/- mice. Peptides *29*, 1575–1581.

Yoder, A.R., Stone, M.D., Griffin, T.J., and Potter, L.R. (2010). Mass spectrometric identification of phosphorylation sites in guanylyl cyclase A and B. Biochemistry *49*, 10137–10145.

Yoder, A.R., Robinson, J.W., Dickey, D.M., Andersland, J., Rose, B. a, Stone, M.D., Griffin, T.J., and Potter, L.R. (2012). A functional screen provides evidence for a conserved, regulatory, juxtamembrane phosphorylation site in guanylyl cyclase a and B. PLoS One *7*, e36747.

Yu, D., Ellis, H.M., Lee, E.C., Jenkins, N. a, Copeland, N.G., and Court, D.L. (2000). An efficient recombination system for chromosome engineering in Escherichia coli. Proc. Natl. Acad. Sci. U. S. A. *97*, 5978–5983.

Zehir, A., Hua, L.L., Maska, E.L., Morikawa, Y., and Cserjesi, P. (2010). Dicer is required for survival of differentiating neural crest cells. Dev. Biol. *340*, 459–467.

Zhao, Z., and Ma, L. (2009). Regulation of axonal development by natriuretic peptide hormones. Proc. Natl. Acad. Sci. U. S. A. *106*, 18016–18021.

Zhao, Z., Wang, Z., Gu, Y., Feil, R., Hofmann, F., and Ma, L. (2009). Regulate axon branching by the cyclic GMP pathway via inhibition of glycogen synthase kinase 3 in dorsal root ganglion sensory neurons. J. Neurosci. *29*, 1350–1360.

Zirlinger, M., Lo, L., McMahon, J., McMahon, A.P., and Anderson, D.J. (2002). Transient expression of the bHLH factor neurogenin-2 marks a subpopulation of neural crest cells biased for a sensory but not a neuronal fate. Proc. Natl. Acad. Sci. U. S. A. *99*, 8084–8089.

Zurborg, S., Piszczek, A., Martínez, C., Hublitz, P., Al Banchaabouchi, M., Moreira, P., Perlas, E., and Heppenstall, P. a (2011). Generation and characterization of an Advillin-Cre driver mouse line. Mol. Pain *7*, 66.

Der Lebenslauf ist in der Online-Version aus Gründen des Datenschutzes nicht enthalten.

Der Lebenslauf ist in der Online-Version aus Gründen des Datenschutzes nicht enthalten.

Selbstständigkeitserklärung

Ich erkläre hiermit, dass ich die vorliegende Arbeit selbständig und nur unter Verwendung der angegebenen Literatur und Hilfsmittel angefertigt habe. Wurden Ergebnisse in Kooperation produziert, ist dies entsprechend angegeben.

Berlin, den 19.02.2015 Philip Tröster